



## ISTITUTO NAZIONALE DI RICERCA METROLOGICA Repository Istituzionale

### GUIDE FOR SAMPLING POWER AND POWER QUALITY MEASUREMENTS

This is the author's submitted version of the contribution published as:

*Original*

GUIDE FOR SAMPLING POWER AND POWER QUALITY MEASUREMENTS / Hadzhistoykova, Radoslava; Yovcheva, Antoaneta; Alvarez Sanmamed, Yolanda; Diaz de Aguilar, Javier; Maslan, Stanislav; Sera, Martin; Novakova Zachovalova, Vera; Trinchera, BRUNO OTTAVIO; Ellingsberg, Kristian; Malmbeek, Helge; Soccalingame, Soureche; Philominraj, Aristo; Pokatilov, Andrei; Power, Oliver; Berginc, Marko; Bergsten, Tobias; Svensson, Stefan; Cayci, Huseyin; Yilmaz, Ozlem; Kefeli, Tansu. - (2019).

*Availability:*

This version is available at: 11696/61733 since: 2020-03-03T01:00:18Z

*Publisher:*

*Published*

DOI:

*Terms of use:*

This article is made available under terms and conditions as specified in the corresponding bibliographic description in the repository

*Publisher copyright*

(Article begins on next page)



# GUIDE FOR SAMPLING POWER AND POWER QUALITY MEASUREMENTS

Radoslava Hadzhistoykova<sup>1)</sup>, Antoaneta Yovcheva,<sup>1)</sup> Yolanda Álvarez Sanmamed<sup>2)</sup>, Javier Díaz de Aguilar<sup>2)</sup>, Stanislav Mašláň<sup>3)</sup>, Martin Šíra<sup>3)</sup>, Věra Nováková Zachovalová<sup>3)</sup>, Bruno Trinchera<sup>6)</sup>, Kristian Ellingsberg<sup>7)</sup>, Helge Malmбекk<sup>7)</sup>, Soureche Soccalingame<sup>8)</sup>, Aristo Philominraj<sup>8)</sup>, Andrei Pokatilov<sup>9)</sup>, Oliver Power<sup>10)</sup>, Marko Berginc<sup>11)</sup>, Tobias Bergsten<sup>12)</sup>, Stefan Svensson<sup>12)</sup>, Hüseyin Çaycı<sup>13)</sup>, Özlem Yilmaz<sup>13)</sup>, Tansu Kefeli<sup>13)</sup>

May 31, 2019





# Affiliation

- <sup>1</sup> Bulgarian Institute of Metrology (**BIM**), Street G.M. Dimitrov 52-B, 1040 Sofia, Bulgaria
- <sup>2</sup> Centro Español de Metrología (**CEM**), C/del Alfar 2, 28760 Tres Cantos, Madrid, Spain
- <sup>3</sup> Czech Metrology Institute (**CMI**), Okružní 31, 638 00 Brno, Czech Republic
- <sup>6</sup> Istituto Nazionale di Ricerca Metrologica (**INRIM**), Strada delle Cacce 91, 10135 Torino, Italy
- <sup>7</sup> Justervesenet (**JV**), Fetveien 99, 2007 Kjeller, Norway
- <sup>8</sup> Laboratoire national de métrologie et d'essais (**LNE**), 1 rue Gaston Boissier, 75724 Paris Cedex 15, France
- <sup>9</sup> AS Metrosert (**Metrosert**), Teaduspargi 8, 12618 Tallinn, Estonia
- <sup>10</sup> National Standards Authority of Ireland (**NSAI**), 1 Swift Square, Northwood, Santry, Dublin 9, Ireland
- <sup>11</sup> Slovenski Institut za Kakovost in Meroslovje (**SIQ**), Tržaška cesta 2, 1000 Ljubljana, Slovenia
- <sup>12</sup> RISE Research Institutes of Sweden AB (**RISE**), Brinellgatan 4, 50462 Borås, Sweden
- <sup>13</sup> Türkiye Bilimsel ve Teknolojik Arastirma Kurumu (**TUBITAK**), Ataturk Bulvari 221, 06100 Ankara, Turkey





# Overview

Sampling techniques have been used in the field of electrical metrology for more than 20 years. These techniques are particularly suited to the sub-field of electrical power measurements where there is a necessity to make simultaneous measurement of several quantities. Digital sampling wattmeters with state-of-the-art performance have been developed and details are available in the literature. Sampling techniques are also eminently suited to the measurement of power quality parameters which involves measurements of complex, extended waveforms.

This Good Practice Guide, which has been developed within EMPIR project 15RPT04 TracePQM “Traceability routes for electrical power quality measurements”, is intended to provide, in a coherent and compact form, all the material concerned with metrology-grade sampling systems suitable for the measurement of power and power quality measurements. It is intended for those who wish to establish a reference measuring system for AC power, including high frequency power up to 1 MHz, and a selection of power quality parameters such as harmonics, dips, swells, flicker etc.

The first part of the guide deals with hardware. Designs for both a low frequency, high accuracy set-up and a high frequency set-up with reduced uncertainty are described. The commonly used hardware components, such as digitizers, voltage dividers and current shunts are introduced and their performance outlined. Schemes for interference free connections are described. Methods of evaluating the measurement uncertainties are provided together with some examples for commonly measured quantities.

The characterization of the hardware components plays a vital role in establishing the achievable uncertainty of the measuring system. Calibration methods for the various components are described including extension to high frequencies.

As part of the TracePQM project two open software tools which handle the control of the instrumentation, the data acquisition and the data processing were developed. These tools as well as updated version of the guide may be downloaded from a link provided on the project’s website <http://tracepqm.cmi.cz/>. Section 3 of this guide contains a full description of the tools including instructions for installing, configuring, and operating the tools.

The project 15RPT04 TracePQM has received funding from the EMPIR programme co-financed by the Participating States and from the European Union's Horizon 2020 research and innovation programme. This guide reflects only the author's view and EURAMET is not responsible for any use that may be made of the information it contains.

You are free to share, copy and redistribute the Guide. You must give appropriate credit.



The EMPIR initiative is co-funded by the European Union's Horizon 2020 research and innovation programme and the EMPIR Participating States

# Glossary

AC	Alternating Current
ADC	Analogue to Digital Converter
AVNA	Vector Network Analyzer
AWG	Arbitrary Waveform Generator
AWS	Arbitrary Waveform Synthesizer
<b>BIPM</b>	International Bureau of Weights and Measures
BNC	Bayonet Neill-Concelman connector
CMRR	Common Mode Rejection Ratio
CPEM	Conference on Precision Electromagnetic Measurements
CSV	2D text matrix of Comma-Separated Values (unless defined otherwise)
CS	Current Shunt
CT	Current Transformer
DAC	Digital to Analog Converter
DC	Direct Current
DFT	Discrete Fourier Transform
DMM	Digital Multimeter
DSWM	Digital Sampling Wattmeter
DUT	Device Under Test
DVM	Digital Voltmeter
EMPIR	European Metrology Programme for Innovation and Research
<b>EURAMET</b>	European Association of National Metrology Institutes
FFT	Fast Fourier Transform
FS	Full-Scale
GPIB	HP-IB, IEEE 488, or IEC625 ; General Purpose Interface Bus
GUF	Guide to the expression of Uncertainty Framework
GUI	Graphical User Interface
GUM	Guide to the expression of Uncertainty in Measurement

HF	High Frequency
HW	Hardware
IADC	Integrating Analogue to Digital Converter
IEC	International Electrotechnical Commission
IVD	Inductive Voltage Divider
JAWS	Josephson Arbitrary Waveform Synthesizer
LF	Low Frequency
MCM	Monte Carlo Method for uncertainty calculation
NI	National Instruments
NMI	National Metrology Institutes
PCR	Power Coefficient of Resistance
PLL	Phase-Locked Loop
PQ	Power Quality
PQM	Power Quality Measurements
PTFE	Polytetrafluoroethylene
PXI	PCI eXtensions for Instrumentation
RMS	Root Mean Square
RVD	Resistive Voltage Divider
SI	International System of Units
SW	Software
TCC	Thermal Current Converter
TCR	Temperature Coefficient of Resistance
THD	Total Harmonic Distortion
TVC	Thermal Voltage Converters
TWM / TPQA	Developed softwares in scope of EMPIR project 15RPT04 TracePQM
UUT	Unit Under Test
VT	Voltage Transformer
WB	Wide Band
ZPF	Zero-power factors standards

# Contents

<b>1</b>	<b>Description of the modular measurement setup</b>	<b>25</b>
1.1	Methods for proper interference-free connections . . . . .	26
1.1.1	Modular measurement setups . . . . .	26
1.1.1.1	Low frequency (LF) measurement setups . . . . .	28
1.1.1.2	High frequency (HF - wideband) measurement setups . . . . .	29
1.1.2	Components of modular measurement setups . . . . .	32
1.1.2.1	Cables and Wiring . . . . .	32
1.1.2.2	Current equalization - The coaxial chokes . . . . .	33
1.1.2.3	Power source . . . . .	34
1.1.2.4	Voltage divider . . . . .	36
1.1.2.5	Current shunt . . . . .	39
1.1.2.6	Current transformers . . . . .	42
1.1.2.7	DMM & Digitizers . . . . .	42
1.2	Hardware configuration of the digitizers . . . . .	43
1.2.1	Low frequency domain (DMM 3458A) . . . . .	43
1.2.1.1	Sampling mode . . . . .	43
1.2.1.2	Input impedance and ranging . . . . .	44
1.2.1.3	Guarding . . . . .	45
1.2.1.4	Synchronization . . . . .	47
1.2.2	High frequency domain (NI PXI5922) . . . . .	50
1.2.2.1	Principle . . . . .	50
1.2.2.2	Input range . . . . .	52
1.2.2.3	Input impedance . . . . .	52
1.2.2.4	Clocking . . . . .	53
1.2.2.5	Input connections . . . . .	53
1.3	Selecting the relevant components . . . . .	55
1.3.1	Selecting the digitizers . . . . .	55
1.3.1.1	Digitizers - Low frequency setups . . . . .	56
1.3.1.2	Digitizers - High frequency setups . . . . .	58
1.3.2	Selecting the input transducers . . . . .	61
1.3.2.1	Selecting the voltage transducers for wideband measurements . . . . .	62
1.3.2.2	Selecting the current transducers . . . . .	63
1.4	Achievable uncertainties . . . . .	65
1.4.1	Uncertainty Calculation Methods . . . . .	65

1.4.1.1	Uncertainty evaluation based on the Law of Propagation of Uncertainty . . . . .	65
1.4.1.2	Numerical calculation by Monte Carlo Method . . . . .	66
1.4.2	Example (GUF) - Uncertainty evaluation for the DSWM . . . . .	68
1.4.3	Examples - Achievable uncertainties . . . . .	71
1.4.3.1	Example 1 - Frequency measurement . . . . .	72
1.4.3.2	Example 2 - Phase shift measurement . . . . .	72
1.4.3.3	Example 3 - Harmonic distortion measurement . . . . .	73
1.4.3.4	Example 4 - LF power and RMS measurements . . . . .	75
1.4.3.5	Example 5 - HF measurements . . . . .	77
<b>2</b>	<b>Calibration methods for the modular measurement setup components</b>	<b>81</b>
2.1	Methods for calibration of current shunts . . . . .	82
2.1.1	Current shunts - Amplitude . . . . .	82
2.1.1.1	Leakage currents . . . . .	82
2.1.1.2	Major contributions to the uncertainty . . . . .	83
2.1.2	Current shunts - Phase angle error . . . . .	83
2.1.2.1	Measurement considerations . . . . .	85
2.1.3	Current shunts - Level dependence . . . . .	87
2.1.3.1	Introduction . . . . .	87
2.1.3.2	Measurement setup . . . . .	87
2.1.3.3	Set of resistance standards . . . . .	88
2.1.3.4	Level dependence (power coefficient) measurement . . . . .	89
2.1.3.5	Uncertainty calculation . . . . .	90
2.1.4	Current shunts - Temperature dependence . . . . .	92
2.1.4.1	Introduction . . . . .	92
2.1.4.2	Temperature dependence (temperature coefficient) measurements . . . . .	92
2.1.4.3	Uncertainty calculation . . . . .	94
2.2	Methods for calibration of voltage dividers . . . . .	96
2.2.1	Voltage divider - Amplitude . . . . .	96
2.2.1.1	Ac-dc difference method . . . . .	96
2.2.1.2	Digitizer method . . . . .	97
2.2.1.3	Digital sampling impedance bridge method . . . . .	97
2.2.1.4	Measurement considerations . . . . .	98
2.2.2	Voltage divider - Phase angle error . . . . .	99
2.2.2.1	Step up method at low frequencies using 3458A . . . . .	100
2.2.3	Voltage divider - Level dependence . . . . .	102
2.2.4	Voltage divider - Temperature and humidity dependence . . . . .	103
2.3	Methods for calibration of the DMM (3458A) . . . . .	105
2.3.1	DMM (3458A) - Frequency response . . . . .	105
2.3.1.1	Introduction . . . . .	105
2.3.1.2	Equipment . . . . .	105
2.3.1.3	Procedure . . . . .	106
2.3.1.4	Calibration connection . . . . .	106
2.3.1.5	Uncertainty evaluation . . . . .	108
2.3.1.6	Results . . . . .	109

2.3.2	DMM (3458A) - Dynamic linearity . . . . .	110
2.3.2.1	Introduction . . . . .	110
2.3.2.2	Equipment and connection . . . . .	111
2.3.2.3	Procedure . . . . .	111
2.3.2.4	Amplitude linearity and phase angle dependence . . . . .	115
2.3.3	DMM (3458A) - Distortion . . . . .	118
2.3.4	DMM (3458A) - Evaluation of the stability . . . . .	120
2.3.5	DMM (3458A) - Temperature dependence . . . . .	121
2.3.5.1	Introduction . . . . .	121
2.3.5.2	Equipment . . . . .	121
2.3.5.3	Procedure . . . . .	122
2.3.5.4	Calibration connection . . . . .	122
2.3.5.5	Uncertainty evaluation . . . . .	123
2.3.6	DMM (3458A) - Input impedance . . . . .	123
2.4	Methods for calibration of the digitizers (NI 5922) . . . . .	125
2.4.1	Digitizer (NI 5922) - Frequency response . . . . .	126
2.4.2	Digitizer (NI 5922) - Level dependence . . . . .	128
2.4.2.1	Example of measured characteristics . . . . .	130
2.4.3	Digitizer (NI 5922) - Phase angle error between channels . . . . .	132
2.4.4	Digitizer (NI 5922) - Distortion . . . . .	133
2.4.4.1	Example of measurement . . . . .	134
2.4.5	Digitizer (NI 5922) - Evaluation of the stability of phase and amplitude . . . . .	135
2.4.6	Digitizer (NI 5922) - Evaluation of the input impedance . . . . .	140
2.5	Methods for calibration of the entire system . . . . .	143
<b>3</b>	<b>User's guide for the open software tool</b>	<b>145</b>
3.1	Software introduction - TWM manual - LabView Environnement . . . . .	146
3.1.1	Installation . . . . .	146
3.1.1.1	Installing TWM tool . . . . .	146
3.1.1.2	Installing TWM prerequisites . . . . .	147
3.1.1.3	Installing GNU Octave . . . . .	148
3.1.1.4	Installing Matlab . . . . .	149
3.1.2	Before starting TWM – Set decimal separator . . . . .	149
3.1.3	Startup . . . . .	149
3.1.4	User guide . . . . .	149
3.1.4.1	Configuring the processing environment . . . . .	150
3.1.4.2	Configuring the digitizer . . . . .	152
3.1.4.3	Configuring setup and corrections . . . . .	156
3.1.4.4	Configuring new measurement . . . . .	162
3.1.4.5	Initiating measurement . . . . .	169
3.1.4.6	Viewing the results . . . . .	169
3.1.4.7	Batch processing . . . . .	172
3.2	TWM Corrections Reference Manual . . . . .	174
3.2.1	CSV marices . . . . .	174
3.2.2	Correction model . . . . .	177
3.2.3	Calibration concept . . . . .	179



3.2.4	Transducer corrections . . . . .	180
3.2.4.1	Transducer correction items . . . . .	182
3.2.5	Digitizer corrections . . . . .	190
3.2.5.1	Digitizer correction files format . . . . .	191
3.2.5.2	Digitizer corrections . . . . .	194
3.2.5.3	Channel corrections . . . . .	196
3.2.5.4	Nominal gain (optional) . . . . .	197
3.2.5.5	Gain frequency transfer (optional) . . . . .	197
3.2.5.6	Phase frequency transfer (optional) . . . . .	198
3.2.5.7	DC offset (optional) . . . . .	199
3.2.5.8	Aperture correction (optional) . . . . .	199
3.2.5.9	SFDR value (optional) . . . . .	200
3.2.5.10	RMS jitter (optional) . . . . .	201
3.2.5.11	Input admittance (optional) . . . . .	201
3.3	Software introduction - TPQA manual - LabWindows Environnement . . . . .	203
3.3.1	Installation of drivers and development environments . . . . .	203
3.3.1.1	Installing TPQA tool . . . . .	203
3.3.1.2	Installing TPQA prerequisites . . . . .	205
3.3.1.3	Installing Matlab . . . . .	205
3.3.2	Startup . . . . .	206
3.3.3	User guide . . . . .	206
3.3.3.1	Configuring digitizers for a new measurement setup . . . . .	207
3.3.3.2	Configuration of measurement corrections . . . . .	211
3.3.3.3	TPQA data processing . . . . .	215
3.4	Software configuration of the built-in digitizers . . . . .	223
3.4.1	DMM 3458A . . . . .	223
3.4.1.1	Voltage range selection . . . . .	223
3.4.1.2	Input frequency bandwidth . . . . .	223
3.4.1.3	Aperture time . . . . .	223
3.4.1.4	Sampling rate . . . . .	223
3.4.1.5	Samples count . . . . .	224
3.4.2	Digitizer NI PXI 5922 . . . . .	224
3.4.2.1	Measurement setup for testing TPQA . . . . .	224
3.4.2.2	Measurement configuration for LabWindows environment (TPQA) . . . . .	225
3.5	Integration of new types of digitizers . . . . .	228
3.5.1	LabVIEW environment . . . . .	228
3.5.2	LabWindows environment . . . . .	228
3.5.2.1	Flow chart LabWindowsTM/CVI environment . . . . .	228
3.5.2.2	Integration of new digitizers in LabWindows/CVI environment . . . . .	229
3.6	Power and PQ tests - Algorithms . . . . .	231
3.6.1	Existing algorithms . . . . .	231
3.6.1.1	TWM-PSFE - Phase Sensitive Frequency Estimator . . . . .	231
3.6.1.2	TWM-FPNLSF - Four Parameter Non Linear Sine Fit . . . . .	232
3.6.1.3	TWM-MFSF - Multi-Frequency Sine Fit . . . . .	232
3.6.1.4	TWM-WRMS - RMS value by Windowed Time Domain Integration . . . . .	233

3.6.1.5	TWM-WFFT - Windowed FFT spectrum analysis . . . . .	233
3.6.1.6	TWM-THDWFFT - THD from Windowed FFT . . . . .	233
3.6.1.7	TWM-PWRDI - Power by Time Domain Integration . . . . .	234
3.6.1.8	TWM-PWRFFT - Power by FFT . . . . .	234
3.6.1.9	TWM-Flicker - Flicker algorithm . . . . .	235
3.6.1.10	TWM-MODTDPS - Modulation analyzer in Time Domain, by quadrature Phase Shifting . . . . .	235
3.6.1.11	TWM-HCRMS - Half Cycle RMS algorithm . . . . .	235
3.6.1.12	TWM-InDiSwell - Interruption, Dip, Swell event detector . . . .	236
3.6.1.13	TWM-InpZ – Estimator of Digitizer Input Impedance . . . . .	236
3.6.2	Integration of new algorithms . . . . .	236

<b>Bibliography</b>	<b>239</b>
---------------------	------------



# List of Figures

<b>1</b>	<b>Description of the modular measurement setup</b>	<b>25</b>
1.1	Calibration of power source using DSWM setup using floating digitizers. . . . .	27
1.2	Calibration of power meter UUT source using DSWM setup using floating digitizers. . . . .	27
1.3	Calibration of power meter UUT source using DSWM setup using floating digitizers 3458A. . . . .	28
1.4	Calibration of power meter UUT source using DSWM setup using floating digitizers 3458A - workaround reducing the leakage current $I_g$ effect. . . . .	29
1.5	Calibration of power meter UUT source using DSWM setup using grounded digitizers NI 5922 in full differential mode. . . . .	30
1.6	Calibration of power meter UUT source using DSWM setup using grounded digitizers NI 5922 in mixed single ended and differential mode. . . . .	30
1.7	HF modular measurement setup electric block diagram. . . . .	31
1.8	Connection of power source, power analyzer (UUT) and reference sampling wattmeter (DSWM) transducers using twisted wires. . . . .	32
1.9	Current equalizer (Choke). . . . .	33
1.10	Power source - Fluke 6100A. . . . .	35
1.11	Power source - Fluke 5720A (Left) & AWG - NI PXI-5421 (Right). . . . .	35
1.12	HF power source schematic. . . . .	35
1.13	Transconductance amplifier - Clarke Hess 8100. . . . .	36
1.14	NMIA Inductive Voltage Divider (IVD) [8] . . . . .	38
1.15	RISE Resistive Voltage Divider (RVD). . . . .	39
1.16	RISE current shunts. . . . .	40
1.17	JV current shunts. . . . .	41
1.18	LNE 10 A current shunt. . . . .	42
1.19	DMM 3458A front panel [14]. . . . .	43
1.20	The 3458A's front panel input terminals, including Guard terminal and the Guard switch [14]. . . . .	45
1.21	DMM 3458A Guard terminal - Open [7]. . . . .	46
1.22	DMM 3458A Guard terminal to LO [7]. . . . .	46
1.23	DMM 3458A synchronization in Master-Slave topology with Master generating sample clock. . . . .	48
1.24	DMM 3458A synchronization in Master-Slave topology with sample clock generated by the external AWG. . . . .	48

1.25	DMM 3458A synchronization in topology with sample clock generated by the external AWG for all DMMs at once. . . . .	49
1.26	DMM 3458A synchronization in Master-Slave topology with sample clock generated by source. . . . .	49
1.27	Dual channel high-speed digitizer NI PXI-5922 [15]. . . . .	50
1.28	Block diagram of the NI PXI-5922 board [15]. . . . .	51
1.29	Single-ended input measurement setup. . . . .	53
1.30	Differential input measurement setup. . . . .	54
1.31	ADCs performance according to main figure of merit as sampling rate, vertical resolution and the signal-to-noise ratio. . . . .	56
1.32	Switching sampling power meter setup. . . . .	59
1.33	Basic structure of synchronized digitizers in a digital sampling wattmeter. . . . .	60
1.34	INRIM unified measurement setup based on DMMs and wideband digitizers for power and PQ measurements. . . . .	61
1.35	Voltage dividers and current shunts available at the labs in the survey. . . . .	62
1.36	Set of wideband coaxial compensated RVD for voltage scaling with ratio from 1:3 to 1:52 constructed at INRIM. . . . .	63
1.37	Coaxial shunts: (Left) Cage design (manufactured by Fluke), (Middle) Coaxial foil structure (manufactured by BEV), (Right) Coaxial disk design (manufactured by INRIM). . . . .	64
1.38	Illustration of the propagation of distribution for 3 input quantities [24]. . . . .	66
1.39	Schematic flow graph of uncertainty evaluation using Monte Carlo Method [24]. . . . .	67
1.40	Uncertainty - Harmonic distortion measurement. . . . .	75
1.41	Uncertainty - HF measurement connection . . . . .	78
<b>2</b>	<b>Calibration methods for the modular measurement setup components</b>	<b>81</b>
2.1	Shunt's schematic description of the ac-dc difference setup at JV. . . . .	83
2.2	Digital bridge for wideband current shunt calibration at RISE. . . . .	84
2.3	Wideband digital phase comparator for high current shunt calibration at INRIM. . . . .	85
2.4	Shunt's level dependence measurement setup. . . . .	88
2.5	Typical level dependence of cage shunt (Left) and Fluke A40A shunt (Right). . . . .	89
2.6	Typical level dependence of foil shunt. . . . .	90
2.7	R(T) characteristic of foil shunt. . . . .	93
2.8	R(T) characteristic of cage shunt. . . . .	93
2.9	R(T) characteristic of Fluke A40A shunt. . . . .	94
2.10	INRIM setup based on an automatic ac-dc transfer facility for high precision characterization of ac-dc amplitude error of RVDs and buffers. . . . .	96
2.11	RISE setup for wideband calibration of voltage dividers. . . . .	97
2.12	CMI setup for calibration of voltage dividers using digital sampling impedance bridge. . . . .	98
2.13	INRIM setup for calibration of high ratio voltage dividers. . . . .	100
2.14	Step up method for calibration of phase angle of RVD dividiars. . . . .	101
2.15	DMM 3458A - Frequency response - A simplified calibration connection where AC voltage source is used as a reference. . . . .	107

2.16	DMM 3458A - Frequency response - A simplified calibration connection where ac voltage standard is used as a reference. . . . .	107
2.17	DMM 3458A - Frequency response - A calibration connection where thermal convertors are used as a reference. . . . .	108
2.18	Frequency response of the DMM 3458 where the set value on the Fluke 5720A calibrator was used as a reference. . . . .	110
2.19	Frequency response of the DMM 3458 where the ac voltage standard Fluke 5790A was used as a reference. . . . .	110
2.20	Schematic diagram (left) and picture (right) of the measurement setup used in characterization of the sampling DMM - Dynamic linearity. . . . .	111
2.21	Voltage deviation vs. frequency for the input signal of 0.8 V (100% FS). . . . .	113
2.22	Voltage deviation relative to the input signal of 0.8 V. . . . .	113
2.23	Voltage deviation vs. frequency for the input signal of 0.8 V (100% FS) at the fixed sampling rate. . . . .	114
2.24	Voltage deviation relative to the input signal of 0.8 V at the fixed sampling rate. . . . .	115
2.25	Calibration of amplitude nonlinearity and phase dependence of the DMM 3458A. . . . .	116
2.26	Nonlinearity of the DMM 3458A amplitude transfer for 53 Hz. Dashed lines are expanded uncertainty limits. . . . .	116
2.27	Nonlinearity of the DMM 3458A amplitude transfer for 53 Hz (details). Dashed lines are expanded uncertainty limits. . . . .	117
2.28	Phase shift dependence on the amplitude of DMM 3458A for 53 Hz. Dashed lines are expanded uncertainty limits. . . . .	117
2.29	Nonlinearity of the DMM 3458A amplitude transfer for 1500 Hz. . . . .	117
2.30	Phase shift of the DMM 3458A vs input amplitude for 1500 Hz. . . . .	118
2.31	Spectrum of the sampled signal generated by the Josephson source (150 mV RMS, 52 Hz). The signal was sampled at $T_s = 420 \mu s$ and $T_a = 120 \mu s$ using $N = 23810$ samples. . . . .	119
2.32	The spectrum of the remaining signal when the estimated fundamental signal (i.e. 150 mV / 52 Hz) was subtracted from the original sampled signal. All distortions are more than 105 dBV below the level of the fundamental signal. . . . .	120
2.33	Voltage deviations and expanded uncertainties at 0.8 V input voltage for 1-year calibration interval (low harmonic distortion mode). . . . .	120
2.34	Voltage deviations and expanded uncertainties at 0.8 V input voltage for 1-year calibration interval (fixed sampling rate mode). . . . .	121
2.35	DMM 3458A - Temperature dependence - Recommended temperature profile in the climatic chamber. . . . .	122
2.36	A calibration connection for measuring temperature dependence of DMM 3458. . . . .	123
2.37	Example of measurement of a input impedance of the digitizer 3458A using autobalance bridge. . . . .	124
2.38	Example of measured input impedance of the digitizer 3458A using autobalance bridge. DMM was set to DCV mode and 1 V range. . . . .	124
2.39	Calibration setup for characterization of NI 5922 wideband digitizer. . . . .	126
2.40	Calibration of NI 5922 gain and phase using any source and precision ACMS to measure reference applied voltage. Optional buffer reduces changes in the applied voltage due to the time varying input impedance of the ACMS. . . . .	127

2.41	NI 5922 Frequency Response Measurements for sampling rate 10 MSa/s. . . . .	127
2.42	NI 5922 – Linearity – A simplified calibration connection where ac voltage source is used as a reference. . . . .	128
2.43	NI 5922 – Linearity – Calibration connection where ac voltage standard is used as a reference. . . . .	128
2.44	NI 5922 – Linearity – Calibration connection where thermal convertor is used as a reference. . . . .	129
2.45	NI 5922 – Linearity – Linearity test in synchronized ADCs using calibrated wideband IVD realized at INRIM. . . . .	130
2.46	NI 5922 – Linearity – Advanced calibration connection where Josephson arbitrary waveform synthesizer (JAWS) is used as a reference. . . . .	130
2.47	Level dependence measurements at 50 kS/s (Channel Ch0). . . . .	131
2.48	Level dependence measurements at 50 kS/s (Channel Ch1). . . . .	131
2.49	Level dependence measurements at 100 kS/s (Channel Ch0). . . . .	131
2.50	Level dependence measurements at 100 kS/s (Channel Ch1). . . . .	131
2.51	Level dependence measurements at 500 kS/s (Channel Ch0). . . . .	131
2.52	Level dependence measurements at 500 kS/s (Channel Ch1). . . . .	131
2.53	Level dependence measurements at 1 MS/s (Channel Ch0). . . . .	132
2.54	Level dependence measurements at 1 MS/s (Channel Ch1). . . . .	132
2.55	Level dependence measurements at 10 MS/s (Channel Ch0). . . . .	132
2.56	Level dependence measurements at 10 MS/s (Channel Ch1). . . . .	132
2.57	Example of measurement of a phase angle between channels 0 and 1 of the digitizer NI 5922. . . . .	133
2.58	Stability of amplitude measurements at 50 kS/s (Channel Ch0). . . . .	136
2.59	Stability of amplitude measurements at 50 kS/s (Channel Ch1). . . . .	136
2.60	Stability of phase error measurements at 50 kS/s (Channel Ch1-Ch0). . . . .	136
2.61	Stability of amplitude measurements at 100 kS/s (Channel Ch0). . . . .	136
2.62	Stability of amplitude measurements at 100 kS/s (Channel Ch1). . . . .	136
2.63	Stability of phase error measurements at 100 kS/s (Channel Ch1-Ch0). . . . .	137
2.64	Stability of amplitude measurements at 500 kS/s (Channel Ch0). . . . .	137
2.65	Stability of amplitude measurements at 500 kS/s (Channel Ch1). . . . .	137
2.66	Stability of phase error measurements at 500 kS/s (Channel Ch1-Ch0). . . . .	137
2.67	Stability of amplitude measurements at 1 MS/s (Channel Ch0). . . . .	138
2.68	Stability of amplitude measurements at 1 MS/s (Channel Ch1). . . . .	138
2.69	Stability of phase error measurements at 1 MS/s (Channel Ch1-Ch0). . . . .	138
2.70	Stability of amplitude measurements at 10 MS/s (Channel Ch0). . . . .	138
2.71	Stability of amplitude measurements at 10 MS/s (Channel Ch1). . . . .	138
2.72	Stability of phase error measurements at 10 MS/s (Channel Ch1-Ch0). . . . .	139
2.73	Example of repeatability of NI 5922 self-cal routine (red diamonds) and calculated stability of internal reference (blue curve). . . . .	140
2.74	Example of measurement of a input impedance of the digitizer NI 5922. . . . .	141
2.75	Example of measurement of a input impedance of the digitizer NI 5922 using TWM/TPQA tool itself. . . . .	141
2.76	Example of measured input impedance of NI 5922 using TWM/TPQA tool itself. . . . .	142
2.77	ac-dc calibration system modified for ac calibration of the voltage channel. . . . .	143

2.78 ac-dc calibration system modified for ac calibration of the current channel. . . .	144
---	-----

### 3 User's guide for the open software tool 145

3.1 Location of TWM download on the TWM GitHub webpage. . . . .	147
3.2 Downloading development version of TWM from GitHub webpage. . . . .	147
3.3 Front panel of TWM. . . . .	150
3.4 TWM processing environment configuration. . . . .	151
3.5 TWM GNU Octave package assistant. . . . .	152
3.6 TWM configuration panel for the niScope digitizers (for NI 5922). . . . .	153
3.7 TWM configuration panel for Agilent 3458A sampling multimeters. . . . .	154
3.8 TWM transducer configuration panel. . . . .	156
3.9 TWM operation for analyzing with single input algorithms. . . . .	157
3.10 TWM operation for analyzing single phase with paired input algorithms (power). . . . .	158
3.11 TWM operation for analyzing multiple phases with paired input algorithms (power). . . . .	158
3.12 TWM transducer correction editor. . . . .	159
3.13 TWM CSV correction matrix editor. . . . .	160
3.14 TWM digitizer corrections configuration panel. . . . .	161
3.15 TWM digitizer correction editor. . . . .	162
3.16 TWM new measurement configuration panel. . . . .	163
3.17 TWM sampling setup assistant. . . . .	164
3.18 TWM sampling setup assistant - fundamental frequency measurement panel. . . . .	165
3.19 TWM processing configuration panel (raw Matlab commands mode). . . . .	166
3.20 TWM processing configuration panel. . . . .	167
3.21 TWM multicore processing setup panel. . . . .	168
3.22 TWM multicore processing GNU Octave servers. . . . .	169
3.23 TWM record viewer panel. . . . .	170
3.24 TWM spectrum viewer panel. . . . .	170
3.25 TWM processing results viewer. . . . .	171
3.26 TWM QWTB batch processing panel. . . . .	173
3.27 Transducer-digitizer loading correction model for single ended connections. . . . .	177
3.28 Transducer-digitizer loading correction model for single ended connections with buffer amplifier. . . . .	178
3.29 Transducer-digitizer loading correction model for differential connection. . . . .	178
3.30 Transducer-digitizer loading correction model for differential connection with buffer amplifier. . . . .	178
3.31 Separate transducer-cable-digitizer calibration. . . . .	179
3.32 Separate transducer-(cable+digitizer) calibration. . . . .	180
3.33 System calibration concept. . . . .	180
3.34 Location of TPQA download on the TPQA GitHub webpage. . . . .	204
3.35 Downloading development version of TPQA from GitHub webpage. . . . .	205
3.36 Front panel of TPQA. . . . .	207
3.37 TPQA - (Left) single-ended measurements; (Right) differential measurements. . . . .	208
3.38 TPQA configuration panel for vertical and horizontal setting of digitizer physical channels. . . . .	209



3.39	TPQA configuration panel for trigger resources and setting. . . . .	209
3.40	TPQA configuration panel for HP-3458a DMMs digitizer. . . . .	210
3.41	TPQA hardware corrections configuration panel. . . . .	212
3.42	TPQA - Example of transducers configuration when ADC1 and ADC2 are set Single-ended mode. . . . .	213
3.43	TPQA - Example of transducers configuration when ADC1 and ADC2 are set in Differential mode. . . . .	214
3.44	TPQA - Example of digitizer configuration panel. . . . .	214
3.45	TPQA (TWM processing panel). . . . .	216
3.46	TPQA - Algorithm setup panel. . . . .	217
3.47	TPQA (TWM processing panel) when processing record is finished. . . . .	218
3.48	TPQA (TWM-Result Viewer). . . . .	219
3.49	TPQA - Acquisition and Data Processing Control section and the measurement plot. . . . .	220
3.50	TPQA - Preliminary (on-line) data processing using NI-CVI FFT algorithms. . . . .	221
3.51	TPQA - Selected Measured value graph. . . . .	222
3.52	Macro setups modular system . . . . .	225
3.53	Flow chart for TPQA open software tool. . . . .	229
3.54	Header structure of the translator used with ni.scope driver. . . . .	230
3.55	Example of a structure for generic Virtual digitizer. . . . .	230

# List of Tables

<b>1</b>	<b>Description of the modular measurement setup</b>	<b>25</b>
1.1	RISE 10 A Shunt's AC/DC transfer difference & Phase angle. . . . .	40
1.2	JV 10 A Shunt's AC/DC transfer difference & Phase angle. . . . .	41
1.3	LNE 10 A Shunt's AC/DC transfer difference & Phase angle. . . . .	42
1.4	Characteristics of sampling modes [14]. . . . .	44
1.5	Characteristics depending on input range [14]. . . . .	45
1.6	Resolution and bandwidth of the NI PXI-5922 [15]. . . . .	51
1.7	Summary of uncertainty evaluation of active power in W/VA . . . . .	70
1.8	Uncertainty - Frequency measurement. . . . .	72
1.9	Uncertainty - Phase shift measurement. . . . .	73
1.10	Uncertainty - Harmonic distortion measurement. . . . .	74
1.11	Uncertainty - LF power and RMS measurements - WITH Corrections. . . . .	76
1.12	Uncertainty - LF power and RMS measurements - WITHOUT Corrections. . . . .	77
1.13	Uncertainty - HF measurements. . . . .	79
<b>2</b>	<b>Calibration methods for the modular measurement setup components</b>	<b>81</b>
2.1	Typical power coefficients of different type of shunts. . . . .	90
2.2	Typical temperature coefficients of different types of shunts. . . . .	94
2.3	Input ranges of ac-dc transfer standard. . . . .	111
2.4	Sampling parameters used for measurements of signals with low harmonic distortion. . . . .	112
2.5	Ac voltage deviation from nominal value in mV/V. . . . .	112
2.6	Expanded uncertainty in mV/V. . . . .	112
2.7	Ac voltage deviation from nominal value (fixed sampling rate), $\mu\text{V/V}$ . . . . .	114
2.8	Expanded uncertainty (fixed sampling rate), $\mu\text{V/V}$ . . . . .	114
2.9	Example of NI 5922 THD measurement. THD was set measure up to 30 harmonics, sampling rate was fixed 2 MSa/s and the band stop for the THD+N was set to 500 kHz. . . . .	135
<b>3</b>	<b>User's guide for the open software tool</b>	<b>145</b>
3.1	Typical GNU Octave packages required for TWM. . . . .	148
3.2	Example of 1D CSV table with one quantity . . . . .	175

3.3	Example of 1D CSV table with multiple quantities . . . . .	175
3.4	Example of 1D CSV table with multiple quantities and missing elements . . . .	175
3.5	Example of 1D CSV table with multiple quantities independent to axis $Y$ . . . .	175
3.6	Example of 2D CSV matrix with single quantity . . . . .	176
3.7	Example of 2D CSV matrix with multiple quantities . . . . .	176
3.8	Example of 2D CSV matrix with multiple quantities independent on axis $Y$ . . .	176
3.9	Example of 2D CSV matrix with multiple quantities independent on axis $X$ . .	176
3.10	Example of 2D CSV matrix with multiple quantities independent on both axes $X$ and $Y$ . . . . .	177
3.11	Example of measured impedance of a current shunt. . . . .	183
3.12	Example of gain transfer CSV matrix corresponding to the Table 3.11 measured impedance of a current shunt. . . . .	183
3.13	CSV matrix header for amplitude transfer correction. $f$ : frequency axis [Hz]; $rms$ : input rms value [V] or [A]; $gain$ : relative transfer [V/V] or [A/A]; $u(gain)$ : absolute std. uncertainty of gain. . . . .	183
3.14	Quantity names passed to the QWTB algorithm. . . . .	184
3.15	CSV matrix header for phase transfer correction. $f$ : frequency axis [Hz]; $rms$ : input rms value [V] or [A]; $phi$ : phase shift [rad]; $u(phi)$ : absolute std. uncertainty of phi [rad]. . . . .	184
3.16	Quantity names passed to the QWTB algorithm. . . . .	184
3.17	CSV matrix header for SFDR correction. $f$ : frequency axis [Hz]; $a$ : input amplitude value [V] or [A]; $sfdr$ : SFDR value [dB]. . . . .	185
3.18	Quantity names passed to the QWTB algorithm. . . . .	185
3.19	CSV matrix header for RVD low-side impedance correction. $f$ : frequency axis [Hz]; $Rp$ : Parallel resistance value [ $\Omega$ ]; $Cp$ : Parallel capacitance value [F]; $u(Rp)$ : Abs. std. uncertainty of $Rp$ [ $\Omega$ ]; $u(Cp)$ : Abs. std. uncertainty of $Cp$ [F]. . . . .	185
3.20	Quantity names passed to the QWTB algorithm. . . . .	186
3.21	CSV matrix header for transducer terminal high-side series impedance. $f$ : fre- quency axis [Hz]; $Rs$ : Series resistance [ $\Omega$ ]; $Ls$ : Series inductance [H]; $u(Rs)$ : Abs. std. uncertainty of $Rs$ [ $\Omega$ ]; $u(Ls)$ : Abs. std. uncertainty of $Ls$ [H]. . . . .	186
3.22	Quantity names passed to the QWTB algorithm. . . . .	186
3.23	CSV matrix header for transducer terminal low-side series impedance. $f$ : fre- quency axis [Hz]; $Rs$ : Series resistance [ $\Omega$ ]; $Ls$ : Series inductance [H]; $u(Rs)$ : Abs. std. uncertainty of $Rs$ [ $\Omega$ ]; $u(Ls)$ : Abs. std. uncertainty of $Ls$ [H]. . . . .	187
3.24	Quantity names passed to the QWTB algorithm. . . . .	187
3.25	CSV matrix header for transducer terminals mutual inductance. $f$ : frequency axis [Hz]; $M$ : Mutual inductance [H]; $u(M)$ : Abs. std. uncertainty of $M$ [H]. . .	188
3.26	Quantity names passed to the QWTB algorithm. . . . .	188
3.27	CSV matrix header for transducer terminals shunting admittance. $f$ : frequency axis [Hz]; $Cp$ : Parallel capacitance [F]; $D$ : Loss tangent [-]; $u(Cp)$ : Abs. std. uncertainty of $Cp$ [F]; $u(D)$ : Abs. std. uncertainty of $D$ [-]. . . . .	188
3.28	Quantity names passed to the QWTB algorithm. . . . .	188
3.29	CSV matrix header for transducer buffer output impedance. $f$ : frequency axis [Hz]; $Rs$ : Series resistance [ $\Omega$ ]; $Ls$ : Series inductance [H]; $u(Rs)$ : Abs. std. uncertainty of $Rs$ [ $\Omega$ ]; $u(Ls)$ : Abs. std. uncertainty of $Ls$ [H]. . . . .	189

3.30	Quantity names passed to the QWTB algorithm. . . . .	189
3.31	CSV matrix header for cable series impedance. <i>f</i> : frequency axis [Hz]; <i>Rs</i> : Series resistance [ $\Omega$ ]; <i>Ls</i> : Series inductance [H]; <i>u(Rs)</i> : Abs. std. uncertainty of <i>Rs</i> [ $\Omega$ ]; <i>u(Ls)</i> : Abs. std. uncertainty of <i>Ls</i> [H]. . . . .	189
3.32	Quantity names passed to the QWTB algorithm. . . . .	190
3.33	CSV matrix header for cables shunting admittance. <i>f</i> : frequency axis [Hz]; <i>Cp</i> : Parallel capacitance [F]; <i>D</i> : Loss tangent [-]; <i>u(Cp)</i> : Abs. std. uncertainty of <i>Cp</i> [F]; <i>u(D)</i> : Abs. std. uncertainty of <i>D</i> [-]. . . . .	190
3.34	Quantity names passed to the QWTB algorithm. . . . .	190
3.35	Quantity names passed to the QWTB algorithm. . . . .	196
3.36	CSV matrix header for digitizer gain correction. <i>f</i> : frequency axis [Hz]; <i>a</i> : input amplitude axis [V]; <i>gain</i> : gain correction [V/V]; <i>u(gain)</i> : absolute std. uncertainty of gain [V/V]. . . . .	198
3.37	Quantity names passed to the QWTB algorithm. . . . .	198
3.38	CSV matrix header for digitizer phase correction. <i>f</i> : frequency axis [Hz]; <i>a</i> : input amplitude axis [V]; <i>phi</i> : phase correction [rad]; <i>u(phi)</i> : absolute std. uncertainty of phase [rad]. . . . .	199
3.39	Quantity names passed to the QWTB algorithm. . . . .	199
3.40	Quantity names passed to the QWTB algorithm. . . . .	199
3.41	Quantity names passed to the QWTB algorithm. . . . .	200
3.42	CSV matrix header for digitizer SFDR correction. <i>f</i> : frequency axis [Hz]; <i>a</i> : amplitude axis value [V]; <i>sfdr</i> : SFDR value [dB]. . . . .	201
3.43	Quantity names passed to the QWTB algorithm. . . . .	201
3.44	Quantity names passed to the QWTB algorithm. . . . .	201
3.45	CSV matrix header for input admittance of digitizer channel. <i>f</i> : frequency axis [Hz]; <i>Cp</i> : Parallel capacitance [F]; <i>Gp</i> : Parallel loss conductance [S]; <i>u(Cp)</i> : Abs. std. uncertainty of <i>Cp</i> [F]; <i>u(Gp)</i> : Abs. std. uncertainty of <i>Gp</i> [S]. . . . .	202
3.46	Quantity names passed to the QWTB algorithm. . . . .	202
3.47	List of algorithms in scope of TracePQM project. . . . .	231



# Chapter 1

## Description of the modular measurement setup

This chapter provides a description of the modular power and power quality (PQ) measurement setups for low frequency (LF) and high frequency (HF) measurements. In the LF measurement setup the sampling DMMs 3458A are employed and it can be used for measurements up to 10 kHz. The HF measurement setup is based on high performance digitizers such as the NI 5922 and its measurement bandwidth goes up to 1 MHz.

Proper, interference free connection and digitizer's configuration of the two modular measurements setups are described.

Guidance on selecting suitable system components and the typical achievable uncertainties for appropriate power and PQ measurements is provided to help end users to build a system most suited to their needs.

## 1.1 Methods for proper interference-free connections

This section deals with a review of “best-in-class” metrology grade power and PQ measurement systems based on sampling techniques. It is intended to give a general overview about the most suitable metrology grade experimental setups designed to ensure traceable sampled power and PQ measurements within the SI system of units. Moreover, it can be used as a quick starting point for the design of a new expandable sampling power and PQ measurement system and as a reference guideline to speed up the design of new highly specialized sampling systems.

The requirement for the new modular setup is to ensure both the lowest possible uncertainties and the highest possible bandwidth using commercially available devices. These contradictory requirements cannot be met by means of a single setup. Therefore, the setup developed in TracePQM project comprises of two macro-setups:

- one using the best sampling DMM such as 3458A for LF measurements with low uncertainties and a frequency range limited up to approximately 10 kHz [1]
- and the other setup using high-bandwidth digitizers such as the NI PXI-5922 for wideband measurements up to 1 MHz or special measurements that require many channels [2] [3] [4] [5]

The design of both LF and HF setups described in this section will ensure proper interference free connection of the particular components with special focus on cancelling ground loops and elimination of leakage currents. A guidance on selecting suitable system components (power sources, current shunts voltage dividers) will also be described, taking into account the availability of the components in most NMIs/DIs, commercial calibration laboratories and other end-users.

### 1.1.1 Modular measurement setups

There are two main modes of operation of the developed sampling wattmeter (it will be referred to a DSWM in the following text): (i) To calibrate a source (e.g. power or PQ calibrator); (ii) To calibrate a meter (power analyser, PQ monitor, etc.).

The first case (i) is usually straightforward as it simply requires a direct connection of the DSWM to the source as shown in Figure 1.1. The example shows a single phase measurement, however the same principle applies to measurement of a multiphase power. The source typically has isolated and floating outputs for current and voltage, so it is trivial to connect it to the DSWM even if the digitizers have grounded inputs (e.g NI 5922). Even the grounded source is not a significant problem as the ground loop may be canceled by insertion of the coaxial chokes between the transducers and digitizers (see later chapters for explanation). In any case it is important that both voltage and current (or other phases) are provided with a ground connection. It is not a good practice to leave the circuit floating as it easily leads to common mode voltages. In the example shown in Figure 1.1 the source was grounded on its output terminals.

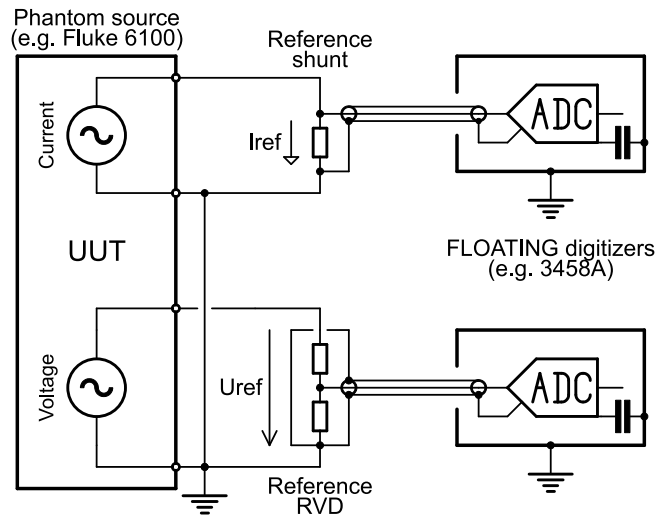


Figure 1.1: Calibration of power source using DSWM setup using floating digitizers.

The latter case (ii) is more challenging as it requires the reference DSWM and wattmeter under test (UUT) to be connected together so that the deviation between the UUT and DSWM readings can be measured. Although the DSWM and UUT may be connected to the source in sequence, it is not a good practice due to the different loading errors of the source. Therefore it is necessary to connect the voltage channels of UUT and DSWM in parallel and current inputs in series. The voltage connection is not a problem since the common mode voltage is insignificant. However, the series connection of current channels is problematic as either the UUT or DSWM current input must be placed on the high-side (floating), and a significant common mode voltage  $U_{cm}$  appears at the input of the current transducer. This may lead to a leakage current  $I_g$  as shown in the Figure 1.2. This unwanted current will flow even in floating digitizers such as the 3458A due to the capacitive coupling between guard and ground of the digitizer. It is usually not a concern for low frequencies, such as industrial 50 Hz, however it may affect measurements at higher frequencies such as harmonic components, with the main effect being on the phase measurements.

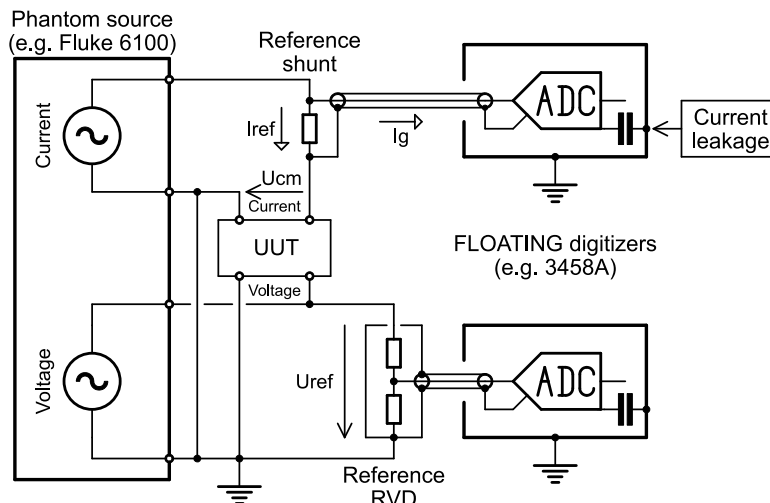


Figure 1.2: Calibration of power meter UUT source using DSWM setup using floating digitizers.



### 1.1.1.1 Low frequency (LF) measurement setups

Figure 1.3 shows an example of the interference free connection of the modular setup in the low frequency domain for the measurement of power and PQ quantities using sampling multimeters DMM 3458A. Coaxial chokes may be placed between the transducer outputs and the digitizers but, at these low frequencies they may not have a noticeable effect.

It is important to note that this connection scheme has two problems as noted earlier. Firstly, the leakage current  $I_g$  via the Low-to-Ground terminal of 3458A and secondly, the loading of the transducers by the finite input impedance of the the 3458A. The algorithms used by the open DSWM SW tools developed in TracePQM project (TWM/TPQA) are capable of correcting the loading errors. However, they are not capable of correcting the errors caused by the leakage current since the common mode  $U_{cm}$  voltage at the current shunt is unknown.

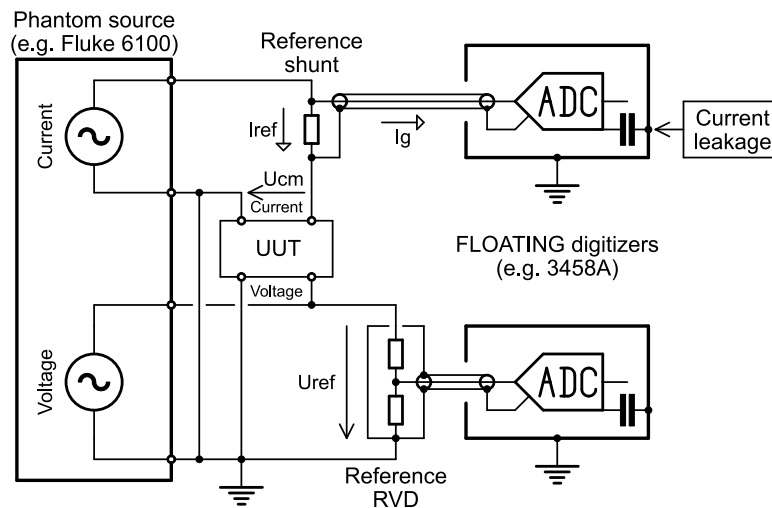


Figure 1.3: Calibration of power meter UUT source using DSWM setup using floating digitizers 3458A.

The effect of the leakage current  $I_g$  can be evaluated experimentally by inserting an additional known capacitance between the LO terminal of the 3458A and Ground and observing the change in the measured amplitude and phase. From a known value of the actual Low-to-Ground capacitance it is possible to deduce the unloaded condition or at least estimate its uncertainty contribution.

Another approach to reduce the effect of the leakage is to swap the UUT and DSWM current input, so DSWM is the low-side shunt. However, that just moves the problem to the UUT, which will be affected by the same effect.

Possible workaround is to change the polarity of the DSWM current shunt as shown in Figure 1.4. The effect is that the leakage current now flows from the high output of the source, so the current via the DSWM and UUT current input should remain equal. However, the remaining problem is the current  $I_g$  flowing via the shield of the coaxial cable between DSWM shunt and the digitizer, as it leads to the unbalance of current in the cable and thus to an error voltage induced in the live conductor. This may be improved by placing a coaxial choke to the cable. The situation

may be also significantly improved by using the 3458A external guard, i.e. by connecting it to the high output terminal of the source. This will reduce the apparent capacitance of the 3458A shunt input. The disadvantage of this workaround is that the DSWM SW tools will indicate current phase inverted by  $180^\circ$ .

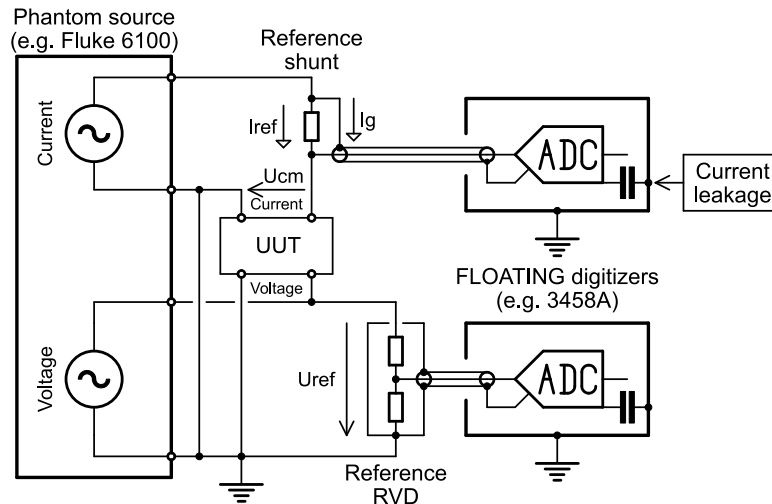


Figure 1.4: Calibration of power meter UUT source using DSWM setup using floating digitizers 3458A - workaround reducing the leakage current  $I_g$  effect.

The last possibility, although very unusual, would be to use a differential connection to the current shunt as described later for the HF setup. The TWM tool is capable of controlling the differential mode even with 3458A multimeters.

#### 1.1.1.2 High frequency (HF - wideband) measurement setups

The HF setup is more challenging. Although it is in some cases still possible to measure in the single ended connection mode as for the LF setup (e.g. direct calibration of source shown in Figure 1.1), it is not recommended, at least for the current shunt input. The main reason is the impedance of the conductors, even the grounding ones, increases proportionally with frequency. So the grounded part of the circuit is at nonzero potential, which leads to a common mode voltages at the inputs of the digitizers. The problem can be reduced by using coaxial chokes, which in general works better at higher frequencies. The chokes can be used if the common mode is just a small fraction of the measured voltage. Such a solution cannot be used with floating digitizers, e.g. setup in Figure 1.2.

For this reason a differential connection to the digitizer(s) as shown schematically in Figure 1.5 is introduced. The voltage channel(s) connection may remain single-ended, as shown in Figure 1.6, because TracePQM algorithms can handle even the mixed single-ended and differential modes.

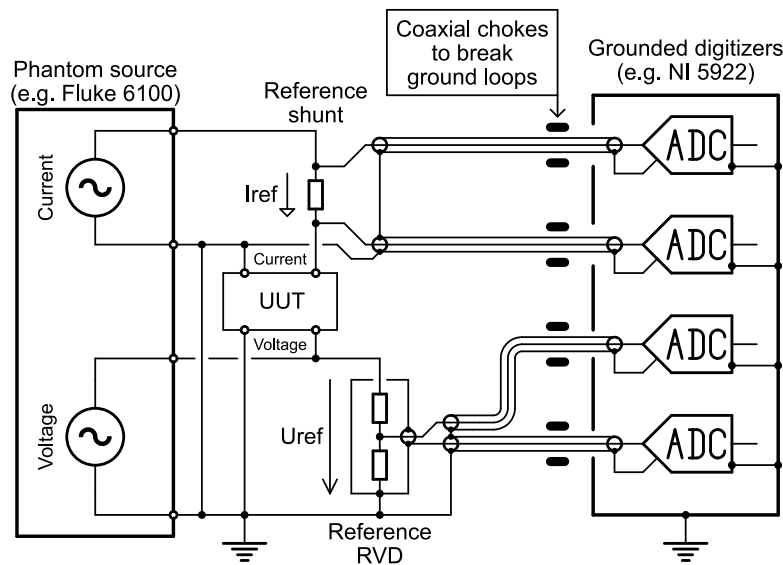


Figure 1.5: Calibration of power meter UUT source using DSWM setup using grounded digitizers NI 5922 in full differential mode.

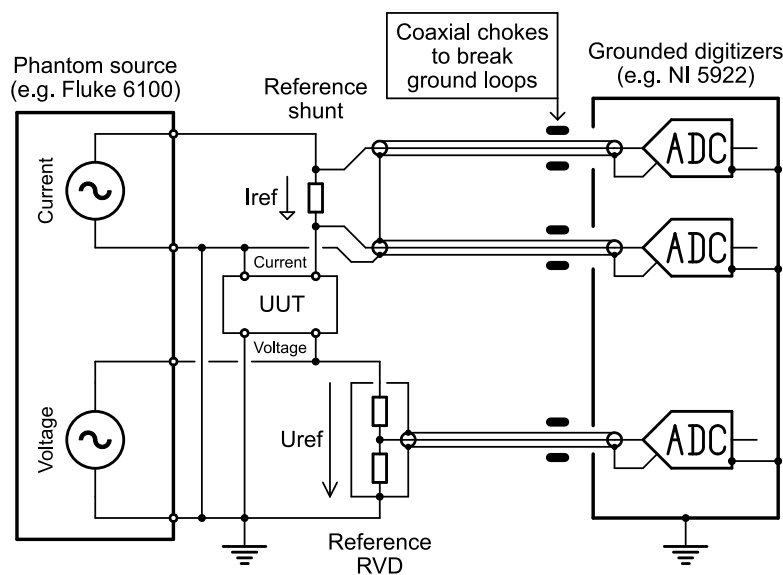


Figure 1.6: Calibration of power meter UUT source using DSWM setup using grounded digitizers NI 5922 in mixed single ended and differential mode.

The schematic diagrams show the connection of wires to the source as bare wires. However, especially for high frequencies it is essential to maintain balanced currents in the coaxial cables in order to reduce magnetic interference. Therefore a more suitable connection is shown in Figure 1.7.

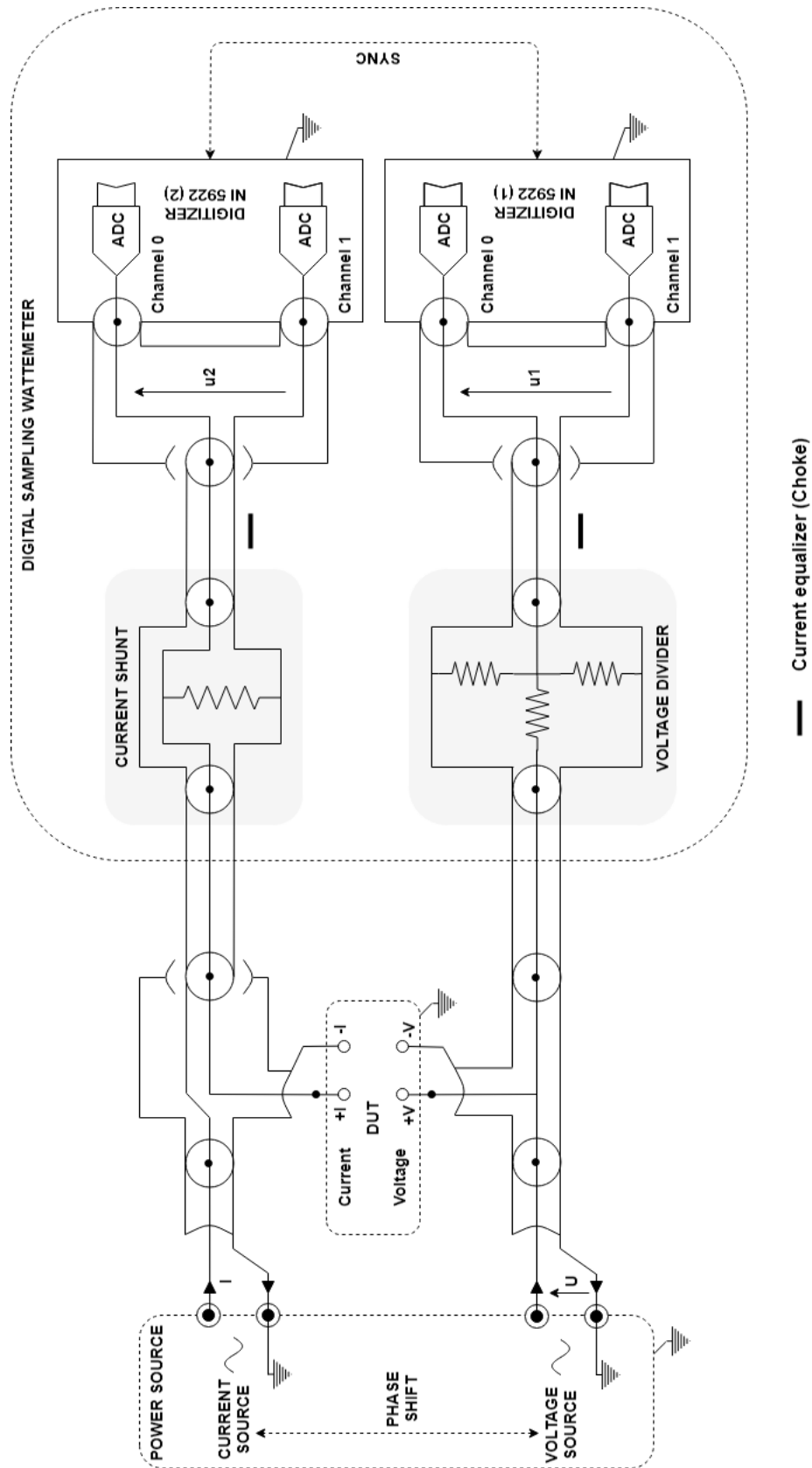


Figure 1.7: HF modular measurement setup electric block diagram.

## 1.1.2 Components of modular measurement setups

### 1.1.2.1 Cables and Wiring

An important aspect of the proper interference free connection is the proper wiring of the components. At low frequencies it is a common practice to use ordinary cables with banana plugs or screwing terminals. In such case it is a good practice to twist the high and low (forward and return) cables tightly as shown in Figure 1.8. This has a positive effect to both voltage and current loops. For currents it is essential to eliminate magnetic radiation. For voltage circuit it is important because it minimizes the area of the loop and this minimizes the induced voltage from magnetic fields. However it is not practical to use separate conductor or even twisted pair conductors to connect the transducers' outputs to the digitizer's inputs. Such connections are still somewhat sensitive to external fields and furthermore the capacitance between the cables of the pair is unpredictable and unstable. Thus it would lead to large phase angle errors due to variable loading effect of the transducers.

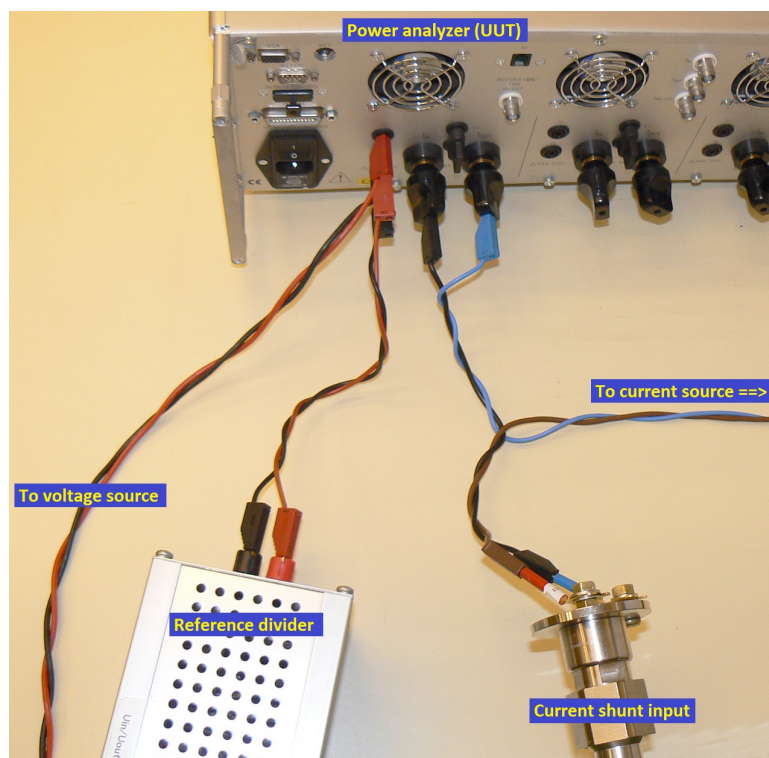


Figure 1.8: Connection of power source, power analyzer (UUT) and reference sampling wattmeter (DSWM) transducers using twisted wires.

As shown in previous section, it is recommended to use coaxial connections from the transducers to the digitizers. Precision measurements of AC signals typically requires use of coaxial cables. There are two advantages of using a coaxial cable. First, its shield provides an electrostatic shielding, so it reduces capacitive coupling from external potentials to the live conductor. Second, if the currents via the live and shield conductors are balanced (equal), the magnetic fields are

eliminated similarly as for twisted pairs. The current equalization can be enforced by use of coaxial chokes.

### 1.1.2.2 Current equalization - The coaxial chokes

If the current between the live and shield conductors are balanced (equal), the magnetic fields are eliminated. This may not happen automatically. If multiple places in the setup's coaxial network are grounded, the problem of ground loops will appear. Note that for the higher frequencies it is essential to take into account even grounding via large capacitances, such as Guard-to-Ground capacitance between the instrument shields. E.g. 3458A has capacitance in order of nanofarads between the shields. In such case current equalizers (coaxial chokes) are inserted to break the loops. The choke has no effect on the useful balanced signal in the cable, because the fields from forward and return current are canceled, but it acts like an AC resistance to any ground loop currents. Example of such coil realization is shown in (Figure 1.9).



Figure 1.9: Current equalizer (Choke).

If a coaxial circuit has a current equalizer in each of its independent ground loops, it is insensitive to external electromagnetic fields. In addition, the currents flowing in the different branches of the circuit do not generate fields and the different loops do not interact with each other.

This element (choke) is made by winding a coaxial cable around a magnetic core with high permeability. This assembly forms a current transformer of ratio 1:1, the core of the cable being the primary winding with high impedance, its shield the secondary winding with low impedance. For frequencies around 50 Hz, the inductance of the choke should be at of the order of 50 mH, however higher inductance, such as 200 mH is desirable. The reactance of the coil is defined as:

$$X_L = j \cdot \omega L, \quad (1.1)$$

where  $\omega$  is angular frequency in rad/s. So for inductance 100 mH and frequency 50 Hz the AC resistance is  $X_L \approx 31 \Omega$ . Therefore, if we have a situation as in Figure 1.6 with the source and digitizer grounded, and the voltage difference between the ends of the coaxial cable shields is just 1 mV due to finite impedance of the grounding lugs, the residual unwanted current via the chokes will still be 31  $\mu$ A. Thus the choke itself may not solve the problem. It will only work

together with a technique that brings the potentials at the sides of the coaxial cable to as close as possible, e.g. in this case grounding to the common point with thick grounding leads.

Although the equalization can be improved by larger inductances, the trade off is of course higher length of the cables and thus higher shunting capacitance, which leads to higher loading of the transducers. TracePQM algorithms can perform loading correction, but it will introduce additional uncertainty.

Typical cores selected for LF operation are NANOPERM or ULTRAPERM strip wound cores having relative permeability of over 50000. Their permeability drops with frequency, however it is not a problem, as the inductance at HF can be lower to achieve the same reactance. Thus it is possible to use the same choke for wider range of frequencies.

The problem of balancing currents in coaxial networks is a topic for a standalone guide itself, so it will not be described in further detail here. Fortunately, the topic is excellently described in a book [6]. Potential users of coaxial setups, especially those for measurements at higher frequencies or complex topologies are strongly advised to consult this book.

### 1.1.2.3 Power source

The power calibrator is a so called phantom power supply which delivers a sinusoidal voltage and a sinusoidal current with a phase shift at an appropriate frequency. The voltage and current sources in a phantom power generator are typically electrically isolated from each other to make the connection to the calibrated instruments easier, although the allowable common mode voltage is very limited for the vast majority of calibrators.

Below is a brief description of commonly used power calibrator in most of NMI:

- The power calibrator Fluke 6100A/B (Figure 1.10) or its newer version 6105A is a dual-channel voltage source associated with voltage amplifiers and transconductance amplifiers which delivers a maximum voltage of 1008 V and a maximum current of 20 A and 80 A with its extended version for low frequency measurement setup. This power calibrator uses digital synthesis method and simulates harmonic distortions, under-voltages, transient voltages and flickers. It is also possible to connect up to three additional channel units to the calibrator in order to generate three phase and neutral signals. The additional units can be also connected together to sum the current from particular channels.





Figure 1.10: Power source - Fluke 6100A.

- For high frequency measurement setup, two multifunction calibrators Fluke 5700A/5720A are often used, associated in certain range of voltage, current or frequency with voltage amplifier and/or transconductance amplifier. The phase between the current and voltage signals has to be controlled externally by multichannel arbitrary waveform generator(s) such as NI PXI-5421/5441 which provide synchronized sine waves to the phase lock inputs of both AC calibrators (Figures 1.11 and 1.12).



Figure 1.11: Power source - Fluke 5720A (Left) & AWG - NI PXI-5421 (Right).

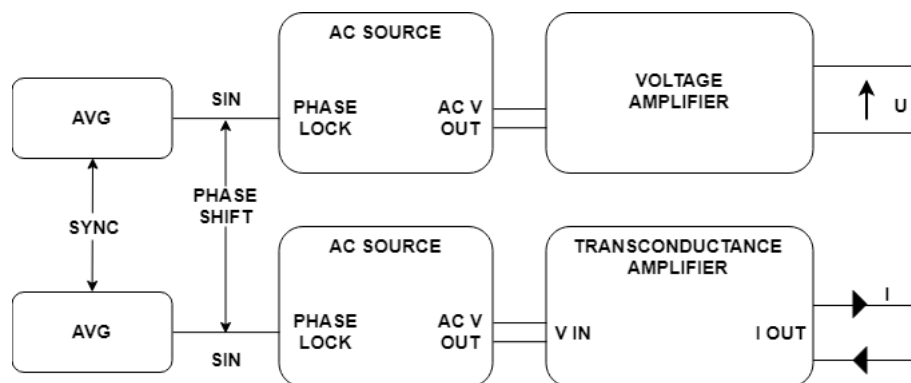


Figure 1.12: HF power source schematic.



Advantage is very stable amplitude, but the disadvantage is the analogue phase locking produces limited phase stability which may be a problem for some operations.

- For voltage measurement, an appropriate voltage amplifier can be added optionally to amplify the voltage from the voltage source or more specifically to be used as an isolation transformer in order to avoid any direct current flow which could cause saturation of the magnetic cores in case of an inductive voltage divider present in the DSWM setup.

There are numerous commercially available voltage amplifiers for LF signals. However, when measuring PQ or HF power, it is often desirable to have a wideband amplifier, preferably with DC coupling, so a complex waveform shapes can be amplified correctly. One example of such specific amplifier is obsolete, yet still very popular amplifier Fluke 5205A with vacuum tube power stage. It has bandwidth over 100 kHz at rms voltage 1000 V and can deliver currents over 100 mA. The amplifier was designed to operate together with a Fluke calibrators, however it can be used as a standalone unit as well together with modern arbitrary waveform generators.

- For current measurements, either the current source of the Fluke 6100A/B or the Fluke 5700A/5720A in AC voltage mode associated with a transconductance amplifiers (such as Clarke Hess 8100 (Figure 1.13) which can generate current up to 100 A depending on the compliance voltage) are used. The Clarke Hess 8100 has following current ranges: 2 mA, 20 mA, 0.2 A, 2 A, 20 A and 100 A; Its output current is directly proportional to the input voltage over the frequency range from DC to 100 kHz. It is also possible to operate it beyond specified bandwidth up to 1 MHz for low current ranges (typically up to 2 A).



Figure 1.13: Transconductance amplifier - Clarke Hess 8100.

#### 1.1.2.4 Voltage divider

In LF measurement setups based on the sampling DMMs 3458A, both multimeters are typically used in the DC voltage sampling mode. In the absence of the voltage divider, the measurement

of the voltage can be done on the higher ranges such as 1000 V, while the measurement of the current, by means of a shunt, is made typically on the 1 V range. However, using voltage ranges above 10 V is not recommended as the stability of the gain and phase is limited [7].

The analogue bandwidth is 150 kHz for 1 V and 10 V ranges and 30 kHz for 100 V and 1000 V ranges. Experimental results and theoretical calculations show that the main source of error on measurements is related to the use of the two DMM 3458A on ranges of different bandwidths [7].

To overcome this issue, in a power measurement system it is essential to introduce a voltage divider into the voltage circuit with high amplitude accuracy, low phase angle errors and low distortion, especially under non-sinusoidal conditions, in order to reduce the nominal voltage to a level measureable on 1 V or 10 V ranges of the DMMs.

Note: The NI PXI-5922 digitizer has only two ranges, 2 Vpp and 10 Vpp. This implies the necessity to use a voltage divider for the HF setup because voltage signals to analyze can be around hundreds of volts.

Several types of voltage dividers exist. It necessary to choose the suitable option among them in relation with the measurement to be done:

- **Inductive Voltage Divider (IVD):** These inductive dividers, widely used in low frequency applications have the advantage of an intrinsic accuracy defined by their turns ratio. On the other hand, they do not allow DC voltage components as it leads to saturation of the magnetic cores and thus fast drop in the permeability. To avoid saturation of the magnetic cores it is necessary to check the voltage source is not supplying DC offset or to use an isolation transformer between the source and divider.

An example of a high performance IVD is the IVD developed and manufactured by the NMIA (Figure 1.14). This is a separately excited 3-stage inductive voltage divider with a maximum input RMS voltage of 1100 V or 20 V/Hz covering the frequency range 40 Hz to 1 kHz. Its typical ratio errors at power frequencies are specified as 0.001 ppm of input (in phase) and 0.005 ppm of input for (quadrature). [8].



Figure 1.14: NMIA Inductive Voltage Divider (IVD) [8]

- Resistive Voltage Divider (RVD):** Resistive dividers play an important role in high frequency applications. RISE has developed a set of dividers [9] (Figure 1.15) covering a broad range of input voltages from 50 mV to 1000 V, at frequency from 16 Hz up to 100 kHz and beyond. They are built with Vishay S102K precision foil resistors which have an extremely low temperature coefficients. The divider construction keeps the AC-DC transfer difference within 20  $\mu\text{V}/\text{V}$  and the phase error within 8  $\mu\text{rad}$  for frequencies up to 65 Hz if the dividers are loaded by an expected capacitance of the DMM 3458A and fixed cable. Similar design dividers are developed and produced also at other NMIs.

It is important to note these dividers are generally usable up to at least 100 kHz without buffers at the output. However, several problems arise if they are used at higher frequencies. First, especially the real component of input impedance of the digitizer is frequency dependent, which causes variable loading errors with frequency (ac-dc transfer changes). Second, the cable capacitance is unstable and will vary with any flexing of the cable leading to changes in the phase angle. E.g. for a typical divider with low-side resistance of 200  $\Omega$  the change of capacitance by 1 pF at 1 MHz leads to a change of phase angle by roughly  $\Delta\phi \approx \frac{1}{\omega \cdot R \cdot C} = 1.25 \text{ mrad}$ . Therefore the high frequency operation usually requires a buffer to be inserted between the divider and digitizer.

The list of custom built dividers and other components for AC applications that can be purchased from NMIs is available on demand from the chair of EURAMET TC group SC & LF or Power & Energy.



Figure 1.15: RISE Resistive Voltage Divider (RVD).

#### 1.1.2.5 Current shunt

At NMIs current shunts of special designs are used for high accuracy current measurements. These shunts convert a measured current to a voltage convenient for the input range of the meter. In electrical metrology applications, the frequency dependence of the current shunt's impedance is essentially characterized by the following two parameters:

- **AC/DC transfer difference ( $\mu\Omega/\Omega$ )**

$$\delta = \frac{|Z_{\text{shunt}}| - R_{\text{DC}}}{R_{\text{DC}}} \quad (1.2)$$

- **Phase angle (rad)**

$$\phi = \arctan\left(\frac{\Re(Z_{\text{shunt}})}{\Im(Z_{\text{shunt}})}\right) \quad (1.3)$$

where:

$Z_{\text{shunt}}$	- Shunt's impedance
$ Z_{\text{shunt}} $	- modulus of the shunt's impedance
$R_{\text{DC}}$	- DC resistance of the shunt
$\Re(Z_{\text{shunt}})$	- Real part of $Z_{\text{shunt}}$
$\Im(Z_{\text{shunt}})$	- Imaginary part of $Z_{\text{shunt}}$

There are several types of high accuracy current shunts. The following table summarizes specifications of the two common types of current shunts used in power and power quality measurements systems:

- **Current shunt based on a “cage” structure (Figure 1.16):**
  - Developed by: RISE (former SP)

- Current range: [100 mA; 100 A]
- Resistors used in these shunts are placed in parallel in a squirrel cage like structure. The even number of fins as well as their positions relative to the traverse axis of the structure implies a quasi-coaxiality of the geometry which limits the electromagnetic disturbances around the shunt. The value of the shunt resistor is defined between four terminals, two terminals to inject the electric current and two terminals to measure the voltage.
- The example of values measured for a 10 A RISE shunt using “AVNA” [10] calibration method (Table 1.1):

Frequency	AC/DC transfer difference ( $\mu\Omega/\Omega$ )	Phase Angle (mrad)
53 Hz	$9.80 \cdot 10^{-4}$	$8.70 \cdot 10^{-4}$
1 kHz	$1.87 \cdot 10^{-2}$	$1.64 \cdot 10^{-2}$
100 kHz	3.77	1.64
1 MHz	211	16.4

Table 1.1: RISE 10 A Shunt’s AC/DC transfer difference & Phase angle.



Figure 1.16: RISE current shunts.

- **Current shunt based on “MELF” resistors (Figure 1.17):**

- Developed by: JV
- Current range: [30 mA; 20 A]
- This type of shunt is based on surface-mounted resistors in straight lines called MELF. These resistors are cylindrical and fit well in holes of appropriate diameter made in the printed circuit boards (PCB). To reduce the shunt inductance a large number of resistors are paralleled. To reduce the parasitic capacitance of the shunt, polytetrafluoroethylene (PTFE) has been used as a dielectric for the PCB.
- Typical values measured for 10 A JV shunt using “AVNA” [10] calibration method (Table 1.2):

Frequency	AC/DC transfer difference ( $\mu\Omega/\Omega$ )	Phase Angle (mrad)
53 Hz	$8.29 \cdot 10^{-3}$	$-2.78 \cdot 10^{-4}$
1 kHz	$-1.56 \cdot 10^{-1}$	$-5.25 \cdot 10^{-3}$
100 kHz	-15.7	-0.53
1 MHz	-160	-5.25

Table 1.2: JV 10 A Shunt's AC/DC transfer difference &amp; Phase angle.



Figure 1.17: JV current shunts.

- “Broadband” current shunt (Figure 1.18):

- Developed by: LNE
- Current range: 10 A (extension of the range ongoing)
- This current shunt [11] [12] is composed of a resistive disk and of a coaxial line made up of an inner conductor and an outer conductor (shielding). Two N-Type connectors are placed in the same axis as the inner conductor of the coaxial line. The electrical resistance of the shunt is obtained by the use of a solid resistive circular disk with a uniform thickness and drilled in its center. The inner conductor passes through the resistive disk which is connected electrically to the inner and outer conductors. Due to the radial distribution of the current between its inner and outer radii, the resistive disk does not exhibit any inductive effects, thus improving its AC performance. The thickness of the resistive disk has been selected in order to make negligible the skin effect on the resistance to a frequency of 1 MHz. The impedance of the resistive disk can be consequently considered equal to its DC resistance value.
- Typical values measured for 10 A LNE shunt using “AVNA” [10] calibration method (Table 1.3):



Frequency	AC/DC transfer difference ( $\mu\Omega/\Omega$ )	Phase Angle (mrad)
53 Hz	$6.94 \cdot 10^{-8}$	$-6.25 \cdot 10^{-7}$
1 kHz	$-2.12 \cdot 10^{-5}$	$-1.18 \cdot 10^{-5}$
100 kHz	0.15	$-1.19 \cdot 10^{-3}$
1 MHz	14.99	-0.012

Table 1.3: LNE 10 A Shunt's AC/DC transfer difference &amp; Phase angle.

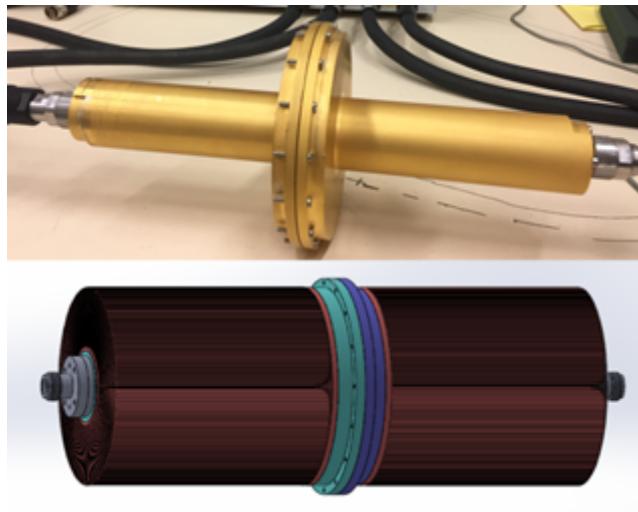


Figure 1.18: LNE 10 A current shunt.

#### 1.1.2.6 Current transformers

Higher currents than 100 A are typically measured using current transformers. There are numerous transformers developed at NMIs and also commercially available ones. However, this topic is more related to the high voltage and high current research groups than TracePQM project, so these will not be discussed here.

One exception worthy of mentioning is an automatic current ranging transformer developed at NMIA [13] capable of providing ranges from 125 mA up to 200 A for a frequency range 40 Hz to 1 kHz. The transformer uses a single shunt resistor as a reference, so its calibration is significantly easier than that of a large set of coaxial current shunts. An additional advantage is the ratio of the transformer remains stable.

#### 1.1.2.7 DMM & Digitizers

A core of a sampling measurement setup is an analog-to-digital converter (ADC). In TracePQM project two types of ADC were employed to meet the requirements stated at the beginning of the project: the DMM 3458A in sampling mode for LF measurement and wideband digitizers NI PXI-5922 for HF applications. Details about DMM 3458A and digitizers NI PXI-5922, especially about their hardware configuration, will be described in section 1.2.

## 1.2 Hardware configuration of the digitizers

### 1.2.1 Low frequency domain (DMM 3458A)

The low frequency (LF) measurement setup used to calculate the power and the power quality (PQ) quantities includes two 3458A digital multimeters (DMMs). The first 3458A DMM is used to sample the voltage  $U(t)$  scaled through a voltage divider and the second DMM 3458A is used to sample the current  $I(t)$  scaled through a current shunt. The measurement consists of sampling simultaneously these signals. For this purpose an external trigger provides a simultaneous trigger signal for both 3458As.



Figure 1.19: DMM 3458A front panel [14].

The 3458A has proven for more than 20 years to have a remarkable capacity for measuring voltage, current and resistance based on its very stable internal voltage reference standard and resistors. In addition, the 3458A has a large number of programmable parameters, which allows it to be adapted to the desired configuration. Despite the evolution of multimeters over the last ten years the digital multimeter 3458A remains the instrument of choice for precision sampling applications. Considering the sampling rate of the DMM 3458A, measurements with low uncertainties is only appropriate for a limited frequency range up to approximately 10 kHz.

The following sections will identify the essential characteristics of the DMM 3458A [14] needed to understand how the digital sampling multimeter concept is used in the low frequency measurement setup. The book “Sampling with 3458A - Understanding, Programming, Sampling and Signal Processing”, authored by Rado Lapuh [7] covers the entire sampling capabilities of the 3458A that can be used in various practical applications.

#### 1.2.1.1 Sampling mode

The DMM 3458A has three sampling modes for DC voltage measurements:

- **DC voltage (DCV):** DCV mode is a basic DC voltage measurement mode. In this mode the 3458A achieves its state-of-the-art accuracy when measuring DC voltage. The DCV bandwidth of 150 kHz limits its inherent accuracy to few hundred Hertz. Operation at higher frequencies is possible with reduced accuracy. The maximum sampling frequency is



100 kSa/s, at which the resolution is limited to 15 bits. No compromises are made when this mode is used, except for the trade off between sampling rate and consequently aperture time and resolution, which are defined by its integrating analogue to digital converter (IADC). The aperture time is selectable from 500 ns to 1 s. The DCV mode ensures high input parallel resistance of the order of gigaohms.

- **Direct sampling (DSDC):** DSDC mode uses a sample and hold circuit (S/H) with fixed aperture of 2 ns to freeze a signal at a sampling instant, which is then digitized by an integrating analogue to digital converter (IADC). The short aperture ensures high analogue bandwidth, despite the sampling rate being limited to only 50 kSa/s in this mode. On the other hand the mode of operation exhibits higher noise and lower resolution even for low frequency signals. The input impedance in this mode is lower than for DCV. Parallel input capacitance is lower than for DCV, but parallel input resistance is only 1 M $\Omega$ , so the loading of transducers is higher.
- **Sub-Sampling (SSDC):** SSDC mode uses the same S/H circuit as the DSDC mode. It uses precision S/H trigger interpolator to realize equivalent time sampling with effective sampling rate up to 100 MSa/s, so the usable bandwidth extends to frequencies up to 50 MHz. However, the equivalent time sampling in principle requires stable periodic signal with no interharmonics.

The Table 1.4 shows significant characteristics of these sampling modes.

Sampling mode	Maximum sampling frequency	Bandwidth	Best uncertainty	Repetitive signal required
DCV	100 kHz	30 - 150 kHz	0.00005 - 0.01 %	No
DSDC	50 kHz	12 MHz	0.02 %	No
SSDC	100 MHz	12 MHz	0.02 %	Yes

Table 1.4: Characteristics of sampling modes [14].

### 1.2.1.2 Input impedance and ranging

In addition to the sampling mode, a fixed input voltage range should be specified in order to disable the auto-range functionality which would slow down the sampling speed considerably.

Table 1.5 shows the full scale reading, maximum resolution and input parallel resistance depending on selected input range. The input parallel capacitance is typically 270 pF in the DCV mode.

Input range	Full scale	Maximum resolution	Input impedance
100 mV	120 mV	10 nV	$> 10 \text{ G}\Omega$
1 V	1.2 V	10 nV	$> 10 \text{ G}\Omega$
10 V	12 V	100 nV	$> 10 \text{ G}\Omega$
100 V	120 V	1 $\mu\text{V}$	10 M $\Omega$
1000 V	1050 V	10 $\mu\text{V}$	10 M $\Omega$

Table 1.5: Characteristics depending on input range [14].

### 1.2.1.3 Guarding

The Guard terminal was introduced to precision digital multimeters with the main aim of reducing the effect of the power line related noise on measurement. A guarded DMM 3458A employs a special sheet-metal structure between its analogue circuitry and the instrument's chassis ground which is connected to the Guard terminal.

The Guard connection is primarily implemented to help minimize the influence of common mode signals in the floating voltage measurements. When used correctly, it can increase the DMM rejection of AC common mode signals (CMRR).

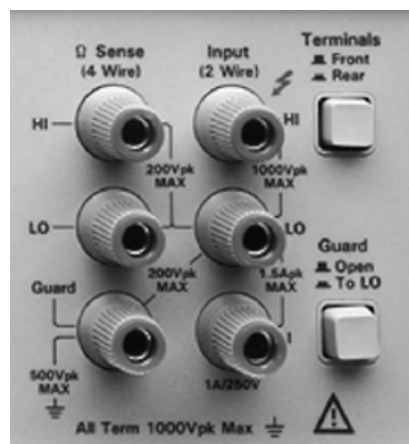


Figure 1.20: The 3458A's front panel input terminals, including Guard terminal and the Guard switch [14].

Figure 1.21 and Figure 1.22 show a simplified internal 3458A circuit with respectively Guard Open and Guard To LO with:

- IADC: Integrating analog to digital converter
- C1: Capacitance between the Internal analogue circuitry and the guard
- C2: Capacitance between the guard and the DMM's chassis

On Figure 1.21 with no connection to the Guard, when common mode voltage  $V_{\text{cm}}$  is present, it forces the common mode current  $I_{\text{cm}}$  to flow through  $R_{\text{LO}}$ . The voltage drop on the  $R_{\text{LO}}$  will

add to the measured voltage  $V_i$  and the 3458A will not be able to differentiate between the two, causing errors.

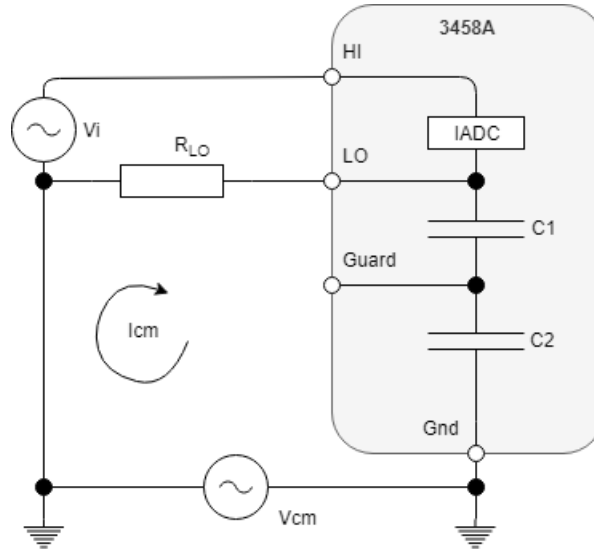


Figure 1.21: DMM 3458A Guard terminal - Open [7].

On Figure 1.22 with the Guard connected to the low terminal on the source, the common mode voltage  $V_{cm}$  sees the low impedance path through the Guard terminal back to the instrument earth and the common mode current  $I_{cm}$  will flow mostly through the lower loop as indicated. As the common mode current  $I_{cm}$  is routed away from the leads connected to the measuring terminals, it does not cause additional error.

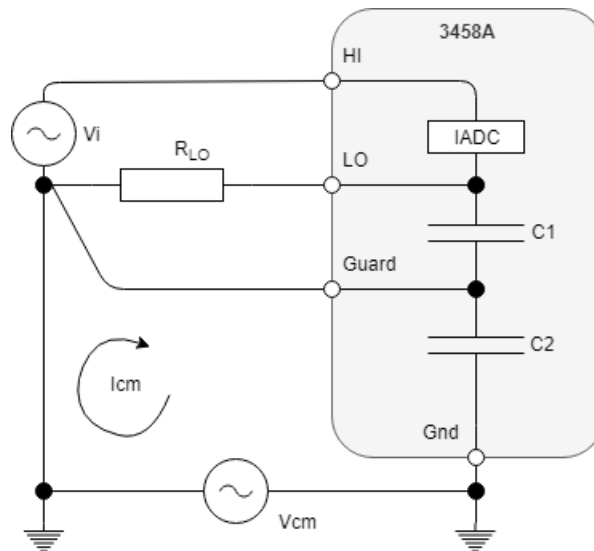


Figure 1.22: DMM 3458A Guard terminal to LO [7].

The 3458A, like with any other DMM, responds to input voltages in two ways:

- Normal mode voltage: the voltage is measured between the HI and LO input terminals.

- Common mode voltage: The voltage is applied between the GND and both HI and LO input terminals simultaneously.

Note that the 3458A is and should always be referenced to the ground potential through its mains power cable connection. It is always important to know the 3458A's common mode rejection ratio (CMRR) where  $V_0$  is the measured voltage caused by the applied common mode voltage  $V_{cm}$  and CMRR is expressed in dB:

$$CMRR = 20\log\left(\frac{V_0}{V_{cm}}\right) \quad (1.4)$$

The CMRR highly depends on the actual measurement setup and the user should ensure that the optimum connection to the guard is made so as to reduce the effect of common mode voltages as far as possible. Further guidance on this matter may be found in HP Application Note 123 Floating Measurements and Guarding. It is recommended to measure the CMRR between the following three configurations:

1. Guard switch in the To LO position and no guard connection
2. Guard switch left to open and no guard connection
3. Guard switch left to open and guard connected

And then choose the best solution which is the configuration with the highest CMRR.

The solution to correctly connecting the Guard terminal is not always so straightforward and the Guard switch should be used with care. For the low frequency (LF) setups, when common mode voltage is negligible, the differences between internal connection, external connection to the source and no connection will be minimal. When using setup with floating shunt or at higher frequencies, such as in Figure 1.2, the general rule is to keep voltage difference between LO terminal and Guard as low as possible and at the same time to divert the capacitive current to the Guard terminal outside from the LO conductor/terminal, so no voltage drops are induced to the LO conductor.

Also note the Guard switch changes input impedance. Especially capacitance by at least few picofarads. This changes the loading effect to the transducer, mainly the phase angle error.

#### 1.2.1.4 Synchronization

When designing the setup with 3458A multimeters, one must also decide the method of synchronization between multiple voltage and current channels. As is noted in the section 3.1, the TWM/TPQA tools allow several modes of synchronization schemes. As most of the algorithms were designed for non-coherent sampling, it is not necessary to phase lock the DMMs to the source. Thus the most basic connection uses Master-Slave topology, where Master's sample clock is generated by its own internal timer. The wiring is shown in Figure 1.23. The eventual additional channel Slave 2 and others should be all connected by their EXT TRIG inputs to the Master's EXT OUT. Daisy chaining of each following Slave to the previous one is not allowed for the TWM/TPQA tools as there is a problem of fake EXT OUT caused by

the auto-zero feature. The TWM/TPQA tools were designed to compensate only for a given synchronization topology.

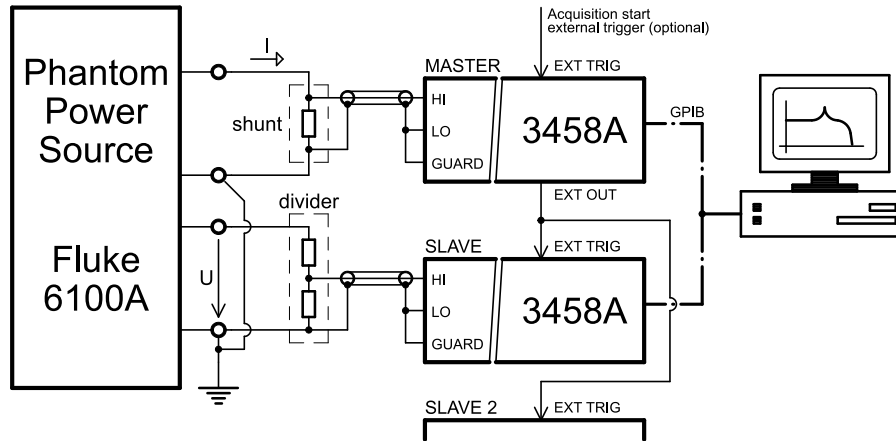


Figure 1.23: DMM 3458A synchronization in Master-Slave topology with Master generating sample clock.

Another option is to generate a sample clock signal for the Master from an external arbitrary waveform generator (AWG) as shown in Figure 1.24. This has the advantage that the AWG can be also phase locked to the 10 MHz same as the source, so the sampling can be coherent. The user also has another possibility to connect all DMMs to the AWG directly as shown in Figure 1.25, which has to be configured in the TWM/TPQA tool (see section 3.1.4.2).

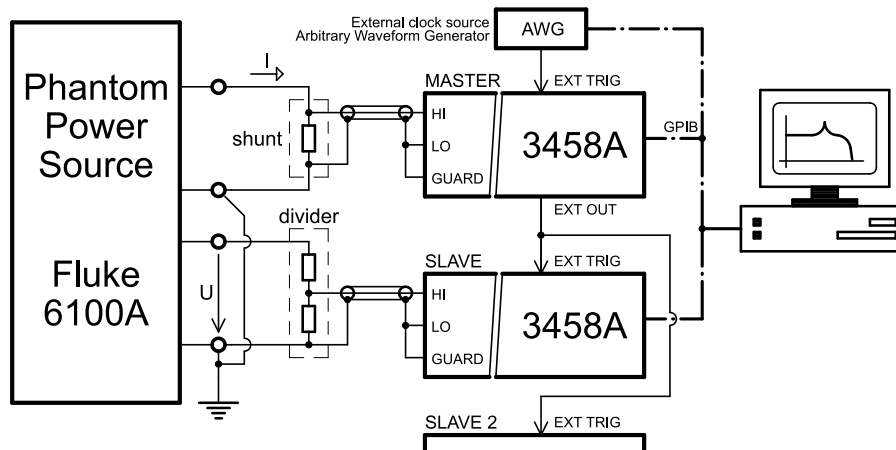


Figure 1.24: DMM 3458A synchronization in Master-Slave topology with sample clock generated by the external AWG.

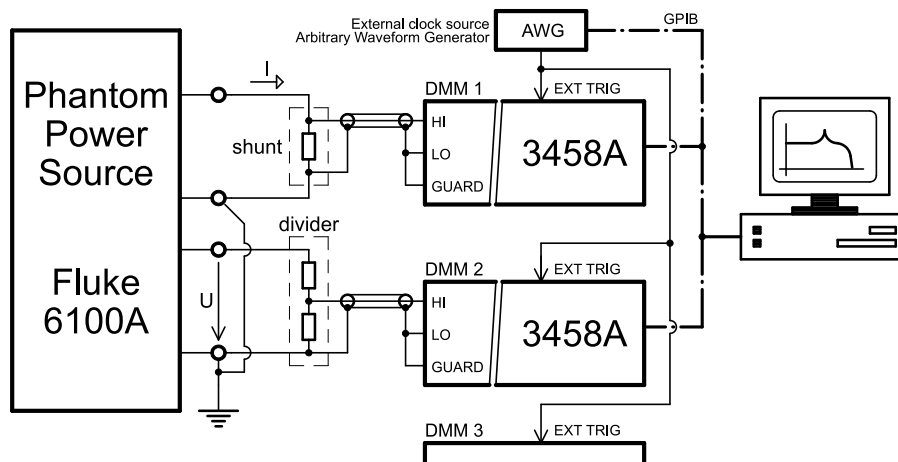


Figure 1.25: DMM 3458A synchronization in topology with sample clock generated by the external AWG for all DMMs at once.

Yet another option is to use the sample clock pulses exported by the source itself. This is often used for the Fluke 6100 series calibrator which can output  $N$  multiples of the fundamental frequency to its Sample Ref Output. This output can be linked directly to the Master DMM's EXT TRIG as shown in Figure 1.26, or to all DMMs as in Figure 1.25. The only disadvantage is that the Fluke 6100A by itself generates too high a sampling frequency, which forces the user to use short aperture on the DMMs. That leads to too much noise. So it is helpful to use an optional clock divider  $\div M$  set to e.g.  $\div 5$  or  $\div 7$  to reduce the sampling clock, so the aperture can be extended. Note the prime number values of  $\div M$  are advised so that the aliased harmonics will not overlay the lower frequency harmonics.

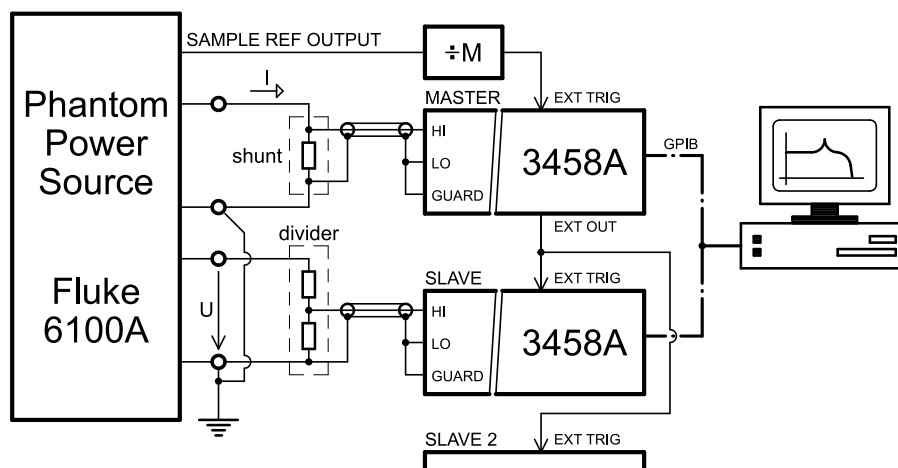


Figure 1.26: DMM 3458A synchronization in Master-Slave topology with sample clock generated by source.

For all cases the interconnection between the DMMs is done via ordinary coaxial cables. No chokes are needed in this case. The EXT TRIG and EXT OUT connectors are referred to instrument chassis ground and internally optically isolated from the measurement board, so no ground loops via the measurement input can appear.

## 1.2.2 High frequency domain (NI PXI5922)

The wideband (HF) measurement setup used to calculate the power and PQ quantities includes one or more dual channel high-speed digitizers developed by National Instruments NI PXI 5922 for sampling simultaneously the voltage  $U(t)$  scaled through a voltage divider and the current  $I(t)$  scaled through a current shunt.



Figure 1.27: Dual channel high-speed digitizer NI PXI-5922 [15].

### 1.2.2.1 Principle

This digitizer is based on a flexible resolution technology, which enables the possibility of analyzing waveforms from 50 Hz to 1 MHz by choosing the right combination between the sampling frequency and the vertical resolution, because most of the precise properties of the NI 5922 digitizer depend on the sampling rate.

Figure 1.28 shows a detailed block diagram of the NI PXI-5922 board.

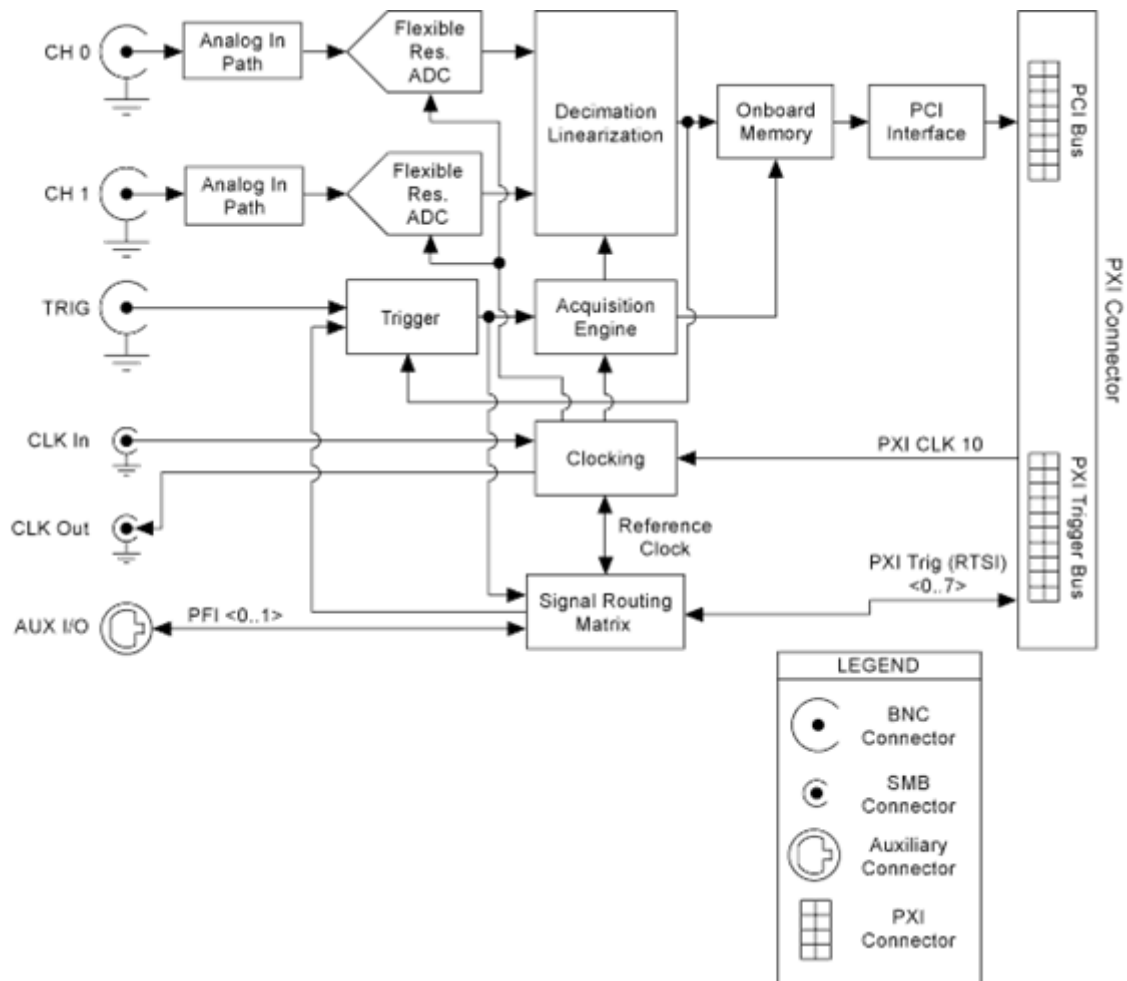


Figure 1.28: Block diagram of the NI PXI-5922 board [15].

Flexible resolution is a National Instruments proprietary technology for a very high-resolution ADC. The Flex ADC trades off resolution for speed and provides the best possible resolution over a wide range of sampling rates. Table 1.6 shows the resolution of the NI 5922 for different sampling rates.

Sample rate	Resolution	Bandwidth ( $0.4 \times$ Sample rate)
100 kS/s	24 bit	40 kHz
1 MS/s	22 bit	400 kHz
5 MS/s	20 bit	2 MHz
10 MS/s	18 bit	4 MHz
15 MS/s	16 bit	6 MHz

Table 1.6: Resolution and bandwidth of the NI PXI-5922 [15].

The NI 5922 uses an internal 6-bit 120 MS/s ADC sourced through a noise-shaping  $\Sigma\Delta$  circuit that moves quantization noise on the output of the ADC from lower frequencies to higher frequencies. Data from the ADC is then corrected in real time in a digital linearization block



to an accuracy of 24 bits, which corrects for static as well as dynamic errors in the ADC. The linearization block is configured during self-calibration, which also means the linearity is slightly changed every time when self-calibration is performed. The repeatability of the linearization should be taken into account when assigning the calibration uncertainties to the gain corrections. A digital low pass filter applied to the data from the linearization block removes all but a fraction of the original shaped quantization noise. The signal is then re-sampled to a lower sampling frequency and a higher resolution. Flexible resolution provides antialiasing protection due to the digital low pass filter.

Like any other type of converter that uses noise shaping to enhance resolution, the frequency response of the converter is only flat to its maximum useful bandwidth. The NI 5922 has a maximum bandwidth of 6 MHz. Beyond this frequency there is a span where the converter acts resonant and where a signal is amplified before being converted. These signals are attenuated in the subsequent digital filter to prevent aliasing. However, if the applied signal contains major signal components in this frequency range, such as harmonics or noise, the converter may overload, and signal data may become invalid. In this case, you receive an overload error message. You must then either select a higher input range or attenuate the signal.

#### 1.2.2.2 Input range

There are two full scale input ranges  $2 V_{pp}$  and  $10 V_{pp}$  within which the digitizer operates with all sampling rates. The choice of the most appropriate input range depends on the output level of the voltage and current transducers. Most of the voltage and current transducers available provide a voltage output from 0.8 V to 1.0 V when operating at the nominal voltage or current.

#### 1.2.2.3 Input impedance

Input impedance can be set to  $1 M\Omega$  or  $50 \Omega$ . The  $50 \Omega$  is in most cases pointless to use as it would load the source too much. Exception may be measurement on the HF sources designed for  $50 \Omega$  output. So typical setup is always  $1 M\Omega$ . This setting is particularly convenient when additional amplifier buffer stages are avoided between the output of the transducers and the input of the digitizer so the transducer is loaded as little as possible.

The knowledge of the input impedance of a digitizer's channel is important since it gives rise to the loading errors when connected to the voltage and current transducers in the modular measurement setup. Manufacturer specifications give a resistance value of  $1 M\Omega$  in parallel to a capacitance value of 60 pF. However, although the capacitance value is mostly frequency independent, the parallel resistance drops quickly with the rising frequency to around 100 k $\Omega$  at 1 MHz. This of course causes frequency dependent loading effect to the transducer gain transfer. Therefore it must be calibrated in order to be able to evaluate the loading effect (see section [2.4.6](#)).

#### 1.2.2.4 Clocking

The clock circuitry on the NI PXI-5922 offers versatile clocking options. We can use the phase-locked loop (PLL) circuit on the NI PXI-5922 to phase lock the internal 120 MHz reference oscillator with the PXI 10 MHz reference or with a provided external reference clock. Locking the particular cards in the chassis to common reference (internal chassis or external “CLK IN”) is a must when the cards should operate synchronously.

#### 1.2.2.5 Input connections

##### 1.2.2.5.1 Single ended input measurement setup

Single ended experimental setups for wideband sampled power and PQ measurements might be realized and validated when both signals coming from voltage and current transducers are preferably floating. Example is shown in Figure 1.29.

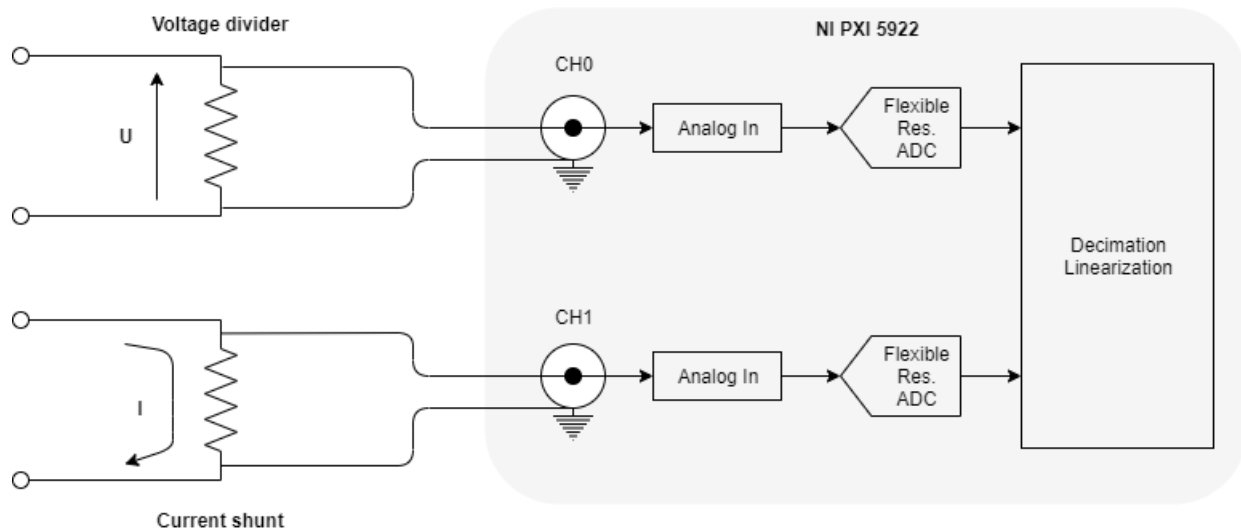


Figure 1.29: Single-ended input measurement setup.

The design shown Figure 1.29 is a principle connection to the NI PXI-5922 digitizer. All channels of the NI PXI-5922 digitizer are sampled simultaneously, and the inputs of the board are equipped with female BNC connectors, where the outer shells are connected to the same ground. In such a configuration one must take into consideration the effect of the ground loops and capacitive loading of the input signals. Note the developed algorithms are designed to compensate the loading.

##### 1.2.2.5.2 Differential input measurement setup

If the voltage and current channels are referenced to ground it is not advisable to use single ended sampling, because this will create ground loops in the system, and undefined current paths.

In this case differential sampling is preferred where the ground of the digitizer is separated from the ground of the sources as shown in Figure 1.30.

The NI PXI-5922 board supports differential mode, but this is an internal digital operation on the board, equivalent with single ended sampling and then subtracting the signals in the computer. It is better to use single ended mode for the board and then perform the signal processing in the computer, because the gain and phase corrections can be applied to the channel signals for better accuracy.

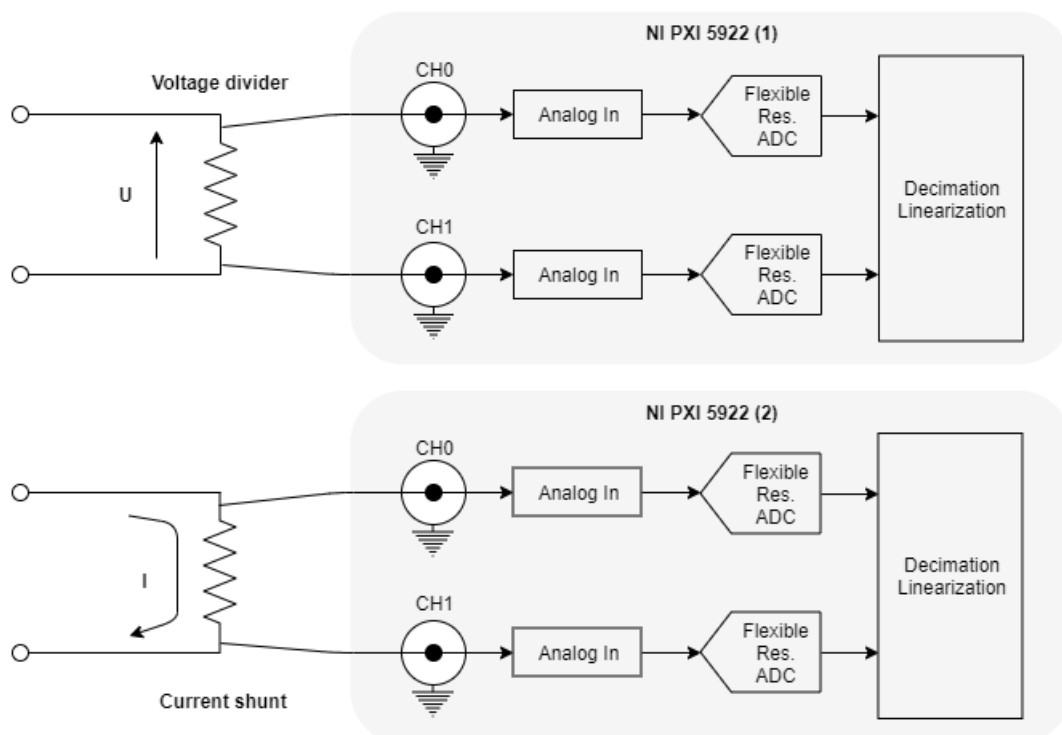


Figure 1.30: Differential input measurement setup.

The design is based on the use of two NI PXI-5922 digitizers in differential mode for voltage and current signal measurement as described in the modular measurement setup for high frequency domain in section 1.1.1.2.

## 1.3 Selecting the relevant components

This section describes the guidance documentation on selecting the relevant digitizers, current and voltage transducers depending on the frequency domain addressed. It has been accepted, after a review of existing measurement and calibration setups, that the most abundant setups for power and PQ measurements among NMIs are based on:

- Sampling DMMs 3458A, for LF power and PQ measurements (up to 10 kHz);
- High performance digitizers such as the NI 5922, for high frequency power and PQ measurements (up to 1 MHz).

Starting from the already developed setups the selection of components, i.e. digitizers, voltage and current transducers, must reflect the impact that the project aims to achieve on the metrological and scientific community. For this purpose, the selection of components should take into account the following steps:

- Establish the ability to measure various power and PQ parameters by assembling the various components within the modular measurement setup.
- Establish the ability to maintain a clear and unbroken traceability chain to the SI for all commonly measured power and PQ parameters.
- Bring assistance to less experienced NMIs/DIs to enable them to start or enhance their research capability in power and PQ metrology by using directly the outputs of the project, e.g. as the open software tool, which enables the possibility of remote control and processes the data automatically thus reducing calibration time for all selected components and associated resource and costs.

### 1.3.1 Selecting the digitizers

Recent trends in precise measurements of voltage and current under sinusoidal and non-sinusoidal waveforms aim on the use of semiconductor based digitizers having increasingly higher sampling frequency, vertical resolution and improved SNR. Figure 1.31 reports some of the main digitizer parameters when LF and HF waveforms are analysed using sampling strategy. For wideband measurements high sampling frequencies are required, according to the Nyquist-Shannon sampling theorem, at the expense of a lower vertical resolution and SNR ratio.

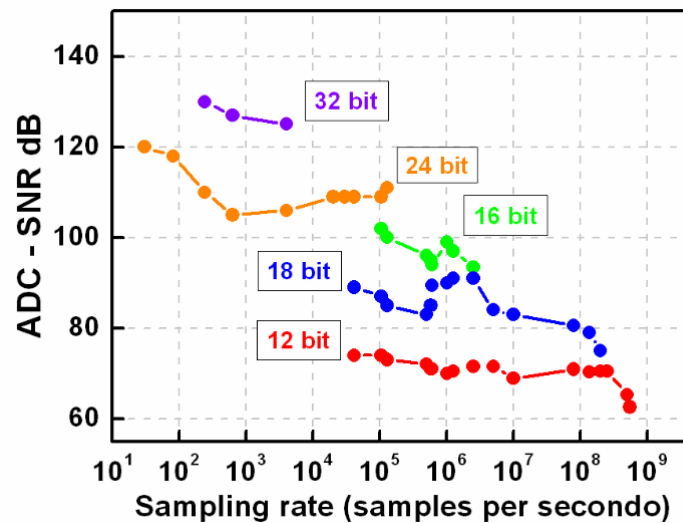


Figure 1.31: ADCs performance according to main figure of merit as sampling rate, vertical resolution and the signal-to-noise ratio.

The selecting of the digitizers depends on the accuracy and bandwidth that the end user wants to achieve. It has been accepted after the survey that the more appropriate solution suitable to cover the whole frequency domain comprises two macro-setups. Each macro-setup covers a distinct frequency domain depending on the choice of the digitizers and voltage and current transducers, according to the possibility of investigation and developing of new capabilities and calibration methods for power and PQ measurements with the aim of improving the current attainable uncertainties as well as extending traceability of power and PQ measurements at high frequencies.

#### 1.3.1.1 Digitizers - Low frequency setups

Candidate experimental setups for low frequency Power and PQ measurements are based on DMMs 3458A digitizers. The proposed solutions are based on these digital multimeters but in general they can be replaced by other samplers. To obtain the best possible accuracy at least the following parameter should be evaluated:

- Temperature and humidity gain dependence
- Time aperture gain dependence
- Gain frequency dependence (within the frequency operation range)
- Time aperture error needs to be corrected. The error of the internal clock may cause an error of this correction at long aperture times and higher frequencies.
- Stability, especially for gain.
- Frequency error may be important if the 3458A internal clock is used, which is not very precise.

It is possible but not trivial to re-build 3458A to accept an external 10 MHz clock to the 3458A. Some laboratories have already done this but do not recommend doing this without detailed knowledge of the internal circuitry.

LF experimental setups are divided in two groups, depending if there is synchronization between the sources and the samplers or not.

1. **Synchronous setups** There are several synchronous digitizing options. There are some advantages of synchronised digitizing: Windowing errors can be easily avoided, and Discrete Fourier transform can easily be applied. The drawback is that it generally required a more elaborate setup. The digitizers can be configured as follow:

- **Using a single digitizer with a coaxial switch:** The setup is based on simultaneous synchronous signal synthesis and sampling. To obtain the best accuracy the RMS value of the voltage is obtained separately by using a thermal converter or a high-grade voltmeter. Thanks to the synchronousness, the voltage and the current need not to be sampled simultaneously but can be sampled after each other, by the same digitizer, and analysed to find the phase angle and voltage/current ratio. This approach is called time multiplexing. In these systems the traceability of amplitudes is from the rms measurement and the phase from the digitizers and the synchronization. The main advantage of this system is that uncertainties in the order of 1  $\mu$ W/VA can be achieved. The main disadvantage is that the system is more complex in the hardware and in the integration, and it is only valid for the calibration of meters and cannot easily be used for harmonics measurements. Thus this mode is currently not supported by the TWM not TPQA SW tools.
- **Phase locking solution:** Both digitizers are connected to the same trigger signal (sample clock). The trigger signal is obtained from the source using an ( $M/N$ ) divider to get the required sampling frequency.  
Advantages: Very versatile, can be used with almost any voltage and current sources, including regular power supply voltages.  
Disadvantages: requires extra hardware, phase-lock adds sampling jitter, trigger source should not contain large inter-harmonics or extra zero-crossings. This method is supported by the TWM/TPQA tools, however without ability to control the  $M/N$  ratio from the SW itself.
- **Synchronized sources and measurement references:** Both samplers are connected to the same trigger signal, from an Arbitrary Waveform Generator (AWG) (or uncontrolled source such as Fluke 6100A). An external frequency reference is then connected both to source and the AWG (and possibly to the source) to avoid any frequency error. It is also possible that the source provides the frequency reference that is connected to the AWG and the frequency meter, so this approach can achieve coherent sampling even when source has only 10 MHz output and no input.

2. **Non-Synchronous setups** There is no synchronization between source and samplers and is the only choice when the hardware does not allow synchronization. However, synchronization between the samplers are necessary to obtain the phase angle. There are some ways of doing that:

- **Using the clock of one of the DMMs and master-slave configuration:** There is a time delay between the two DMMs samplers that can be measured and corrected for, together with the influence of the different bandwidths. There is a limitation in the possible sampling rates due to the DMM clock resolution. This problem is due to the DMM clock frequency and cannot be solved.
- **Using an external source (AWG) for triggering:** The jitter in the two DMMs is the same but the AWG jitter is added to both. With the adequate AWG it can be much better than using the 3458A clock for triggering. There is still a small delay between the two samplers although it is more limited, and it is still necessary to apply the correction for the bandwidth differences of the two DMMs. The corrections for bandwidth difference can be done simultaneously with a time delay correction. It works for the lower frequency and in the lower ranges of the 3458A. But the idea is to use only the 1 V range, so it is not a big problem. The frequency of the AWG must be known or the AWG must be connected to an external frequency reference. The main advantage is that the same hardware configuration can be used for synchronous and asynchronous measurements.

For the TracePQM project the straightforward solution with one digitizer per channel was chosen. Thus the achievable uncertainty for amplitude measurements is limited to few parts in  $10^6$ . For power measurement the phase uncertainty is introduced, so the realistic conservative guess of the limiting uncertainty is say  $7 \mu\text{W}/\text{VA}$  ( $k = 2$ ) without effects of the transducers. The DMMs are stable enough and their auto-cal procedure repeatable enough to allow this.

### 1.3.1.2 Digitizers - High frequency setups

The experimental setups already developed during the last decades can be grouped into three macro-methods or setups depending on the method implemented for the detection of voltage and current signals coming from the scaling transducers.

1. **Zero-power factors (ZPF) standards:** The ZPF standards offer wide-bandwidth (from power line frequencies up to 1 MHz) and high precision (from  $10^{-6} \text{ W}/\text{VA}$  at low frequencies to  $10^{-4} \text{ W}/\text{VA}$  up to 200 kHz). ZPF standards, based on thermal converter technology, are the most accurate instruments capable of reaching uncertainties of  $1 \mu\text{W}/\text{VA}$  and are employed for calibration of various type of wattmeters. Even if thermal power standards offer wide bandwidth, they do not ensure the same performances at any power factor and in presence of distorted waveforms but can be used for multi-frequency investigations of systematic deviations in other ac power systems.
2. **Coaxial bridges:** These are complex measurement systems, based on current comparators and electromagnetic devices, suitable for establishing the unit of electrical energy, power measurements and calibration of power and energy meters with uncertainties of less than  $30 \mu\text{W}/\text{VA}$  at almost all power factors. Such a system can in principle operate at least up to the acoustic band but the frequency operating margins of CC bridges for power measurements are limited by the frequency behaviour of the electromagnetic devices.
3. **WB digitizing methods:** Digital sampling power meters represent the state-of-the-art



in the field of power measurements with pure and distorted waveforms and at any power factor at frequencies ranging from power line frequencies to the megahertz range. Two digitizing approaches have been developed in parallel, both based on the use of mixed analog – digital technologies, i.e.,

- those based on the synthesis of bi-phase sine waves by means of semiconductor digital-to-analog devices (DACs) [16] [17] [18] employed as power standard;
- those based on the concept of waveform sampling/digitizing by using analog-to-digital converters (ADCs), for fast and precise digitizing of waveforms coming from voltage and current transducers.

With respect to the use of sampling strategy for power and PQ parameters estimation in an extended bandwidth of frequencies the proposed solutions and those adopted from several NMIs can be subdivided in two macro-setups, namely:

- **Switching sampling power meter**

The main components of the setup consist of a commercial digitizer together with a switch unit, and buffer amplifiers to alternatively measure the voltage and current channel suitable to operate at power frequencies up to 400 Hz. An improved version of the setup suitable to operate in the megahertz region was proposed in the framework of an European project to calibrate high frequency power meters able to measure up to the megahertz region under sinusoidal regime. Figure 1.32 shows a simplified block overview of the proposed setup for sampled power measurements.

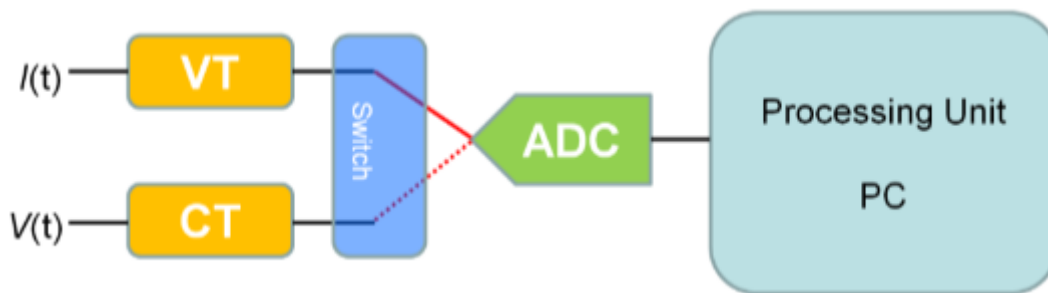


Figure 1.32: Switching sampling power meter setup.

- **Digital sampling wattmeter based on high-speed synchronized digitizers**

Synchronized digitizers represent the method adopted and accepted by most NMIs, accredited laboratories and instrumentation manufactures to ensure reliable and accurate power and PQ parameters measurements in a wide range of frequencies, ranging from power line frequencies to the kilohertz range. In this configuration the synchronized digitizers carry out instantaneous sampling of both voltage and current waveforms. The digital sampling approach for power and PQ parameters has a great advantage compared with other methods, e.g. those based on analogue multiplication, because the digital multiplication process is carried out in equally-spaced simultaneous samples of voltage and current, within a time interval corresponding to an exact number of periods of the



fundamental frequency, is precise and does not cause linearity problems. Post-processing and/or real-time processing on data streaming of voltage and current enable fast and accurate power measurements under distorted waveforms and of the different harmonics.



Figure 1.33: Basic structure of synchronized digitizers in a digital sampling wattmeter.

The Analog-to Digital converter is the most important part of the modular setup. The ADC system selected for the design of the wideband modular setup is based on two-channel high-speed digitizer developed and commercialized by National Instruments, NI 5922. Further information can be found in [15] and in section 1.2.2.

In TracePQM project the straightforward solution with synchronized digitizers was chosen. Therefore the amplitude accuracy fully depends on the gain stability and self-cal procedure repeatability of the selected NI 5922 digitizer. Thus the achievable uncertainty even at low frequencies is limited. The observations made on several digitizers in scope of the TracePQM shown occasional deviation of the self-cal procedure of NI 5922 up to  $\pm 100 \mu\text{V/V}$ . So for the power measurement it is not realistic to expect better performance, then some  $150 \mu\text{W/VA}$  ( $k = 2$ ). Only exception would be to perform LF gain calibration of each NI 5922 channel by higher accuracy instrument, such as Fluke 5790 just after the self-calibration and correcting the nominal gain correction of the particular channel just before the measurement itself starts. However, even then, due to the short term instability, it is not reasonable to expect power uncertainty below some  $50 \mu\text{W/VA}$  ( $k = 2$ ) even if the temperature of the cards is held stable and temperature dependent gain correction is applied (TWM/TPQA tools in principle allows that).

#### 1.3.1.2.1 Mixed LF and HF approach

In addition following paragraphs show example of mixed LF and HF approach setup developed at INRIM. A simplified block diagram of the modular measurement setup developed at INRIM which comprises both macro-setups based on high precision DMMs for power and PQ measurements in the kilohertz range and wideband digitizers for measurement up to 1 MHz is shown in Figure 1.34. The system can be set up with several voltage (IVD, voltage transformers (VT) and RVD) and current (current transformers CT) or shunts CS) transducers. Extension to three-phase power measurements is also possible.

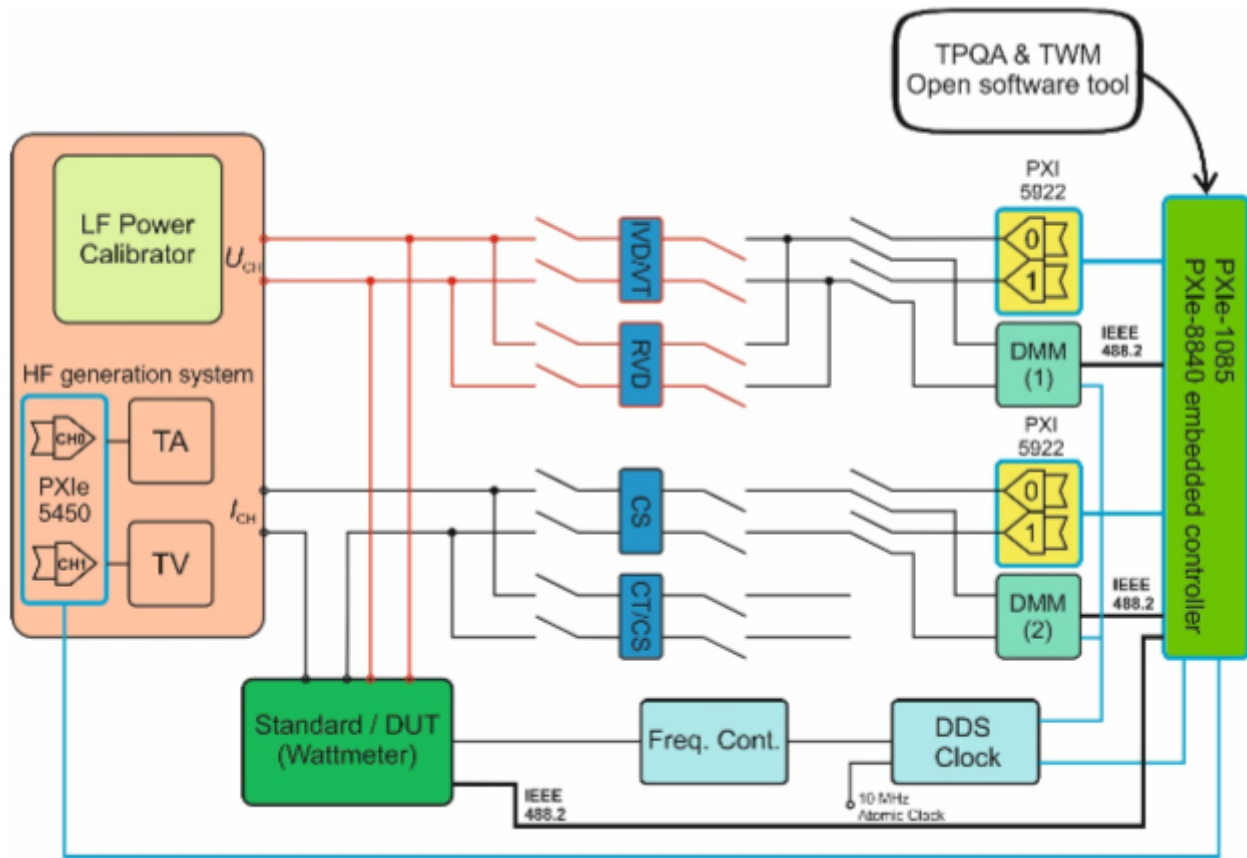


Figure 1.34: INRIM unified measurement setup based on DMMs and wideband digitizers for power and PQ measurements.

The measurement can be handled by both TPQA and TWM open tool software and a synchronization between them is also possible using the embedded controller of the PXI-chassis. The generation system is based on a power calibrator for the generation of voltage and current waveforms at power line frequencies or a dual-phase high speed DAC equipped with wideband voltage and current amplifiers.

### 1.3.2 Selecting the input transducers

The input transducers for voltage and current down-scaling process are typically:

1. voltage ratio devices;
2. current ratio devices.

The most accurate voltage ratio device are those based on inductive voltage dividers (IVD), which ensures the voltage ratio with sub-ppm uncertainty from 10 Hz up to 1 MHz [19] [20] [21]. Furthermore, improved ratio devices are available which enable accurate voltage and current ratios [22]. These ratio devices are voltage and current transformers, constructed to minimize the overall losses and thread as much as possible the magnetic flux between the windings. This is

accomplished using appropriate winding geometry and magnetic materials of high permeability. In these devices the ratio of electromotive force induced, or current flowing, in the two windings is the ratio of the number of turns of the two windings to within a part in a million or better. The major disadvantage is different types of devices are needed to cover the whole bandwidth of interest and their calibration is time-consuming.

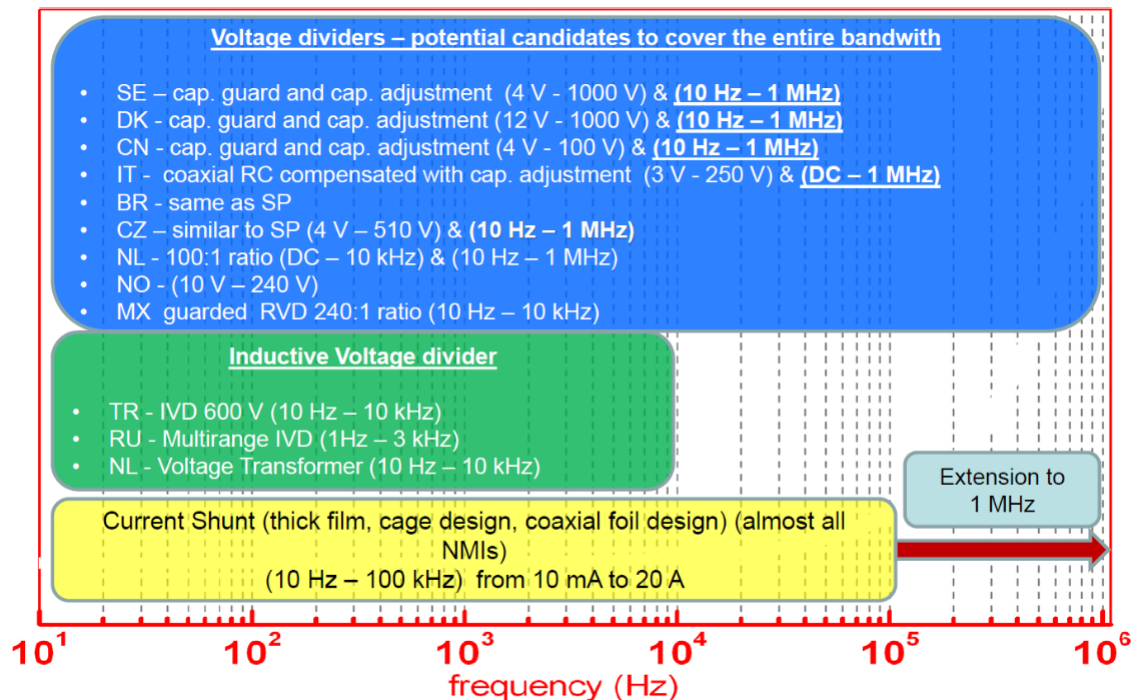


Figure 1.35: Voltage dividers and current shunts available at the labs in the survey.

### 1.3.2.1 Selecting the voltage transducers for wideband measurements

For wideband applications resistive voltage dividers represent the most commonly used solution because they don't present the typical bandwidth limitations of the inductive ones.

In wideband power measuring system voltage dividers must have high ratio accuracy, low distortion, and low frequency dependence of the amplitude ratio and input-output phase difference. They are designed using series-parallel configuration. Input-output phase difference and the effect of stray capacitance to ground can be minimized using a capacitive divider in parallel with the resistive divider. Moreover, the value of the capacitive network can be finely trimmed to compensate the capacitive loading of the output, i.e. cables and input of the sampling system. Such a compensation can be carried out at a fixed frequency and is difficult to make it in a wideband.

The output impedance of a resistive divider is typically of the order of 100  $\Omega$ , which makes it sensitive to capacitive loading at higher frequencies.

It is therefore recommended to use a buffer amplifier to unload the divider output. The buffer should ideally be connected directly to the divider output without a cable, and the combination

divider + buffer should be calibrated as a unit.

Figure 1.36 shows the schematic and a set of wideband coaxial RVD realized at INRIM operating from 3 V to 150 V.



Figure 1.36: Set of wideband coaxial compensated RVD for voltage scaling with ratio from 1:3 to 1:52 constructed at INRIM.

### 1.3.2.2 Selecting the current transducers

Coaxial current shunts are passive devices and are the transducers most frequently employed for routine AC current measurements at the primary level. The current shunts are resistive devices suitable to detect alternating current in terms of voltage drop by using Ohm's law.

They are generally characterized by high stability impedance with the variation of the current, temperature and time, and low reactive parameters (inductance and capacitance). The main technologies prevalently used are:

- Cage design, where several resistive elements are connected in parallel, in a cage like design;
- Coaxial foil structures, where resistive metal alloys are arranged in coaxial structures;
- Coaxial disk design, where a resistive disk is made of parallel precision resistors or a thick resistive film.

The circuital model of these shunts is a two port transresistance and the parameters of interest for the measurements are the transresistance ratio and the phase difference between output voltage and input current.

The main purpose of all designs is to minimize the mutual inductance between the output of the shunt and the current path leading to the resistive elements and also other, external, current paths. The influence of magnetic fields is further minimized using cylindrical symmetry and sheet-metal casing as in the case of coaxial foil shunts. Moreover, the use of discrete resistors, e.g. the cage design, reduces the error associated with the distributed resistance due to skin effect at higher frequencies.

Current shunts are already used as primary standards for AC current and phase for frequencies ranging from 10 Hz to 100 kHz and an extension up to 1 MHz is also possible.

Figure 1.37 shows the set of current shunts routinely used at INRIM as primary AC standard for current and power and PQ measurements. For currents from 10 mA up to 1 A the reference set is based on the coaxial disk design. For currents from 2 A to 100 A the shunts are of cage design and coaxial foil design.



Figure 1.37: Coaxial shunts: (Left) Cage design (manufactured by Fluke), (Middle) Coaxial foil structure (manufactured by BEV), (Right) Coaxial disk design (manufactured by INRIM).

## 1.4 Achievable uncertainties

Measurement results generally need to be accompanied by quantitative statements about their accuracy. This is particularly important when the result of a measurement is part of a measurement chain tracing back to national standards or when decisions about product specifications are taken. Standardized treatment of measurement uncertainty is essential.

This section will provide:

- A brief description of the two main uncertainty evaluation methods:
  1. GUM Uncertainty Framework (GUF) based on the Guide to the expression of uncertainty in measurement (GUM) [23],
  2. Monte Carlo Method (MCM) based on the first and second supplement to the GUM [24], [25].
- A detailed example of uncertainty evaluation for the DSWM according to the GUF
- And finally, typical achievable uncertainties for the developed algorithms of this project.

### 1.4.1 Uncertainty Calculation Methods

#### 1.4.1.1 Uncertainty evaluation based on the Law of Propagation of Uncertainty

This method [23] uses the concept of standard uncertainty, and does not distinguish between standard uncertainties obtained from analysis of measurement data and those obtained by other means.

The measurement model (functional relationship) between the measure quantity  $Y$  and the input quantities  $X_i$  is given by:

$$Y = f(X_1, X_2, X_3, \dots, X_N) \quad (1.5)$$

Given the measurement results  $x_i$  of the input quantities  $X_i$  and their associated standard uncertainties  $u(x_i)$  and covariances  $u(x_i, x_j)$ ,  $i \neq j$ , the measurement result  $y$  of  $Y$  is determined as:

$$y = f(x_1, \dots, x_N) \quad (1.6)$$

and its associated standard uncertainty as:

$$u^2(y) = \sum_{i=1}^N \left( \frac{\partial y}{\partial x_i} \right)^2 u^2(x_i) + 2 \sum_{i=1}^{N-1} \sum_{j=i+1}^N \frac{\partial y}{\partial x_i} \frac{\partial y}{\partial x_j} u(x_i, x_j) \quad (1.7)$$

The first term of the equation 1.7 shows the calculation of the standard uncertainty of the output signal using the law of propagation of uncertainties. The second part of the equation 1.7 is used in the case of correlated input quantities.



The GUM states rules for the construction of the expanded uncertainty:

$$U(y) = k \cdot u(y) \quad (1.8)$$

This expanded uncertainty is used to express the confidence of the interval about the measurement result that encompasses a large fraction  $p$  of the probability distribution characterized by that result and its combined uncertainty.  $k$  is the coverage factor. For a level of confidence  $p$  of approximately 95.45 % the value of  $k$  is 2 for normal distributed measurement. In the other words,  $y$  is in the interval  $[y - U(y), y + U(y)]$  encompasses true value of the measurement with 95 % level of confidence

#### 1.4.1.2 Numerical calculation by Monte Carlo Method

Monte Carlo method (MCM) was devised as an experimental probabilistic method to solve difficult deterministic problems since computers can easily simulate a large number of experimental trials that have random outcomes. The method is used for solving differential equations or computation of definite integrals. MCM can be easily used for propagation of uncertainties [24], [25] through a measurement model that is non-linear or is too complicated for the Law of Propagation to be applied.

This method basically consists of a number  $M$  of Monte Carlo trials in which the distribution function of the value of the output quantity  $Y$  will be numerically approximated. A sample vector of the input quantities can be drawn repeatedly using random number generators. For each input sample vector the corresponding value of the output quantity is calculated by measurement model. The set of the  $M$  output sample vectors yields an empirical distribution which can be used to approximate the random distribution of the output quantity.

Based on the complexity of the measurement model, one needs to use  $M \geq 10^6$  to estimate a 95 % coverage interval for the output quantity such that this length is correct to one or two significant decimal digits.

The single steps of the algorithm of Monte Carlo method for uncertainty estimation, show in Figure 1.39 as a schematic flow graph, are as follows:

1. Select the number  $M$  of Monte Carlo trials to be made. The input quantity  $X_i$  is described by mean value  $x_i$  and the probability density.

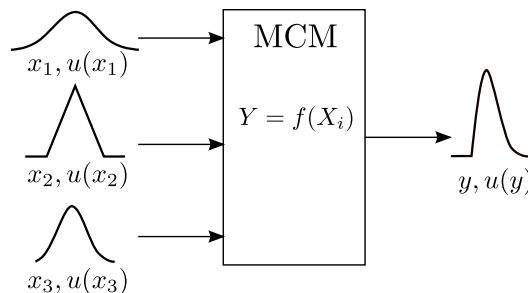


Figure 1.38: Illustration of the propagation of distribution for 3 input quantities [24].

2. Generate a set of  $N$  input parameters  $x_1, x_2, \dots, x_N$ , which are random variables distributed according to a probability density function assigned to each input parameter. This process should be repeated  $M$  times for every input quantity.
3. Calculate using model the corresponding value of measure quantity  $Y$ :

$$y_j = f(x_{1,j}, x_{2,j}, \dots, x_{N,j}), \text{ for } j = 1, 2, \dots, M \quad (1.9)$$

From this sample it is possible to estimate the probability density function of  $y$ .

4. Calculate the mean and the standard deviation from output vector  $y_1, y_2, \dots, y_M$  as the measurement result  $y$  for  $Y$  and its associated standard uncertainty  $u(y)$ .
5. Sort the output vector in ascending order and determine a coverage interval  $[y_L, y_H]$  at coverage probability  $p$ :

$$L = \text{round}\left((M + 1)\gamma\right) \quad (1.10)$$

$$H = \text{round}\left((M + 1)(1 - \gamma)\right) \quad (1.11)$$

where  $\gamma$  is the significance level ( $\gamma = 0.025$  for 95 % coverage probability) and the function  $\text{round}(x)$  is used to represent the nearest integer to  $x$ .

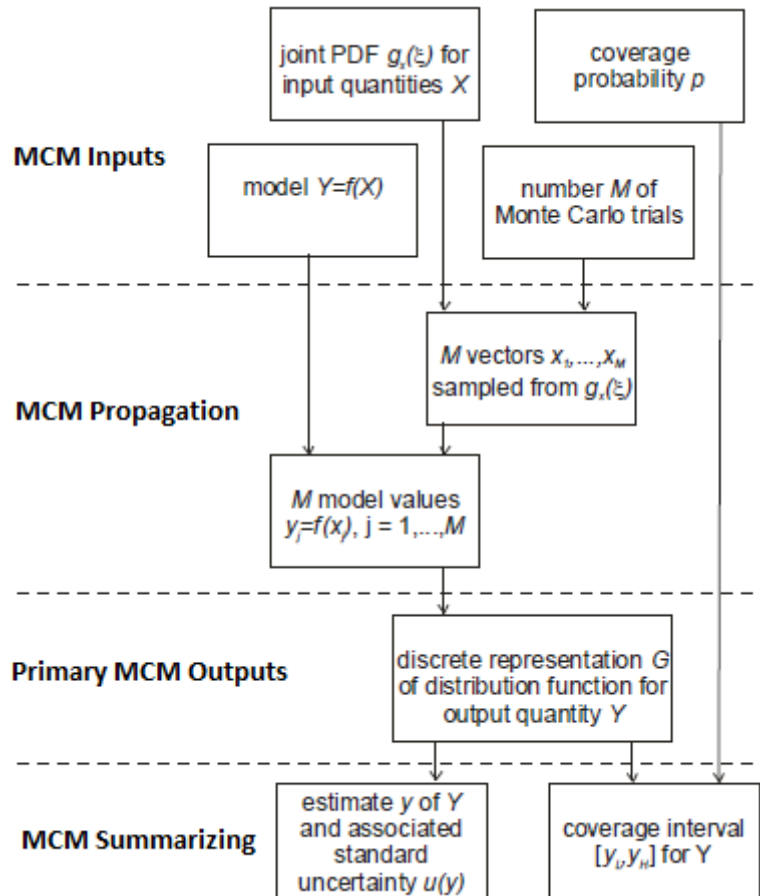


Figure 1.39: Schematic flow graph of uncertainty evaluation using Monte Carlo Method [24].



### 1.4.2 Example (GUF) - Uncertainty evaluation for the DSWM

The following example shows the main terms to take into account for the uncertainty evaluation of the active power in low frequency domain using the DSWM under sinusoidal steady state. The uncertainty is evaluated using GUF.

1. Let's recall that in sinusoidal mode, the active power  $P$  is defined by the relation:

$$P = U \cdot I \cdot \cos(\phi) \quad (1.12)$$

where  $U$  and  $I$  are respectively the voltage and the current of the signals  $u(t)$  and  $i(t)$ , and  $\phi$  represents their phase shift. The quantities  $U$ ,  $I$  and  $\phi$  are independent.

2. By applying the law of propagation of the uncertainties to the relation 1.12, appears an expression with terms of uncertainties in phase and in quadrature:

$$\left(\frac{u(P)}{P}\right)^2 = \overbrace{\left(\frac{u(U)}{U}\right)^2 + \left(\frac{u(I)}{I}\right)^2}^{\text{uncertainties in phase}} + \overbrace{\tan^2\phi \cdot u^2(\phi)}^{\text{uncertainties in quadrature}} \quad (1.13)$$

3. The quadrature uncertainty terms have a zero contribution on the global balance for  $\phi = 0^\circ$  and a contribution that tends towards infinity when  $\phi$  tends to  $90^\circ$ . The relative uncertainty will therefore always be expressed as a function of the apparent power  $S = I \cdot U$  in the form:

$$\left(\frac{u(P)}{P}\right)^2 = \left[\left(\frac{u(U)}{U}\right)^2 + \left(\frac{u(I)}{I}\right)^2\right] \cdot \cos^2\phi + \sin^2\phi \cdot u^2(\phi) \quad (1.14)$$

4. The voltage  $U$  is brought back, by means of a voltage divider of ratio  $k$ , to a level of voltage  $u_1$  which can be measured on the 1 V range:

$$U = k \cdot u_1 \quad (1.15)$$

The term  $\frac{u(U)}{U}$  is:

$$\left(\frac{u(U)}{U}\right)^2 = \left(\frac{u(u_1)}{u_1}\right)^2 + \left(\frac{u(k)}{k}\right)^2 \quad (1.16)$$

5. The current  $I$  is measured via a shunt of impedance  $Z$ :

$$I = \frac{u_2}{|Z|} \text{ with } |Z| = \frac{R}{1 + \delta} \quad (1.17)$$

where  $|Z|$  is the module of the impedance of the shunt,  $R$  is the value of its DC resistance and  $\delta$  is its AC/DC transfer difference.

The term  $\frac{u(I)}{I}$  is:

$$\left(\frac{u(I)}{I}\right)^2 = \left[\left(\frac{u(R)}{R}\right)^2 + \left(\frac{u(\delta)}{1 + \delta}\right)^2\right] + \left(\frac{u(u_2)}{u_2}\right)^2 \quad (1.18)$$

6. In equations 1.16 and 1.18,  $u_1$  and  $u_2$  are measured voltages by the two DMMs in DCV mode. They are affected by errors due to DMM bandwidth limitation  $\varepsilon_{BP}$ , integration time  $\varepsilon_{Ta}$ , signal quantization  $\varepsilon_Q$ , and sampling jitter  $\varepsilon_J$ :

$$u_{1,2} = u_{DCV} \cdot \left(1 + \varepsilon_{BP} + \varepsilon_{Ta} + \varepsilon_Q + \varepsilon_J\right) \quad (1.19)$$

The terms  $\frac{u(u_1)}{u_1}$  and  $\frac{u(u_2)}{u_2}$  are:

$$\left(\frac{u(u_{1,2})}{u_{1,2}}\right)^2 = \left(\frac{u(u_{DCV})}{u_{DCV}}\right)^2 + \frac{u^2(\varepsilon_{BP}) + u^2(\varepsilon_{Ta}) + u^2(\varepsilon_Q) + u^2(\varepsilon_J)}{1 + \varepsilon_{BP} + \varepsilon_{Ta} + \varepsilon_Q + \varepsilon_J} \quad (1.20)$$

7. Finally, the last parameter to be analyzed is the phase shift  $\phi$  between the voltage  $u(t)$  and the current  $i(t)$ . The different sources of phase shift are the voltage divider  $\phi_{VD}$ , the current shunt  $\phi_{Shunt}$  and the DMMs. The DMMs can phase out the signals due to their bandwidth difference  $\phi_{BP}$ , their integration time  $\phi_{Ta}$ , their tripping delay  $\phi_r$ , and their sampling jitter  $\phi_J$ . To all these sources of error is added the phase shift  $\phi_Q$  due to the quantization of the signals. We finally have:

$$\phi = \phi_0 + \phi_{VD} + \phi_{Shunt} + \left[\phi_{BP} + \phi_{Ta} + \phi_r + \phi_J\right] + \phi_Q \quad (1.21)$$

The term  $u(\phi)$  is:

$$u^2(\phi) = u^2(\phi_0) + u^2(\phi_{VD}) + u^2(\phi_{Shunt}) + \left[u^2(\phi_{BP}) + u^2(\phi_{Ta}) + u^2(\phi_r) + u^2(\phi_J)\right] + u^2(\phi_Q) \quad (1.22)$$

8. Additionally to this, following terms can be take into account:

- Current shunt's DC resistance, AC/DC transfer difference and phase shift drift
- Voltage divider's ratio and phase shift drift
- DMMs resolution for voltage and current measurements

All individual error terms and their associated uncertainties should be evaluated experimentally and/or by calculation. Below Table 1.7 summarize the uncertainty estimation for active power calculation with the three independent terms described above.

Note: Calibration methods of all components related to the three main independent components  $\frac{u(U)}{U}$ ,  $\frac{u(I)}{I}$  and  $u(\phi)$  are described in chapter 2.

Uncertainty evaluation for active power $P$ in W/VA				
Main uncertainty components	Type method of evaluation	Standard uncertainty value $u(x_i)$	Sensitivity coefficient $C_i$	Standard uncertainty $u_i =  C_i u(x_i)$
Voltage $\frac{u(U)}{U}$	Here specify the type A or B of all sub uncertainty components	Here specify the value of all sub uncertainty components	$\cos(\phi)$	Root square sum of all sub uncertainty components value and sensibility coefficient (in V/V)
Current $\frac{u(I)}{I}$	Here specify the type A or B of all sub uncertainty components	Here specify the value of all sub uncertainty components	$\cos(\phi)$	Root square sum of all sub uncertainty components value and sensibility coefficient (in A/A)
Phase shift $u(\phi)$	Here specify the type A or B of all sub uncertainty components	Here specify the value of all sub uncertainty components	1	Root square sum of all sub uncertainty components value and sensibility coefficient (in rad)
<b>The standard uncertainty for active power <math>P</math> in W/VA is the root square sum of the standard uncertainty of the three independent components: 1) Voltage <math>\frac{u(U)}{U}</math>; 2) Current <math>\frac{u(I)}{I}</math>; 3) Phase shift <math>u(\phi)</math></b>				
<b>Expanded uncertainty for active power <math>P</math> in W/VA is equal to standard uncertainty multiplied by 2 which gives 95.45 % coverage factor</b>				

Table 1.7: Summary of uncertainty evaluation of active power in W/VA

### 1.4.3 Examples - Achievable uncertainties

This section shows examples of achievable uncertainties for several typical examples of developed setups and SW tool TWM/TPQA.

Uncertainties achievable with setup and SW tools depend on several factors:

1. Calibration uncertainty of HW components, i.e. the digitizer and the transducers.
2. Uncertainty introduced by the algorithm itself:
  - (a) Standard deviation (can be suppressed by averaging measurements)
  - (b) Systematic errors (cannot be eliminated by repeating the measurement)
3. Uncertainty introduced by sources that were intentionally omitted during algorithms design (e.g. crosstalk).
4. Uncertainty introduced by imperfection in the setup, e.g.: interferences, ground loops.

The component (2a) Standard deviation can be reduced by repeating the measurement and averaging. For most of the algorithms the component (2b) can be reduced by changing the sampling parameters. Most of the algorithms are very sensitive to selection of sampling-to-measured frequency ratio, i.e. number of sampled per period of a signal. The algorithms are also sensitive to length of the record, i.e. number of signal periods recorded. Due to the non-linear behavior of the algorithms it is not trivial to give general uncertainty for each algorithm.

In real measurement, the dominant source of uncertainty for the simple algorithms such as FFT based estimators, PSFE, WRMS etc. will be mostly (1) Calibration uncertainty. It is e.g. not possible to achieve amplitude measurement uncertainty below some 0.005 % for the setups based on the wideband digitizers NI 5922, because their gain stability and repeatability is limited. Similarly, the dominant component the HF measurements will be the loading correction, which will grow at least to the order of 0.01 % despite the algorithm itself is frequency independent and may have errors in order of parts per million.

The component (3) Setup interferences is not possible to evaluate by developed SW tools as it depends on particular grounding, balancing of currents in the coaxial cables, cable layout, etc. These sources must be evaluated manually, e.g. by changing positions of cables and observing the changes in the measured values. Also techniques typical from coaxial impedance bridges such as described in [6] can be valuable for estimating these effects.

Last component are the omitted sources (4). Several simplifications were done during the design of the algorithms to make them effective enough. One of the major simplifications was leaving out the inter-channel crosstalk correction. The main reason for this step was it is easy to implement such a correction for two-channel algorithms such as power, but very complex to implement it for the multiphase measurements, where it would be necessary to correct mutual crosstalk between each pair of digitizer channels. Such a solution would complicate the algorithms to indecipherable level and significantly decrease their performance. Therefore, in particular for the crosstalk, it was decided to assume the highest accuracy setup based on the 3458A will have negligible crosstalk, as the channels are well separated. For NI 5922, where crosstalk is up to some -106 dBc, the effect will be masked by another, more relevant sources.

However, for extreme cases, e.g. when measuring high inter-channel voltage ratios, such as 1:100, the crosstalk effect must be evaluated manually.

Following sections show actual examples of measurements and uncertainties that can be achieved. Note all uncertainties are expressed for confidence level of 95 % as it is the mostly used one among the NMIs.

#### 1.4.3.1 Example 1 - Frequency measurement

One of the most typical and simple usage is the measurement of a frequency. For such application the vast majority of corrections are irrelevant. The only relevant correction is time-base correction of the digitizer. However, if the digitizer is phase locked to some higher accuracy reference, such as GPS clock distribution unit, the dominant remaining component of uncertainty becomes the algorithm itself. The uncertainty can be as low as few parts in  $10^9$  for high purity signals (no harmonics). When distortion and noise grows, the estimator will increase the uncertainty accordingly, depending on the sensitivity of the algorithm. Several algorithms implemented in TracePQM can be used for a frequency estimation: PSFE, FPNLSF and MFSF. Example of minimum achievable uncertainties for the particular algorithms without contribution of corrections are shown in following table:

Signal	Algorithm	Conditions/setup	Rel. uncertainty
Sine wave $f_S = 50 \text{ kHz}$ $f_0 = 53 \text{ Hz}$ $N = 50000$ $SFDR = -90 \text{ dBc}$ $SNR = -110 \text{ dBc}$	TWM-PSFE	None	$0.71 \mu\text{ Hz/Hz}$
	TWM-FPNLSF	Initial guess 53.0 Hz	$110 \text{ nHz/Hz}$
	TWM-MFSF	Three harmonics [1 2 3]	$24 \text{ nHz/Hz}$

Table 1.8: Uncertainty - Frequency measurement.

#### 1.4.3.2 Example 2 - Phase shift measurement

TracePQM algorithms were not designed directly for measurement of a phase shift between channels. Instead, the TWM tool is designed so it calculates phase of each channel (or phase) relative to the timestamp (or record start) and then allows to display the differences between the particular channels. Thus, the phase shift uncertainty is always combination of two uncertainties from subtracted channels. Variety of single or multi-harmonic estimation algorithms can be used this way: WFFT, PSFE, FPNLSF and MFSF. Note PSFE has no assigned uncertainty for phase angle, so it can be used, but without uncertainty.

Note TracePQM algorithms and processing module was designed to be able to perform the phase correction by timestamp for the digitizers that support it (e.g. NI 5922):

$$\varphi' = \varphi - f_x \cdot t_0 \cdot 2\pi \quad (1.23)$$

where  $f_x$  is harmonic frequency and  $t_0$  is the timestamp. This ensures the repeated measurements of a stable signal will show the same phase angle independent of digitizer trigger point, so the particular results can be averaged. This approach works best for the FFT algorithm, where  $f_x$  is exact value known from the selected DFT bin. However, for the fitting algorithms,  $f_x$  has its own uncertainty so it produces an uncertainty component proportional to the absolute value of timestamp  $t_0$ . The timestamp for NI 5922 digitizers is relative to their reset, so it may grow easily to over  $10^4$  s. Thus it may easily become dominant component of uncertainty. See TWM manual, section processing setup 3.1.4.4.2, for possible counter measures, such as making the timestamp relative to first record before calculation.

Minimum achievable uncertainties without contribution of corrections can be found in the following table:

Signal	Algorithm	Conditions/setup	Rel. uncertainty
Sine wave $f_s = 50$ kHz $f_0 = 53$ Hz $N = 50000$ $SFDR = -90$ dBc $SNR = -110$ dBc	TWM-WFFT	Window: Hanning	2.3 $\mu$ rad
	TWM-FPNLSF	Initial guess 53.0 Hz	3.1 $\mu$ rad
	TWM-MFSF	Three harmonics [1 2 3]	6.1 $\mu$ rad
Sine wave $f_s = 10$ MHz $f_0 = 987$ kHz $N = 10^6$ $SFDR = -70$ dBc $SNR = -110$ dBc	TWM-WFFT	Window: Hanning RVD: 1:15 RVD: $Z_{lo} = (200 \pm 1) \Omega$ ADC: $Y_{in} = (100 \pm 1) \text{ pF}$	1.7 mrad

Table 1.9: Uncertainty - Phase shift measurement.

### 1.4.3.3 Example 3 - Harmonic distortion measurement

TWM-THDWFFT algorithm was directly designed for THD evaluation. It is using windowed FFT with very wide window function "Flatop\_248D", which gives the algorithm capability to evaluate harmonics with uncertainty down to 50  $\mu$ V/V (limited by low SNR). Uncertainty of the algorithm is thus limited by three main factors:

- accuracy of the harmonic amplitude readings;
- SFDR of the digitizer and transducer;
- Gain correction of digitizer and transducer.

Following example is measurement of triangular waveform of frequency 1 kHz and voltage amplitude 1 V using 5922 digitizer at 5 V range. Following corrections were applied to the algorithm:

- SFDR = 116 dBc
- $U(\text{adc-gain}) = \pm 20 \mu\text{V/V}$

Sampling setup:

- $f_s = 50 \text{ kHz}$
- $N = 50000$
- Records processed = 5

Measured THD (fundamental referenced):

- THD =  $(12.0329 \pm 0.0014) \%$

Example of measured harmonics and their uncertainties is shown in Table 1.10.

<b>h</b>	<b>A<sub>x</sub></b>	<b>U(A<sub>x</sub>)</b>	<b>U(A<sub>x</sub>)</b>
-	V	V	%
1	1.000 168	$\pm 0.000\,077$	0.007 7
2	0.000 1513	$\pm 0.000\,006\,8$	4.5
3	0.110 959	$\pm 0.000\,011$	0.010
4	0.000 049 8	$\pm 0.000\,004\,0$	8.1
5	0.040 016 8	$\pm 0.000\,005\,9$	0.015
6	0.000 020 3	$\pm 0.000\,004\,7$	23
7	0.020 441 0	$\pm 0.000\,004\,7$	0.023
8	0.000 009 6	$\pm 0.000\,003\,7$	38
9	0.012 384 4	$\pm 0.000\,003\,9$	0.032
10	0.000 004 9	$\pm 0.000\,003\,7$	76

Table 1.10: Uncertainty - Harmonic distortion measurement.

Harmonics plot for the example measurement is shown in Figure 1.40.

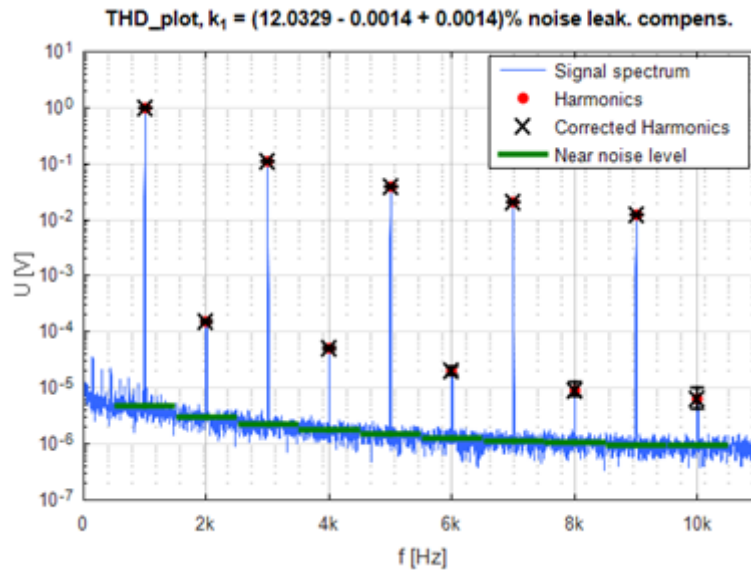


Figure 1.40: Uncertainty - Harmonic distortion measurement.

#### 1.4.3.4 Example 4 - LF power and RMS measurements

Two algorithms are available for power evaluation:

- TWM-PWRTDI for time domain integration method;
- TWM-PWRFFT for FFT based evaluation.

Following examples were obtained from actual measurements using setup based on multimeters 3458A. Following corrections were applied:

- ADC  $U(\text{time-shift}) = \pm 2 \text{ ns}$
- ADC  $U(\text{gain}) = \pm 5 \text{ } \mu\text{V/V}$
- ADC  $U(\text{dc}) = \pm 2 \text{ } \mu\text{V}$
- ADC  $U(\text{Cin}) = (376 \pm 3.5) \text{ pF}$
- ADC  $U(\text{Gin}) = (10 \pm 5) \text{ G}\Omega$
- RVD  $U(\text{nom-gain}) = (300.0000 \pm 0.0016) \text{ V/V}$
- RVD  $U(\text{phi}) = \pm 3.6 \text{ } \mu\text{rad}$
- RVD  $U(\text{Zlo}) = (200 \pm 2) \text{ } \Omega$
- Shunt  $U(\text{nom}) = (120.0000 \pm 0.0006) \text{ m}\Omega$
- Shunt  $U(\text{phi}) = \pm 0.7 \text{ } \mu\text{rad}$

The tables 1.11 and 1.12 below apply for following sampling setup (coherent sampling):

- $f_s = 5427.2 \text{ kHz}$



- $f_0 = 53 \text{ Hz}$
- $N = 27136$

Signal	Algorithm	uncertainty
Sine power: $SFDR = -90 \text{ dBc}$ $SNR = -110 \text{ dBc}$  $U = 240 \text{ V}$ $I = 5 \text{ A}$ $PF = 1.00000$ $P = 1.2 \text{ kW}$ $S = 1.2 \text{ kVA}$	TWM-PWRDI	$U(P) = 12 \mu\text{W/VA}$ $U(S) = 12 \mu\text{VA/VA}$ $U(U) = 7.5 \mu\text{V/VA}$ $U(I) = 7.2 \mu\text{A/VA}$ $U(PF) = 0.000021$
	TWM-PWRFFT	$U(P) = 10 \mu\text{W/VA}$ $U(S) = 10 \mu\text{VA/VA}$ $U(U) = 7.5 \mu\text{V/VA}$ $U(I) = 7.2 \mu\text{A/VA}$ $U(PF) = 0.000021$
Sine power: $SFDR = -90 \text{ dBc}$ $SNR = -110 \text{ dBc}$  $U = 240 \text{ V}$ $I = 5 \text{ A}$ $PF = 0.50000$ $P = 600 \text{ W}$ $S = 1.2 \text{ kVA}$	TWM-PWRDI	$U(P) = 8.1 \mu\text{W/VA}$ $U(S) = 11 \mu\text{VA/VA}$ $U(U) = 7.9 \mu\text{V/VA}$ $U(I) = 7.6 \mu\text{A/VA}$ $U(PF) = 0.000013$
	TWM-PWRFFT	$U(P) = 6.3 \mu\text{W/VA}$ $U(S) = 10 \mu\text{VA/VA}$ $U(U) = 7.5 \mu\text{V/VA}$ $U(I) = 7.2 \mu\text{A/VA}$ $U(PF) = 0.000011$

Table 1.11: Uncertainty - LF power and RMS measurements - WITH Corrections.

Minimum achievable uncertainty when all corrections listed above are disabled:

Signal	Algorithm	uncertainty
Sine power: <i>SFDR</i> = -90 dBc <i>SNR</i> = -110 dBc  <i>U</i> = 240 V <i>I</i> = 5 A <i>PF</i> = 1.00000 <i>P</i> = 1.2 kW <i>S</i> = 1.2 kVA	TWM-PWRTDI	$U(P) = 3.3 \mu\text{W/VA}$ $U(S) = 3.2 \mu\text{VA/VA}$ $U(U) = 2.6 \mu\text{V/VA}$ $U(I) = 1.4 \mu\text{A/VA}$ $U(PF) = 0.0000060$
	TWM-PWRFFT	$U(P) = 1.5 \mu\text{W/VA}$ $U(S) = 1.5 \mu\text{VA/VA}$ $U(U) = 1.3 \mu\text{V/VA}$ $U(I) = 0.58 \mu\text{A/VA}$ $U(PF) = 0.000029$
Sine power: <i>SFDR</i> = -90 dBc <i>SNR</i> = -110 dBc  <i>U</i> = 240 V <i>I</i> = 5 A <i>PF</i> = 0.50000 <i>P</i> = 600 W <i>S</i> = 1.2 kVA	TWM-PWRTDI	$U(P) = 3.3 \mu\text{W/VA}$ $U(S) = 3.2 \mu\text{VA/VA}$ $U(U) = 2.9 \mu\text{V/VA}$ $U(I) = 1.4 \mu\text{A/VA}$ $U(PF) = 0.0000048$
	TWM-PWRFFT	$U(P) = 1.5 \mu\text{W/VA}$ $U(S) = 1.5 \mu\text{VA/VA}$ $U(U) = 1.4 \mu\text{V/VA}$ $U(I) = 0.56 \mu\text{A/VA}$ $U(PF) = 0.0000022$

Table 1.12: Uncertainty - LF power and RMS measurements - WITHOUT Corrections.

#### 1.4.3.5 Example 5 - HF measurements

Goals of TracePQM call for wideband measurements in a frequency range up to at least 1 MHz. Following example shows achievable uncertainties of amplitude and phase difference measurement between two current channels, where one of the channels is floating (differential connection). The test was made with following corrections:

- ADC  $U(\text{phase}) = \pm 100 \mu\text{rad}$
- ADC  $U(\text{gain}) = \pm 100 \mu\text{V/V}$
- ADC  $U(C_{\text{in}}) = (250 \pm 2) \text{ pF}$
- ADC  $U(G_{\text{in}}) = (120 \pm 12) \text{ k}\Omega$
- High-side shunt  $U(\text{gain}) = (6.00000 \pm 0.00042) \text{ A/V}$
- High-side shunt  $U(\text{phi}) = \pm 700 \mu\text{rad}$
- High-side shunt  $U(Z_{\text{ca-L}}) = (40 \pm 10) \text{ nH}$
- High-side shunt  $U(Z_{\text{ca-R}}) = (10 \pm 5) \text{ m}\Omega$

- High-side shunt  $U(Z_{cal-L}) = (30 \pm 10) \text{ nH}$
- High-side shunt  $U(Z_{cal-R}) = (5 \pm 5) \text{ m}\Omega$
- High-side shunt  $U(Z_{cam}) = (10 \pm 10) \text{ nH}$
- High-side shunt  $U(\text{gain}) = (2.00000 \pm 0.00020) \text{ A/V}$
- High-side shunt  $U(\phi) = \pm 700 \mu\text{rad}$
- High-side shunt  $U(Z_{ca-L}) = (20 \pm 10) \text{ nH}$
- High-side shunt  $U(Z_{ca-R}) = (5 \pm 5) \text{ m}\Omega$

Signal and connection:

- $I = 100 \text{ mA}$
- $f_0 = 1 \text{ MHz}$
- $SFDR > 70 \text{ dBc}$
- $SNR > 100 \text{ dBc}$

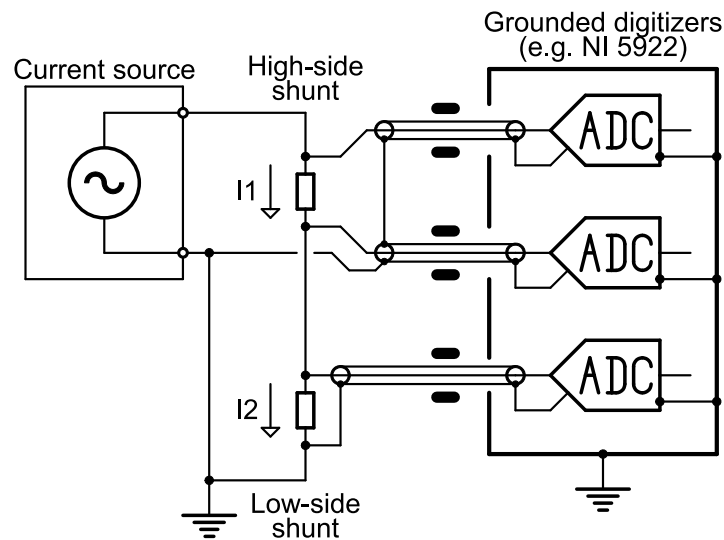


Figure 1.41: Uncertainty - HF measurement connection

Sampling setup:

- $f_s = 10 \text{ MHz}$
- $N = 100\,000$

Achieved uncertainties for high-side and low-side shunt:

Algorithm	Uncertainty
TWM-WFFT	$U(A - high) = 580 \mu A/A$ $U(A - low) = 180 \mu A/A$ $U(\varphi - high) = 930 \mu rad$ $U(\varphi - low) = 710 \mu rad$ $U(\varphi - diff) = 1.2 mrad$
TWM-WRMS	$U(A - high) = 810 \mu A/A$ $U(A - low) = 180 \mu A/A$

Table 1.13: Uncertainty - HF measurements.



## Chapter 2

# Calibration methods for the modular measurement setup components

This chapter provides an overview of the methods used to calibrate all the components of the modular power and PQ measurement setup to establish full traceability to the SI for the electrical power and PQ parameters measured. The modular measurement setup comprises current shunts, voltage dividers and digitizers. The calibration of individual components is performed for all of the parameters that are relevant to the power and PQ measurements over the appropriate frequency range dependent on the PQ parameters to be measured.

In the case of the current shunts and voltage dividers, the amplitude, phase angle error, the level dependence (power coefficient) and the temperature coefficient are all important performance parameters that need to be traceably measured.

The calibration of the digitizers includes, as a minimum, calibration of the amplitude including level dependence, phase angle error between the channels and evaluation of the stability. Different calibration procedures are required for sampling DMMs 3458A and wideband ADCs such as NI 5922 digitizers.

Finally a method for calibration of the entire system is described to provide an opportunity to check the calibration of the individual components.

## 2.1 Methods for calibration of current shunts

### 2.1.1 Current shunts - Amplitude

Ac-dc measurements are used to transfer the traceability from dc to ac, by using Thermal Voltage Converters (TVC) and currents shunts. The ac-dc difference for voltage is defined as (2.1).

$$\delta = \frac{V_{AC} - V_{DC}}{V_{DC}}, \text{ when } E_{AC} = E_{DC} \quad (2.1)$$

where  $V_{AC,DC}$  and  $E_{AC,DC}$  are the input and output voltages from the TVC, respectively.

When TVCs are compared, they are connected in parallel but when measuring the ac-dc difference of a current shunt, the Device-Under-Test (DUT) and the reference must be connected in series so that the same current passes through both devices. The voltage drop across the current shunt is measured by connecting a TVC to the output of the shunt and measuring its output. By interchanging the position of the TVCs and averaging the results, the contribution from the ac-dc difference of the TVCs can be eliminated. This means that only the ac-dc difference of the reference shunt must be known to calibrate an unknown shunt.

A sequence of 13 measurements are taken as: ac, dc+, ac, dc-, ac, dc+, etc. of current shunts in order minimize thermal voltages, current direction dependent effects in the setup and drift in the TVCs during the measuring sequence [26]. Usually the current is switched by operating two separate sources (one for ac and one for dc) and using a fast relay to switch between the sources.

#### 2.1.1.1 Leakage currents

When an alternating current is sent through the current shunts there are alternating voltages developing in different parts of the setup that drives leakage currents through capacitors outside the main current path. For frequencies below 10 kHz, these leakages can be made insignificant with a simple guarding, but for frequencies from 50 kHz and above the problem becomes much harder.

The leakage current will give a rise to asymmetry in the setup, so the Low and High positions for the shunts will be different. However reduction of the leakage can also reduce this error to well below 1  $\mu\text{A}/\text{A}$ . One way to reduce the leakage current for the multimeter on the High side, is to have the multimeter floating relative to ground, by powering it on an isolation transformer. The screen of the GPIB cable will be connected to the multimeter chassis, so this connection also needs to be broken.

The simplest way to reduce the leakage current through the isolation transformer, is to use transformers with a low capacitance between the primary and secondary windings. By using two transformers, this capacitance might be reduced to around 100 pF.

Figure 2.1 is a schematic description of a setup that isolates the high side of the setup.

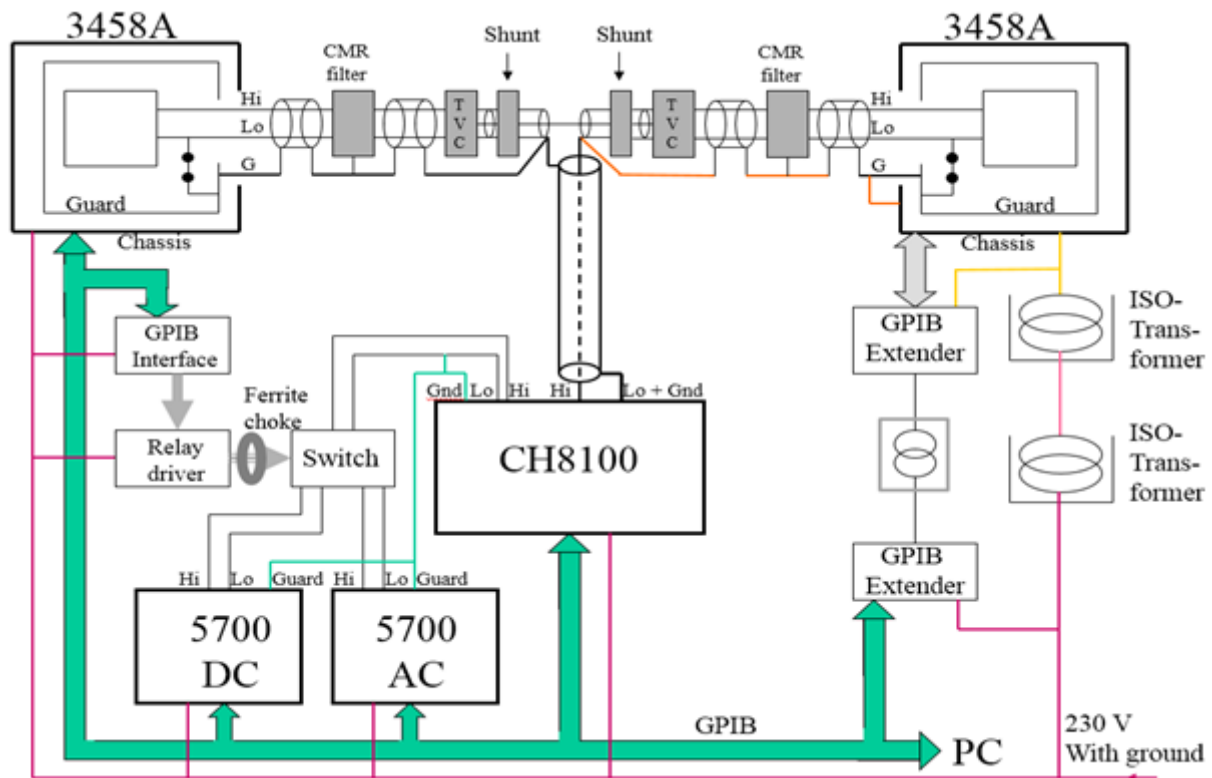


Figure 2.1: Shunt's schematic description of the ac-dc difference setup at JV.

### 2.1.1.2 Major contributions to the uncertainty

The major contributions to the uncertainty of ac-dc difference calibration are related to the shunts used and the efforts taken to reduce the leakage current, as described above. If the sources are delivering stable currents, the standard deviations can be kept below  $0.5 \mu\text{A/A}$  for most frequencies. Asymmetry in the setup might be a significant contribution, but this can be checked by interchanging the position of the shunts and TVCs. In the setup described, this difference is negligible, and often as low as  $0.1 \mu\text{A/A}$ . All current shunts have a significant power dependency, and often this effect, as well as the uncertainty in the reference shunt are the dominant contributions to the uncertainty. Measurements by Funck and Klönz [27] have shown that the power dependency can be up to  $5 \mu\text{A/A}$  at 100 kHz for a JV 5 A current shunt. The uncertainty of the reference shunt is related to the accumulated uncertainty from the step up calibration process starting from low current shunts, which often have a calculable ac-dc difference.

### 2.1.2 Current shunts - Phase angle error

Wideband current shunts are designed to have very low parasitic reactance, i.e. series inductance and parallel capacitance. This is in order to have a small phase error and ac-dc difference at high frequencies. The small phase error makes it a challenge to measure the effective inductance



or capacitance with an LCR meter [28] [29]. Therefore, the most common solution is to use a digital bridge [30] [31] [30] such as the one pictured in Figure 2.2. It consists of an ac current source which feeds a current to two shunts connected in series. The output voltages from the shunts are sampled using synchronized digitizers, such as NI 5922. In this example, four digitizer channels are used to measure the output voltages differentially, but several other configurations are used in different labs. This setup is capable of measuring the phase difference between the shunts very accurately. (It actually measures the full complex impedance ratio, but ac-dc difference methods are generally more accurate for amplitude ratio.) One of the shunts is usually the reference with a known phase, and the other shunt is the device under test.

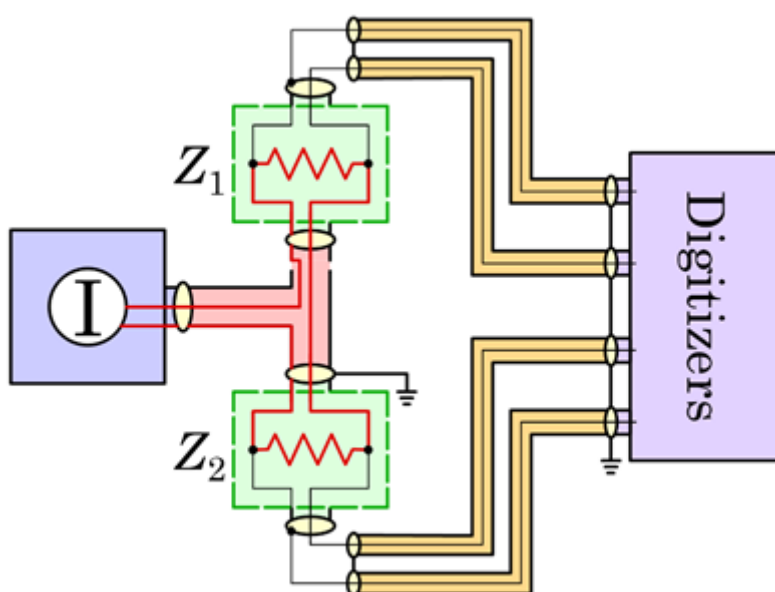


Figure 2.2: Digital bridge for wideband current shunt calibration at RISE.

A second solution employed for precise measurement of phase difference of high current shunts is based on the use of wideband digital phase comparator. The two-input digital phase detector is realized with a precision wideband digitizer connected to the outputs of the coaxial shunts under comparison, through a pair of symmetric active guarded transformers, employed as wideband decoupled precision voltage transmitters having high galvanic isolation.

The system was developed to compare shunts from 2 A to 100 A [32], and frequencies ranging from 500 Hz to 100 kHz, but an extension to lower currents and frequencies is also possible. The active guarded transformers are of identical construction and are made as a special type of double stage transformer using magnetizing windings and wideband buffers. This approach leads to increase the input impedance of the transformer at intermediate frequencies and to use single-ended sampling digitizers. Triaxle cables and separate screens, connected to suitable voltages, are employed in order to reduce the interwinding capacitance. The schematic of the digital phase comparator is shown in Figure 2.3. The shunts are connected in series through a suitable T-current node. The phase difference of the shunts is computed by taking a combination of the measurements performed by reversing the shunt position respect to the current node.

The phase of the unknown shunt is calibrated using the reference shunt and the phase difference measured by the system.

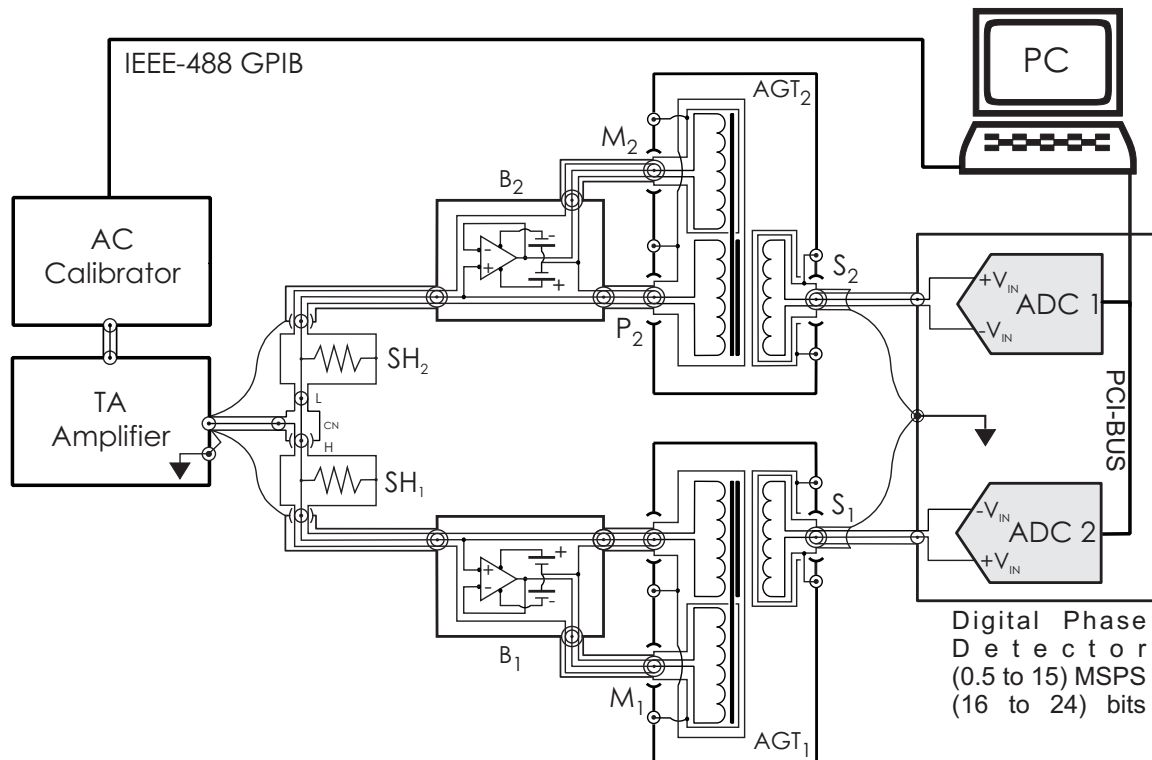


Figure 2.3: Wideband digital phase comparator for high current shunt calibration at INRIM.

## 2.1.2.1 Measurement considerations

### 2.1.2.1.1 Grounding

It is important to avoid ground loops in the measurement setup. First, because they are sensitive to magnetic field pick-up, second because they can result in undefined current return paths. It is equally important to avoid floating sections in the setup, because they are sensitive to an electric field interference and a stray capacitance. In the example setup the digitizer inputs are coaxial contacts with grounded screens (NI 5922 digitizers). This digitizer ground is separated from the current source ground by the differential connection to the shunt outputs. In other setups they may be separated using chokes, transformers or differential amplifiers.

### 2.1.2.1.2 Output loading

The instrument measuring the output voltages of the shunts has necessarily a finite input impedance which will load the shunt and change the effective shunt impedance. If the shunt will be connected in the same way for current measurements, this input impedance can be considered part of the shunt impedance, and no loading corrections are needed. However, if

the shunt will be used in another configuration, the input impedance must be characterized, and a loading correction applied to the measurement results. With the setup in Figure 2.2, this loading correction can be done indirectly by measuring the ratio twice while turning the current T-connector (pink in the figure) 180° between the measurements, effectively exchanging the high and low potentials of the shunts [29]. If we denote the two complex ratios A and B, where:

$$A = \frac{Z_1}{Z_2} (Z_1 \text{ high}) \quad \text{and} \quad B = \frac{Z_2}{Z_1} (Z_2 \text{ high}) \quad (2.2)$$

then we can calculate the unloaded ratio by:

$$\frac{Z_1}{Z_2} = \frac{A + 1}{B + 1} \quad (2.3)$$

#### 2.1.2.1.3 Digitizer calibration

The digitizer channels must be calibrated for relative channel delays and gain before they will be used for calibration of phase angle error of the shunts. This can be done by simply connecting the same signal in parallel to all channels and comparing the measured signal amplitudes and phases for the frequencies of interest. However, since the channels will measure signals with different voltages, the linearity should also be considered. Calibration of linearity can be done e.g. using ac-dc difference or IVD methods.

If only one digitizer channel is used per shunt, it is enough to calibrate the channel delays to measure the shunt phase difference, ignoring the gain and linearity.

See section 2.4 for details about digitizer calibration.

#### 2.1.2.1.4 Absolute phase reference

The bridges in Figure 2.2 and Figure 2.3 measure complex impedance ratio, including phase difference between the shunts. But they do not measure the absolute phase, which is needed for power measurements. There are a number of methods to realize an absolute phase, including calculable time constant standards, LCR meter methods and a method developed in this project based on impedance ratios of geometrically identical shunts [33] [31] [34] [35] [36] [37] [38]. See references for details. The key principle is to realize an absolute phase at the impedance level which gives the best uncertainty, and then step up and down in impedance using the ratio bridge, since the uncertainty in phase difference is much lower than the absolute phase uncertainty. Using these methods an uncertainty of around 100 ps is possible for the time constant (equivalent to 600 prad at 1 MHz).

### 2.1.3 Current shunts - Level dependence

#### 2.1.3.1 Introduction

Most of the resistance standards (current shunts) are usually used at one current level or at narrow band current level with non significant changes of resistance value. For resistance standards which are demand for using in large current range it is necessary to know their current level dependence. To this dependence is close related the power coefficient of resistance (PCR).

At national metrology institutes (NMI) dc resistance measurement systems in wide resistance range (from  $0.0001\ \Omega$  up to  $100\ \text{T}\Omega$ ) in high accuracy are used, but mainly for calibration of the resistance standards at one current level or at narrow band current level with non significant resistance changes of used reference standard.

#### 2.1.3.2 Measurement setup

The measurement set up is based on the measurement of ratio of output voltages of the tested and the reference standard by dual channel multimeter as the basic measurement method. Thus, the resistance of tested standard is calculated (2.4):

$$R_X = \frac{U_X}{U_S} \cdot R_S \quad (2.4)$$

The diagram below (Figure 2.4) presents the measurement setup in general.

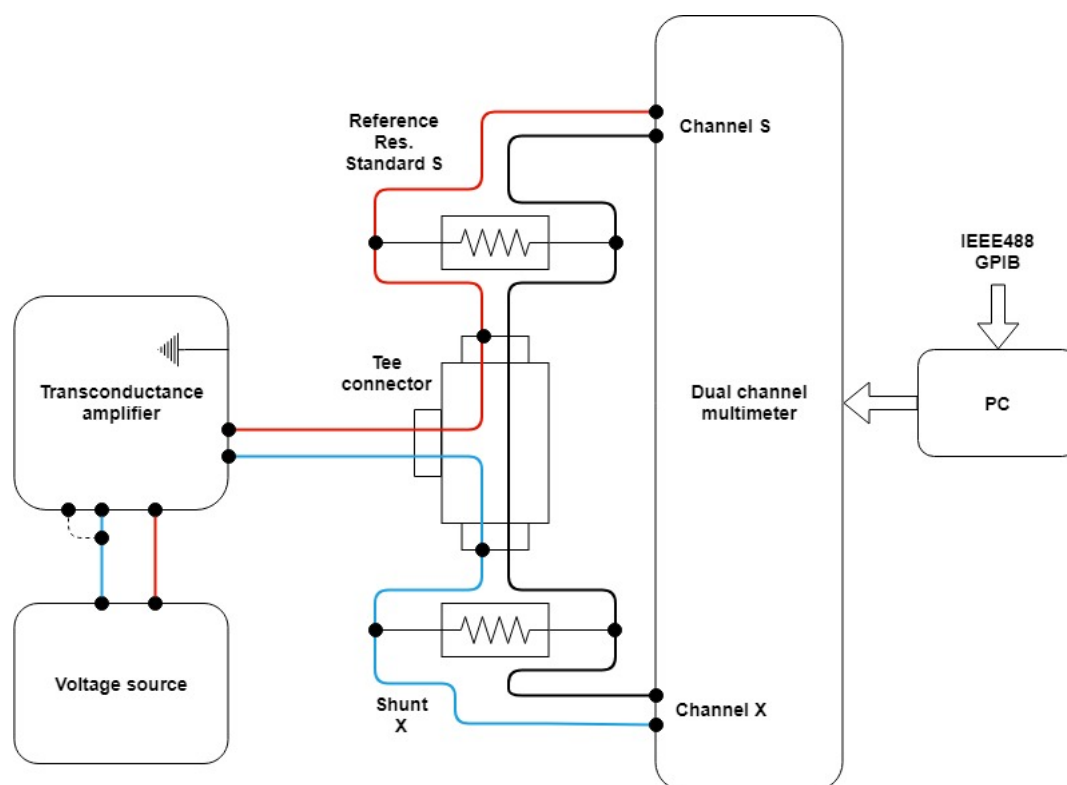


Figure 2.4: Shunt's level dependence measurement setup.

For the voltage measurements the digital multimeters FLUKE 8508A or Wavetek 1281 with math function for immediate calculation of the ratio of the two input channels are employed. As dc current source the transconductance amplifiers Clark Hess 8100 for currents up to 100 A or Wavetek 4600 for currents up to 10 A driven by high accuracy voltage sources (e.g. Wavetek 4808) can be used. It guarantees a high stability of dc current. A stable thermostatic oil bath such as Guildline 9730 CR should be used to place reference resistance standard. For placing a shunt into a temperature-stabilized air bath during characterization of its temperature dependence the MI 9300 may be used.

The heart of this set up is set of working resistance standards ( $0.1\ \Omega$  -  $0.0001\ \Omega$ ) which is used as reference and covers the current range from 1 A up to 100 A.

### 2.1.3.3 Set of resistance standards

Verification of working resistance standards is made in different ways depending on laboratory calibration procedure:

- comparison with primary resistance standards by using measurement of output voltages ratio. These primary standards are also oil filled (placed in the oil bath) and they are periodically calibrated in primary laboratory e.g. using Quantum Hall Effect (QHE). Primary standards are calibrated only at narrow band of current levels with non significant changes of resistance value. Thus, for the verification of one working standard in wide

current range a several of primary standards have to be used. And measured voltage ratio is not equal to 1:1 in all comparisons.

- comparison to the reference standard resistors 1  $\Omega$  using a direct current comparator bridge MI 6010C. Thus some of the working standard could be calibrated in different current levels (from 1 A up to 100 A). Traceability is provided by calibrations of 1  $\Omega$  standard resistors at BIPM. All working and reference standards are oil filled and are placed in the oil bath (with uncertainty contribution two hundredths of degrees of Celsius) during all measurements.

The reference resistance standards should be with a long history of their resistance changes in a time, so for the calculation of the reference value  $R_s$ , the predicted value or correction from the regression can be used.

These standards should be tested on the stability and dependence of their resistance on the current level should be characterized. Thus for the next measurements out of compared currents, the linear approximation can be calculated.

After the characterization of the working standards group the set up was ready to use for the level dependence measurements.

#### 2.1.3.4 Level dependence (power coefficient) measurement

The working standards should be placed in the oil bath. The shunts are air cooled, thus the stability of the ambient temperature in the laboratory is important. A stability equal or less then  $\pm 1^\circ\text{C}$  during the measurements should be achieved which next will be taken into account by uncertainty calculation.

The shunts should be warmed up before measurements depending on their type and construction.

A typical level dependence of current shunts is shown in Figure 2.5 and 2.6. The shape of the characteristic can be monotonous (nearly linear) and/or near of the apex.

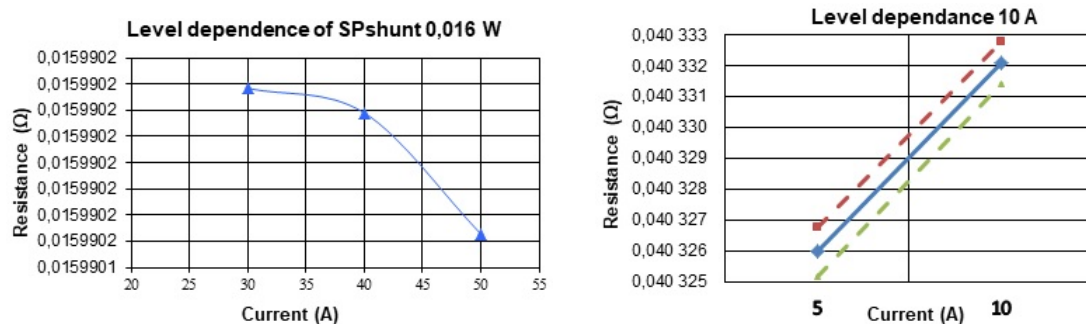


Figure 2.5: Typical level dependence of cage shunt (Left) and Fluke A40A shunt (Right).

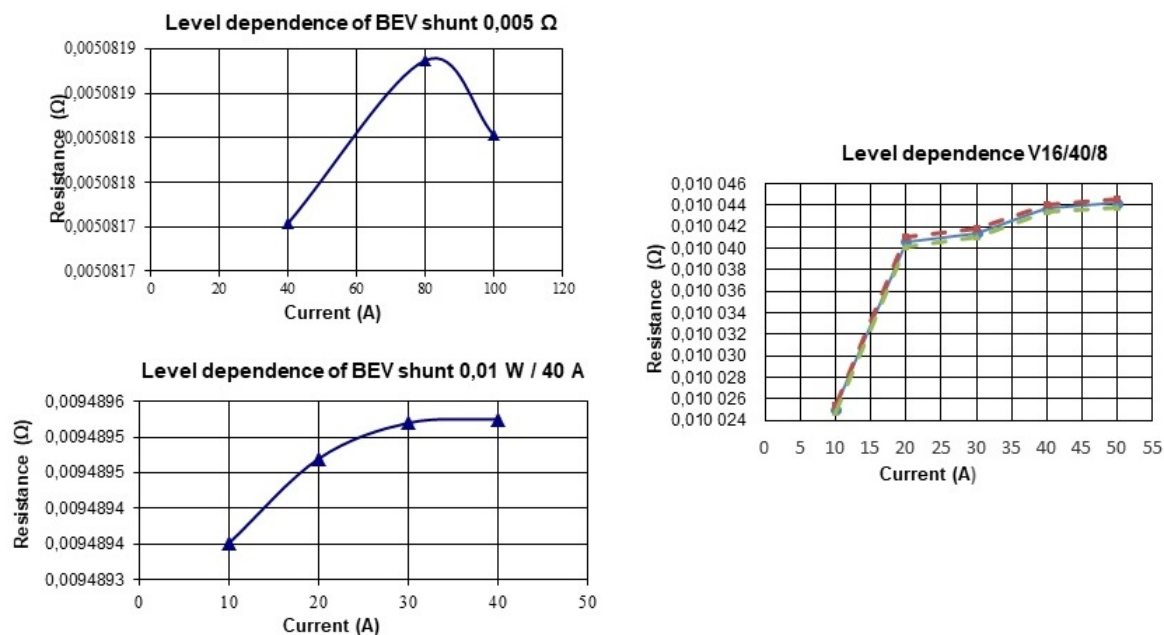


Figure 2.6: Typical level dependence of foil shunt.

The power coefficient  $PC_R$  is calculated according as in (2.5):

$$PC_R = \frac{\Delta R}{\Delta P}, \quad (2.5)$$

where  $\Delta R$  is change of the resistance in power interval  $\Delta P$ .

The power coefficient of measured shunts is calculated in different current ranges 75 % - 125 % and 50 % - 100 % of a nominal current.

If the resistance standard is used in wide current range the whole level dependence should be verified. The knowledge of only a power coefficient does not give the information about the current dependence shape.

### 2.1.3.5 Uncertainty calculation

Typical values for different type of shunts are presented in Table 2.1:

Shunt type	$PC_R$ , ppm/W	Uncertainty, ppm/W
Foil	< 4	< 3.1
Cage	< 1.5	< 1.5
Fluke A40A	< 69	< 9

Table 2.1: Typical power coefficients of different type of shunts.

### 2.1.3.5.1 Dc resistance model

The mathematical model for calculation of dc resistance of the tested shunts is as follows [39] in (2.6):

$$R = \left[ R_s + \delta R_{dr} + R_s \cdot \alpha \cdot (\bar{t} - t_{cal}) \right] \cdot r_c \cdot \bar{r} - \delta R_t \quad (2.6)$$

where:

$R_s$	-	resistance value of the working standard
$\bar{r}$	-	estimation of ratio of output voltage
$\delta R_{dr}$	-	estimation of the working standard drift since last calibration
$\bar{t}$	-	estimation of temperature in the oil bath room temperature
$t_{cal}$	-	calibration temperature of the working standard
$\alpha$	-	temperature coefficient of the working standard
$\delta t$	-	correction due to the thermometer measurements
$\delta R_t$	-	correction of the changes of shunt resistance with temperature
$r_c$	-	correction factor of DMM Fluke 8508 or Wavetek 1281 specifications

Combined uncertainty is calculated as in (2.7) :

$$\begin{aligned} u^2(R) = & c^2(R_s) \cdot u^2(R_s) + c^2(R_{dr}) \cdot u^2(R_{dr}) + c^2(\alpha) \cdot u^2(\alpha) \\ & + c^2(\bar{t}) \cdot u^2(\bar{t}) + c^2(\delta t) \cdot u^2(\delta t) + c^2(\bar{r}) \cdot u^2(\bar{r}) \\ & + c^2(r_c) \cdot u^2(r_c) + c^2(\delta R_t) \cdot u^2(\delta R_t) \end{aligned} \quad (2.7)$$

where:

$$\begin{aligned} c(R_s) &= r_c \cdot \bar{r} \cdot \left[ 1 + \alpha (\bar{t} - t_{cal} + \delta t) \right] \\ c(\delta R_{dr}) &= r_c \cdot \bar{r} \\ c(\bar{t}) &= R_s \cdot \alpha \cdot r_c \cdot \bar{r} \\ c(r_c) &= \left[ R_s + \delta R_{dr} + R_s \cdot \alpha \cdot (\bar{t} - t_{cal} + \delta t) \right] \cdot \bar{r} \\ c(\bar{r}) &= \left[ R_s + \delta R_{dr} + \delta R_v + R_s \cdot \alpha \cdot (\bar{t} - t_{cal} + \delta t) \right] \cdot r_c \\ c(\delta R_t) &= -1 \end{aligned}$$

The analysis of the realized measurements shown that the most significant influences (except working resistance standard calibration and drift) are the temperature influence and standard deviation of the measured voltage ratio.

### 2.1.3.5.2 Power coefficient

The combined uncertainty of the power coefficient measurements is calculated from (2.5) as in (2.8):

$$u^2(PC_R) = c^2(\Delta R) \cdot u^2(\Delta R) + c^2(\Delta P) \cdot u^2(\Delta P) \quad (2.8)$$



where:

- sensitivity coefficients equate to (2.9):

$$c(\Delta R) = \frac{1}{\Delta P} \quad , \quad c(\Delta P) = -\frac{\Delta R}{\Delta P^2} \quad (2.9)$$

- contribution  $\Delta R$  is calculated as in (2.10), where  $u(R_1)$  and  $u(R_2)$  are the uncertainties of the shunt resistance calculated from (2.7):

$$u^2(\Delta R) = u^2(R_1) + u^2(R_2) \quad (2.10)$$

- contribution  $\Delta P$  is calculated as in (2.11), taking into account that  $P = R \cdot I^2$ :

$$u^2(\Delta P) = c^2(R_1) \cdot u^2(R_1) + c^2(I_1) \cdot u^2(I_1) + c^2(R_2) \cdot u^2(R_2) + c^2(I_2) \cdot u^2(I_2) \quad (2.11)$$

- sensitivity coefficients equate to (2.12), where the contribution of  $R_i$  is calculated from (2.7) and the contribution of  $I_i$  is calculated from the specification of dc current source or its calibration certificate :

$$c(R_i) = I_i^2 \quad , \quad c(I_i) = 2 \cdot I_i \cdot R_i \quad (2.12)$$

## 2.1.4 Current shunts - Temperature dependence

### 2.1.4.1 Introduction

The resistance of all resistors varies with temperature. This variation is characterized by the temperature coefficient of resistance (TCR). Its influence is more significant especially for air cooled resistance standards. The TCR is used for making of corrections and/or for the uncertainty calculation.

The measurement setup and characterization of the set of working resistance standards are as described in sections 2.1.3.2 and 2.1.3.3.

### 2.1.4.2 Temperature dependence (temperature coefficient) measurements

The shunts should be tested on the ambient temperature dependence. These measurements are carried out at 1/10 of nominal current to reduce the warming of shunt due to passing current. In addition also the measurements at nominal current level are performed. The temperature range was selected from 18 °C to 30 °C.

The working standards should be placed in the oil bath. The tested shunts should be placed in the thermostatic box, temperature-stabilized air bath or in the laboratory. The temperature uncertainty contribution is taken into account by uncertainty calculations.

As dc current sources the transconductance amplifiers Clark Hess 8100 or Wavetek 4600 driven by a stable dc voltage source can be employed.

The typical  $R(T)$  dependences of measured current shunts are shown in Figure 2.7, 2.8 and 2.9:

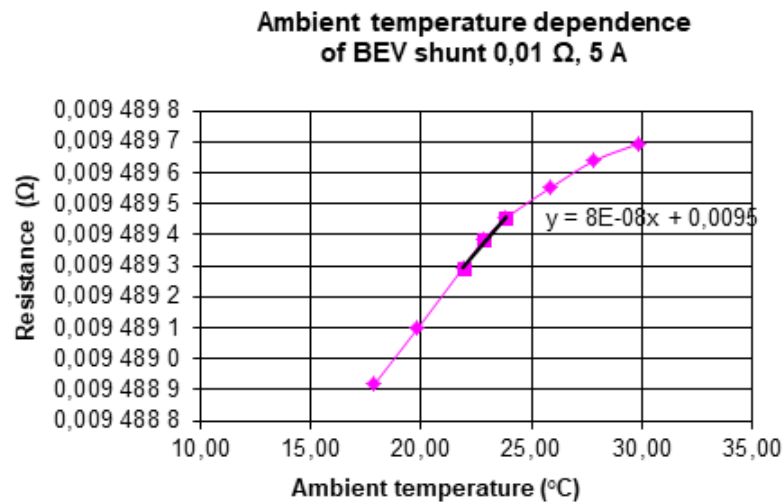


Figure 2.7:  $R(T)$  characteristic of foil shunt.

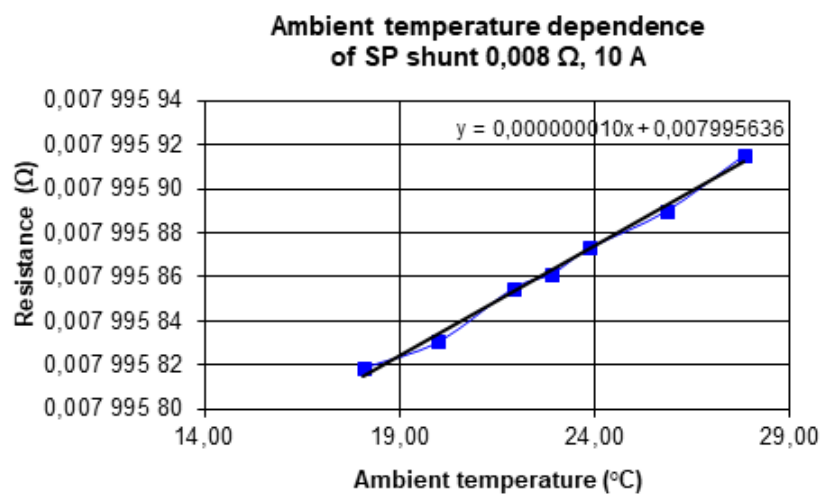


Figure 2.8:  $R(T)$  characteristic of cage shunt.

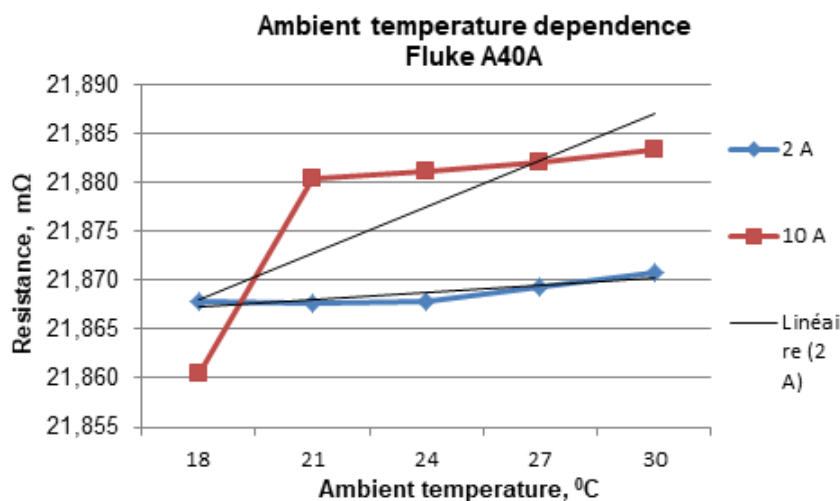


Figure 2.9: R(T) characteristic of Fluke A40A shunt.

The temperature coefficient TCR is calculated according (2.13):

$$TC_R = \frac{\Delta R}{\Delta T}, \quad (2.13)$$

where  $\Delta R$  is change of the resistance in the temperature interval  $\Delta T$ .

### 2.1.4.3 Uncertainty calculation

The typical values of calculated uncertainty of temperature coefficient for different types of shunts are presented in Table 2.2:

Shunt type	TC <sub>R</sub> , ppm/W	Uncertainty, ppm/W
Foil	−2.8 to +8.4	< 2.1
Cage	+1.2 to +1.7	< 1.7
Fluke A40A	+7 to +67	< 10

Table 2.2: Typical temperature coefficients of different types of shunts.

#### 2.1.4.3.1 Temperature coefficient

Combined uncertainty of temperature coefficient measurements is calculated from (2.13) as in (2.14):

$$u^2(TC_R) = c^2(\Delta R) \cdot u^2(\Delta R) + c^2(\Delta T) \cdot u^2(\Delta T) \quad (2.14)$$

where:

- sensitivity coefficients equate to (2.15) :

$$c(\Delta R) = \frac{1}{\Delta T}, \quad c(\Delta T) = -\frac{\Delta R}{\Delta T^2} \quad (2.15)$$

- contribution  $\Delta R$  is calculated according (2.16), where  $u(R_1)$  and  $u(R_2)$  are uncertainties of shunt resistance calculated from (2.7) :

$$u^2(\Delta R) = u^2(R_1) + u^2(R_2) \quad (2.16)$$

- contribution  $\Delta T$  is equal to (2.17), where  $u(T_1)$  and  $u(T_2)$  are calculated from calibration certificate of the used thermometer and/or thermometer specification type PT100.

$$u^2(\Delta T) = u^2(T_1) + u^2(T_2) \quad (2.17)$$

## 2.2 Methods for calibration of voltage dividers

### 2.2.1 Voltage divider - Amplitude

#### 2.2.1.1 Ac-dc difference method

Resistive voltage dividers can be calibrated using traditional ac-dc-difference methods [40]. Figure 2.10 illustrates typical experimental setup employed for direct comparison of ac-dc thermal converters or F792A electronic ac-dc transfer standards. It is based on an automatic ac-dc low electromotive forces comparator, equipped with two synchronized nanovoltmeters.

In the method proposed, a special T-voltage node is used to connect both the inputs of the ac-dc voltage standard and of the device under test. The ac-dc voltage standard is based on a coaxial resistor (CR) connected in series with a planar multijunction thermal converter (PMJTC), instead the device under test consists of a coaxial resistive voltage divider (RVD) connected to a wideband buffer. The output of the buffer is then measured with a calibrated PMJTC or with other thermal voltage converters such as Fluke 792A.

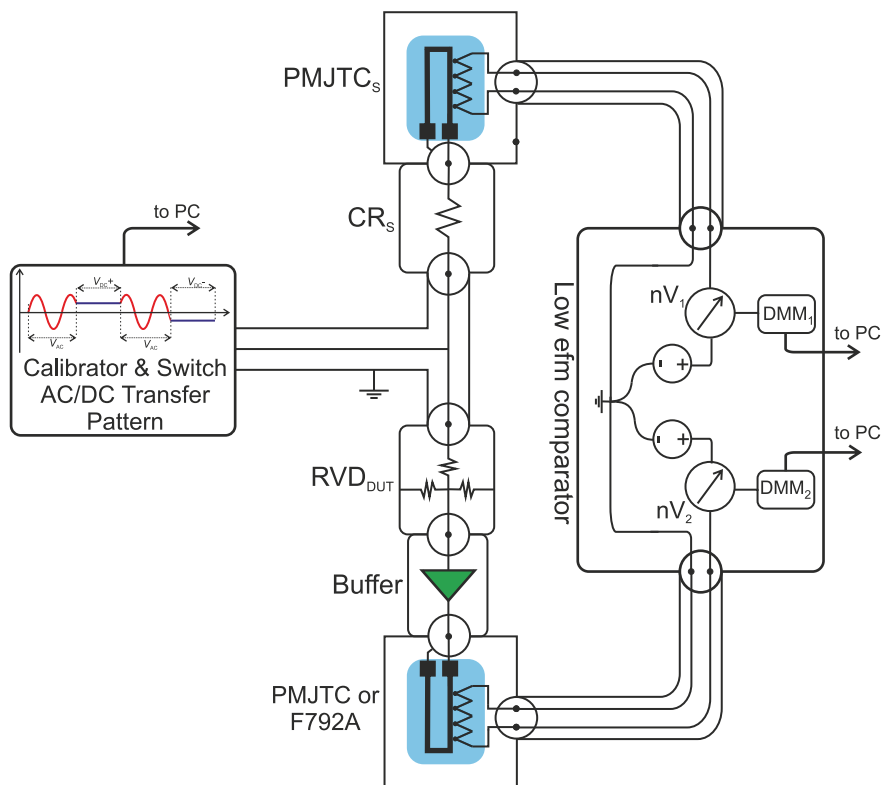


Figure 2.10: INRIM setup based on an automatic ac-dc transfer facility for high precision characterization of ac-dc amplitude error of RVDs and buffers.

### 2.2.1.2 Digitizer method

While the ac-dc difference methods are very accurate, they are generally a quite time consuming, and they require thermal transfer standards which are not available at all metrology labs. A faster and simpler method, although not as accurate, is to use the same digitizers which are used for power measurements. Figure 2.11 shows an example of such a setup. In this figure, the ratio of two voltage dividers are compared. The absolute divider ratio of one divider can be measured by measuring the input and output voltages directly. The divider outputs are measured differentially in this setup to avoid ground loops, but other solutions involving transformers or chokes can also be used.

Another advantage with this setup is that both amplitude and phase response can be measured simultaneously.

The gain of the 5922 digitizer is not as stable as the 3458A DMM. Therefore, it is recommended to include a low frequency point (e.g. around 50 Hz) where the divider ratio can be assumed to be the same as the dc ratio and scale the ac results using the calibrated dc ratio.

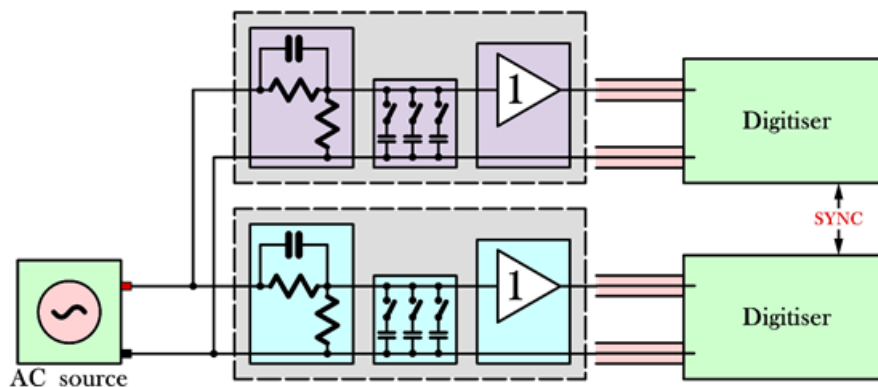


Figure 2.11: RISE setup for wideband calibration of voltage dividers.

### 2.2.1.3 Digital sampling impedance bridge method

Another option for calibration of the dividers is use of a digital sampling impedance bridge [30]. Traditionally, the bridge is used to measure complex voltage ratio of two impedance standards, however the same setup can be used to measure ratio of dividers or direct input-to-output ratio as shown in Figure 2.12. This solution has the advantage the digital bridge (complex voltage ratio measurement system) can be linearized using well characterized or calculable impedance standards as shown in the [30]. Then the ratio of the RVD measured by the linearized setup is traceable to the unit of impedance. The achievable expanded uncertainty at 100 kHz is below  $20 \mu\text{V/V}$  and  $50 \mu\text{rad}$  and at 1 MHz is below  $100 \mu\text{V/V}$  and below  $360 \mu\text{rad}$  for voltage ratios up to at least 1:16. Higher ratio devices can be measured using step-up, i.e. connecting two dividers' inputs in parallel and output to the arms of the bridge.

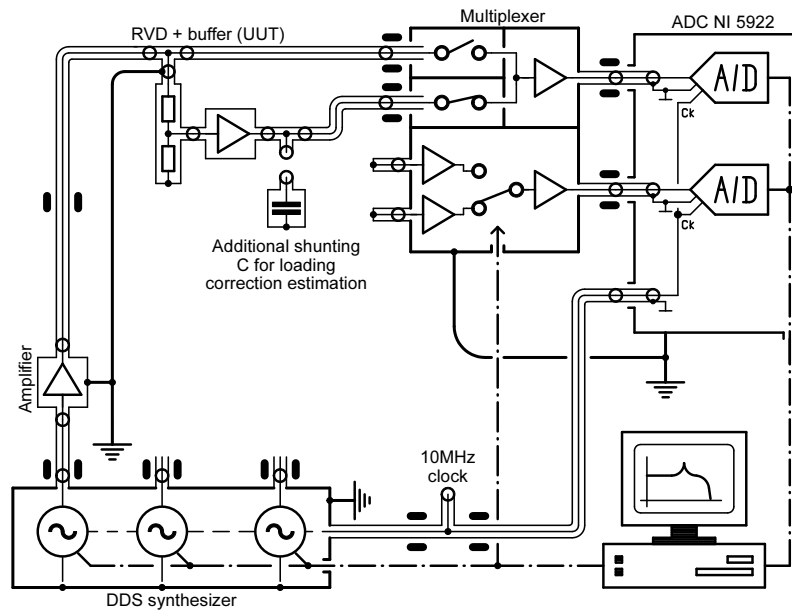


Figure 2.12: CMI setup for calibration of voltage dividers using digital sampling impedance bridge.

## 2.2.1.4 Measurement considerations

### 2.2.1.4.1 Grounding

It is important to avoid ground loops in the signal path of the measurement setup. First because they are sensitive to magnetic field pick-up, second because they can result in undefined current return paths. It is equally important to avoid floating sections in the setup, because they are sensitive to electric field interference and stray capacitance. In the Figure 2.11 setup the digitizer inputs are coaxial contacts with grounded screens (NI 5922 digitizers) and the ac source low output is grounded. This digitizer ground is separated from the current source ground by the differential connection to the shunt outputs. In other setups they may be separated using chokes, transformers or differential amplifiers. The differential connection also forces the current through the divider to return by the input low of the same divider, rather than by the digitizer ground or the input low of the other divider.

### 2.2.1.4.2 Output loading

The instrument measuring the output voltages of the dividers has necessarily a finite input impedance which will load the divider output and change the effective divider ratio. In particular, at high frequencies the capacitance of the digitizer inputs and connecting cables will severely affect the ratio. This is why a buffer amplifier is necessary for accurate high frequency

measurements, to unload the divider output [41] [42]. The buffer amplifier still has a small output impedance which should be taken into account, however. If the divider will be connected the same way for voltage measurements, the loading effect can be considered part of the divider characteristics, and no loading corrections are needed. However, if the divider will be used in another configuration, the output loading must be characterized, and a loading correction applied to the measurement results.

#### 2.2.1.4.3 Digitizer calibration

The digitizer channels must be calibrated for relative gain. For phase measurements the relative channel delays also need to be calibrated. This can be done by simply connecting the same signal in parallel to all channels and comparing the measured signal amplitudes at the frequencies of interest. However, since the channels will measure signals with different voltages, the linearity should also be considered. Calibration of linearity can be done e.g. using ac-dc difference or IVD methods.

See section 2.4 for details about digitizer calibration.

### 2.2.2 Voltage divider - Phase angle error

The phase angle error is typically measured with a digitizer setup, such as the one in Figure 2.11. For phase calibration the capacitive loading is the most important error source. If we assume that the low voltage arm of the divider is  $100\ \Omega$ , a change in capacitive load by  $1\ \text{pF}$  changes the output phase by  $600\ \mu\text{rad}$  at  $1\ \text{MHz}$ . A regular flexible coaxial cable can easily change its capacitance by  $1\ \text{pF}$  just by bending it. Therefore, it is important that the output is connected rigidly to the buffer amplifier, to have a constant capacitive load.

For high ratio dividers the output amplitude is very small compared to the input, which will result in higher noise if the input and output are measured directly. Therefore, it is better to use a step up procedure [9] [42] [40], where the lowest ratio divider is measured directly, and the higher ratios are measured against the next lower ratio divider as a reference.

An experimental setup based on an automatic asynchronous digital phase comparator and the step-up procedure [43] for phase angle calibration of high ratio voltage resistive dividers is shown in Figure 2.13. The setup was used for calibration of coaxial resistive voltage dividers having ratios ranging from 1:3 to 1:52 and voltages from  $3\ \text{V}$  up to  $150\ \text{V}$  and frequencies from  $10\ \text{Hz}$  up to  $1\ \text{MHz}$ .



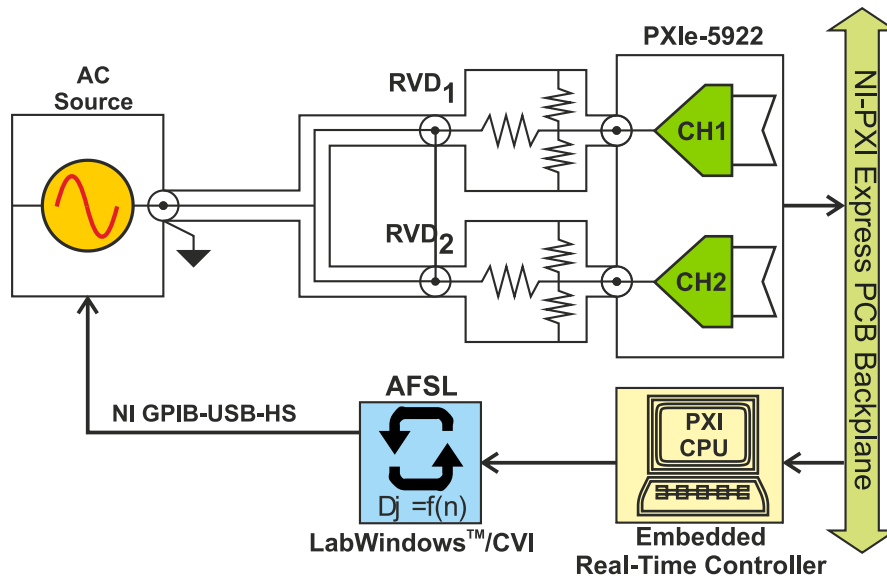


Figure 2.13: INRIM setup for calibration of high ratio voltage dividers.

### 2.2.2.1 Step up method at low frequencies using 3458A

One of the possible ways how to measure phase angle error of the voltage dividers is a step-up method performed directly with the any sampling wattmeter (DSWM) capable of showing phase difference or by TWM tool itself using harmonic analysis algorithms for phase difference estimation.

Block diagram is shown in Figure 2.14. In the first step, both voltage and current channel is connected to the stable function generator or ac calibrator. DSWM correction are cleared, so the system measures pure phase difference. Measured phase error between the channels is marked  $\Delta\phi_1$ . Next, the current channel is connected via the lowest range divider, e.g. 4 V divider. Measurement of the phase is repeated and marked  $\Delta\phi_2$ . In the third step, voltage channel is connected via next higher voltage divider, e.g. 12 V divider and the previous 4 V divider is moved to the current channel. Measurement is repeated once more and result is marked  $\Delta\phi_3$ . Rest of the dividers is calibrated in the same manner.

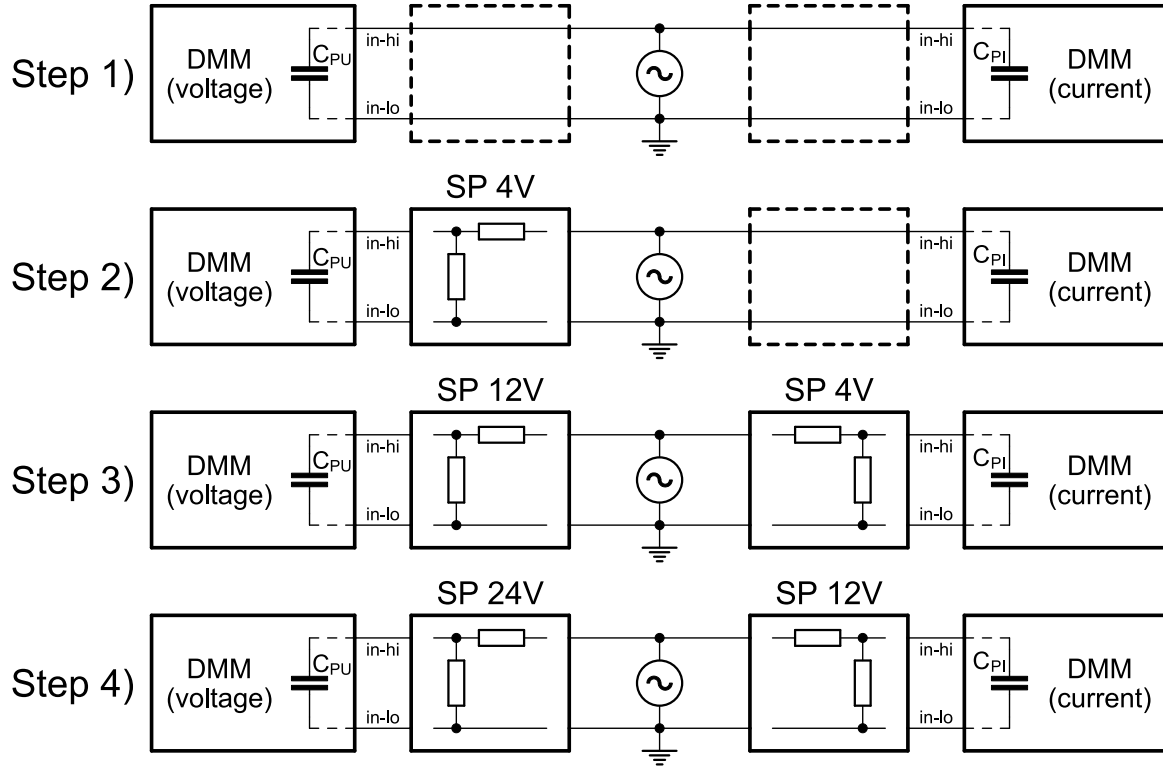


Figure 2.14: Step up method for calibration of phase angle of RVD dividers.

The problem of the method is possible different loading capacitance of both DMMs, i.e.  $C_{PU}$  is not equal to  $C_{PI}$ . For the step 2) the phase error of the 4 V divider is measured directly including the loading effect so no correction is needed, i.e. the absolute phase error of the 4 V divider is:

$$\phi_{E4V} = \Delta\phi_2 - \Delta\phi_1 \quad (2.18)$$

However, for next steps the previously calibrated divider is connected to the current channel so it is loaded by different capacitance. The difference is  $\Delta C_P = C_{PI} - C_{PU}$ . That causes phase shift error:

$$\phi_c = -2\pi f \cdot \frac{R_1 \cdot R_2}{R_1 + R_2} \cdot \Delta C_P, \quad (2.19)$$

where  $R_2$  is lower arm resistor (e.g. for RVDs manufactured by RISE Sweden  $200 \Omega$ ) and  $R_1$  is the upper arm resistor and  $f$  is frequency of the measurement. So for the step 3) the phase angle error of the 12 V divider is calculated:

$$\phi_{E12V} = \Delta\phi_3 - \Delta\phi_1 + (\phi_{E4V} + \phi_c) = \Delta\phi_3 - \Delta\phi_1 + \phi_{E4V} - 2\pi f \cdot \frac{R_1 \cdot R_2}{R_1 + R_2} \cdot \Delta C_P, \quad (2.20)$$

where  $R_1$  and  $R_2$  are upper and lower arm resistors of the divider 4 V. The same technique is used for all following steps. The capacitance correction term  $\phi_c$  can be eventually eliminated by balancing the input capacitances of both DMMs by a small external ceramic capacitor connected in parallel to the input. The set of phase shifts realized using this procedure is already loaded by input capacitance of the DMMs, so no loading correction is needed. If it should be used in TWM tool, the loading correction must be deactivated by simply defining zero input capacitance of digitizer channels (see section 3.2.5.11).

Another approach suitable for TWM/TPQA tools is possible. The step 1) is performed to calibrate and correct for the residual inter-channel phase error (and/or time shift) and also input impedance of both digitizers must be calibrated and applied as the TWM correction. Once the digitizer correction is applied, TWM/TPQA should show zero phase difference. In step 2), the “voltage” channel is loaded with RVD transducer correction file that contains only nominal ratio (e.g. 5.000 for the RISE 4 V divider) and RVD low side impedance estimate (200  $\Omega$  for RISE 4 V divider). All other components of transducer correction are left blank. The phase shift between the “voltage” and “current” channel is measured and applied to the created 4 V transducer correction file as a phase correction (for currently calibrated frequency). If the measurement is repeated with the modified correction file, the phase difference between the TWM channels should again be zero, which is useful check. This method incorporates the “unloading” correction, so the measured phase error is given for no loading condition and can be used normally in the TWM algorithms. Next steps are performed in the same way, i.e. by creating nominal correction file for 12 V divider, loading it to the “voltage” channel and moving the 4 V correction to the “current” channel. Again the phase error is measured and stored to the 12 V correction and check is performed if the residual phase is zero again.

Note the same method is in theory usable even for step-up of voltage ratio, but it depends on the linearity of 3458A, which must be first evaluated. It can be also used for the current shunts as well.

### 2.2.3 Voltage divider - Level dependence

Although the resistive voltage dividers are in principle linear in voltage, there are several mechanisms which can lead to the voltage level dependence:

1. Self-heating of the resistors by the current, which changes the dc and ac resistance of the resistive material.
2. Self-heating of the encapsulation and substrate of the resistors which changes the leakage resistance at high frequencies.
3. Self-heating of the resistor leads which changes the skin depth and therefore the resistance at high frequencies.
4. Voltage dependence of the dielectric in load compensation capacitors or guard capacitors (if any), which changes the phase error
5. Heating by the resistors of the dielectric in capacitors (if any), which changes the phase error.

Different divider designs exhibit these effects to various degrees, and higher voltages give stronger level dependence. It is important to investigate each design to determine which types of level dependence are present, and whether to make corrections or just include it in the uncertainty budget.

- (1.) Dc level dependence

The dc ratio should be calibrated at least at full and half nominal value of the divider. The level dependence is expected to be quadratic. To verify the quadratic dependence a third level can be added, e.g. at 10 % of nominal.

- **(2.) & (3.) Ac level dependence - amplitude**

The ac-dc difference should also be calibrated at full and half nominal voltage. The level dependence may be quadratic, but it may also be more complex. Therefore, more levels should be calibrated if the level dependence is strong.

- **(4.) Linear ac level dependence - phase**

Some divider designs include capacitors in parallel with the resistors in the high voltage arm to compensate for capacitive loads. They may also include a capacitive guard divider to improve frequency response. The resistors and printed circuit board (PCB) also contribute to capacitance. The dielectric materials in the capacitors are in general voltage dependent which can lead to level dependence of the phase response. This dependence is expected to be mainly linear in voltage.

One way to measure this dependence is to switch between different voltage levels and compare the phase response to a reference divider with known level dependence [44]. The switching should be fairly quick – on the order of seconds or shorter – to avoid temperature changes between the different voltage levels. The reference divider can be e.g. a capacitive divider with air dielectric capacitors (GR1404 series or similar) or an inductive voltage divider, which are not expected to have any level dependence.

- **(5.) Quadratic ac level dependence - phase**

The capacitors in the divider are also dependent on temperature. The resistors will not only warm up themselves, but also (with some delay) nearby capacitors, which can lead to a change in phase response. This dependence is mainly quadratic.

A simple method to measure this effect is by a warm-up test [44]. The divider under test is connected to the digitizer, but not to the voltage source. Another divider is connected in parallel to both the source and the digitizer (another channel). The voltage is applied to the second divider and we wait until the divider temperature has stabilised (probably 10 - 30 minutes). Then the divider under test is connected to the source voltage and at the same time the phase difference between the dividers is recorded until it has stabilised. The difference between the initial and the final phase is the power dependence. An exponential decay function can be fitted to the phase curve to determine the time constant of the divider warm-up.

## 2.2.4 Voltage divider - Temperature and humidity dependence

### – Temperature dependence

Like the current shunts, the resistive voltage dividers are sensitive to temperature changes of the environment. This effect is related to the power sensitivity, but it is a concern at all voltage levels. If the divider design consists of identical resistors (from the same production batch) in

the high and low voltage arms, the temperature dependence may be reduced considerably, but it is still important to characterize it. This can be done with a relatively straightforward dc ratio measurement with the divider operating in different temperatures. The voltage for the test should be low enough to avoid self-heating. See also section [2.1.4](#) on temperature dependence of current shunts.

#### – Humidity dependence

Some resistors are sensitive to humidity level in the air. Again, a dc ratio measurement can be used to characterise the humidity sensitivity. However, the resistors can be quite slow to react to humidity changes, and up to several days may be needed for stabilisation. If hermetically sealed resistors are used in the divider design, the dependence on humidity should be insignificant.

## 2.3 Methods for calibration of the DMM (3458A)

### 2.3.1 DMM (3458A) - Frequency response

#### 2.3.1.1 Introduction

The Keysight 3458, used for low band frequency measurement, presents an input impedance for the voltage and current channels. This input impedance modifies the amplitude and phase of the signal to be sampled. For precise measurements this influence must be known and the corresponding correction applied. For amplitude the correction must be determined independently for each DMM. For phase the interest is not the absolute phase shift introduced for each DMM in the input signal but the difference in the phase shift between the two DMMs. This section deals only with the amplitude measurement. Phase measurement is evaluated in a different section of this guide.

#### 2.3.1.2 Equipment

The following equipment is required to perform the frequency response measurements of the DMM 3458.

- **Ac reference source:** To perform this characterization a calibrated voltage source in the frequency range of interest is necessary. For the low frequency this calibration is performed in the frequency range from 10 Hz to 20 kHz. As the current shunts and voltage dividers used in this configuration are typically designed to provide 0.8 V RMS output (peak will not exceed 1.2 V range of DMM) at the nominal value input. The calibration is performed by applying 0.8 V RMS to the 1 V input range. Nevertheless, the frequency response measurement could be performed also at other ranges (i.e. 100 mV, 1 V, 10 V, 100 V and 1000 V) and in this case appropriate levels are also needed in the 10 Hz to 20 kHz frequency range.
- **Calibration of the ac source:** The reference could be defined by ac voltage measurement standard (e.g. Fluke 5790A) or by thermal converters at several frequencies (e.g. 10 Hz, 20 Hz, 60 Hz, 100 Hz, 200 Hz, 500 Hz, 1 kHz, 5 kHz, and 10 kHz). The value that is set on the AC source could be also used as less accurate reference if the top uncertainty is not critical. It is important to note the Fluke 5790A changes its input impedance when performing the reading. This is a problem when source of the voltage has higher output impedance, because the switching of the loading impedance of 5790A causes changes in the applied voltage to the calibrated 3458A. Solution may be to use a 4-wire connection to the source calibrator and enabling remote sensing, which reduces the apparent source impedance, but this method may not work for all calibrators and at all their ranges. Other possibility is to place a buffer between source and the meters, so the source impedance is reduced and loading effects reduced.
- **Sampling DMMs** used for current and voltage channel measurements
- **Data acquisition and Data processing** used in the PQM system

### 2.3.1.3 Procedure

The frequency response can be calibrated using the TWM/TPQA tool itself or by another sampling system (in general DSWM). For each frequency and eventually for each amplitude of interest, the voltage from an AC source is applied to the DMM input. The applied voltage  $U(f)$  is either known from set value on a source or from reference meter connected in parallel to the source. DSWM is configured to the same range, sampling rate and aperture  $T_a$  as will be used for the actual measurement using TWM/TPQA. DSWM is used to read applied rms value  $U_M(f)$ . For low distortion signals with THD below some -60 dB it is possible to use sine fitting and conversion to effective value. The relative calibration gain to be applied as a gain transfer correction to the TWM tool (see section 3.2.5.5):

$$\text{gain}(f) = \frac{U(f)}{U_M(f)}. \quad (2.21)$$

Note if TWM/TPQA is used for the calibration, the systems will by default apply aperture correction (see section 3.2.5.8). That is it will correct integrating ADC intrinsic error, which is function of frequency  $f$  and aperture time  $T_a$ :

$$K(f, T_a) = \frac{\pi \cdot f \cdot T_a}{\sin(\pi \cdot f \cdot T_a)}. \quad (2.22)$$

In such case the measured correction gain( $f$ ) represents the residual error of the DMM, whereas if the correction was disabled, the gain( $f$ ) is total correction of the error including the aperture error. In both cases the TWM/TPQA correction item “Aperture correction” must be set to the same mode as was for the calibration! The correction values when the aperture correction is enabled are expected to be in order of  $10^{-6}$  for frequencies around 50 Hz and apertures around 100  $\mu\text{s}$  which may be a useful indicator of correctness of the obtained corrections.

In theory the frequency response should be identical for all sampling rates and depend only on the aperture time  $T_a$ . However, it was found it slightly depends even on the sampling rate, resp. on the “dead time” between end of integration of one sample and start of integration for the following one [7]. Thus, for the best accuracy it is necessary to repeat the measurement for various used sampling rates at least once to characterize particular instrument’s behaviour.

From the experimental results [45] on the DCV sampling function of several DMM 3458A, the frequency response is very similar for all the time apertures below 100  $\mu\text{s}$  and a different one for all the times aperture above 100  $\mu\text{s}$ . This has to be verified for each specific DMM 3458A so the first calibration will be performed at several  $T_a$ . If the results of this calibration show that the frequency response does not depend on  $T_a$ . The following calibration can be performed only for two time apertures values below and above 100  $\mu\text{s}$  boundary where 3458A changes its integration circuitry.

### 2.3.1.4 Calibration connection

Several calibration connections for frequency response measurements are possible (Figure 2.15, 2.16 and 2.17).

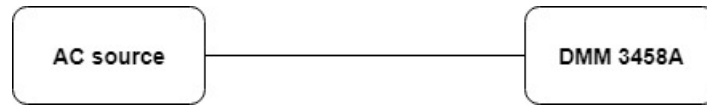


Figure 2.15: DMM 3458A - Frequency response - A simplified calibration connection where AC voltage source is used as a reference.

The DMM 3458A can be connected directly to ac source (e.g. Fluke 5720 calibrator) as in Figure 2.15. The ac source is set to a certain level (depending on the DMM's range of interest) and frequency. The signal is then sampled by the DMM 3458A using desired sampling parameters (aperture time, sampling frequency, number of samples, etc.) which should remain the same during the calibration. Afterwards, the sampled signal is analyzed by one estimating algorithm (e.g. four-parameter sine fitting algorithm [46], phase-sensitive frequency estimation algorithm PSFE [47], etc.) to define the amplitude of the sampled signal  $A_{\text{sampled},f}$ . This procedure is repeated for different frequency, typically in the 10 Hz to 20 kHz range, while keeping the amplitude of the ac source constant. The frequency response at the certain DMM's range is calculated using (2.23), where the  $A_{\text{ref},f}$  denotes the voltage that was set on the ac source (i.e. the reference value). The  $A_{\text{sampled},1}$  and  $A_{\text{ref},1}$  denote the estimated amplitude of the sampled signal and the reference value for the lowest frequency, respectively. Please note that the  $A_{\text{ref},f} = A_{\text{ref},1}$  for this simplified calibration procedure. The same procedure as describe above could be reaped also for other DMM's ranges; only the amplitude of the ac source must be proportionally changed.

$$K_f = \frac{A_{\text{sampled},f} / A_{\text{ref},f}}{A_{\text{sampled},1} / A_{\text{ref},1}} \quad (2.23)$$

The method is very simple and fast. However, the accuracy is limited since the calibrator's output partly varies with the frequency.

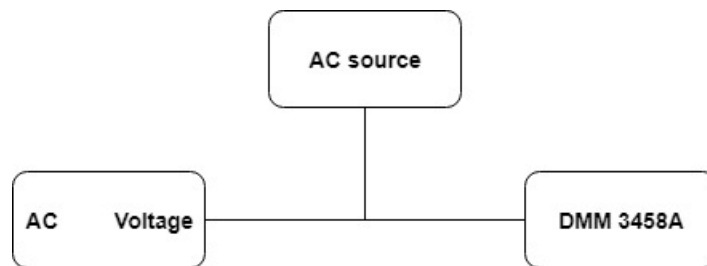


Figure 2.16: DMM 3458A - Frequency response - A simplified calibration connection where ac voltage standard is used as a reference.

Alternatively, the ac voltage standard (e.g. Fluke 5790A) could be used to define the reference value  $A_{\text{ref},f}$  at the certain frequency and level (Figure 2.16). Stable sine-wave signals are generated by the calibrator and connected to DMM and ac voltage standard using coaxial T piece and short cables. Nevertheless, the calibration procedure remains the same as described above. Please note that the  $A_{\text{ref},f} \neq A_{\text{ref},1}$ . The method is also simple and fast with increased accuracy, but it requires the ac voltage standard.



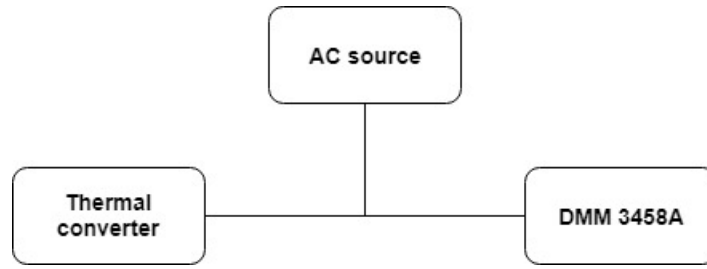


Figure 2.17: DMM 3458A - Frequency response - A calibration connection where thermal converters are used as a reference.

The accuracy of the frequency response measurements could be further improved if the thermal converters instead of the ac voltage standard are used (Figure 2.17). Normally the source used for this characterization is affected by the load. Thermal converters present a low load impedance that modifies the output of the calibrator from the one that is obtained with a high input impedance. Therefore, it is necessary to have the same input impedance used during the calibration of the source. To obtain this condition, a good way is to use a T-piece to connect in parallel the thermal converter and the DMM under test. This configuration is used during the calibration of the source and during the calibration of the frequency response as it is shown in Figure 2.17. This method provides ultimate accuracy but it requires extra equipment. The method is also rather complicated especially since it requires a tricky dc measurement.

### 2.3.1.5 Uncertainty evaluation

The uncertainty evaluation is based on [45].

The output quantity is the gain error of the DMM at a defined frequency  $f$ , time aperture ( $T_a$ ) and temperature ( $T$ ):  $E(f, T_a, T)$

The input quantities are:

- The  $n$  samples taken:  $(V_1, V_2, \dots, V_i, \dots, V_n)$
- The  $n$  time points when the samples are taken:  $t_1, t_2, \dots, t_n$
- The time aperture:  $T_a$
- The temperature:  $T$

The model relating the output quantity and input quantities is as in (2.24):

$$E(f, T_a, T) = A(f) - V_I(f) + C_a(f) + C_{\text{alg}} + C_T + C_R \quad (2.24)$$

where:

- $E(f, T_a, T)$ : DMM gain error for a given frequency  $f$ , time aperture ( $T_a$ ) and temperature  $T$ .
- $A(f)$ : For an specific time aperture ( $T_a$ ) and temperature  $T$ , amplitude value obtained from the  $n$  samples,  $V_n$ , at times  $t_n$ . by means of the estimating algorithm (2.25):

$$A(f) = f_1(V_1, V_2, \dots, V_i, \dots, V_n, t_1, t_2, \dots, t_i, \dots, t_n) \quad (2.25)$$

- \* The function  $f_1$  denotes the estimating algorithm.
- \*  $V_i$ , are the mean dc values obtained by the DAC at time  $t_i$  during the integration time  $T_a$  at temperature  $T$  (2.26):

$$V_i(T_a) = f_2(T_a, t_i) \quad (2.26)$$

- $V_I(f)$  is the reference applied signal from the ac reference standard.
- $C_a(f)$ : The correction term arrives from the fact that the DMM measures the mean value during the integration time and this value is assigned to the mean time of the aperture time  $t_i$ . For a sine signal at frequency  $f$ , there is a difference between the mean value and the signal value at the time  $t_i$ .
- $C_{alg}$ : Correction due to the performance of the applied data processing method other than  $C_a(f)$ .
- $C_T$ : Correction due to temperature influence.
- $C_R$ : Variations in repeated observations under apparently identical conditions.

The source uncertainty evaluation should be done as follow:

- $V_I(f)$  comes from the ac source calibration, according to the method in this section. The ac source is calibrated at several frequencies and by interpolation amplitude and uncertainty at any frequency can be obtained.
- $A(f), C_a(f), C_{alg}$  and  $C_R$ : These components can be obtained following [45].
- $C_T$ : This term can be obtained by multiplying the temperature coefficient uncertainty obtained in section 2.3.5.5 by the estimated temperature variation.

### 2.3.1.6 Results

Typical frequency response of the DMM 3458A for different ranges (i.e. 100 mV, 1 V, 10 V, 100 V and 1000 V) is shown in Figure 2.18. In this case the set voltage on the Fluke 5720 calibrator was used as a reference. The aperture time was  $T_a = 25 \mu\text{s}$ , sampling period  $T_s = 50 \mu\text{s}$  and the number of samples was  $N = 8192$ . The sampled waveform was then analyzed with the PSFE estimation algorithm [47]. The same measurement with exactly the same procedure was repeated but the ac voltage standard Fluke 5790A was used instead (Figure 2.19). Very similar frequency responses were obtained in both cases. There is only a slight difference at higher frequencies above cutoff frequency of the input filter.

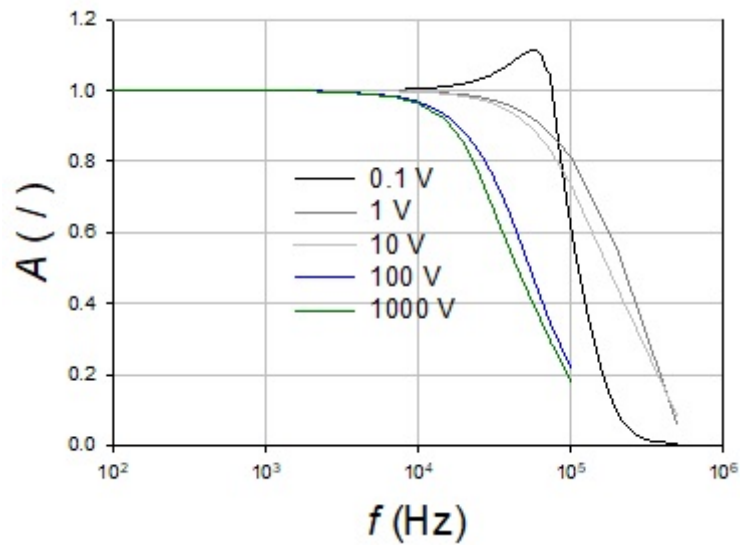


Figure 2.18: Frequency response of the DMM 3458 where the set value on the Fluke 5720A calibrator was used as a reference.

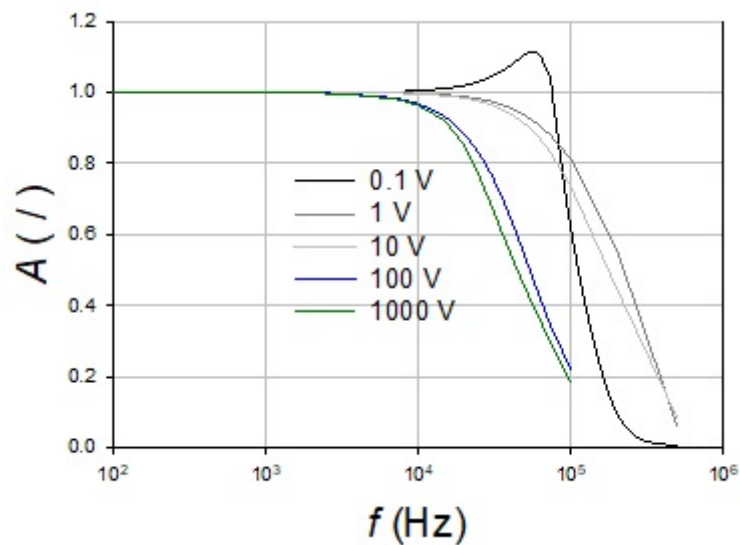


Figure 2.19: Frequency response of the DMM 3458 where the ac voltage standard Fluke 5790A was used as a reference.

## 2.3.2 DMM (3458A) - Dynamic linearity

### 2.3.2.1 Introduction

Current and voltage transducers having voltage outputs around 0.8 V are usually measured by the sampling DMMs at the 1 V range in the DCV function. The frequency response of the DMM at the input voltage levels down to 1 % of the full-scale FS (dynamic linearity) can be

determined by comparison with a calibrated ac-dc transfer standard. At least 5 voltage levels from 100 % FS to 1 % FS should be measured for more accurate interpolation. For example, the ranges of the ac-dc transfer standard Fluke 792A used in calibration are shown in Table 2.3. The input ranges of the ac-dc transfer standard are selected in accordance with the calibration data, applying interpolation between calibration points where necessary [48].

% of FS	Input voltage(V)	Input range of 792A (V)
100	0.8	2.2
50	0.4	2.2
12.5	0.1	0.22
6.25	0.05	0.22
1.25	0.01	0.022

Table 2.3: Input ranges of ac-dc transfer standard.

### 2.3.2.2 Equipment and connection

The automated measurement setup developed for calibration of ac sources has been extended to characterize dynamic linearity of a sampling DMM (Figure 2.20).

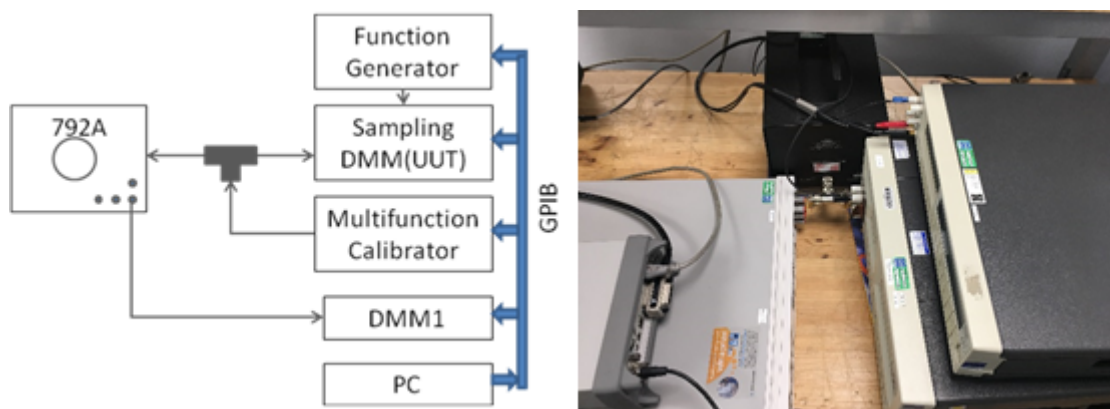


Figure 2.20: Schematic diagram (left) and picture (right) of the measurement setup used in characterization of the sampling DMM - Dynamic linearity.

### 2.3.2.3 Procedure

#### 2.3.2.3.1 Measurement of signals with low harmonic distortion

In measurements of signals with low harmonic distortion ( $THD < 0.1\%$ ) lower sampling rates and longer integration times are applied. For example, the typical sampling parameters are given in [49], see Table 2.4. In the 50 Hz power measurements, characterization of the DMMs at the sampling parameters as given in the first row of Table 2.4 might be enough. However, calibration of the DMMs at different sampling parameters is required for the power measurements at higher frequencies and for characterization of the voltage and current transducers.

Input frequency (Hz)	Sampling time ( $\mu$ s)	Aperture time ( $\mu$ s)
53	400.045	370
100	200.045	170
300	62.545	50
1000	40.045	30
2500	40.045	30
5000	20.045	10
10000	10.045	1.4
20000	10.045	1.4

Table 2.4: Sampling parameters used for measurements of signals with low harmonic distortion.

f, Hz	100% FS	50% FS	12.5% FS	6.25% FS	1.25% FS
53	0.003	0.005	0.006	0.009	0.057
100	0.013	0.010	0.013	0.010	0.059
300	0.002	0.003	0.001	0.008	0.111
1000	-0.031	-0.030	-0.041	-0.027	0.048
2500	-0.285	-0.285	-0.283	-0.281	-0.193
5000	-0.780	-0.778	-0.757	-0.757	-0.711
10000	-2.986	-2.949	-3.029	-3.136	-3.440
20000	-11.291	-11.265	-11.327	-11.438	-11.753

Table 2.5: Ac voltage deviation from nominal value in mV/V.

f, Hz	100% FS	50% FS	12.5% FS	6.25% FS	1.25% FS
53	0.01	0.01	0.02	0.03	0.15
100	0.01	0.02	0.03	0.03	0.18
300	0.01	0.02	0.02	0.03	0.19
1000	0.01	0.01	0.01	0.03	0.11
2500	0.01	0.02	0.02	0.03	0.11
5000	0.01	0.02	0.02	0.03	0.11
10000	0.02	0.02	0.03	0.06	0.27
20000	0.02	0.02	0.03	0.09	0.29

Table 2.6: Expanded uncertainty in mV/V.

As an example, in Tables 2.5 and 2.6, the measurement results and the expanded uncertainties obtained with the previously described calibration setup are shown. The observed frequency dependence (Table 2.5 and Figure 2.21) corresponds approximately to the frequency response of a low pass input filter of the Keysight 3458A DMM. The voltage deviations relative to the 0.8 V input level (100% FS) are presented in Figure 2.22.

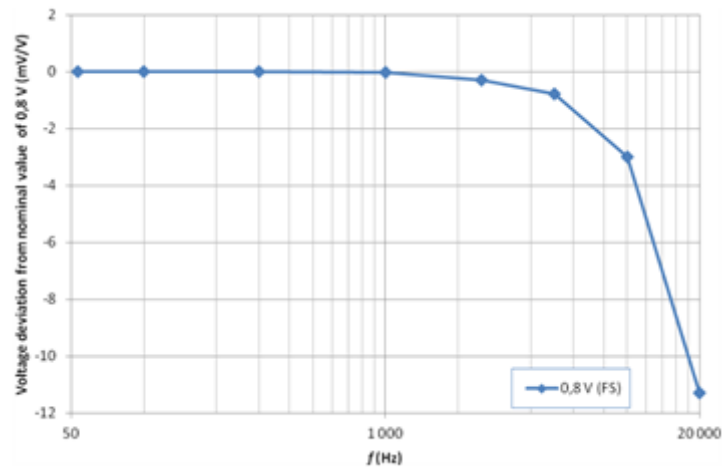


Figure 2.21: Voltage deviation vs. frequency for the input signal of 0.8 V (100% FS).

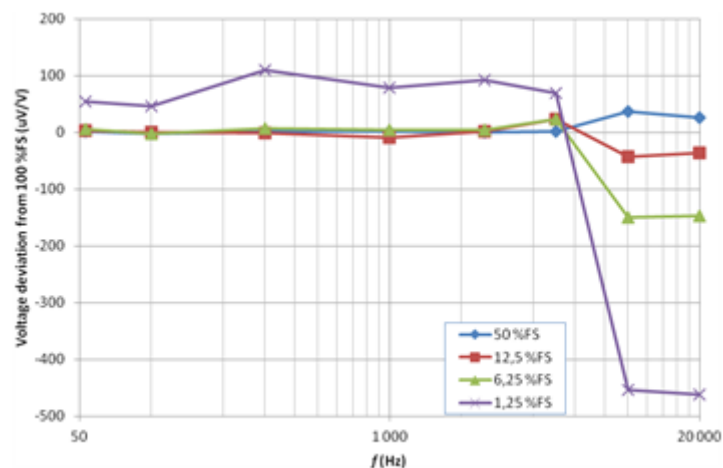


Figure 2.22: Voltage deviation relative to the input signal of 0.8 V.

### 2.3.2.3.2 Measurement of harmonically distorted signals (fixed sampling rate)

In precise measurements of harmonically distorted signals (up to 50th harmonic) higher sampling rates are usually applied:  $f_{\text{sampling}} \geq 500 \cdot f_{\text{signal}}$ . In this mode, the DMM is used and calibrated at a fixed sampling interval, for example  $f_{\text{sampling}} = 25 \text{ kHz}$  (aperture time  $T_a = 20 \mu\text{s}$ ). The measurement results and the associated expanded uncertainty estimates obtained at the fixed sampling rate with the calibration setup described in section 2.3.2.3.1 are presented in Tables 2.7 and 2.8, respectively. The voltage deviation of the input signal of 0.8 V (100% FS) at the fixed sampling rate is shown in Figure 2.23. The voltage deviations relative to the 0.8 V input level (100% FS) are shown in Figure 2.24.

f, Hz	100% FS	50% FS	12.5% FS	6.25% FS	1.25% FS
53	11	14	11	27	41
100	8	7	9	24	42
300	-1	3	2	17	500
1000	-34	-36	-36	-21	-21
1500	-77	-78	-78	-71	-52
2000	-139	-141	-137	-133	-98
2500	-221	-221	-218	-215	-171

Table 2.7: Ac voltage deviation from nominal value (fixed sampling rate),  $\mu\text{V}/\text{V}$ .

f, Hz	100% FS	50% FS	12.5% FS	6.25% FS	1.25% FS
53	10	12	20	34	172
100	13	18	23	33	200
300	13	17	23	29	194
1000	9	10	13	26	106
1500	13	17	19	26	109
2000	13	17	19	26	105
2500	13	17	19	26	108

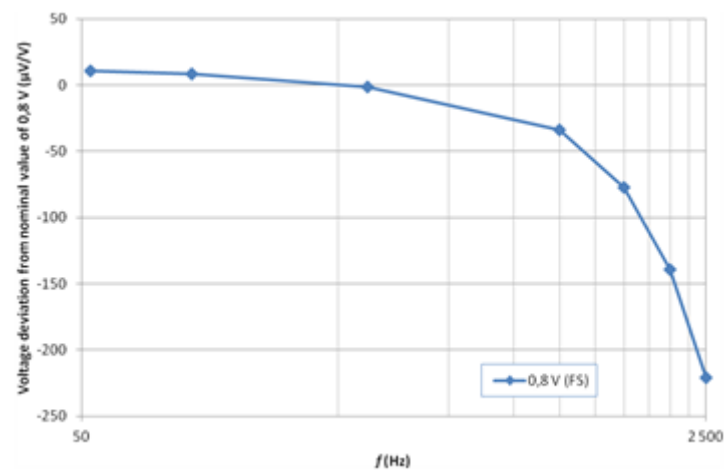
Table 2.8: Expanded uncertainty (fixed sampling rate),  $\mu\text{V}/\text{V}$ .

Figure 2.23: Voltage deviation vs. frequency for the input signal of 0.8 V (100% FS) at the fixed sampling rate.

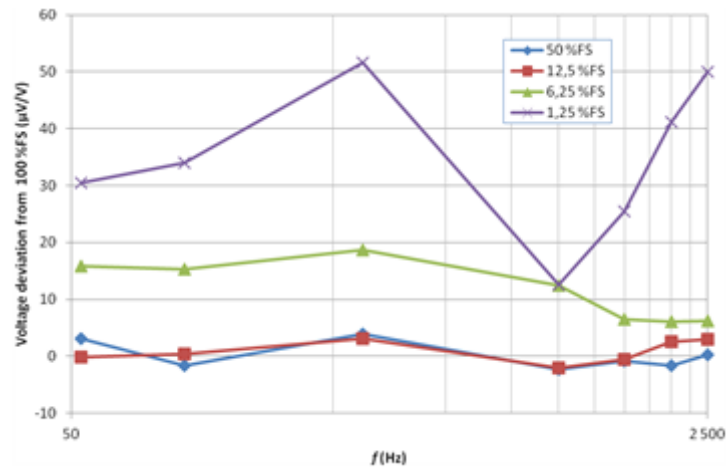


Figure 2.24: Voltage deviation relative to the input signal of 0.8 V at the fixed sampling rate.

#### 2.3.2.4 Amplitude linearity and phase angle dependence

The alternative solution to calibration of a digitizer linearity based in the inductive voltage divider (IVD) is shown in this chapter. When the both voltage and current channel DMMs are used with near full-scale waveforms at its inputs, i.e. with nominal voltage and current at the transducers, the self-calibration of inter channel phase shift is trivial. It can be made by simply connecting the channels to a common source of stable voltage and an inter-channel phase shift can be measured and applied as a correction. The amplitude nonlinearity is also not an issue since the DMM gain can be calibrated at nominal amplitude.

However, when the input voltage or current is not near nominal value it is necessary to consider the amplitude nonlinearity of the DMMs and also a possible dependence of the inter channel phase shift on the ratio of the amplitudes between the two DMMs. For calibration of this dependence a precision inductive voltage divider can be used. Circuit diagram is shown in Figure 2.25. Excitation winding of the IVD and eventual PLL input (depends on synchronization mode of 3458A) is connected directly to the ac voltage source to prevent loading effects. Loading error of the IVD caused by the input capacitance of the DMM is measured and corrected by extrapolation technique, i.e. by repeating the measurement with additional capacitor connected in parallel to the output of the IVD (few hundred of picofarads is convenient value). From known value of the capacitor and known input capacitance of 3458A it is possible to extrapolate correction for virtual no loading of IVD. However the error will be around  $10^{-6}$  for most IVDs.

Example of experimental results are shown in following paragraphs. Two different dividers were used in place of the IVD. For the low frequency a special low frequency 16 Hz to 80 Hz divider with double excitation winding was used. For the 1500 Hz frequency a high precision divider was used. Both dividers have absolute ratio deviation less than  $10^{-7}$  on both in-phase and quadrature component.



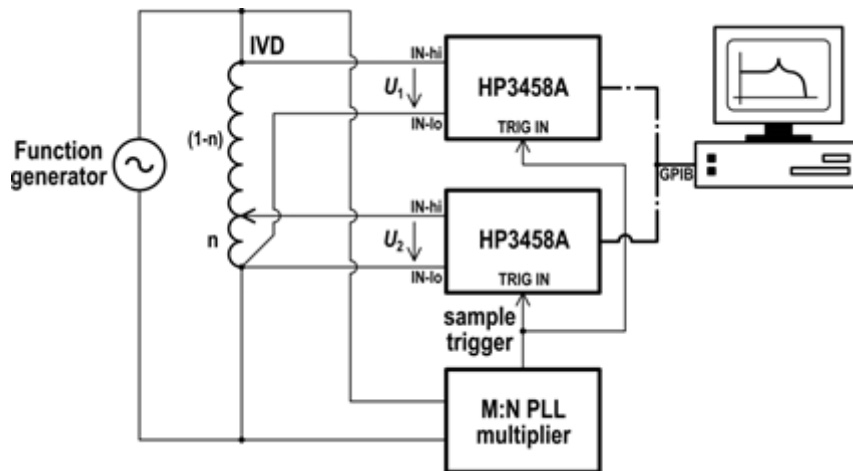


Figure 2.25: Calibration of amplitude nonlinearity and phase dependence of the DMM 3458A.

Because the IVDs have only one decade, the measurement was repeated several times with a different supply voltage and the particular relative dependencies were combined into a single graph. Measured amplitude nonlinearity of the 1 V range at 53 Hz is shown in Figure 2.26 and detailed in Figure 2.27. The error is expressed as a relative deviation from ideal reading of amplitude of the PQM system. The measurement clearly showed the nonlinearity in a RMS voltage range from 300 mV up to 0.8 V (i.e. where the DMM is used), is less than  $3 \mu\text{V/V}$ . Measured phase error dependence on the amplitude at 53 Hz is shown in the Figure 2.28. The error in the range 300 mV up to 0.8 V RMS is up to  $1 \mu\text{rad}$  which is minor source compared to the phase angle uncertainty of the shunts and dividers.

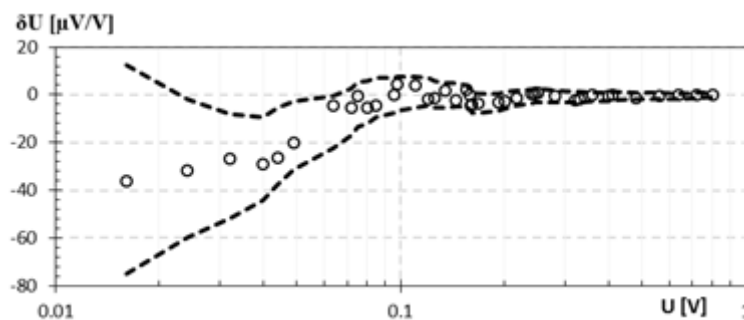


Figure 2.26: Nonlinearity of the DMM 3458A amplitude transfer for 53 Hz. Dashed lines are expanded uncertainty limits.

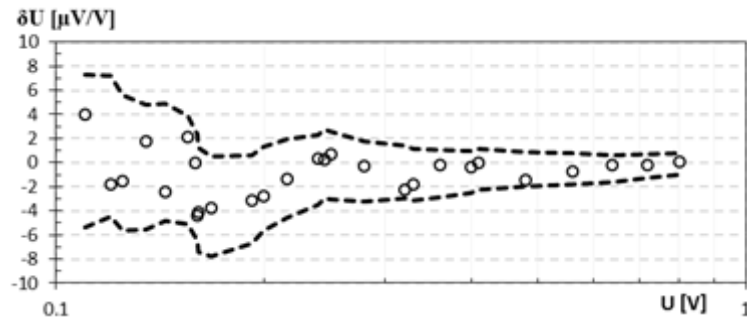


Figure 2.27: Nonlinearity of the DMM 3458A amplitude transfer for 53 Hz (details). Dashed lines are expanded uncertainty limits.

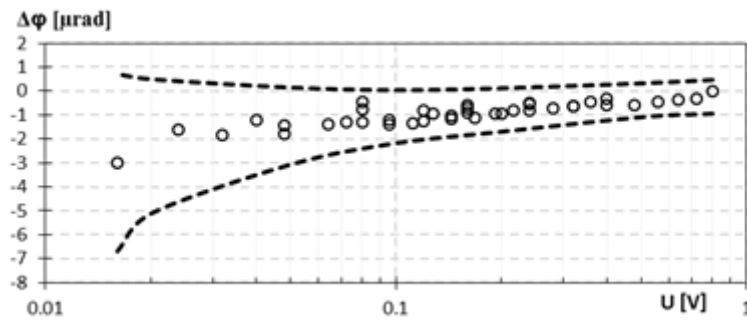


Figure 2.28: Phase shift dependence on the amplitude of DMM 3458A for 53 Hz. Dashed lines are expanded uncertainty limits.

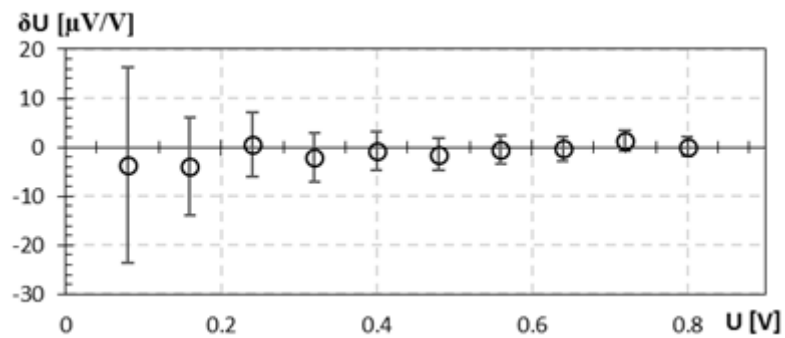


Figure 2.29: Nonlinearity of the DMM 3458A amplitude transfer for 1500 Hz.

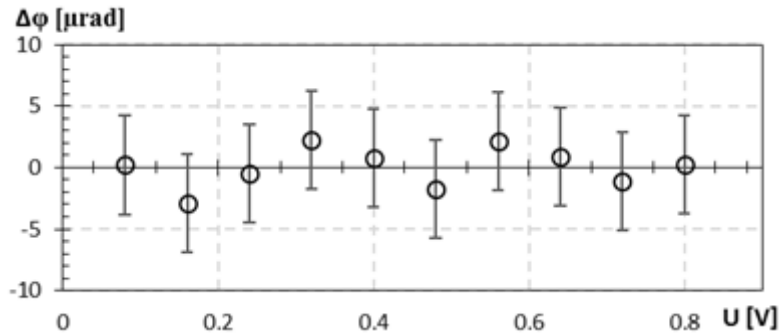


Figure 2.30: Phase shift of the DMM 3458A vs input amplitude for 1500 Hz.

The same measurement was repeated at 1500 Hz however only within a single decade, i.e. from RMS voltage 80 mV to 800 mV. At this frequency the  $\pm 100$  ns sampling jitter of DMMs is much higher compared to 53 Hz so the uncertainty of the phase angle is strongly affected. However, this test is still relevant because of the harmonics measurement. Since in this technique the DMMs measure different amplitudes it is nonsense to perform the calibration without knowledge of eventual inter-channel phase shift dependence on the ratio of the compared amplitudes. Measured amplitude nonlinearity and phase error dependence for 1500 Hz are shown in Figures 2.29 and 2.30 respectively. The same measurement was repeated for the second DMM. However, the results were practically identical (within the uncertainty).

### 2.3.3 DMM (3458A) - Distortion

The sampling systems are often used to measure more or less distorted signals. However, the distortions (harmonics, interharmonics, noise, etc.) do not always originate only from the sampled signal but the sampler itself also introduces a certain level of distortions. Therefore, it is recommended to be aware of this level prior to the sampling and data processing.

The preferred method to measure the DMM's distortions in DCV mode is by applying a pure full scale sine wave signal with much lower noise content and any spurious signals than the distortions contributed by the DMM itself. This requires an extremely clean distortion free signal with a wide range of amplitudes in the audio frequency range [50]. One such source is a spectrally pure Josephson arbitrary waveform synthesizer (JAWS), which can provide adequate signal in audio frequency range, but currently only for amplitudes below one volt [51].

In our study we used the 1 V JAWS system with 63,000 SNS Josephson junctions. Sine waveform with an output voltage of 150 mV RMS and frequency of 52 Hz was synthesized [50]. Due to the small sigma-delta modulator code amplitude of about 10.8 %, no compensation signal was applied [52]. Nevertheless, all distortion components were kept below the noise floor level of -159 dBV (FFT spectrum at  $N = 5000$ ), which corresponds to the SNR of around 112 dB. These JAWS generated signal parameters were additionally verified with a NI PXI 5922 sampler at 10 V range, 1 MOhm input impedance and sampling rate of 500 kS/s [51].

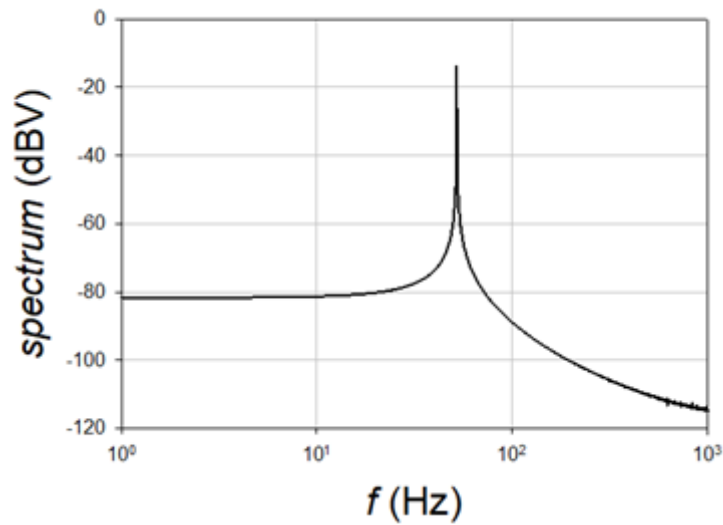


Figure 2.31: Spectrum of the sampled signal generated by the Josephson source (150 mV RMS, 52 Hz). The signal was sampled at  $T_s = 420 \mu\text{s}$  and  $T_a = 120 \mu\text{s}$  using  $N = 23810$  samples.

The spectrally pure sine wave signal (150 mV RMS, 52 Hz) has been sampled with the DMM 3458A at 1 V range (Figure 2.31). The sampling period, aperture time and number of samples were  $T_s = 420 \mu\text{s}$ ,  $T_a = 1.2 \mu\text{s}$ ,  $N = 23810$ , respectively. After the sampling, a phase sensitive sine-fit algorithm (PSFE) [47] was used to estimate sine wave parameters from the sampled data. The estimated sine wave signal was then numerically subtracted from the original sampled data. The remaining signal was analyzed with Fast Fourier Transform to retrieve residual distortion spectra [50] (Figure 2.32). The peak of the remaining spectrum is about 105.8 dBV lower than the peak of the original spectrum containing the whole sampled signal. The difference was even slightly higher when another DMM 3458A was used for sampling.

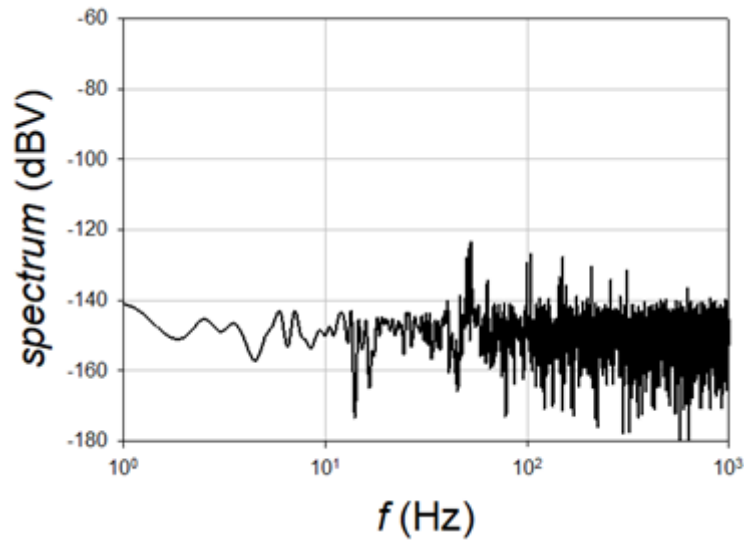


Figure 2.32: The spectrum of the remaining signal when the estimated fundamental signal (i.e. 150 mV / 52 Hz) was subtracted from the original sampled signal. All distortions are more than 105 dBV below the level of the fundamental signal.

### 2.3.4 DMM (3458A) - Evaluation of the stability

The long-term stability of a sampling DMM can be evaluated by performing two calibrations of the frequency dependence in the 1-year time interval. The measurement results for two sampling modes obtained by the calibration setup as described in Section 2.3.1.3 are shown in Figures 2.33 and 2.34.

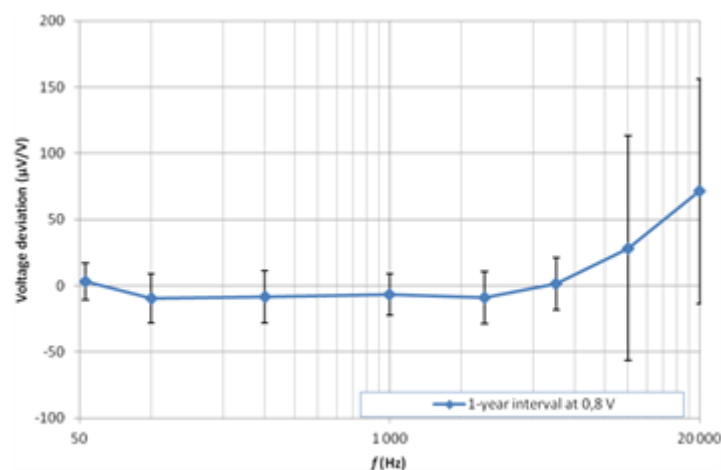


Figure 2.33: Voltage deviations and expanded uncertainties at 0.8 V input voltage for 1-year calibration interval (low harmonic distortion mode).

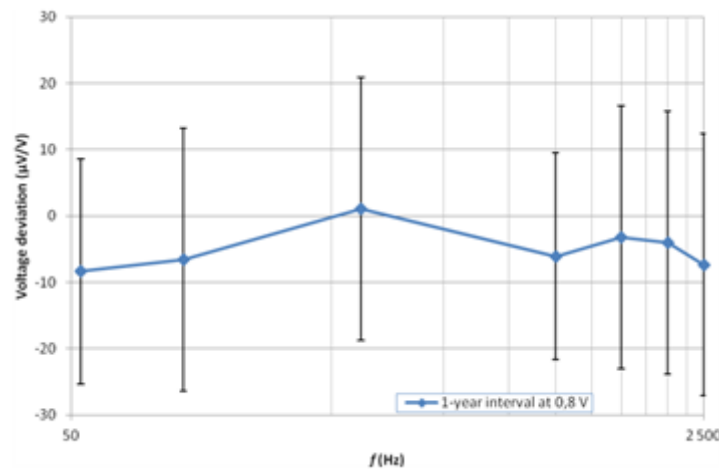


Figure 2.34: Voltage deviations and expanded uncertainties at 0.8 V input voltage for 1-year calibration interval (fixed sampling rate mode).

The observed voltage deviations are within the measurement uncertainties. The slight increase in deviation at the higher frequencies is, probably, caused by the different cabling between the DMM and the thermal transfer standard used in the two measurements: 60 cm banana type leads (Fluke 5440A-7004) and N-type coaxial T-piece.

## 2.3.5 DMM (3458A) - Temperature dependence

### 2.3.5.1 Introduction

Experimental results have shown [53] that the DMM 3458A has a temperature coefficient that is different for each particular DMM and that can be in the order of  $10 \mu\text{V}/\text{V}^{\circ}\text{C}$  for aperture times below  $100 \mu\text{s}$ . The temperature coefficient is lower than  $1 \mu\text{V}/\text{V}^{\circ}\text{C}$  for aperture times above  $100 \mu\text{s}$ .

The DMM 3458A has a sensor that provides the internal temperature measurement, this value should be obtained during the sampling.

The temperature coefficient should be determined for each DMM used in the measurement system and correction applied to the output data.

If the DMM internal sensor is going to be used, this sensor must be calibrated by comparing the external temperature measured with a precise temperature standard. This comparison must be done after waiting enough time for internal thermal stabilization.

### 2.3.5.2 Equipment

- **A stable source:** The measures will take several hours so it is important that the source variation should be lower than  $0.5 \mu\text{V}/\text{V}$ . For a dc source a Zener can be used. For ac

source it will be necessary to check the stability of the source from time to time during the temperature coefficient measurements.

- **Climatic chamber:** A validated climatic chamber with a temperature stability and homogeneity in the order of  $0.2^{\circ}\text{C}$ . Ideally the chamber will have enough homogeneous area to perform the characterization of the two DMMs at the same time.
- **Sampling DMMs** used for current and voltage channel measurements.
- **Data acquisition and Data processing** used in the PQM system.
- **A calibrated precise temperature sensor** to measure the internal chamber temperature. This will be used to calibrate the DMMs internal temperature sensors (PT-100).

### 2.3.5.3 Procedure

The chamber temperature was varied from  $20^{\circ}\text{C}$  to  $26^{\circ}\text{C}$  in  $1^{\circ}\text{C}$  steps (Figure 2.35). At each point, to get the thermal equilibrium the temperature set point is maintained during 4-8 hours. After the stabilization time the temperature of the probe is saved and the sampling measurement are performed for the set of aperture times to be used on the PQM. Two cycles are recommended, the first one starting at  $20^{\circ}\text{C}$  and going up to  $26^{\circ}\text{C}$  and the second one starting at  $26^{\circ}\text{C}$  and going down to  $20^{\circ}\text{C}$ . The values should be the same for both directions.

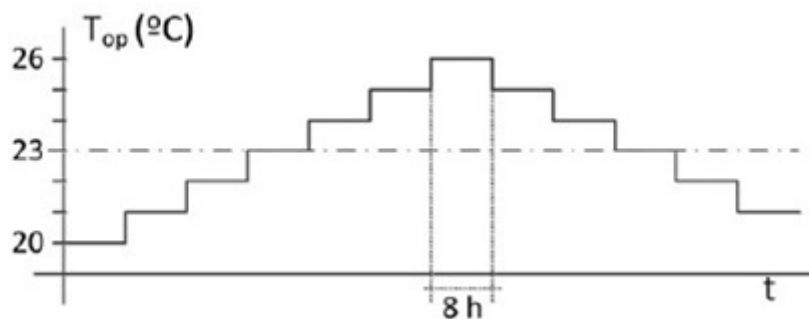


Figure 2.35: DMM 3458A - Temperature dependence - Recommended temperature profile in the climatic chamber.

### 2.3.5.4 Calibration connection

Figure 2.36 shows the calibration connection:

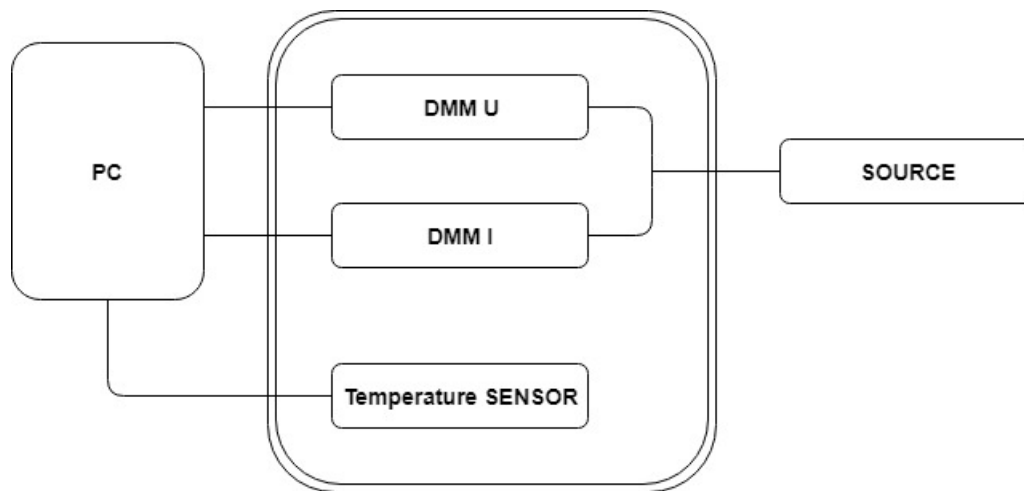


Figure 2.36: A calibration connection for measuring temperature dependence of DMM 3458.

#### 2.3.5.5 Uncertainty evaluation

The uncertainty contributions for this method arise from:

- Temperature stability and uniformity of the climatic chamber and the calibration uncertainty of the thermometer controlling the temperature inside the chamber.
- Standard deviation due to sampling method.
- Uncertainty of linear regression performed for each  $T_a$  value to obtain the temperature coefficients.

#### 2.3.6 DMM (3458A) - Input impedance

TracePQM algorithms supports automatic correction of loading errors caused by the finite input impedance of the digitizer and cable. In order to use the correction, user must calibrate input impedance of the digitize channel.



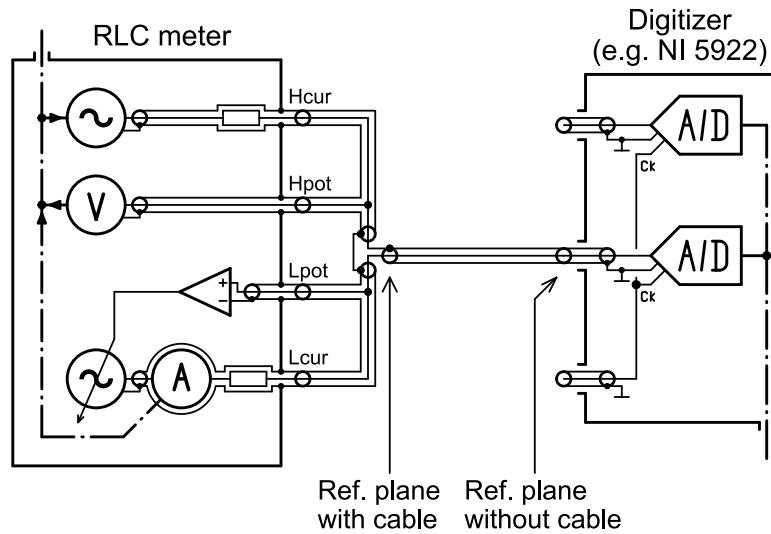


Figure 2.37: Example of measurement of a input impedance of the digitizer 3458A using autobalance bridge.

Measurement of input impedance of floating digitizer such as 3458A is a trivial task as it can be connected to the RLC meter directly as shown in Figure 2.37 using e.g. Keysight E4980A bridge. Note before such measurement it is important to switch the 3458A to the particular input mode and range that will be used for the actual measurements. The example in Figure 2.37 shows two possible reference planes: (i) At the terminals, which means the OPEN and SHORT correction of the RLC bridge is made at the right side of the coaxial cable; (ii) Including the cable to the input of the digitizer, which means to perform OPEN and SHORT of the RLC bridge at the 4TP to coaxial adapter.

Alternative procedure using TWM tool itself is explained in section 2.4.6. Example of measured input impedance of the 3458A is shown in Figure 2.38.

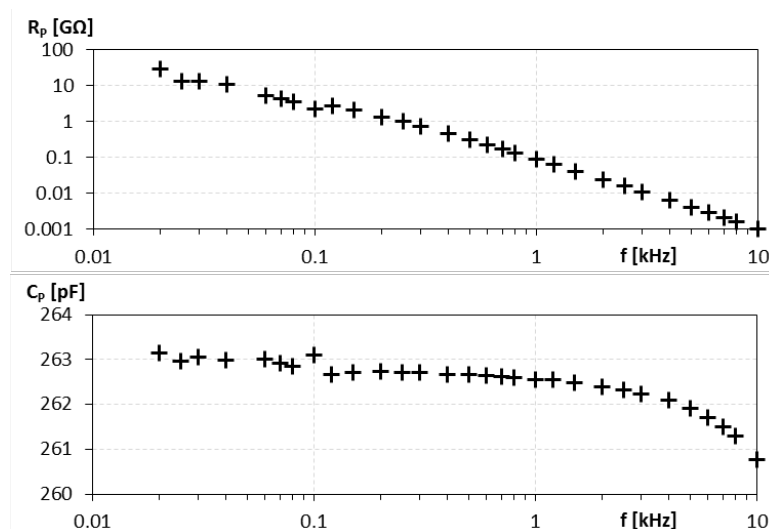


Figure 2.38: Example of measured input impedance of the digitizer 3458A using autobalance bridge. DMM was set to DCV mode and 1 V range.

## 2.4 Methods for calibration of the digitizers (NI 5922)

The heart of wideband commercial power meters consists of a fast digitizer combined with wideband voltage dividers and current shunts, which are used to convert input current and voltage signals into the input voltage levels of the digitizer. For calibration of such power meters, a reference system is needed, where again a digitizer plays an important role. A commercial wideband digitizer (NI PXI-5922) has been characterized for this purpose in the frequency range of 10 Hz to 1 MHz [5].

The National Instruments PXI-5922 two-channel high-speed digitizer [15], which was housed in a PXI-1082 chassis has two ranges, i.e., 2 Vpp and 10 Vpp, and can be operated at sampling rates from 50 kSa/s with 24 bit resolution up to 15 MSa/s with 16 bit resolution. The precise properties of the digitizer NI 5922 have been found to depend on the sampling rate, which is caused by the variable anti aliasing FIR filter. It is thus necessary to pick limited number of fixed sampling rates for certain ranges of measured frequencies and perform the characterization at these rates. Although it is possible to measure 50 Hz signal at 10 MSa/s, it is not advised as the amount of sample data to process would be too high. On the other hand most of the algorithm needs oversampling (ratio:  $0.5f_s/f_0$ ) of at least 5, so the sampling rate must be always significantly higher than measured frequency components. Thus, the typical combinations to be chosen are e.g. 100 kSa/s for frequencies up to 10 kHz, 1 MSa/s for frequencies between 10 Hz and 100 kHz, and finally 10 MSa/s for frequencies from 100 kHz up to 1 MHz. In this way, an oversampling ratio of at least 5 is reached over the complete measurement frequency range.

Five type of characterization methods are advised in order to calibrate NI 5922. These are “Frequency Response”, output/input gain relationship on entire frequency domain, “Level Dependency”, changing of frequency response on different input voltage levels, “Phase Angle error between channels”, in terms of radian/Hertz, “Distortion”, to use SINAD is better and “Evaluation of the stability for phase and amplitude”, middle-term, day-to-day input channels behavior of the digitizer. The calibration setup that can be used for all of them is shown in Figure 2.39.

The suggested system consists of one high accuracy multifunction calibrator, Fluke 5720A, the best device of the shelf, for use as input signal source, one ac measurement standard, Fluke 5790A, for input voltage level measurement, an arbitrary waveform generator, e.g. LeCroy ArbStudio 1104 and a multifunction calibrator, Datron 4808, in order to provide synchronization to make coherent sampling and finally NI 5922 device under test mounted in the chassis. With this setup/system, all characterization methods can be performed without any modification.

All measurements to be presented are carried out with single-frequency low noise sinusoidal signals with synchronization between the digitizer and the signal source. Datron 4808 calibrator in conjunction with LeCroy DAC is used for synchronization of measurement and signal generation. Measurements are performed only at calibrated values of ac measurement standard (ACMS) 5790. Since the measurement is coherent, FFT and RMS formulas are used for evaluating the results. In the final power measurement application, cables between the voltage and current transducers and the digitizer are unavoidable. Since cables also affect the measurement results, a 0.5 m BNC cable was connected to each digitizer input and consider as an internal part of the digitizer.

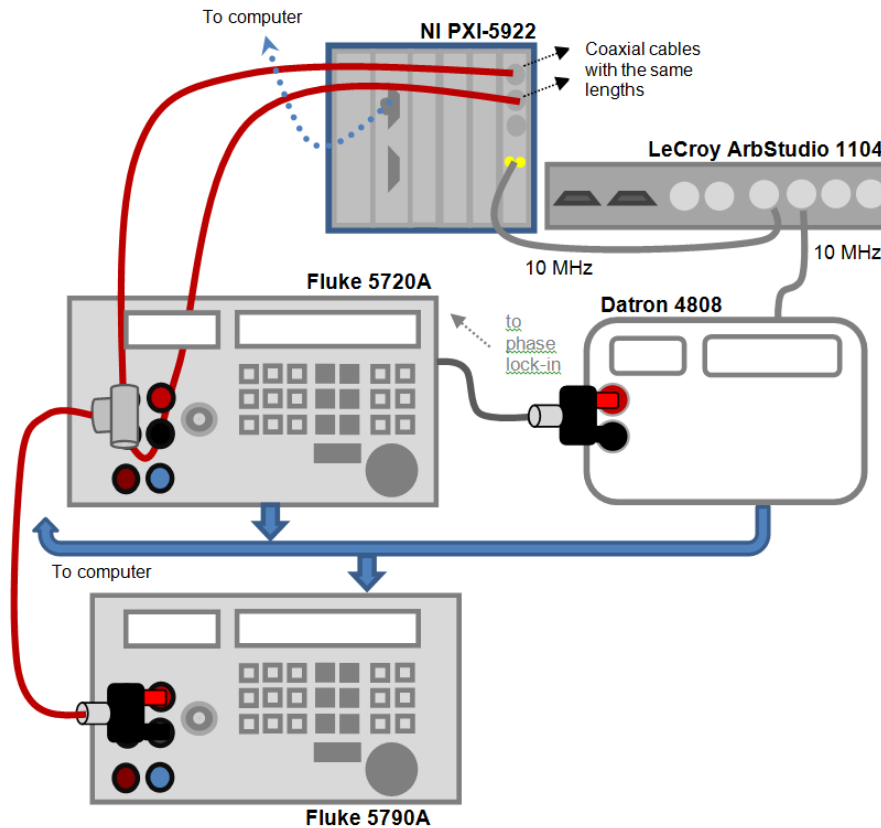


Figure 2.39: Calibration setup for characterization of NI 5922 wideband digitizer.

Measurement software has been developed, providing a simultaneous read out of the two digitizer channels. The software subsequently calculates the root-mean-square (RMS) voltage and, using a Fast Fourier Transform (FFT), the phase between the two channels [5].

### 2.4.1 Digitizer (NI 5922) - Frequency response

In general, frequency response of any system/device is the measurement of the output frequency spectrum in response to a given signal with a known voltage. This response can be drawn as a graph which has a vertical axis that represents the input voltage level, a horizontal axis that represents the frequency.

In order to determine the output spectrum of a digitizer, a frequency and level controlled signal generator is used to generate the input signal. After applying the single tone sinusoidal input signal to the digitizer, the sampled values are collected from the digitizer and the RMS value of the input signal are determined using FFT transformation of these sampled values. Since only one frequency component exists in the input signal, the biggest one of the FFT components represents the peak value of the input signal level at the frequency applied. Also, RMS value can be computed from the definition of RMS, which is used here. The ratio of the RMS of the measured voltage to the RMS of the applied signal voltage gives the frequency response of digitizer at applied frequency and voltage level. This process is repeated in the entire operating

frequency spectrum of the digitizer. Frequency response curves are generally shown in dB format at the vertical axis and logarithmic scaled frequency format at the horizontal axis.

Although this is a simple method in general, it is not enough for characterizing the frequency response of the high accuracy digitizers such as NI PXI-5922. The input signal level must be measured with an ac measurement system to be sure of the actual applied voltage level, even if the source is the high accurate calibrator. At this point it is relevant to mention the most common ACMS Fluke 5790A/B has unpleasant feature of time varying input parallel resistance. It varies during each readout, which leads to a variable loading of the source and thus changes in applied voltage to the digitizer. Reading from the NI 5922 and ACMS is never fully synchronous, so this variation must be suppressed either by placement of a low output impedance buffer between source and NI 5922 with ACMS as shown in Figure 2.40, or by a careful evaluation of the loading effect based on the impedance model of the circuit. The example of the observed resistance jumps at 1 MHz on one piece of Fluke 5790B was roughly 66 to 660 k $\Omega$  and  $\pm 1.5$  pF, so with output impedance of a source just 10  $\Omega$ , which is realistic value at low voltage ranges of calibrators Fluke 5720A, it still changes the applied voltage by some 150  $\mu$ V/V. If it is not corrected, it should be at least taken into account as uncertainty.

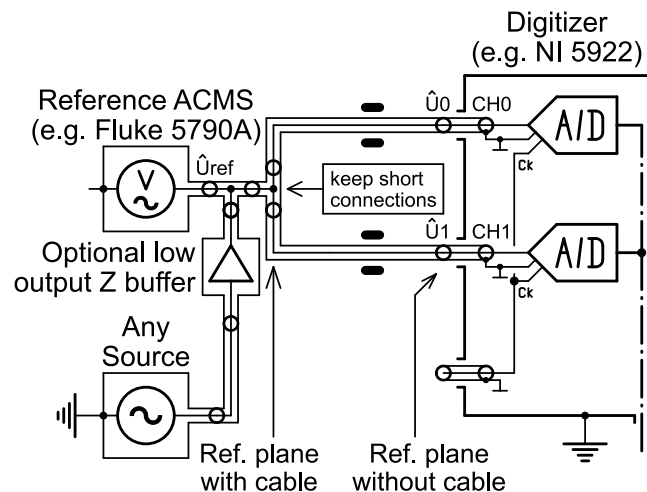


Figure 2.40: Calibration of NI 5922 gain and phase using any source and precision ACMS to measure reference applied voltage. Optional buffer reduces changes in the applied voltage due to the time varying input impedance of the ACMS.

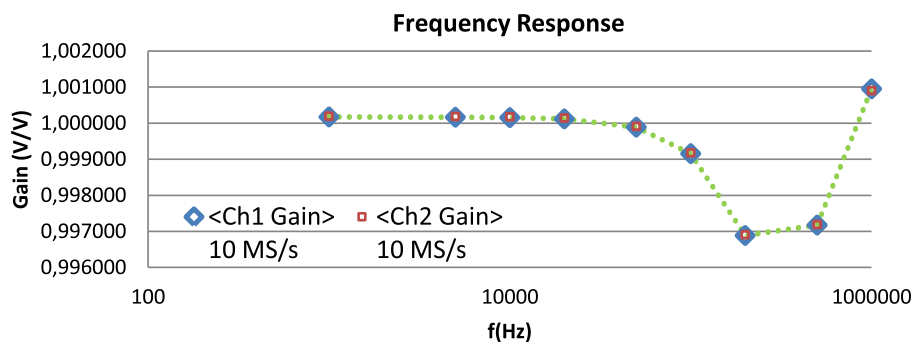


Figure 2.41: NI 5922 Frequency Response Measurements for sampling rate 10 MSa/s.

Example of the measured response for 10 MSa/s sampling rate is shown in Figure 2.41. The calibration was performed using RMS values according formula:

$$\text{gain} = \frac{U_{\text{NI5922 rms}}}{U_{5790}}. \quad (2.27)$$

Note the difference between RMS and amplitude evaluation will be negligible as long as THD of the source is lower then some 60 dB.

## 2.4.2 Digitizer (NI 5922) - Level dependence

Several calibration setups for linearity measurements are possible (Figures 2.42, 2.43, 2.44, 2.45). The NI-5922 digitizer can be connected directly to ac source (e.g. Fluke 5720 calibrator) as shown in Figure 2.42. The ac source is set to a certain frequency of interest and different levels (i.e. the reference values). The applied signal is than sampled by the digitizer using desired sampling settings (triggering, sampling frequency, number of samples, etc.) which should remain unchanged during the calibration. Afterwards, the sampled signal is analysed by the estimating algorithm (e.g. four-parameter sine fitting algorithm [46], phase-sensitive frequency estimation algorithm [47], etc.) to define the amplitude of the sampled signal. This procedure is repeated for different levels of interest, while keeping the frequency of the ac source constant. The method is relatively simple and fast, it requires the equipment which is readily available in different laboratories and it covers a variety of different levels and frequencies. However, the accuracy is limited due to source's (calibrator's) specifications. Alternatively, the ac voltage standard (e.g. Fluke 5790A) could be used to define the reference levels of the signals. This method reduces the measurements uncertainty but it requires additional equipment. Other cons and pros of the setup are similar as described above.



Figure 2.42: NI 5922 – Linearity – A simplified calibration connection where ac voltage source is used as a reference.

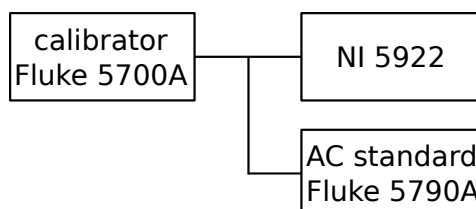


Figure 2.43: NI 5922 – Linearity – Calibration connection where ac voltage standard is used as a reference.

The accuracy of the linearity measurements can be significantly improved if the thermal converters instead of the ac voltage standard is used as a reference (Figure 2.45). Normally the

source used for this characterization is affected by the load. Thermal converters present a low load impedance that modifies the output of the calibrator from the output that is obtained with a high input impedance. Therefore, it is necessary to have the same input impedance used during the calibration of the source. To obtain this condition, a good way is to use a T-piece to connect in parallel to the thermal converter and the NI-5922 under test. This configuration is used during the calibration of the source and during the linearity measurements as shown in Figure 2.45. This linearity measurement provides significantly better accuracy but it requires extra equipment. The method is also rather complicated especially since it requires a tricky dc measurement. Additionally, different load resistors and voltage dividers are needed at lower and higher levels, respectively.

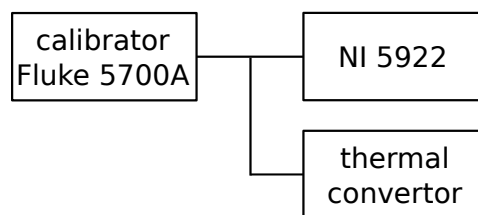


Figure 2.44: NI 5922 – Linearity – Calibration connection where thermal convertor is used as a reference.

For example, a modified version of a wideband inductive divider with guarded cable connections was realized for testing the linearity of wideband digitizers. It is optimized for operating in the frequency range from 500 Hz to 50 kHz but an extension up to 1 MHz is also possible. Simulation with a lumped parameters circuit has shown that the errors in both phase and quadrature are about 1 part in  $10^6$ . By means of this inductive voltage divider the calibration of the linearity of wideband synchronized digitizers is possible using a set of suitable triaxial cables. Figure 2.45 gives a general measurement principle using the proposed wideband IVD.

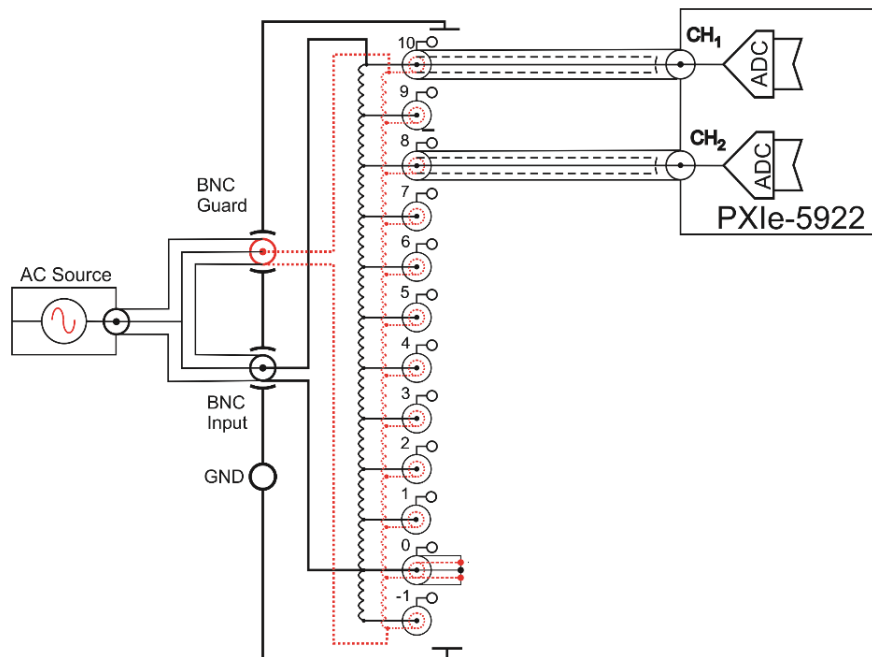


Figure 2.45: NI 5922 – Linearity – Linearity test in synchronized ADCs using calibrated wideband IVD realized at INRIM.

The ultimate accuracy of linearity measurement could be obtained when Josephson arbitrary waveform synthesizer (JAWS) is used as a reference [54] (Figure 2.46). However, this method requires very expensive equipment. Additionally, the high voltage levels (above 1 V) might be difficult to obtain especially at higher frequencies.



Figure 2.46: NI 5922 – Linearity – Advanced calibration connection where Josephson arbitrary waveform synthesizer (JAWS) is used as a reference.

#### 2.4.2.1 Example of measured characteristics

This section shows example of measured level dependencies using setup shown in Figure 2.39. With the level dependency measurements, it is investigated if there is any gain difference from the previous applied voltage or not while applying different voltage levels to either of input channels. This can be considered as extended frequency response measurement at more than one voltage level. Finally, there will be many frequency response curves for each input voltage level. At this point one voltage level frequency response is selected as reference and the other response curves are compared with the reference. Between Figure 2.47 to Figure 2.56, level dependence measurements are shown for four different levels. Gain difference from 3.5 Vrms dependent on frequency of each channel is given for each sampling rate. Level dependence of Ch0 is within the gain stability of the digitizer while level dependence of Ch1 is worse but within 50 ppm.

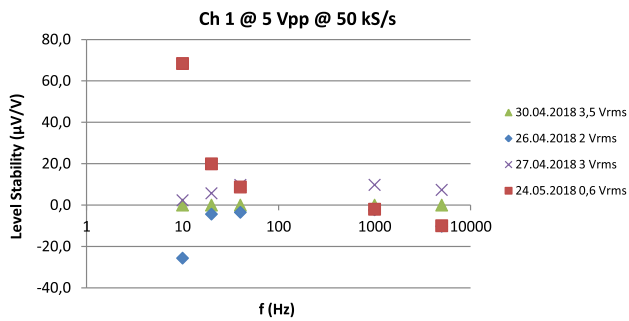


Figure 2.47: Level dependence measurements at 50 kS/s (Channel Ch0).

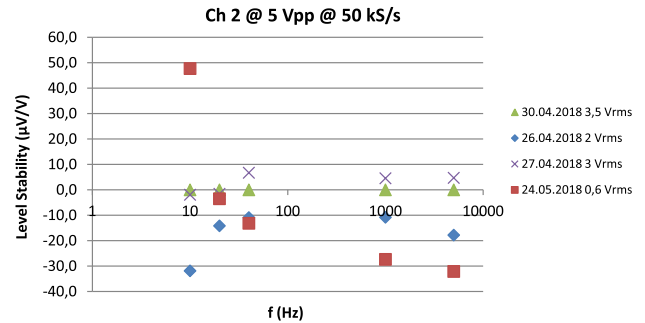


Figure 2.48: Level dependence measurements at 50 kS/s (Channel Ch1).

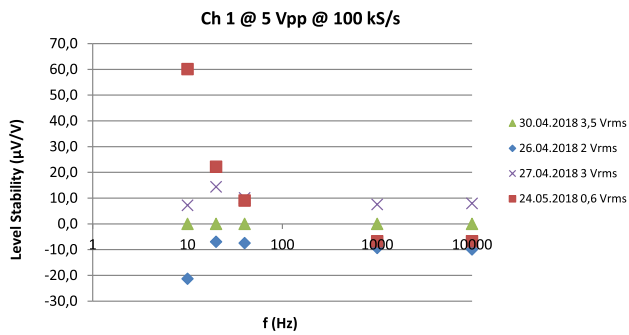


Figure 2.49: Level dependence measurements at 100 kS/s (Channel Ch0).

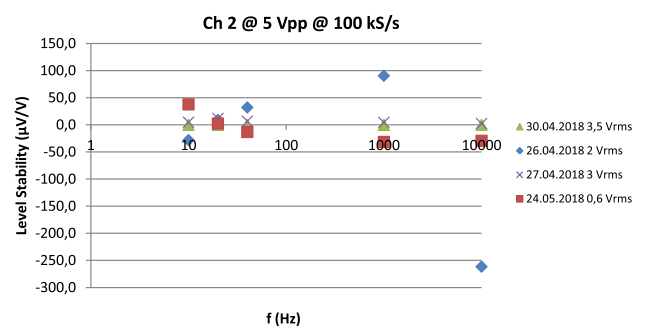


Figure 2.50: Level dependence measurements at 100 kS/s (Channel Ch1).

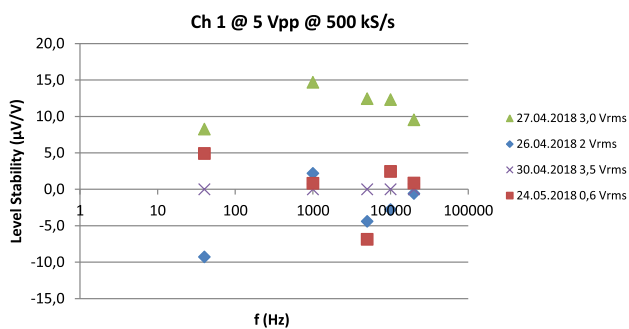


Figure 2.51: Level dependence measurements at 500 kS/s (Channel Ch0).

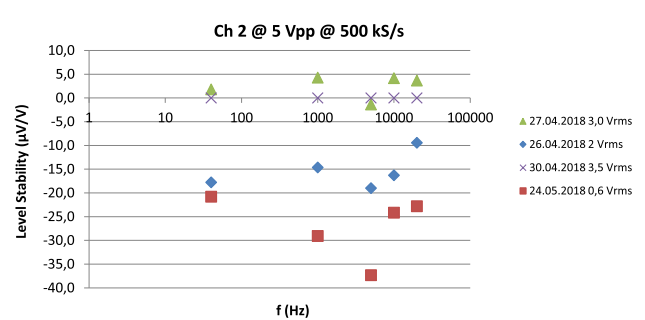


Figure 2.52: Level dependence measurements at 500 kS/s (Channel Ch1).



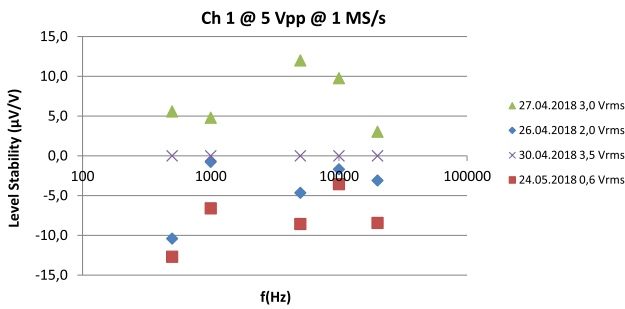


Figure 2.53: Level dependence measurements at 1 MS/s (Channel Ch0).

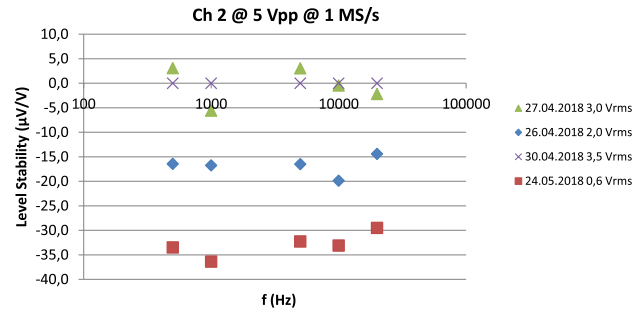


Figure 2.54: Level dependence measurements at 1 MS/s (Channel Ch1).

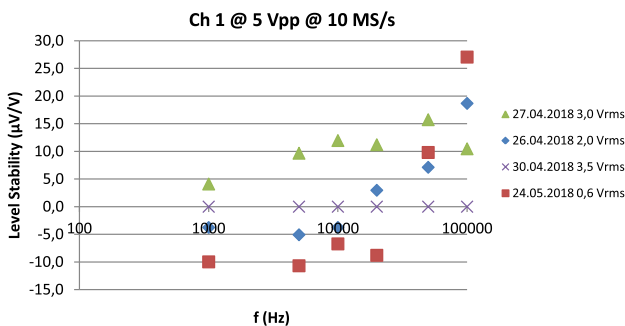


Figure 2.55: Level dependence measurements at 10 MS/s (Channel Ch0).

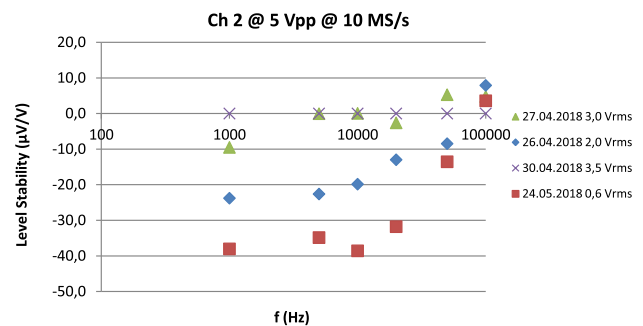


Figure 2.56: Level dependence measurements at 10 MS/s (Channel Ch1).

### 2.4.3 Digitizer (NI 5922) - Phase angle error between channels

Majority of the phase angle error measurements is performed by applying the same signal to both input channels. A perfect digitizer then should show a zero phase difference between the two channels. 0 rad phase difference, with the other words the same signal, is applied to each channels as shown in the setup. FFT is used for evaluating the NI 5922 samples. The phase difference of FFTs of two channels is used as phase difference result. An example of a phase difference measurement is given in Figure 8, below. The phase is almost linear versus frequency, as expected.

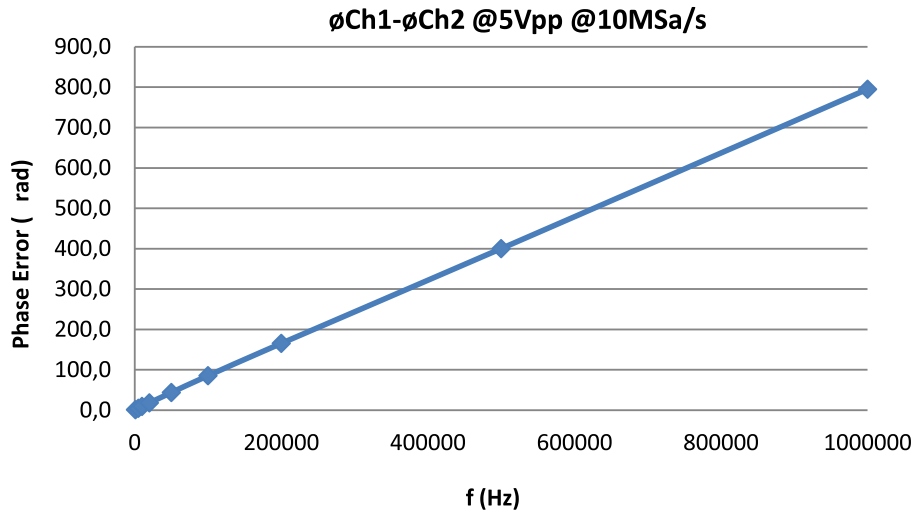


Figure 2.57: Example of measurement of a phase angle between channels 0 and 1 of the digitizer NI 5922.

As an ideal situation, each digitizer channel should be identical and have the same specs. When the digitizer will sample the signal, the software controlling the input channels sends a command or triggering signal, using the same task to begin the sampling process. Although this trigger signal should arrive to the sampling hardware at the same time, but also there can be a slight delay between two channels while getting the first sample, which means the phase difference between channels. As seen, the phase error between CH0 and CH1 behaves almost linearly with the frequency. The phase error has a slope about 800  $\mu\text{rad}/\text{MHz}$ . This suggests the phase error is mostly caused by the time delay, rather than analogue phase shift error in the input stage of the digitizer. Assuming the slope is  $k(\phi) \approx 800 \mu\text{rad}/\text{MHz}$ , we can calculate the time shift from a formula:

$$\Delta t = \frac{k(\phi)}{2\pi}, \quad (2.28)$$

e.g. in example case the  $\Delta t \approx 127 \text{ ps}$ , which is about typical value for NI 5922 inter channel time delay. Note this time shift can be used as a time shift correction for the TWM/TPQA tools as described in section 3.2.5.2.1. The residue after subtracting the time shift caused slope from the measured phase error is then used as a phase error correction for the digitizer as described in section 3.2.5.6.

#### 2.4.4 Digitizer (NI 5922) - Distortion

Any signal other than the applied one to the input of the digitizer seen in the sample data or spectrum is considered as a distortion or noise. If the applied signal is “pure sinusoidal” signal, then it should not contain any spectral components other than fundamental. If the reference signal is already distorted, then the sampled signal will be distorted. Therefore, the noise or distortion levels of the reference signal must be known in order to measure the distortion of the digitizer of interest. There are several specifications and notations for quantifying digitizer performance, such as SINAD (Signal-to-noise-and-distortion), ENOB (Effective Number Of Bits),

SNR (Signal-to-Noise Ratio), THD (Total Harmonic Distortion), THD+N (Total Harmonic Distortion plus Noise) and SFDR [55].

When an analog signal is sampled with a certain sampling rate and number of samples, the spectrum of the sampled signal may have some spectral components, even if the sampled analog signal is pure sinusoidal, which contains no harmonic or noise inside. These spectral components come from the nature of the sampling process and the other electrical or EMI disturbances. The result of FFT of the sampled signal is a complex 1-dimensional array. The array size is the same as the number of samples in the data. Each component of this array represents the corresponding frequency component of the sampled signal with a part of Sampling Rate/Sample Size,  $f_s/M$ , called frequency “bins”. Therefore, the value of  $f_s/M$  must be integer and the value input signal frequency must be a member of these frequency bins. That’s why coherent and synchronized sampling must be used at the all measurement works. When take a look at the spectrum, it can be easily seen some components with a certain and repetitive points above the noise floor. These components come from the harmonics as a result of multiplication with input signal frequency and sampling signal. The frequency values of these components are  $|\pm K \cdot f_s \pm n \cdot f_0|$ . Here,  $n$  represents the number of harmonics and for integer  $K$  values,  $f_s$  sampling rate and  $f_0$  input signal frequency. Determining the distortion with using the notations above is all based on FFT analysis.

Harmonic distortion is normally specified in dBc, decibels below carrier. It may also be specified as a percentage in audio applications. It is the ratio of the RMS signal to the RMS value of the harmonic in question. Since the spectrum contains many harmonics, using this calculation will not be enough. Total Harmonic Distortion (THD) is the ratio of the RMS value of the fundamental signal to the mean value of the root-sum-square of its harmonics, generally only first 5 harmonics are taken into account, better but not enough again. Total Harmonic Distortion plus Noise (THD+N) is the ratio of the RMS value of the fundamental signal to the mean value of the root-sum-square of its harmonics plus all noise components (excluding dc). The bandwidth over which the noise is measured must be specified. In the case of an FFT, the bandwidth is DC to  $f_s/2$ . If the bandwidth of the measurement is dc to  $f_s/2$  (the Nyquist bandwidth), THD+N is equal to SINAD.

#### 2.4.4.1 Example of measurement

The TWM algorithm uses SFDR as their input correction (see section 3.2.5.9). the point of the calibration is this to get worst case estimate of the SFDR (highest spur to carrier ratio), so the TWM/TPQA tools can estimate uncertainty caused by the distortion of digitizer. Unless special sources with known THD are available, the only acceptable method of estimating the SFDR is to use the purest possible frequency source as a signal generator, apply to the digitizer and e.g. use directly the TWM/TPQA algorithm such as TWM-THDWFFT (see section 3.6.1.6) to measure the harmonic levels and thus SFDR.

For low frequencies it is possible to use ultra low distortion generators such as Krohn-Hite 4400 series, which has typically THD better than -105 dBc. For higher frequencies, the precision digital synthesizers or custom built oscillators may be used. The only result of using source with higher distortion is simply more pessimistic estimate of the worst case SFDR, which will

limit the uncertainty of the TWM/TPQA measurement system.

Example of measurement of NI 5922 distortion is shown in Table 2.9. The measurement was performed using Krohn Hite 4400B up to 10 kHz and custom built wien oscillators up to 100 kHz. Higher frequency sources with acceptable distortion were not available. Note the measurement of THD was performed just after self-calibration of the NI 5922. The self-cal also performs linearization of the ADC, so every time it is performed, the THD changes a bit and it was observed it slowly rises with elapsed time due to the temperature changes and drifts.

f Hz	THD		THD+N	
	%	dBc	%	dBc
20	< 0.000 45	< 107.0	< 0.002 0	< 94.0
50	< 0.000 43	< 107.4	< 0.002 0	< 94.0
100	< 0.000 42	< 107.5	< 0.002 0	< 94.0
200	< 0.000 41	< 107.7	< 0.002 0	< 94.1
500	< 0.000 42	< 107.6	< 0.002 0	< 94.1
1k	< 0.000 42	< 107.5	< 0.002 0	< 94.0
2k	< 0.000 44	< 107.1	< 0.002 0	< 94.0
5k	< 0.000 58	< 104.7	< 0.002 1	< 93.7
10k	< 0.000 56	< 105.0	< 0.002 9	< 90.7
20k	< 0.000 45	< 106.9	< 0.003 5	< 89.2
50k	< 0.000 43	< 107.3	< 0.002 6	< 91.6
100k	< 0.000 30	< 110.6	< 0.003 3	< 89.6

Table 2.9: Example of NI 5922 THD measurement. THD was set measure up to 30 harmonics, sampling rate was fixed 2MSa/s and the band stop for the THD+N was set to 500 kHz.

### 2.4.5 Digitizer (NI 5922) - Evaluation of the stability of phase and amplitude

The gain and the phase are measured in different days and the measurements obtained for different frequencies are summarized in the Figures 2.58 to Figure 2.72. The calibrator's stability is worse at 10 Hz and 20 Hz. The stability measurement at these frequencies is the reflection of the calibrator's stability. At the rest of the frequencies the stability is within 20 ppm and there is not any correlation with time as seen in the figures. This stability is valid almost for the all sampling frequencies. At 500 kHz and 1 MHz the SINAD measurement is worse as RMS formula may not reflect the actual result. For this reason these frequencies are omitted from the stability evaluation.

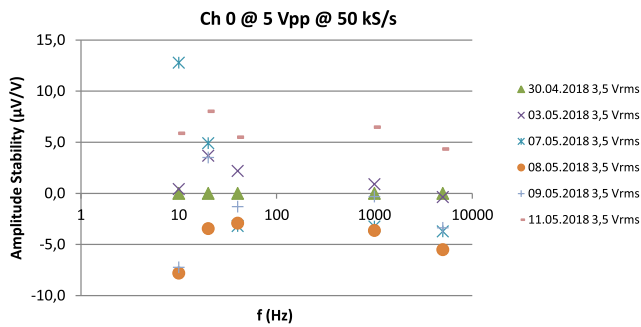


Figure 2.58: Stability of amplitude measurements at 50 kS/s (Channel Ch0).

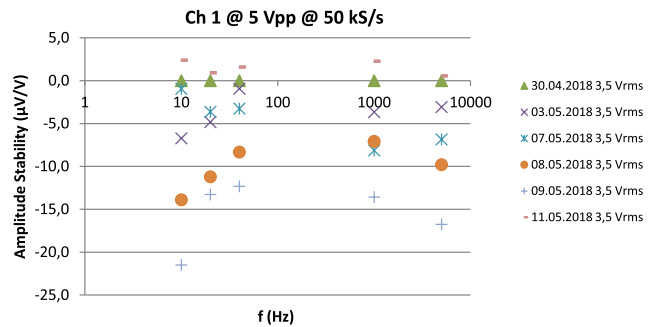


Figure 2.59: Stability of amplitude measurements at 50 kS/s (Channel Ch1).

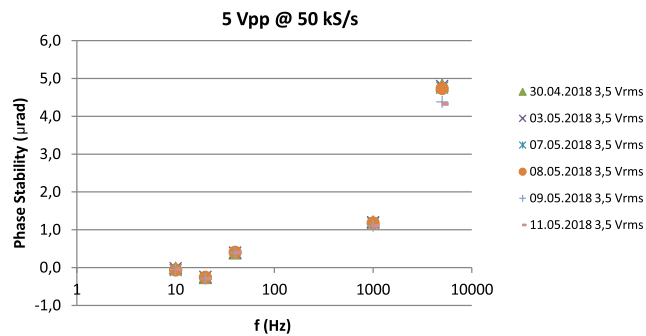


Figure 2.60: Stability of phase error measurements at 50 kS/s (Channel Ch1-Ch0).

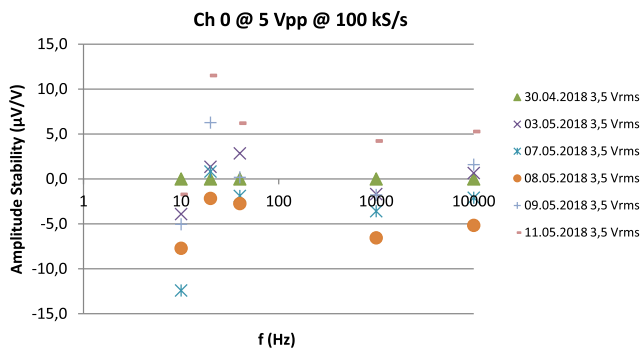


Figure 2.61: Stability of amplitude measurements at 100 kS/s (Channel Ch0).

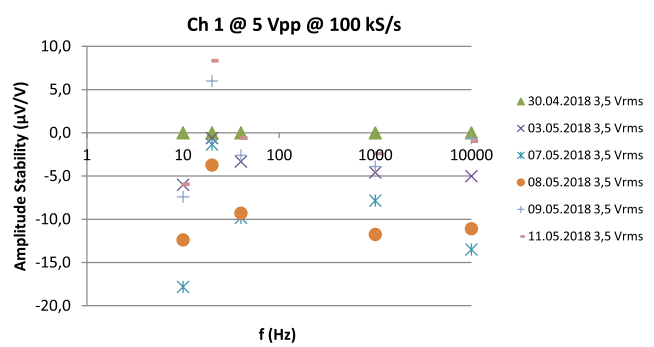


Figure 2.62: Stability of amplitude measurements at 100 kS/s (Channel Ch1).

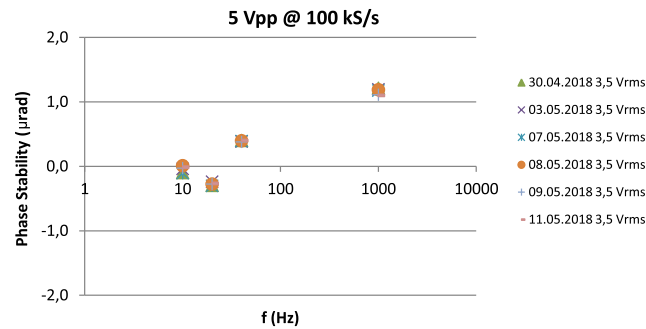


Figure 2.63: Stability of phase error measurements at 100 kS/s (Channel Ch1-Ch0).

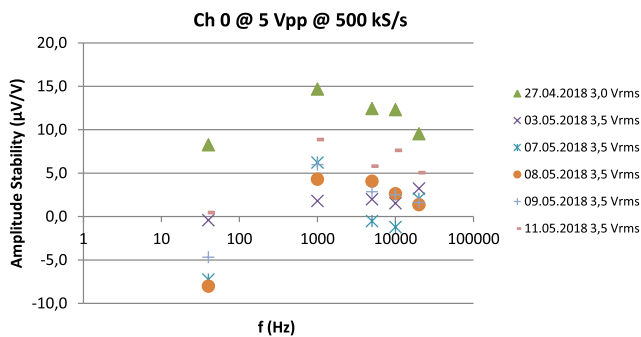


Figure 2.64: Stability of amplitude measurements at 500 kS/s (Channel Ch0).

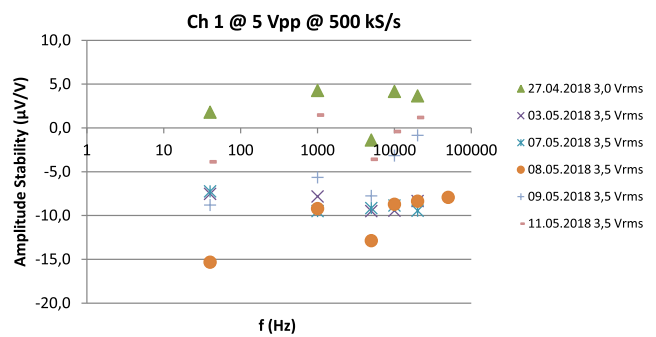


Figure 2.65: Stability of amplitude measurements at 500 kS/s (Channel Ch1).

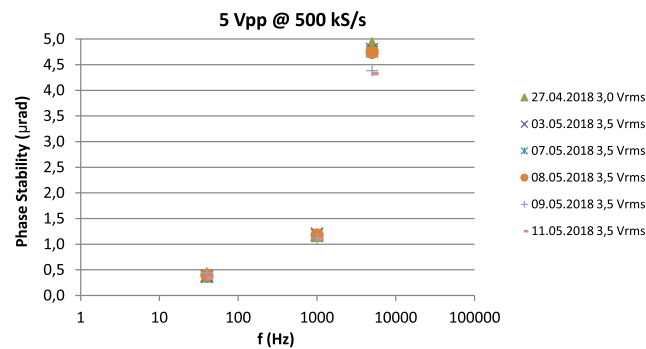


Figure 2.66: Stability of phase error measurements at 500 kS/s (Channel Ch1-Ch0).

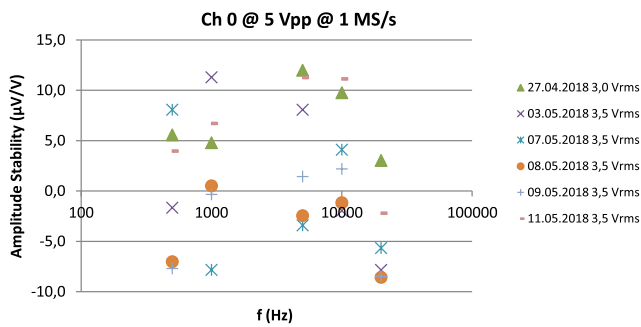


Figure 2.67: Stability of amplitude measurements at 1 MS/s (Channel Ch0).

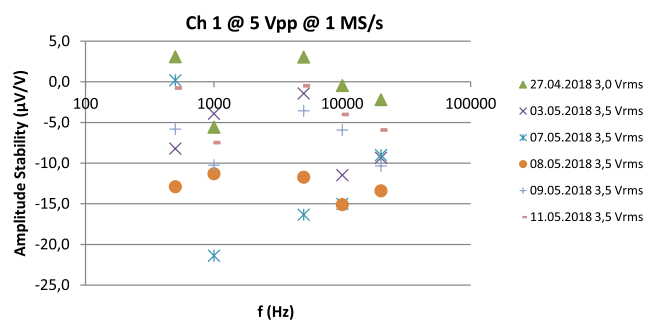


Figure 2.68: Stability of amplitude measurements at 1 MS/s (Channel Ch1).

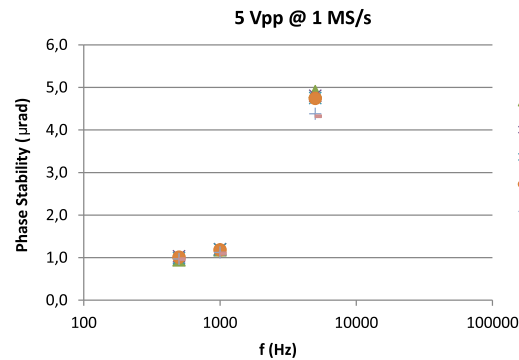


Figure 2.69: Stability of phase error measurements at 1 MS/s (Channel Ch1-Ch0).

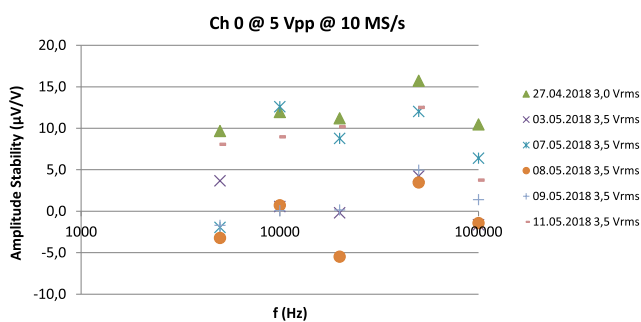


Figure 2.70: Stability of amplitude measurements at 10 MS/s (Channel Ch0).

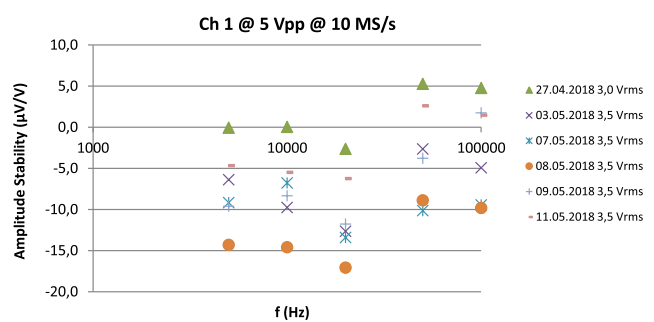


Figure 2.71: Stability of amplitude measurements at 10 MS/s (Channel Ch1).

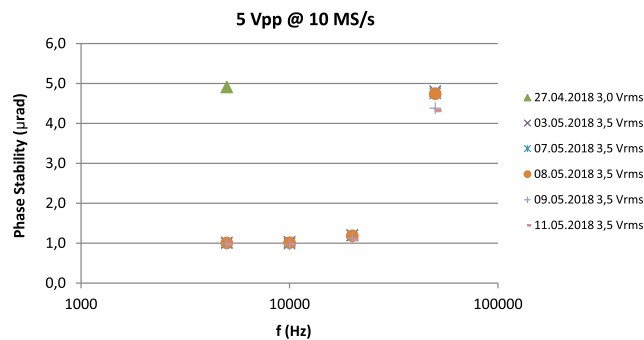


Figure 2.72: Stability of phase error measurements at 10 MS/s (Channel Ch1-Ch0).

Stability of NI 5922 was also tested by second method. The setups was made using stable source Fluke 5720A and one NI 5922. The dc gain error of the card was measured using voltages  $\pm 900$  mV. Following procedure was carried out:

1. self-cal was performed on NI 5922.
2. dc gain error was measured from a difference between the voltage calculated from the sampled data and applied voltage.
3. 10 minute pause was made.
4. Process was repeated 10 times from (1).
5. 5 hour pause was made.
6. Process was repeated 32 times from (1).

Result of the experiment is shown in Figure 2.73. The obtained data allowed to evaluate repeatability of the self-cal procedure and also the stability of the internal reference (average error of 10 repeated self-cal routines). The temperature effect was compensated by temperature coefficient obtained for the same card using the same setup and thermal cycling of the digitizer in thermostat. The test reveals it is not realistic to expect better absolute gain accuracy than  $100 \mu\text{V/V}$ .



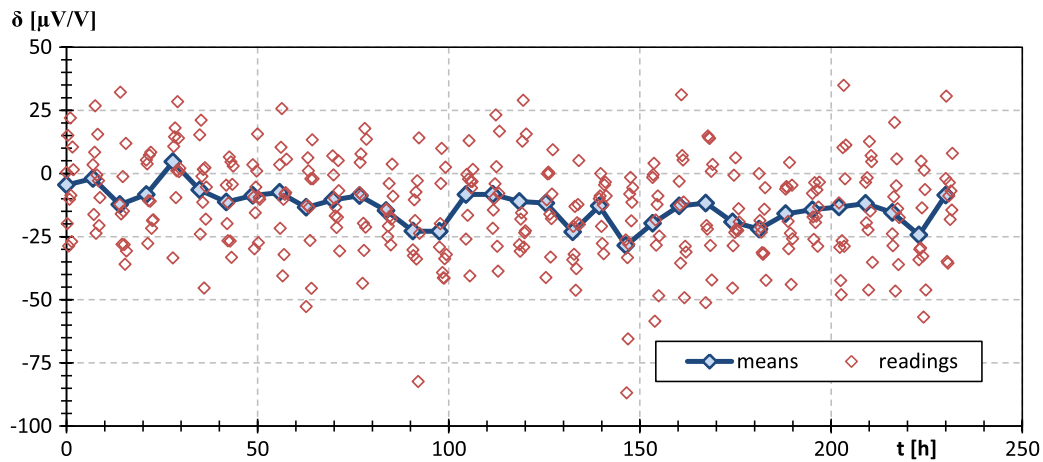


Figure 2.73: Example of repeatability of NI 5922 self-cal routine (red diamonds) and calculated stability of internal reference (blue curve).

#### 2.4.6 Digitizer (NI 5922) - Evaluation of the input impedance

TWM algorithms supports automatic correction of loading errors caused by the finite input impedance of the digitizer and cable. In order to use the correction, user must calibrate input impedance of the digitize channel.

Measurement of input impedance of floating digitizer such as 3458A is trivial task as it can be connected to the RLC meter directly as shown in Figure 2.74 using e.g. Keysight E4980A bridge. Situation for grounded digitizers such as NI 5922 is somewhat more complicated. To be able to use ordinary four terminal pair (4TP) bridge, as shown in Figure 2.74, the bridge or the digitizer must be made floating including the communication bus to the controlling computer. Even after that, there may be some leakage of current via the isolation capacitances, so the measurement above some 100 kHz will become problematic. Solution may be to use VNA analysers, which are capable to operate to grounded loads, but those are typically for higher frequencies only. Note for measurement of the NI 5922 is relevant to mention the input impedance changes for different configuration. Especially it is critical to switch on the input from default “GND” mode to “DC” (or eventually “AC”) coupling, otherwise the input stays unconnected!

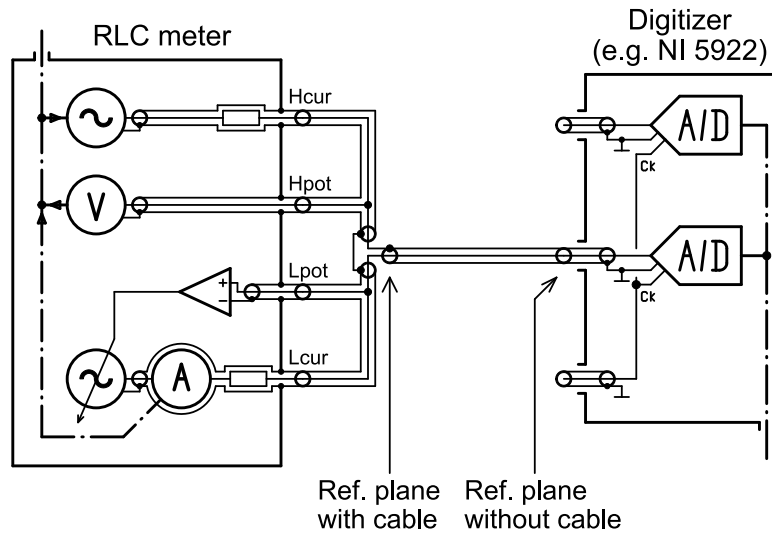


Figure 2.74: Example of measurement of a input impedance of the digitizer NI 5922.

The example in Figure 2.74 shows two possible reference planes: (i) At the terminals, which means the OPEN and SHORT correction of the RLC bridge is made at the right side of the coaxial cable; (ii) Including the cable to the input of the digitizer, which means to perform OPEN and SHORT of the RLC bridge at the 4TP to coaxial adapter.

Therefore, another method is typically used for calibration of input impedance. When two channel digitizer is available, the solution shown in Figure 2.75 is usable. The idea is such the inter-channel gain and phase errors of the two channel digitizer are first calibrated and corrected as shown in previous sections. Then, TWM itself or any other sampling system capable of measuring voltage vectors is used to determine the input impedance  $\hat{Z}_{IN}$  using an impedance standard of known value  $\hat{Z}_{REF}$ .

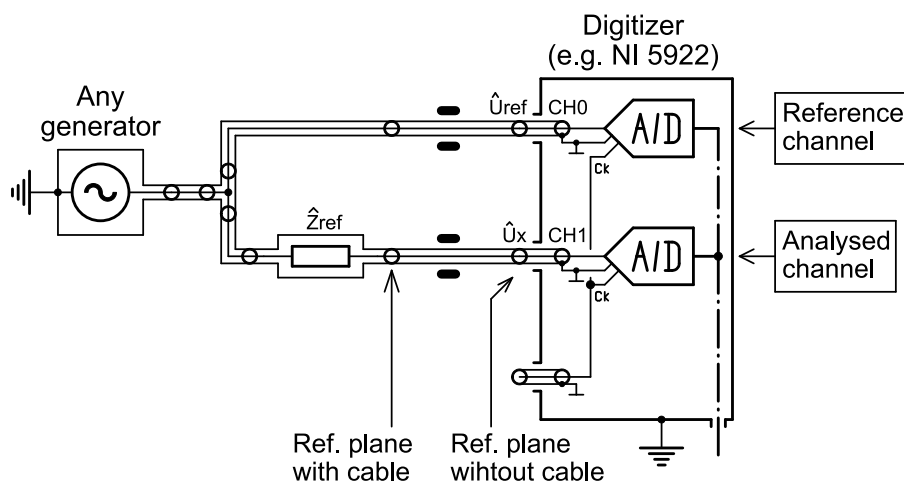


Figure 2.75: Example of measurement of a input impedance of the digitizer NI 5922 using TWM/TPQA tool itself.

If  $\hat{Z}_{REF}$  forms a voltage divider together with input impedance  $\hat{Z}_{IN}$ . When we measure voltage vectors  $U_{REF}$  and  $U_X$  at the inputs of the digitizer, the input impedance can be calculated from

a formula:

$$\hat{Z}_{\text{IN}} = \frac{\hat{Z}_{\text{REF}} \cdot \hat{U}_X}{\hat{U}_{\text{REF}} - \hat{U}_X} \quad (2.29)$$

The value of the standard  $\hat{Z}_{\text{REF}}$  should be comparable to the input impedance of the digitizer. Resistor of value 100 k $\Omega$  in parallel with capacitor 100 pF may be a good choice. Such transfer standard can be calibrated using RLC bridge before the calibration Keysigh E4980A. The measurement of the input impedance can be performed directly by the algorithm TWM-InpZ (see section 3.6.1.13). Example of measured input impedance is shown in Figure 2.76.

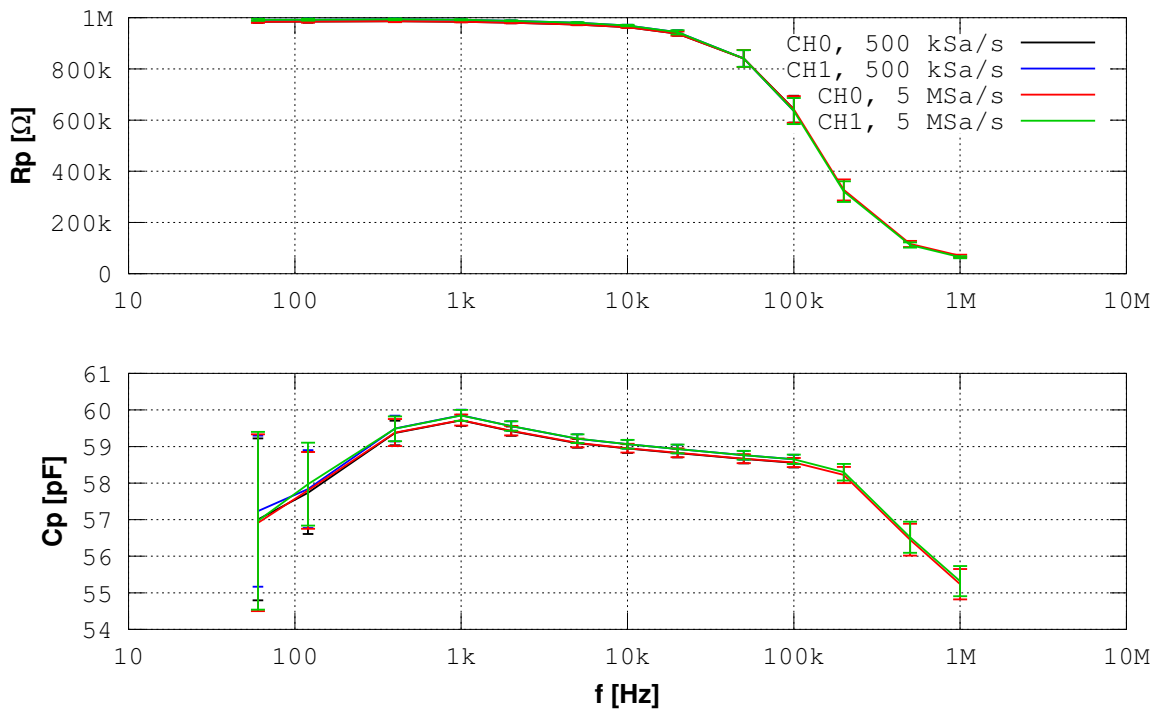


Figure 2.76: Example of measured input impedance of NI 5922 using TWM/TPQA tool itself.

## 2.5 Methods for calibration of the entire system

The most straightforward calibration method for a modular system may be to calibrate the parts and then add possible corrections and uncertainties to take care of issues regarding connecting parts. That is why most NMIs have evaluated the current shunts, the dividers and the digitizers (sampling multimeters) separately. These methods are described in other sections of this guide.

However, the calibration and verification of shunts, dividers and digitizers includes several measurement steps and uncertainty contributions that adds up, and for highest precision, the wiring and digitizer input impedance plays an important role in the uncertainty budget. These can, to some extent, only be estimated and calculated when a parts calibration approach is used. An alternative road to traceability is to calibrate the voltage channel and current channel for ac voltage and current directly. Calibration with an ac calibration system will offer a shorter traceability chain if more primary standards can be used.

The object is then to calibrate the complete voltage channel at ac voltages of e.g. 120 V and 230 V and the current shunts at e.g. 1 A and 5 A, thereby shorten the traceability chain [56], by using the existing ac-dc difference calibration set-up. It is then necessary to add a high-grade DC meter to the ac-dc difference calibration system, in order to go from ac-dc difference to ac voltage.

There are some issues with such a calibration scheme. One issue is that a Thermal Voltage Converter (TVC) is of rather low impedance, and draws a non-negligible load current. Therefore, it is necessary to define the reference plane carefully so that thermal or ohmic voltage differences does not influence the calibration.

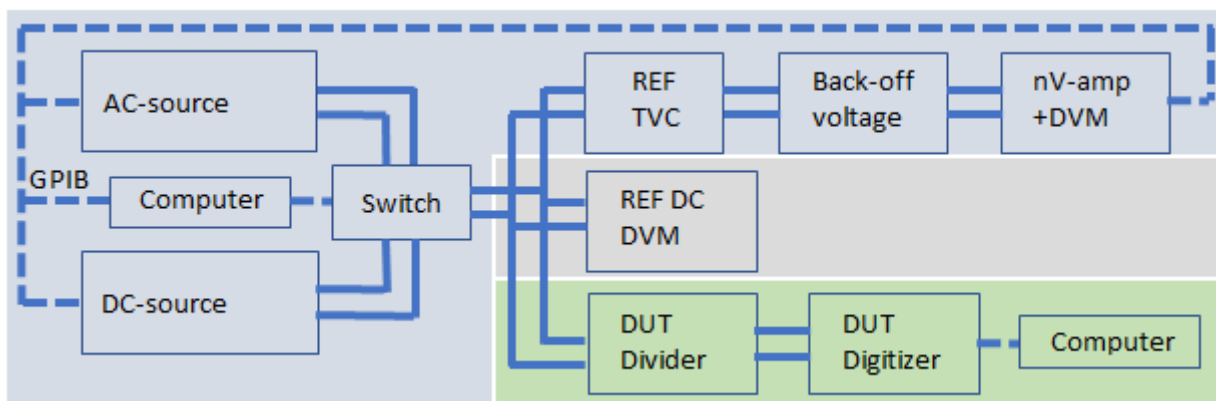


Figure 2.77: ac-dc calibration system modified for ac calibration of the voltage channel.

For ac voltage calibration the ac-dc difference system, the reference dc DVM and the digitizer, with or without divider, are connected in parallel. Instead of the normally used T-connector, an adapter with three outputs is then used for the parallel connection. The REF dc DVM is then read when dc (plus and minus) is provided and the digitizer is read when ac is provided. The true ac voltage is taken as the (corrected) mean dc DVM value plus the (corrected) ac-dc difference measured by the TVC.

For the calibration of ac current, the shunts of the ac-dc system and the modular system is connected in series. Also, the setup is somewhat changed, as the dc current measurement, with the reference dc voltmeter, needs to be done by help of the current shunt of the Thermal Current Converter (TCC). Therefore, it must be investigated whether this added load influences the accuracy of the TCC. It was established that for the RISE TCC and at 50 Hz the influence was negligible.

The current calibration setup will then be as shown in Figure 2.78.

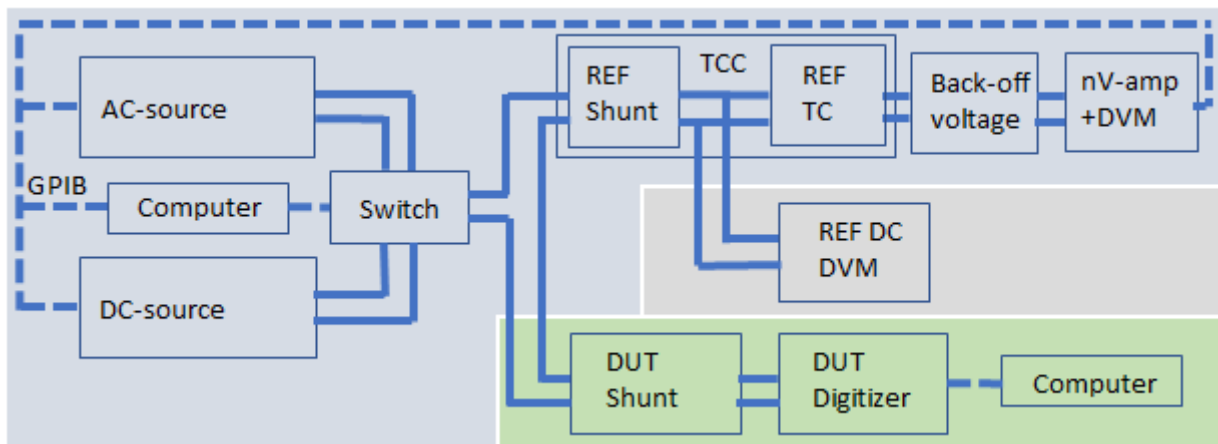


Figure 2.78: ac-dc calibration system modified for ac calibration of the current channel.

RISE have compared the results of this calibration with a modular calibration of the voltage and current channel. The agreement of the calibrations of voltage was within  $2 \mu\text{V/V}$ . The agreement for current was about  $5 \mu\text{A/A}$ .

## Chapter 3

# User's guide for the open software tool

This chapter is a user's guide for the open software tools TWM and TPQA. The software is described in terms of installation, user interface and configuration. The guide also describes concept, data formats and meanings of correction data sets for the hardware setup components which is essential for the use of the tools. The guide also shows the integration of new digitizers into the system. Finally, it provides information about the initial database of integrated algorithms for the power and PQ measurements as well as brief principle of integration of new ones.

## 3.1 Software introduction - TWM manual - LabView Environnement

Following sections will describe installation and basic usage of the TWM tool [57].

### 3.1.1 Installation

Installation of TWM consists of several components:

1. Download and unpacking of the TWM tool itself from GitHub [57].
2. Installation of the prerequisites for the TWM run, which are:
  - (a) LabVIEW 2013 Runtime Engine. This is needed to run any LabVIEW application.
  - (b) Drivers of all integrated instruments, which are currently:
    - i. NI VISA drivers for handling GPIB bus.
    - ii. niScope drivers for handling NI digitizers.
3. Installation of the GNU Octave or Matlab for data processing (optional).

Steps (1) and (2) are mandatory. Current version of TWM is built with several digitizers integrated. Several build versions are available with disabled digitizers which are not needed. If full version is installed, the TWM application will not run unless there are drivers for all integrated digitizers. So it would be necessary to install VISA drivers even for use with NI 5922 cards and “niScope” drivers even for use only with Agilent 3458A multimeters.

Step (3) is needed when processing of the recorder waveforms is to be performed in place. Without GNU Octave or Matlab, the TWM can only record the waveforms.

#### 3.1.1.1 Installing TWM tool

TWM tool requires no installation. Its files just must be unpacked from the ZIP to any user folder, e.g.:

```
c:\Program Files (x86)\TWM
```

The build releases of TWM are relatively rare and usually contains version that was at least partially tested. It can be downloaded from GitHub webpage (see Figure 3.1).

However, user may also download development version which will run only with development version of LabVIEW installed on the computer. Note the TWM was intentionally developed in LabVIEW 2013 Base version. The development version can be obtained either by cloning the TWM Git or manually by downloading the Git as a ZIP file (see Figure 3.2).

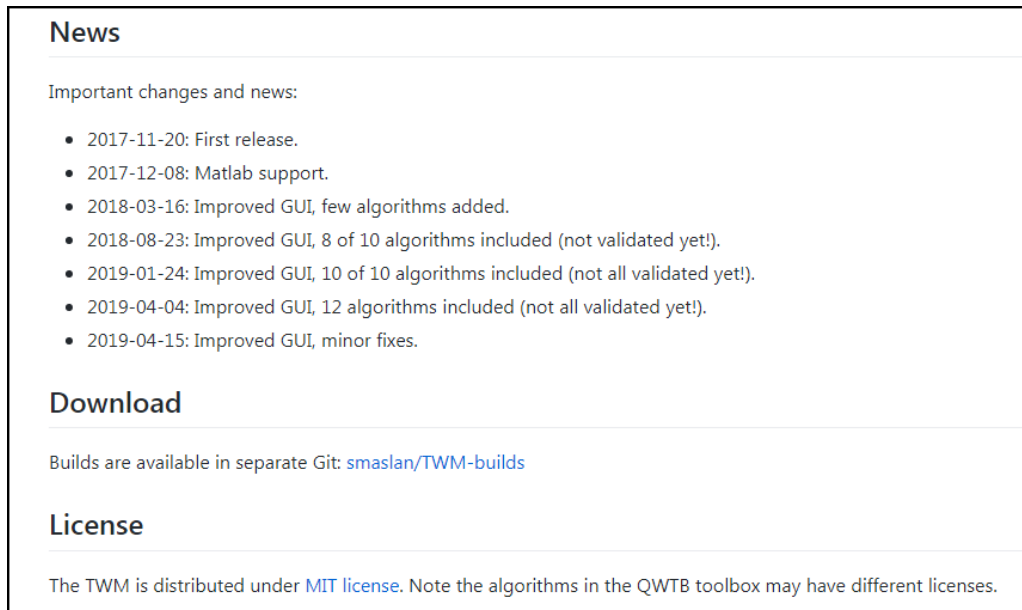


Figure 3.1: Location of TWM download on the TWM GitHub webpage.

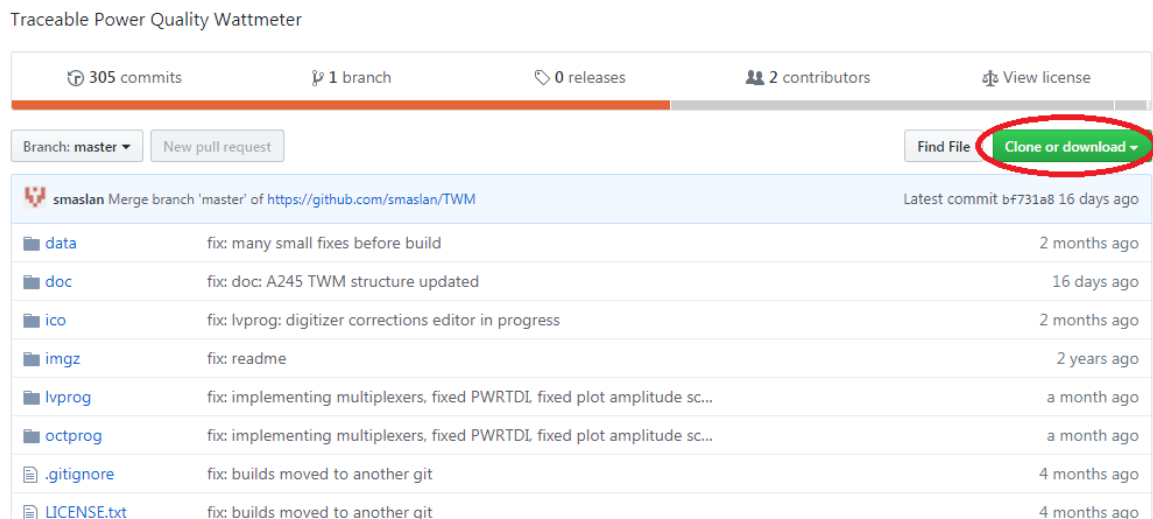


Figure 3.2: Downloading development version of TWM from GitHub webpage.

### 3.1.1.2 Installing TWM prerequisites

LabVIEW applications in general requires large amount of external libraries and drivers to run. First required is LabVIEW 2013 Runtime Engine 32bit [58]. The version must be 32bit as the TWM is built as a 32bit application.

Next component are the VISA drivers, which are needed for communication via GPIB. At least version 5.4 should be installed. The newer versions are partially backward compatible, see [59] for selection.



Last needed component are the “niScope” drivers, which are used to communicate with NI 5922 digitizers. The supported versions are 4.0.5 to 16.1 (see [60] for details). *Note there is also a build version made without “niScope” support, so this part can be optionally skipped.*

### 3.1.1.3 Installing GNU Octave

In order to enable calculations of the PQ parameters from the waveforms, user must install GNU Octave (or Matlab). The TWM was tested with version 4.0.0 and later. The preferred version of GNU Octave is always 64bit, as it has much higher memory limit. That may be useful for some memory demanding algorithms.

The download and guidance to the GNU Octave can be found at [61]. Some of the algorithms do require additional packages to be installed and loaded to the GNU Octave after its startup. This is typically ensured by creating a startup file in the user folder, *but see section 3.1.4.1 Configuring processing environment for alternative approach!* GNU Octave will always execute the sequence of the command on the startup. E.g. in Windows, for the user named “user”, the file location will be:

```
c:\Documents and Settings\user\.octaverc
```

Note the file name actually starts with the dot! Example of the content of the file may be following:

```
more off;
pkg load io;
pkg load optim;
pkg load signal;
pkg load statistics;
pkg load outliers;
graphics_toolkit('gnuplot');
```

One of the main uses of this file is usually to load the packages to the memory on startup. Note the packages must be installed first. Some distributions of the GNU Octave ask user to select the packages to install during the installation. Other distributions are plain without packages and those must be downloaded and installed separately following the documentation [61]. Typical packages needed for the currently implemented algorithms are listed in Table 3.1.

Package	Description
io	Input/output to external formats (CSV files, etc.)
optim	Non-linear optimization toolkit
outliers	Outlier tests and removal
signal	Signal processing routines (e.g. filters)
statistics	Additional statistical functions
multicore	Multicore calculations (for Monte Carlo)
golpi	More effective data exchange between LabVIEW and GNU Octave

Table 3.1: Typical GNU Octave packages required for TWM.

Package “multicore” is not necessary, however it can be used to significantly speedup Monte Carlo uncertainty evaluation of some of the algorithms. Package “golpi” is designed to speed up the data interchange between GNU Octave and LabVIEW GOLPI library [62]. Note the GOLPI library should offer automatic installation of the “golpi” package to the user when the mode of communication is selected (see below).

#### 3.1.1.4 Installing Matlab

Matlab [63] is alternative processing environment for the TWM, however it should be 100 % compatible. TWM was tested with versions 2008b and later. Typical Matlab installation should contain all required packages and they are loaded automatically, so no additional actions after installation should be required.

### 3.1.2 Before starting TWM – Set decimal separator

TWM internally uses GNU Octave or Matlab for processing and result formatting. LabVIEW can switch decimal separator to either dot or comma, whereas Octave or Matlab cannot. This may result in problems when trying to display or copy results when decimal separator is set to comma. Although some changes in TWM were made to prevent these problems, it may still fail in some case, so only safe solution is to **change Windows setup to decimal dot** (Windows Control Panel | Region and Language | Formats | Additional settings).

### 3.1.3 Startup

When all required components are installed, the TWM can be started by its executable “TWM.exe”. When no component is missing, the front panel should appear with no error messages. If some driver is missing, LabVIEW will throw an error with explanation which component cannot be located. Typical missing components are “niScope.dll”, “niTcl.dll” (part of “niScope” drivers) or VISA drivers. If TWM requests the libraries, follow the installation guidance in section 3.1.1 TWM requires no other configurations prior starting the application itself. In some cases TWM may start, but error field will contain an error for a first start. This may be caused by residue of setting from a build computer. The problem should stop once the TWM is restarted.

### 3.1.4 User guide

Main panel of TWM is shown in Figure 3.3. All subpanels with particular configurations can be invoked from the main panel. **Error** indicator at the bottom will show eventual error message of the TWM. User must configure the system before any measurement can be taken. This is done by buttons **Digitizer** for digitizer selection and configuration, button **Octave/Matlab** for processing environment selection and button **HW corrections** for selection of the transducer and digitizer connection and correction files.

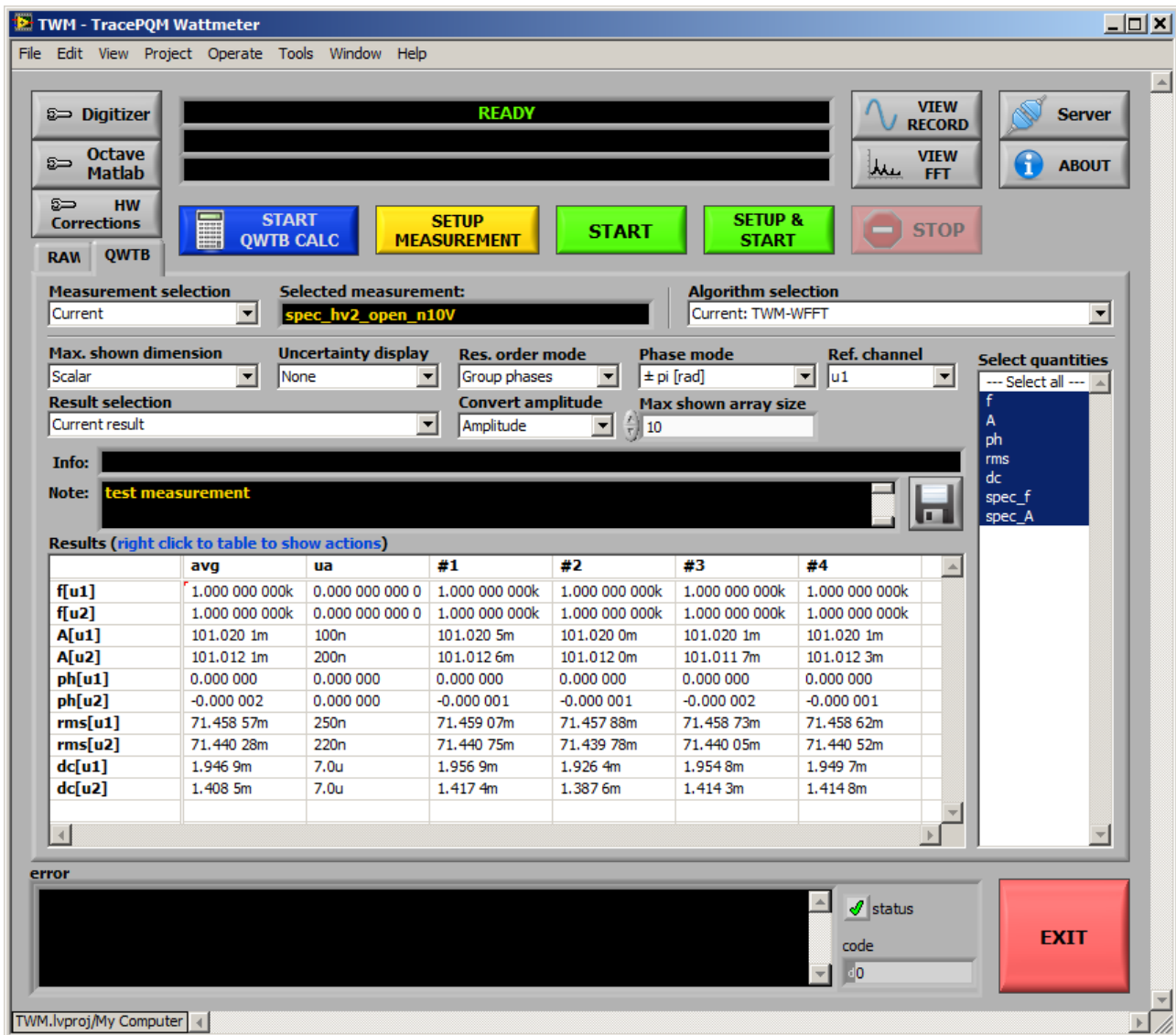


Figure 3.3: Front panel of TWM.

### 3.1.4.1 Configuring the processing environment

First step before any processing can be done is to setup the processing environment, i.e. Matlab or GNU Octave by pressing button **Octave/Matlab** on the front panel. This will invoke panel shown in Figure 3.4. The main option is checkbox **Enable Matlab script mode**. This will select Matlab for processing. If unchecked, the GNU Octave is selected. Matlab has no other options in the top frame. For GNU Octave user must manually list the **GNU Octave binary path** of the selected GNU Octave installation. Example for versions up to 4.x.x is following:

```
c:\Octave\Octave-4.2.2\bin
```

The new version starting with Octave 5.x.x changed the internal location of the binary to either of following subfolders depending on 32/64-bit version selection:

```
c:\Octave\Octave-5.1.0.0\mingw32\bin
c:\Octave\Octave-5.1.0.0\mingw64\bin
```

Next, user may enable option **Always clear function cache**, which has effect only for debugging. This will force GNU Octave to reload the scripts before every command to ensure the changes in them are recognized (do not use for normal operation - it will only slow down operation). Another option is **Use bitstream mode**, which will enable faster communication between LabVIEW and GNU Octave. This requires the package “golpi” to be installed. TWM should offer user automatic installation. However, it is not necessary as there is mostly only small amount of data transferred between the environments. Last option is **Show console window** which will show GNU Octave console window for debugging. Note the Matlab will always show its console window. Do not close neither the Octave’s or Matlab’s console during TWM usage as it will terminate the application! Validity of the setup can be tested by button **Restart**.

Another option to be done is selection of the **QWTB toolbox root folder path**. Although TWM should work with main QWTB distribution, the TWM algorithms are distributed along with the TWM, so always set path to the local copy of QWTB in the TWM installation subfolder:

```
.\octprog\qwtb
```

This is essential as the downloaded TWM will contain the path that was valid at the computer that was used for building the application! Validity of the setup can be tested by **TEST QWTB**.

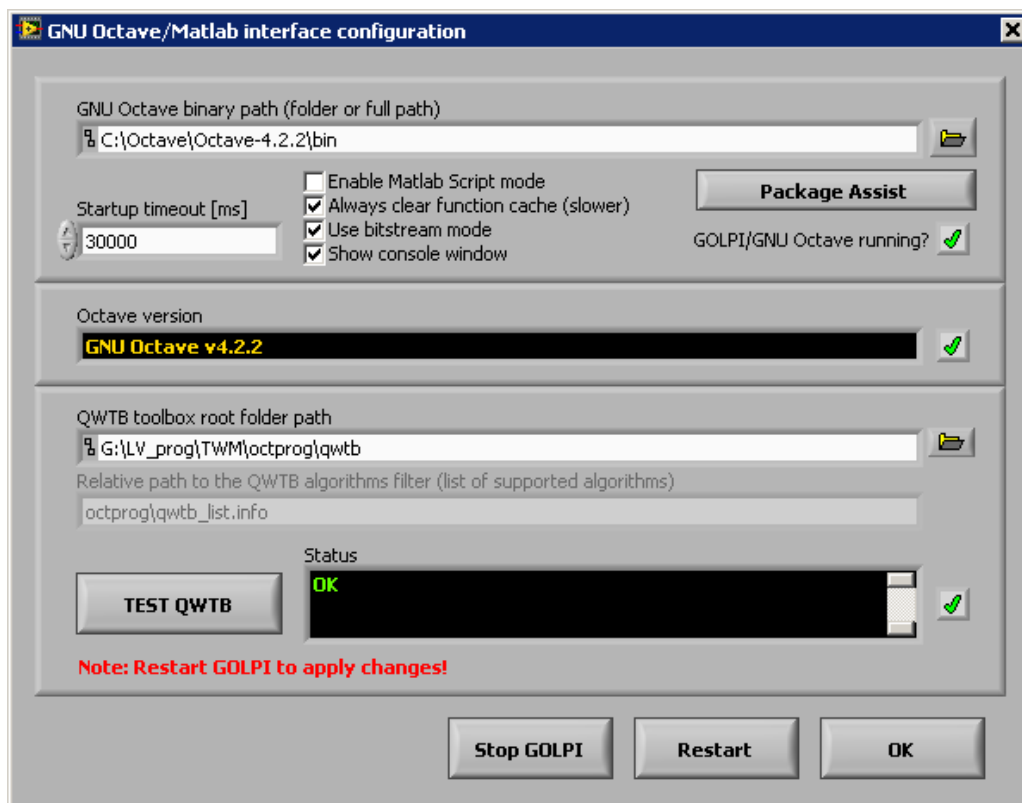


Figure 3.4: TWM processing environment configuration.

A special package assistant shown in Figure 3.5 was made to reduce complexity of initial GNU Octave setup. The panel can be invoked by pressing **Package Assist** button in GNU Octave/Matlab panel. The left list should show the installed packages in the selected installation of GNU Octave. The right panel shows which packages are already loaded after startup (caused by the startup file) or are selected to load by TWM. Select and shift packages you want to load on startup by **right** or **left** buttons. Note the right list will always contain at least the packages that are loaded by startup file `.octaverc`. Also note to apply the changes you must restart Octave in panel Figure 3.4. The selected packages to load should be automatically loaded after the TWM is restarted.

The assistant panel also contains button **Install packages**. This button will display open dialog which can be used to select downloaded package (extension `*.tar.gz`) and TWM will try to install the package to the Octave. The success can be tested by pressing **Reload Packages**. The newly installed packed should appear and must be moved to right panel to be loaded after Octave restart.

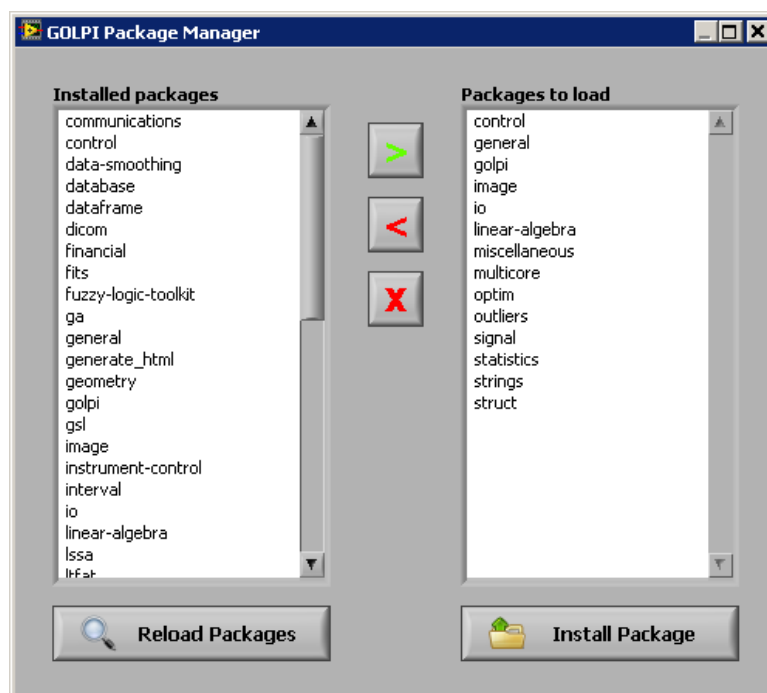


Figure 3.5: TWM GNU Octave package assistant.

### 3.1.4.2 Configuring the digitizer

The button **Digitizer** on the main TWM panel must be pressed in order to invoke **Digitizer configuration** panel. Example of the panels for the **niScope** and **3458A** digitizers are shown in Figure 3.6 and Figure 3.7. The panel contains **Digitizer type** selector which is used to select the HW to be used for digitizing. Below is a text frame with brief description of the selected digitizer.

Next option **On device close** at the bottom-left of the panel is used to determine behavior of

the TWM after the digitizers were used. Selection of **Immediate reset** will reset all HW related to the digitizer to the safe state. Selection of **Delayed reset** will do the same when the HW is not used for preset timeout. This second option is preferred way especially for the sampling multimeters 3458A as it saves the relays for repeated measurements. Option **Force reset on open** will issue reset command to the instruments related to the digitizer every time the digitizer is initialized. Normally this should be disabled.

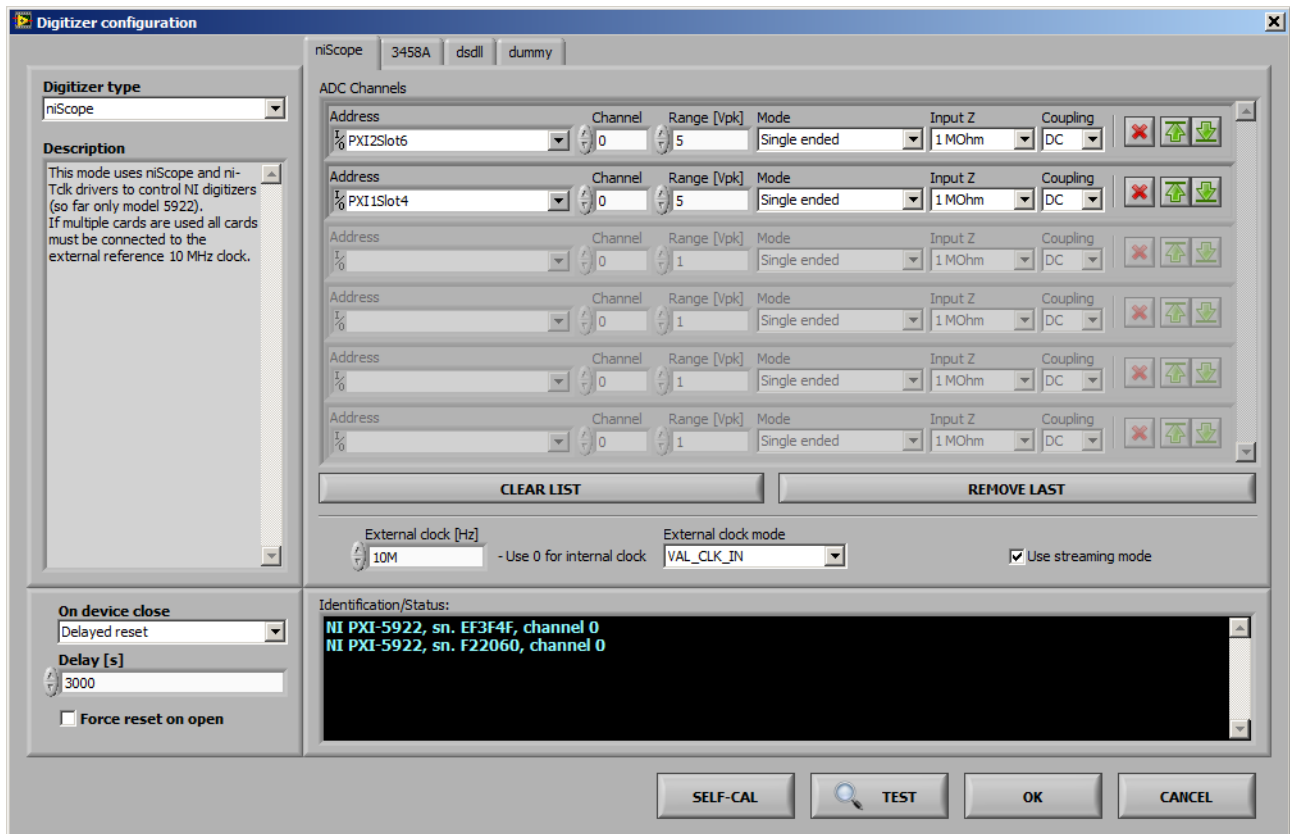


Figure 3.6: TWM configuration panel for the niScope digitizers (for NI 5922).

Each digitizer has one private page with specific options. The page for **niScope** digitizers is shown in Figure 3.6. User can select any number of physical channels of any number of digitizing cards by adding or removing rows to the table **ADC Channels**. Each virtual channel (row) contains **Channel ID** (note niScope counts channels from zero), input **Range [Vpk]**, which is maximum applied voltage (e.g., 5 for range  $\pm 5$  V), **Input Z** is input impedance of the channel and **Coupling** is mode of input coupling. The icons on the right of each row enables reordering or removal of row(s). Note the physical channels of the card(s) which are not selected are automatically set to ground to prevent buildup of noise at near channels. The driver supports PLL synchronization to the external 10 MHz source, which is needed for coherent sampling or when synchronizing multiple cards. Type in nominal sync. frequency to the **External clock [Hz]** entry to enable the PLL. Use value of 0 to switch to the internal clock. Source of the synchronization clock can be selected by **External clock mode**. Selection **VAL\_CLK\_IN** refers to front “CLK IN” SMB of 5922. Options **VAL\_PXI\_CLOCK** should select internal chassis clock distribution. Last option is **Use streaming mode**, which will enable runtime streaming of the sample data from the cards to



the disk storage. This option still uses the internal card memory, but it reads the sample data along with the sampling, so unless the disk storage is too slow, user may digitize indefinitely. Validity of the setup can be tested by the button **TEST**. Eventual problems will be shown in the black area below. The **SELF-CAL** button will initiate self-calibration routine of all selected digitizer cards.

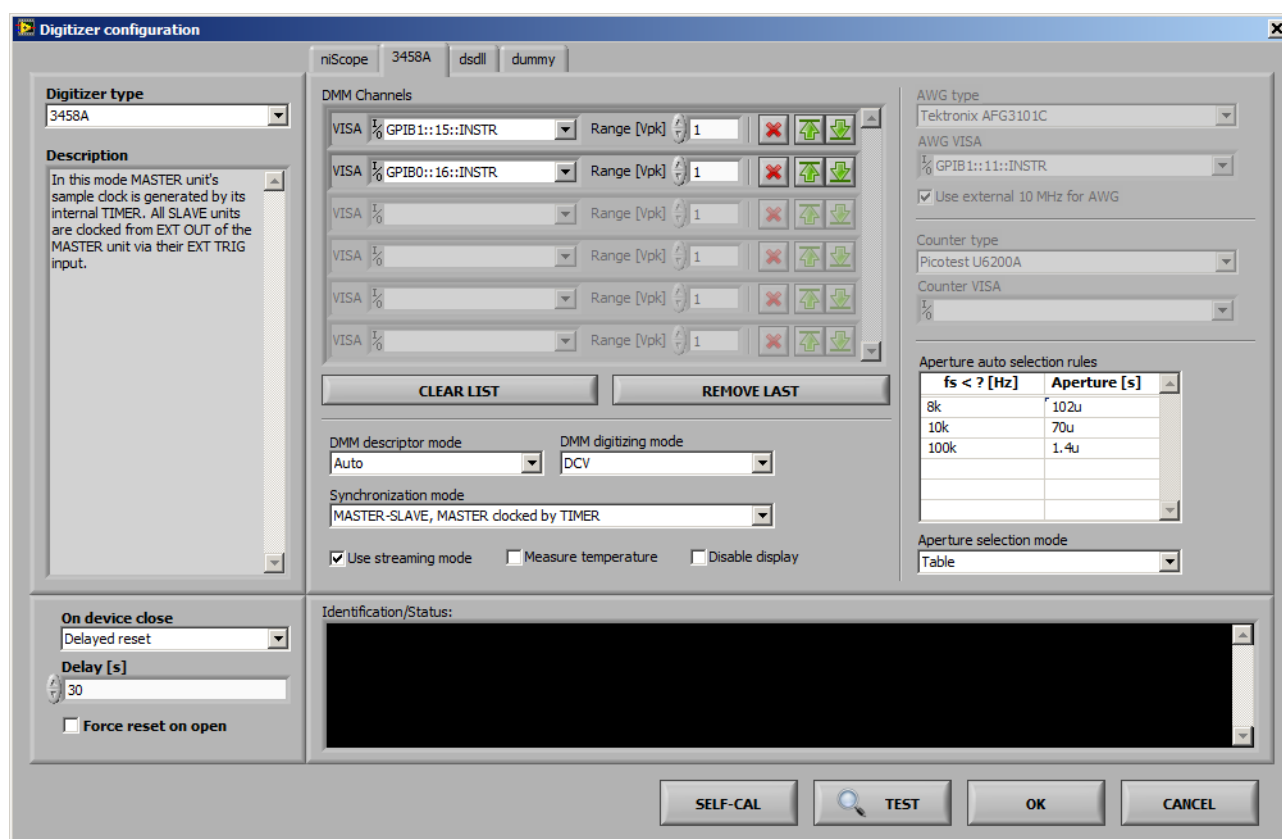


Figure 3.7: TWM configuration panel for Agilent 3458A sampling multimeters.

Configuration panel for the digitizers **3458A** is shown in Figure 3.7. User may create any number of virtual channels by adding or removing rows to the table **DMM Channels**. **VISA** is visa address of the 3458A instruments. **Range [Vpk]** is nominal range of the DMM. Typical value for digitizing is 1 V. Color icons on the right enable reordering or removal of the row(s). Driver has no internal limitation of the channels count. Control **DMM descriptor mode** allows to change the way the multimeters are identified. Selection of **Sequential** will generate fake identifiers “HP3458A, channel 1”, “HP3458A, channel 2”, etc. These are identifiers that must match channel names in the digitizer correction files. Another option **From calibration string** means the TWM will scan the calibration string of each DMM (command “CALSTR?”) and if it discovers serial number in there, it will use it as an identifier. Using CALSTR for serial numbers is common practice for distinguishing the DMMs via GPIB. Selection of Auto will choose automatically with priority of calibration strings. Next option is **DMM digitizing mode**, which selects the digitizing method. Available modes are **DCV**, **DSDC** and **DSAC** (refer to 3458A manual for meaning). Option **Synchronization mode** determines the way how multiple DMMs are synchronized. Four selections are possible:

1. **MASTER-SLAVE, MASTER clocked by TIMER:** Master (first DMM in the list) clocks itself from internal TIMER. All other DMMs takes sample clock (EXT TRIG) from master's EXT OUT. This option means sampling rate of the whole virtual digitizer is determined by the MASTER's internal TIMER and thus by MASTER's reference clock.
2. **MASTER-SLAVE, MASTER clocked by AWG:** Master EXT TRIG is clocked from the arbitrary waveform generator (AWG). All slaves are clocked via EXT TRIG from MASTER's EXT OUT. The sampling clock is determined by the AWG.
3. **All clocked by AWG:** EXT TRIG of all DMMs are clocked from the AWG.
4. **All clocked by TIMER:** All DMM's are clocked from their internal TIMERS. This special mode is dedicated for DMMs with modified internal reference clocks, which can be locked to the external 10 MHz source. The absolute time shift between the channels is determined by additional counter connected between EXT OUT outputs of the DMMs. Note this is intended for two DMMs only.

Typical selection when non-coherent sampling is acceptable is (1). For coherent sampling use modes (2) or (3). Note in modes (2) and (3) user must define AWG type and AWG VISA address and in mode (4) user must define Counter type and Counter VISA address.

Note the modes (2) and (3) can be used with an external non-controlled source of sampling pulses, which may be e.g. some PLL synchronizing unit or other instrument's output. In that case the **AWG type** is set to **dummy**, which means TWM will ignore it. The sample clock generator will be connected to the EXT TRIG of master (2) or EXT TRIG of all DMMs (3). Typical example of such operation is calibration of Fluke 6100 calibrator series, which are equipped by a "Sample Ref Output" connector. This output can be enabled and it outputs fundamental frequency multiplied by certain factor. It is convenient e.g. for achieving coherent sampling.

Next option is **Use streaming mode**, which will enable direct readout of the samples via GPIB without the limitation of the internal DMM memory. This will enable up to 16 MSamples per channel to be captured in one record. However, this mode requires one GPIB controller for each DMM and it may fail for the highest sampling rates. The fail will be indicated by beep and message "trigger too fast" while sampling. The streaming method is faster, as the data are read continuously. Another option is **Measure temperature**, which will read the internal DMM temperature once per record. Note it takes additional time as the reading is made via the main ADC. Last option is **Disable display** which will turn the CFL displays off while digitizing. It is recommended to reduce the noise.

Last option is selection mode of the DMM integration time (aperture) made by control **Aperture selection mode**. Three options are available:

1. **Manual:** user selects the aperture in the new measurement configuration.
2. **Table:** TWM selects the aperture based on the rules in table **Aperture auto selection rules** depending on the sampling frequency. This option is helpful to limit possible apertures to few calibrated values. The example shown in Figure 3.7 defines to select aperture of 102s up to 8 kSa/s sampling rate, 70  $\mu$ s up to 10 kSa/s and 1.4s up to 100 kSa/s.



3. **Maximum:** TWM selects the maximum possible aperture based on empirical formula. Note each aperture needs separate calibration of DMMs, because residual errors of TWM changes e.g. when crossing 100  $\mu$ s aperture.

Configuration of the virtual digitizer can be confirmed and tested by pressing **TEST**. Any error detected should appear in red color in the black area. Autocalibration of the DMMs can be initiated by the **SELF-CAL** button.

### 3.1.4.3 Configuring setup and corrections

TWM was designed to be able to correct each component of the measurement setup: (i) Digitizer; (ii) Transducer; (iii) Loading effects (e.g. cables). Corrections panel shown in Figure 3.8 can be invoked by pressing button HW Corrections on the main panel. The panel contains two pages. One for configuration of Transducers and another one for Digitizers corrections.

#### 3.1.4.3.1 Transducer configuration

User must define connection of the transducers and their correction files before any meaningful measurement can be done. The format of the correction files is described in section 3.2.

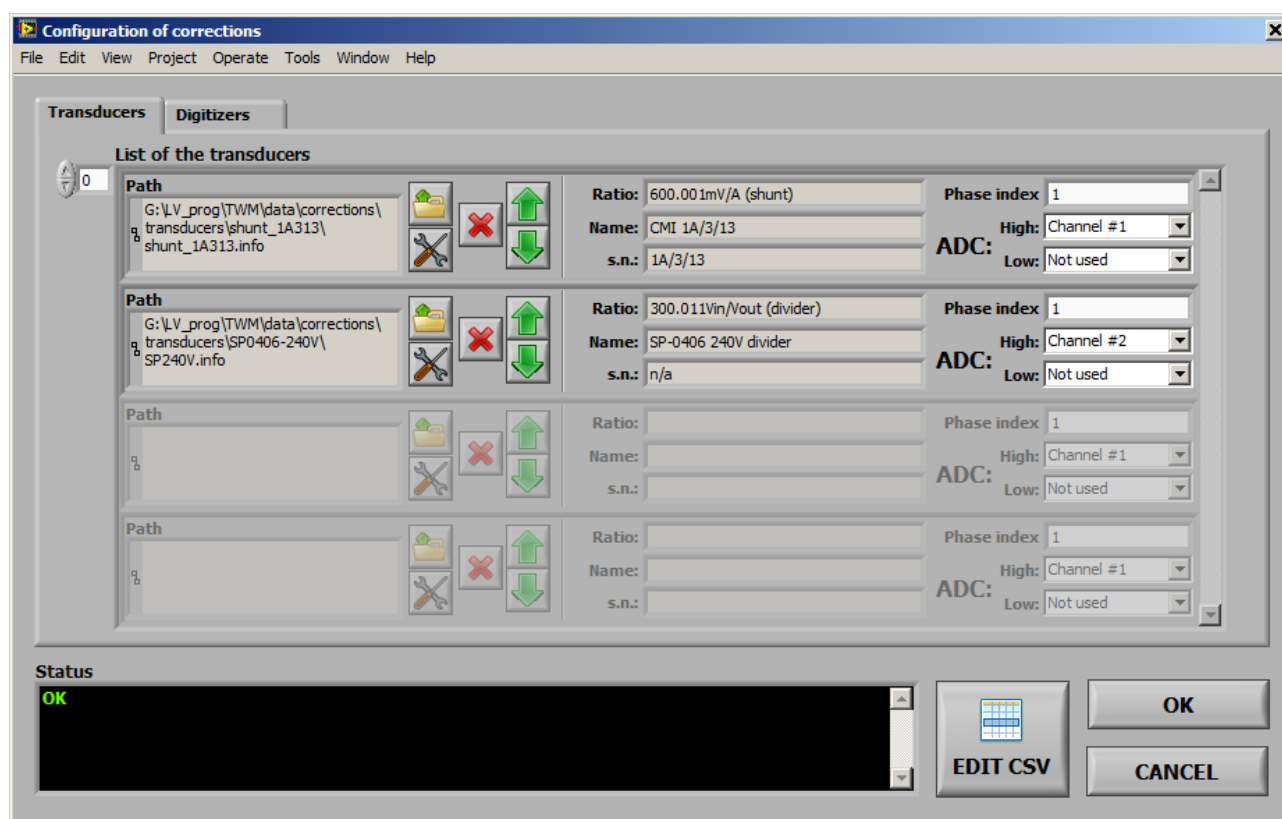


Figure 3.8: TWM transducer configuration panel.

The transducer configuration panel shown in Figure 3.8 is used to: (i) Select correction files of

particular transducers; (ii) To assign the digitizer channels to particular transducers; (iii) To assign transducers to system phases.

The behaviour of TWM depends on the combinations of assigned transducers. First example for analysis of three phase current is shown in Figure 3.9. If single input algorithms, such as harmonic analysis are used, TWM assumes each transducer represents one standalone channel (phase) and it will repeat the same calculation for each of the transducers. Note in this case there cannot be two transducers of the same type (shunt or divider) with the same **phase index**. TWM can accept combination of shunts and dividers or no transducers at all. In such case it will assume the channels are voltages with unity correction value and will assign one automatically to every available digitizer channel.

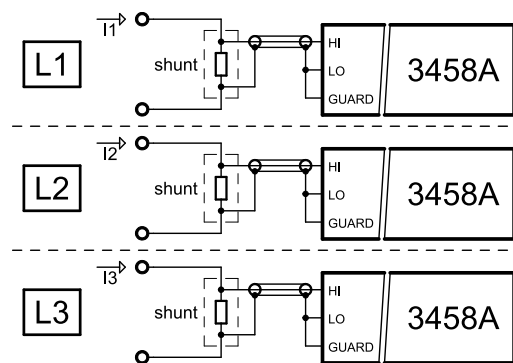


Figure 3.9: TWM operation for analyzing with single input algorithms.

Another example shown in Figure 3.10 is measurement with algorithms requiring pair of inputs, i.e. power algorithms that requires voltage and current channels. In this case there must be always one shunt and one divider of the same **phase index** so TWM can pair them and execute the paired input algorithm. It is also possible to make multiple pairs, each with different **phase index** as shown in Figure 3.11 in which case TWM will repeat calculation for each each pair (phase). Note for the paired-input algorithms TWM always requires transducers assigned even if no correction is needed, because it is not able to distinguish voltage and current channels of the digitizer by itself.

The page **Transducers** of the correction panel allows user to create list of transducers. User may create multiple transducers by adding or removing the rows to the **List of the transducers**. Each row designates one transducer, which may be either for voltage or current channel. **Open** icon is used to select the transducer correction file (voltage divider or shunt). When the load is successful, the type and nominal ratio will be shown in the middle of the row. User must then assign **Phase index** to each transducer. This is integer number that is used by TWM to pair the voltage and current transducers for algorithms such as power. Selectors **High** and **Low** are used to map the transducer output(s) to particular digitizer virtual channels. **High** channel must be always assigned. For differentially connected transducers, user must also assign the **Low** side digitizer channel. For single ended mode assign **Not used** to the **Low**. Every time the change is made, TWM will check the validity and show either “OK” or error message in the black area. Note the TWM does not require the transducers to be defined for single input algorithms, such as PSFE. It will load default unity transfer transducer. But it is required for multi-input algorithms such as power, because TWM must know which is voltage and current

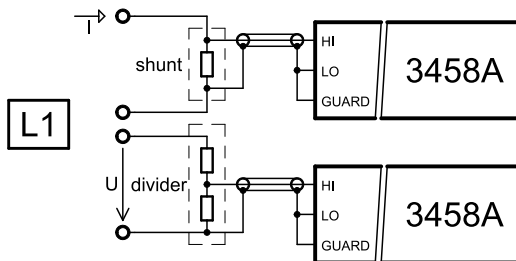


Figure 3.10: TWM operation for analyzing single phase with paired input algorithms (power).

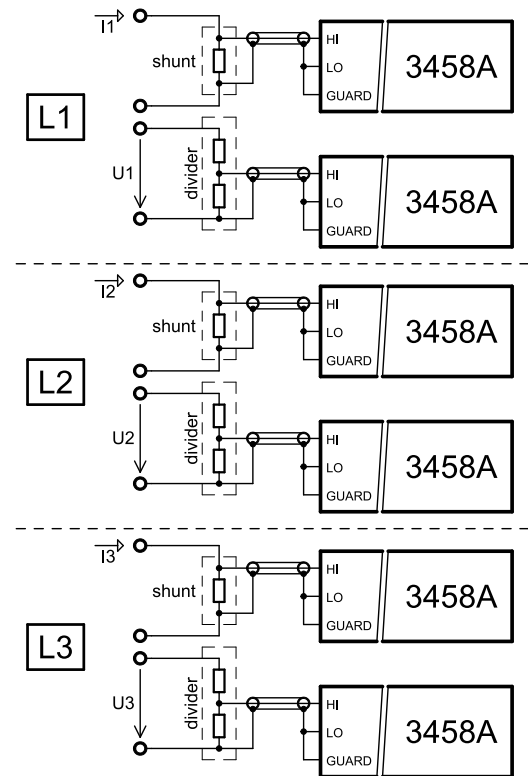


Figure 3.11: TWM operation for analyzing multiple phases with paired input algorithms (power).

and to which phase it belongs. Also note the TWM installation contains examples including “dummy” divider and shunt correction with unity transfers in the TWM folder:

```
.\data\corrections\transducers
```

These should be used if no input correction is needed, but definition of voltage or current channels are required.

The transducer items in the **List of the Transducers** can be also edited directly from TWM. Pressing the **Edit** button will invoke a dialog shown in Figure 3.12. The panel starts with selector of **Correction file path**. Change the path to load another file to the editor. **Type** defines type string of the transducer divider (“shunt” or “divider”). **Name** and **Serial number** are user descriptions of the correction. **Digitizer channel identifier** is optional name of a digitizer channel to which the transducer belongs. TWM will throw an error if non-empty and digitizer channel identifier does not match. Next, user can select **Correction item** to edit. Either numeric entry or CSV editor button **EDIT CSV** will be shown. The numeric values can be typed in directly to the **Value** and **Uncertainty** edits. CSV style correction is edited via **EDIT CSV** button or the relative link to the CSV file can be written directly to **CSV table path (relative)** edit. Note TWM is designed so it prefers CSV files related to the correction to be placed to the same folder (or subfolder) as the correction INFO file. Any changes done must be saved by **SAVE CHANGES** button before leaving.

The screenshot shows a software window titled "Transducer correction INFO file editor". It has a menu bar with "File", "Edit", "View", "Project", "Operate", "Tools", "Window", and "Help". The main area contains several input fields and buttons:

- Correction file path:** A text field containing "G:\LV\_prog\TWM\data\corrections\transducers\SP0406-240V\SP240V.info" with a file explorer icon to its right.
- Type:** A dropdown menu showing "divider".
- Name:** A text field containing "SP-0406 240V divider".
- Serial number:** A text field containing "n/a".
- Digitizer channel identifier (optional):** An empty text field.
- Correction item:** A dropdown menu showing "nominal ratio".
- Value:** A text field with a spinner icon containing "300.0112".
- Uncertainty:** A text field with a spinner icon containing "300u".
- INFO:** A button with an information icon.
- EDIT CSV:** A button with a grid icon.
- CSV table path (relative):** A text field containing "300.0112".
- SAVE CHANGES:** A button with a floppy disk icon.
- OK:** A button.

Figure 3.12: TWM transducer correction editor.

The CSV file editor example is shown in Figure 3.13. The path of selected CSV file is shown in the **File path** selector which can be also used to select another file directly in the panel. Editing the values is possible by typing into the cells or via the pop-up menu. **Copy Data** and **Paste Data** are possible between Excel style editors and the TWM CSV editor. Note the TWM will automatically try to convert all numeric decimal separators to a dot which is only accepted by TWM. In case of a new CSV creation, user may select pop-up item **Create Template** which should generate expected header of the required CSV table according to the correction manual [64]. Note any changes must be saved by **SAVE** button before leaving. If the CSV editor was called from a correction item editor, it will overwrite relative CSV path in the selected correction item by the saved CSV file path.

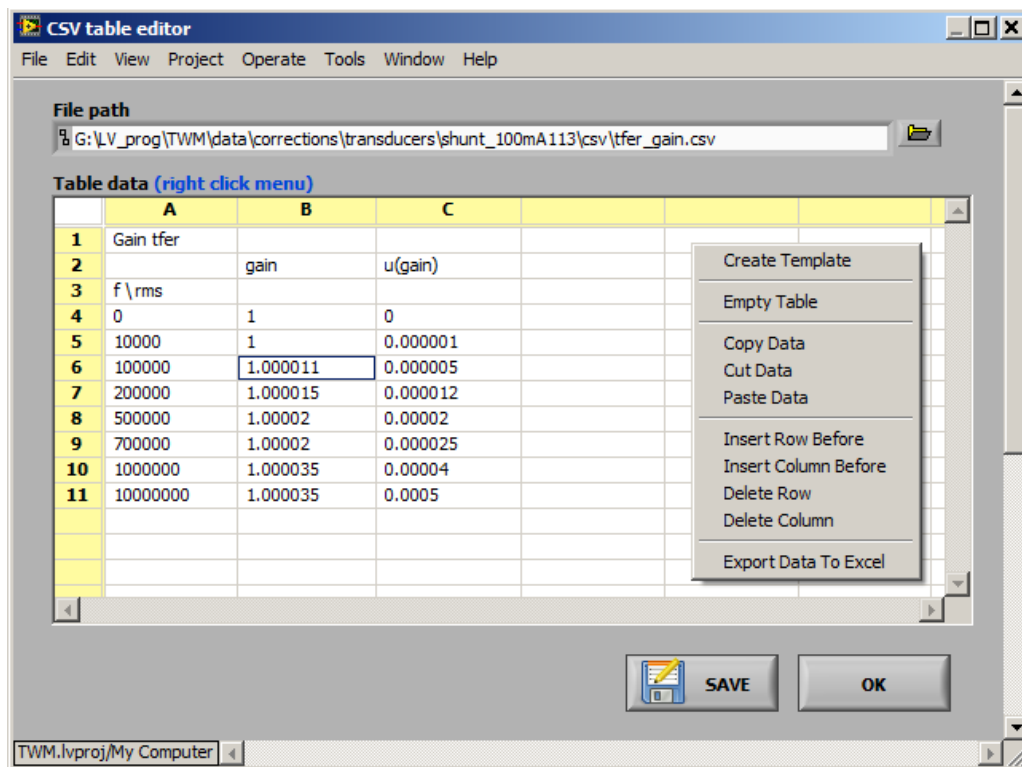


Figure 3.13: TWM CSV correction matrix editor.

### 3.1.4.3.2 Digitizer corrections

**Digitizers** page of corrections panel shown in Figure 3.14 is used for loading the digitizer correction file. The correction file is selected by pressing **LOAD NEW CORRECTIONS**. This is verified by pressing **CHECK HW CONSISTENCY**. The content of the correction file must match the configured digitizer, i.e. the channel names and order must be the same. **RELOAD CORRECTIONS** will just reload the same correction file in case it was modified. **CLEAR CORRECTIONS** is used to clear digitizer corrections. TWM will work without digitizer corrections selected normally, except no correction will be applied. Only exception are the corrections that are enabled by default, i.e. currently only aperture correction (see section 3.2.5.8).

Last option is **EDIT CORRECTION**, which will invoke panel shown in Figure 3.15 for direct editing (or creation) of digitizer correction files. **Correction file path** entry is used for selection of correction INFO file. Change it to load another file if required. **Channel identifiers** is a list of digitizer channels for which the correction will apply. Optionally use pop-up menu to load channel names from currently connected digitizer. **Channels list** must contain one row for each channel. The items are relative paths to the INFO correction files of particular channels. Use pop-up menu to **Insert**, **Remove** or **Edit Channel Correction** items. **Edit** will invoke identical editor panel for a channel correction file. In channel editing mode the **Channel identifiers** will be disabled and **Channel name filter** will appear. This is optional item that may be used to restrict use of the correction file for particular digitizer. Leave it empty in not needed.

Main editor starts with the **Correction item** selector. The list should contain all available

corrections for given correction type (digitizer or channel). Selecting the desired correction should show **Value** and **Uncertainty** matrices. For direct numeric corrections the numeric values are placed directly to the **Value** and **Uncertainty** matrices. For CSV style table corrections the **Uncertainty** matrix is ignored and **Value** matrix is used to define relative CSV matrix path. Use pop-up menu to **Edit/Create CSV matrix**. Note the **Value** and **Uncertainty** matrices allows **Copy Data** and **Paste Data** between Excel style editor and TWM. Also note TWM will automatically convert the decimal separators to dot. User can additionally restrict the correction for given attributes of the digitizer and make it dependent on **Primary** or **Secondary parameter**. Please refer to the corrections manual [64] for details. Pressing the INFO button should show brief description of the correction meaning. If you want to inhibit given correction without removing its data, use **Disable correction** item. Use button **CLEAR** to clear given correction data.

Any changes must be saved by pressing **SAVE CHANGES** before leaving the panel. Note when valid INFO path was selected during save, TWM will override caller's correction path by the newly created/edited file automatically.

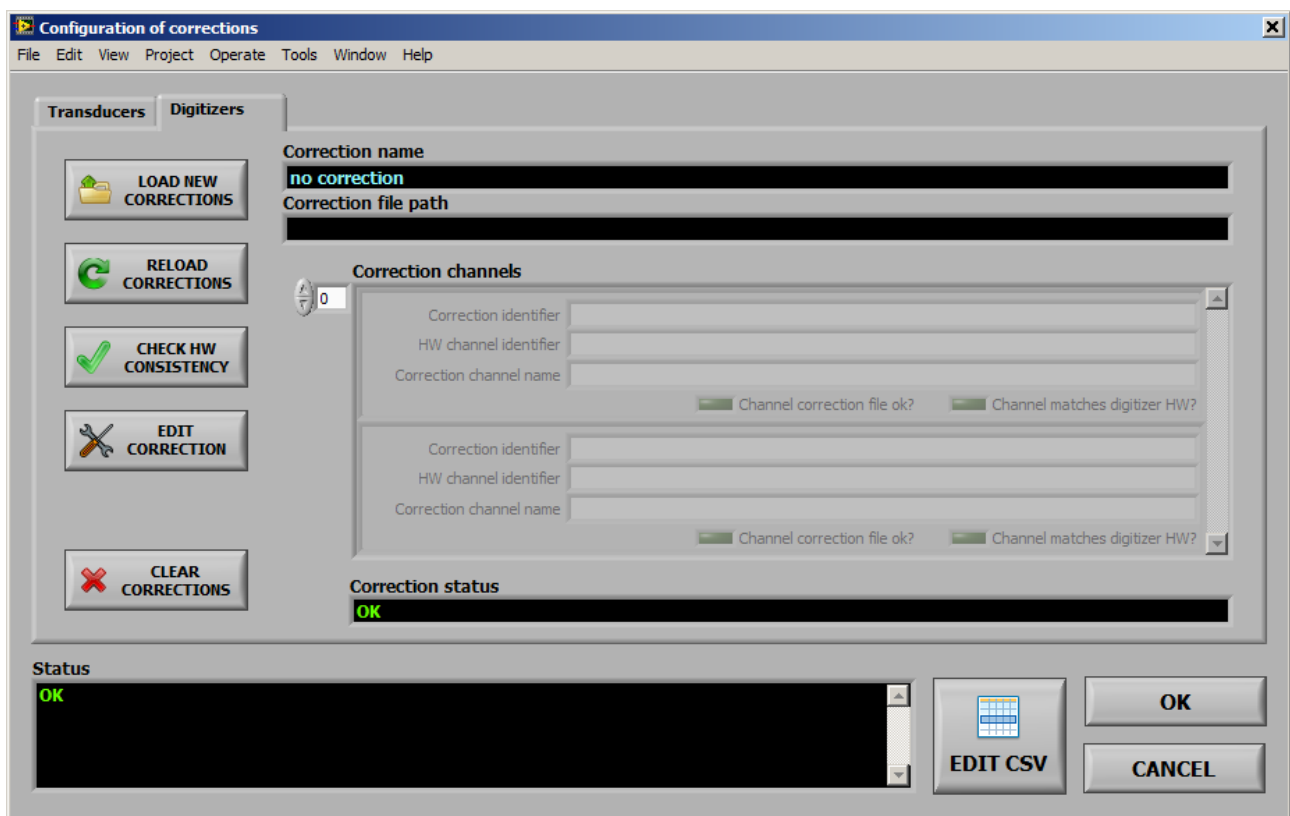


Figure 3.14: TWM digitizer corrections configuration panel.

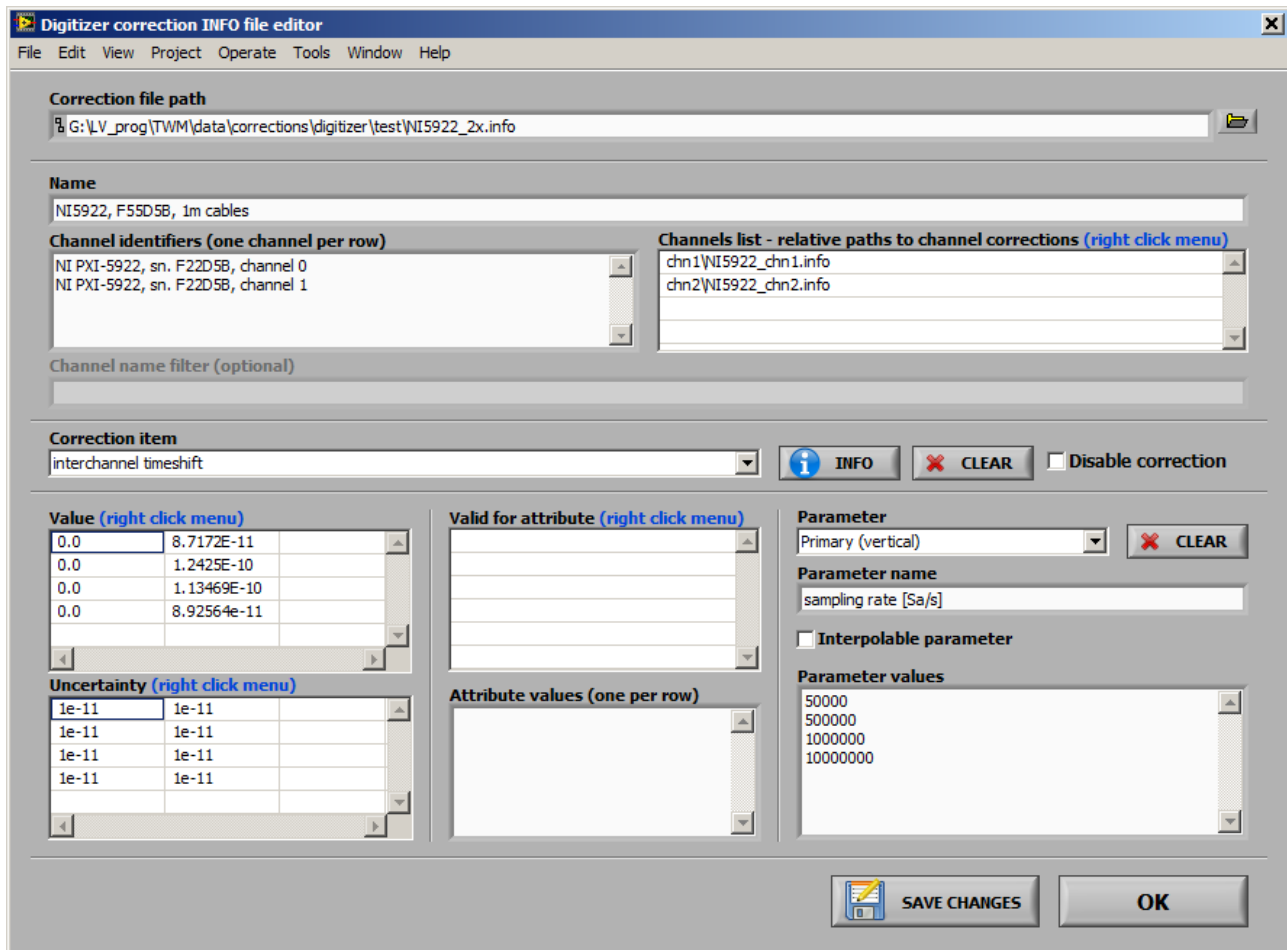


Figure 3.15: TWM digitizer correction editor.

### 3.1.4.4 Configuring new measurement

New measurement configuration can be invoked by button **SETUP NEW MEASUREMENT** or button **SETUP&START**. These will open panel shown in Figure 3.16. The panel is used to setup **Sampling rate**, **Aperture** time of the digitizer ADC, **Samples count** to record or **Measurement time**, measurement **Repetition cycles**, additional **Repetition settling** for extra delay between repetitions. Next group of options is **Trigger mode** and its parameters. Mostly it is not needed, so **Immediate** can be used. Note the mode **Level** is always derived from the first channel of the digitizer. This decision was made because of the DMM synchronization modes MASTER-SLAVE which do not allow principally different operation. The mode **External** is some form of external trigger input dependent on the selected digitizer. For DMMs it is EXT TRIG input of the MASTER DMM (if not used for AWG input). For NI 5922 it is the TRIG input on the first card in the digitizer channels list. The panel also contains **Voltage range selection**. Normally this is not needed, because the ranges can be set in the digitizer configuration, but the default ranges can be overridden from here, when other than **Keep defaults** option is selected. The TWM will allow user to set the same range to all virtual channels, or separately to odd and even (intended for voltage and current channels).



The mandatory part of this panel is setup of the destination folder for the measurement data. User must select some **Folder for measurement data files** to which the TWM will store the data and results. User must also choose a **Measurement name base**, which is subfolder to be created in the **Folder for measurement data files**. This name may contain variables as shown in the panel which will be replaced. Preview of the final path to the measurement is shown in the indicator **Full measurement base path**. Normally, if user does not require to archive the measured data for future processing, the **Measurement name base** may be still the same and TWM will simply overwrite the previous data by new ones (it will always ask to delete old data). By adding the %id% variable to the name, TWM will auto increment the **Measurement number** every time the measurement is taken, so the data will be archived in the **Folder for measurement data files**. User can also define **Measurement comment** to be stored with the data. Use Shift+Enter to break line in the comment editor.

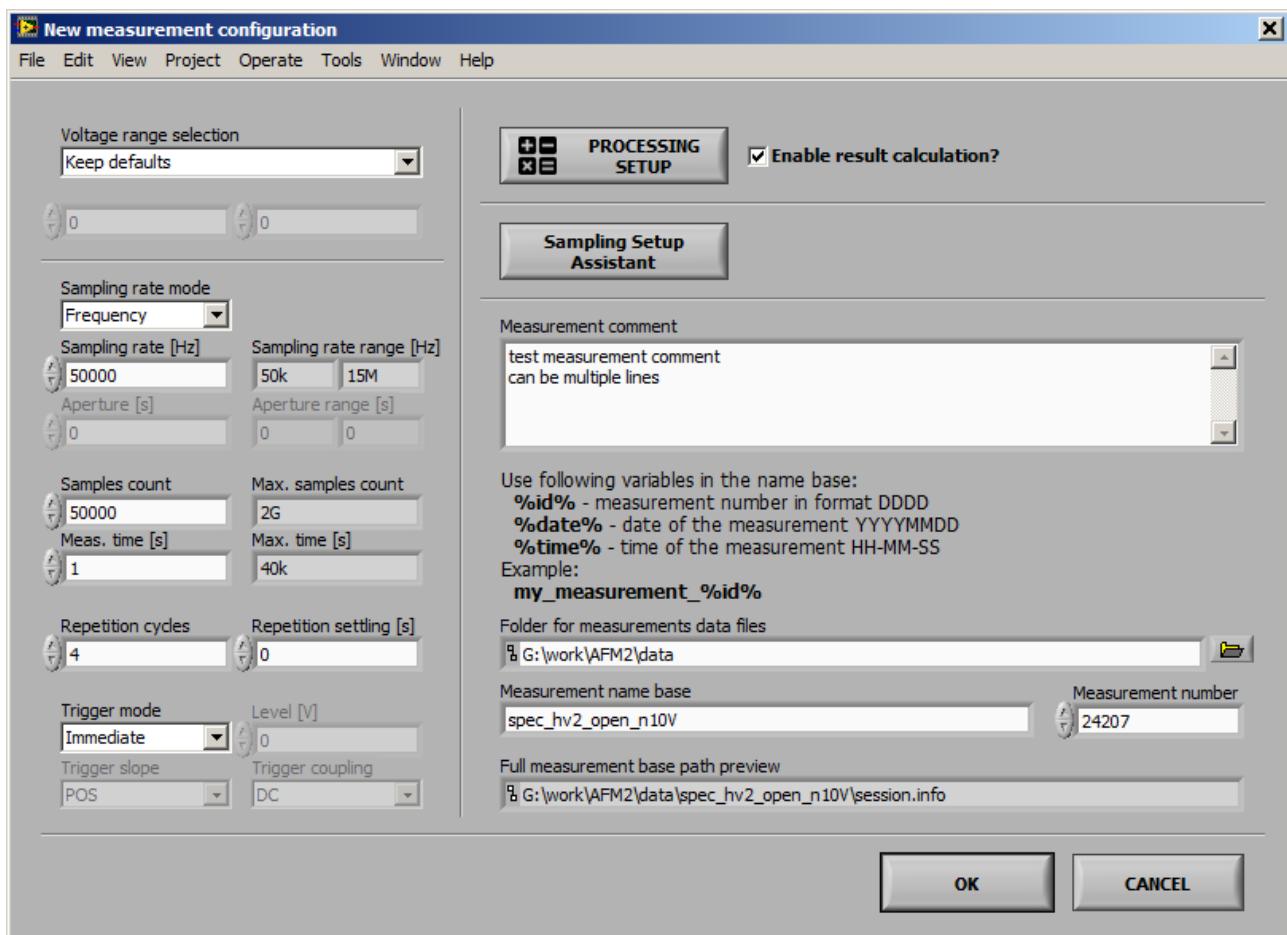


Figure 3.16: TWM new measurement configuration panel.

**Processing setup** and **Sampling Setup Assistant** are described in the following sections. Option **Enable result calculation** must be checked to perform the data processing immediately after digitizing. Otherwise TWM will only record the data to the measurement folder(s) and the processing can be initiated afterwards.

When the setups are done, user may confirm by pressing **OK** or **CANCEL** to return back. If the



panel was invoked by **SETUP&START**, the measurement will start immediately after **OK**.

### 3.1.4.4.1 Sampling setup assistant

In some cases user may need to setup coherent sampling. The **New measurement configuration** panel has integrated **Sampling Setup Assistant** for easing this task. Panel of the assistant is shown in Figure 3.17. Purpose of this panel is to measure or manually enter frequency of the fundamental component of the signal and calculate combination of the sampling rate and samples count which will result in coherent sampling. The frequency can be measured using subpanel shown in Figure 3.18 that can be invoked by pressing **MEASURE**. Alternatively, if it is known, it may be entered directly to the **Reference frequency fr**. The frequency can be multiplied by a factor **P/Q** and shifted by given offset to resulting **Fundamental frequency f0**. At this point user must enter search range of the sampling rate **Minimum fs** and **fs max tolerance** and total measurement time range **Min integration t.**, **Max integration t.** or **Min periods**, **Max periods** counts. By pressing **FIND ROUGH**, the TWM will select nearest possible sampling rate and time, but not coherent. This is just to show user rough calculated parameters of the sampling such as DFT bin spacing, periods count, etc. By pressing **FIND COHERENT**, TWM will call experimental m-function that will try to find coherent setup in the set ranges. The function is quite complicated and may take a while, so **Max timeout [s]** control is used to set maximum time to spent on the calculation. Control **Max setup error** defines how accurately TWM searches the coherent setup. Note the digitizers may have very limited step of sampling period or frequency, so there may be no coherent setup for irrational fundamental frequencies **f0**. This may be prevented by selecting higher tolerance.

The subpanel for automatic frequency measurement of the reference frequency shown in Figure 3.18 is basically a reading loop for a selected counter. It will perform up to **Max averages** readings and calculates average frequency. When **OK** is pressed, the measured value will be transferred to the **Sampling setup assistant panel**.

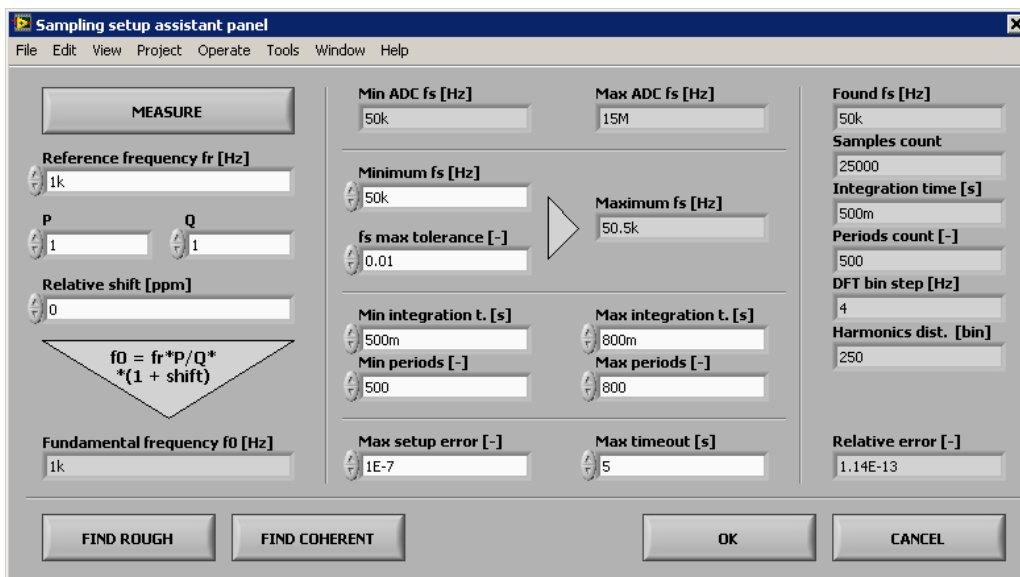


Figure 3.17: TWM sampling setup assistant.

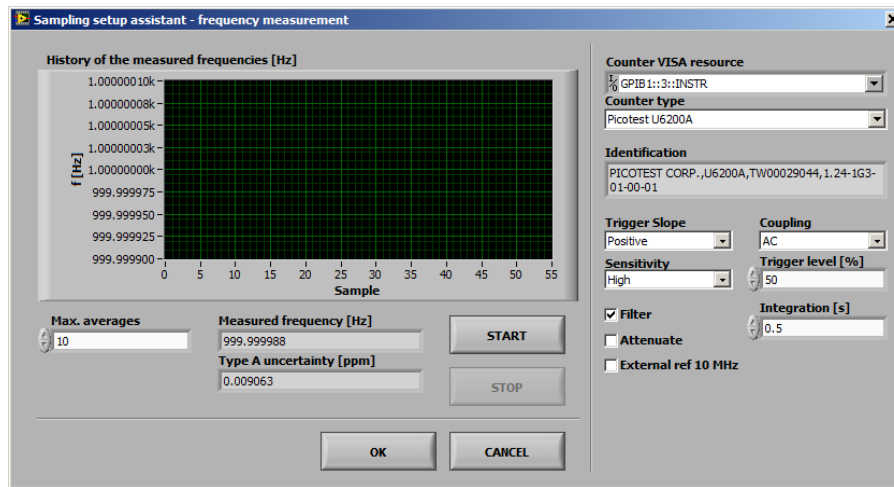


Figure 3.18: TWM sampling setup assistant - fundamental frequency measurement panel.

#### 3.1.4.4.2 Configuring data processing

Panel for configuration of the processing is accessible from the **New measurement configuration panel** shown in Figure 3.16 or from batch processing panel Figure 3.26 (see section 3.1.4.7). There are two main modes of processing which are selected by the page selector. The **RAW command** is a simple debugging mode which enables user to simply type in or load m-code to execute on the raw measured sample data (see panel shown in Figure 3.19).

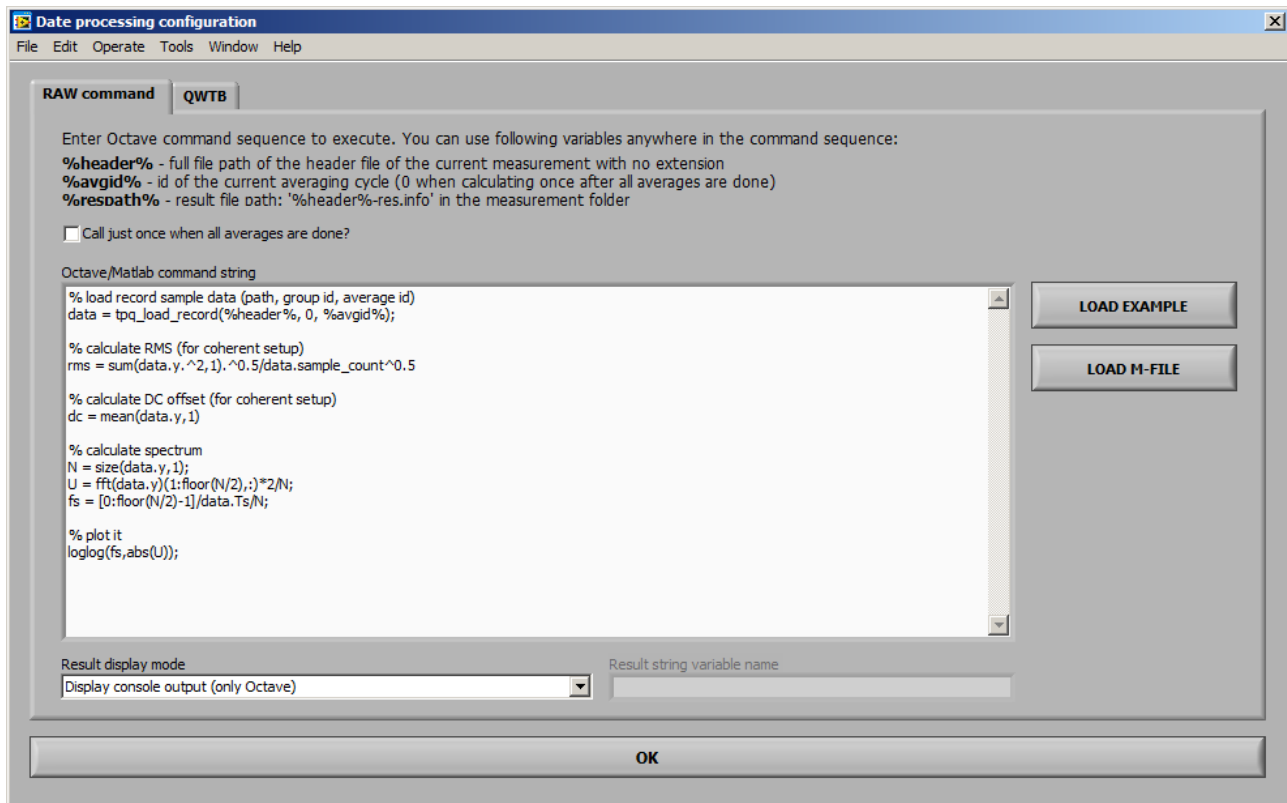


Figure 3.19: TWM processing configuration panel (raw Matlab commands mode).

The other and preferred option is the **QWTB** mode, which is shown in Figure 3.20. When the panel is opened, TWM will fetch the available **List of algorithms** from QWTB distribution linked in the panel **GNU Octave/Matlab configuration** panel in Figure 3.4. Note this operation may take some time during which the controls will be grayed. The algorithms may be reloaded manually by pressing the **RELOAD ALGs** button. Note the actual displayed list is not full list of QWTB algorithms. It is intendedly limited by filtering file (see [65] for details):

```
.\ocprog\qwtb_list.info
```

This decision was made to remove algorithms which are not compatible with TWM. When no error occurred and correct version of QWTB was selected, the list should contain some 10+ algorithms. By selecting one, TWM will fetch the algorithm info, which may also take some time. The description should appear in the indicators on the right side. The **LED indicators** will indicate features of the algorithm. The table **Parameters of the algorithm** will be filled by the user parameters of the algorithm. User may enter the numeric or text into the table following the algorithm manual [66]. The table can be cleared by the button **CLEAR PARAMETERS**. Note each row name may contain a suffix in the parentheses. **Opt.** means the parameter is optional. **Alt.** means it has alternative parameters (details can be found in QWTB guide [67]). Description of the selected parameter (row) is shown in the **Variable description** indicator.

Bottom part of the panel contains several specialized options. First, user can segment the recorded waveform by selecting **Start offset** of the first sample and by limiting the amount of input data to process by **Input data length**. Another option is **Calculate result just once**, which

means to send multiple records to the algorithm at once. This is currently supported only by the TWM-THDFFT algorithm. Last option is **Calculate uncertainty just once**, which means the uncertainty is calculated only for the first repetition cycle (record) and it is disabled in following cycles to save processing time.

One more special processing option **Time-stamp** handling was added to the processing panel. This option will alter the way TWM processing module handles the time-stamps coming from the digitizers. Many algorithms that involve phase angle perform phase correction based on the time-stamp  $ts$  and frequency component  $f$  following formula 3.1:

$$\varphi' = \varphi - ts \cdot f \cdot 2 \cdot \pi \quad (3.1)$$

As long as sampling is coherent, this correction will ensure the measured phase remains constant independent of a trigger point of a digitizer, which may be valuable for averaging multiple record results. It works fine for algorithms such as FFT, where frequency is given exactly by the DFT bin selection. But for fitting algorithms the frequency  $f$  has its own uncertainty and for large values of  $ts$  the correction will produce large uncertainty of a phase angle. Therefore, TWM processing module was extended by option to **Disable** the time-stamp (algorithm will receive only the channel time-shift correction in this case) or to the **Relative to 1. record**, which means the time-stamps of particular records are subtracted from a first record. This will still allow the phase correction within the repeated records, but minimizes the absolute value of the correction and thus the additional phase uncertainty.

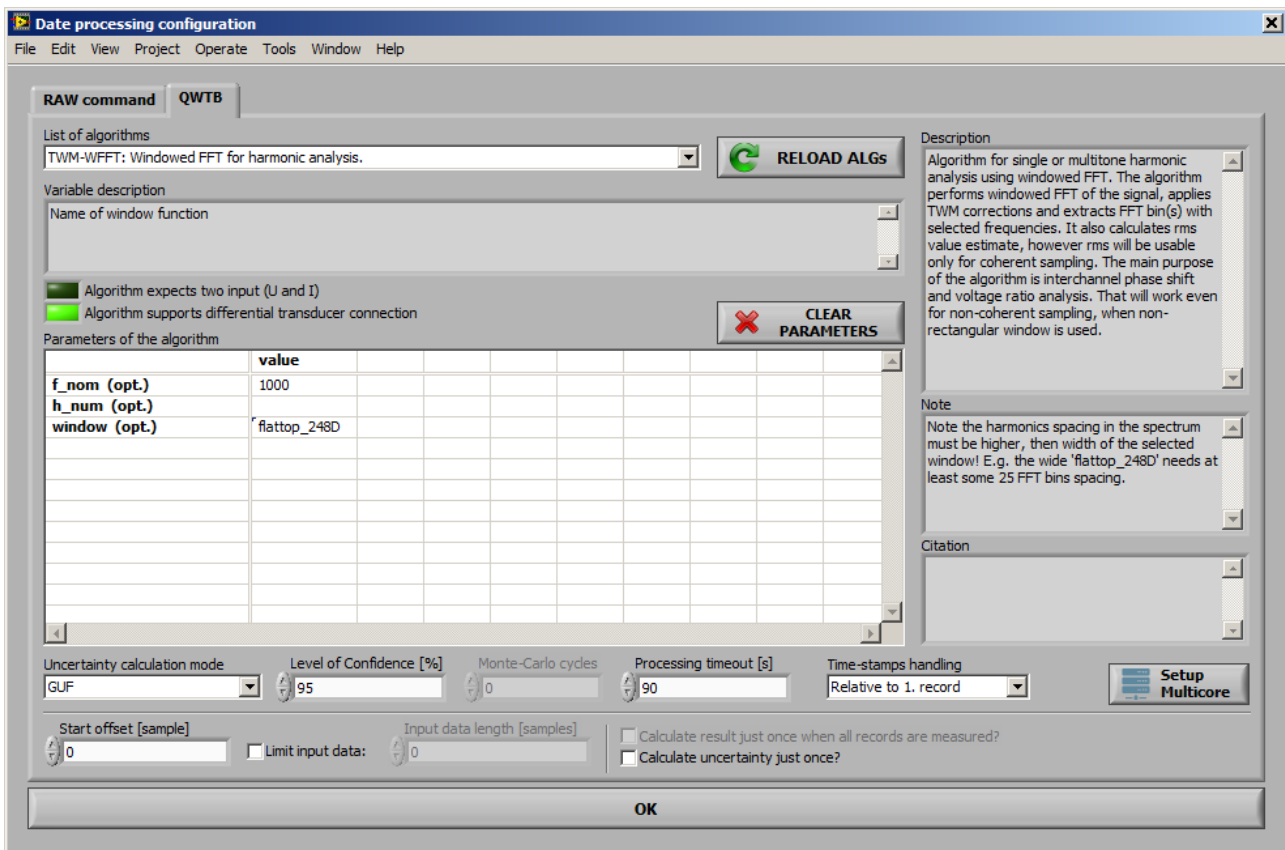


Figure 3.20: TWM processing configuration panel.

Next, user should select **Uncertainty calculation mode**. Depending on the algorithm, there may be **None** (no uncertainty calculation), **GUF** (GUF method or fast estimator) or **Monte Carlo** (numeric Monte Carlo calculation). User should also enter desired Level of Confidence for the calculation. For Monte Carlo there is also entry **Monte Carlo cycles** which should be always set to at least 1000 iterations (refer to algorithms manual [66] for optimal setup). Control **Processing timeout [s]** is maximum allowed calculation timeout. Note this will work only for GNU Octave as Matlab interface has no abort capability from LabVIEW. Also note if the timeout is reached, the TWM will throw an error, but the processing still runs in the GNU Octave, so Octave must be eventually restarted using the Octave/Matlab configuration panel.

The Monte Carlo calculation has one more advanced option – the **Setup Multicore**. By pressing the button, the panel in Figure 3.21 will be shown. The default **Execution mode** is **Singlecore**, which means all iterations of the Monte Carlo will be performed on a single core. Option **Multicore** uses “parfor” command for Matlab or “parcellfun” command from “optim” package [68] for GNU Octave. Note the “parcellfun” will not work in Windows in current version of GNU Octave. Last option is **Multistation**, which will work only for GNU Octave and it uses package “multicore” [69] which must be installed and loaded. This package is using shared **Multistation jobs folder** to distribute so called job files, which are then processed by any number of GNU Octave servers that can be started by pressing **Start Servers**. If the operation was successful, the panel shown in Figure 3.22 will appear. Note all the servers prints to the same console so the content will be most likely unreadable. The only purpose is to see the processing is happening and to enable easy termination. The servers can be terminated by simply closing their console window. This option has significant effect on the performance of Monte Carlo calculation, however it should be used only after the **Singlecore** was tested and working properly.

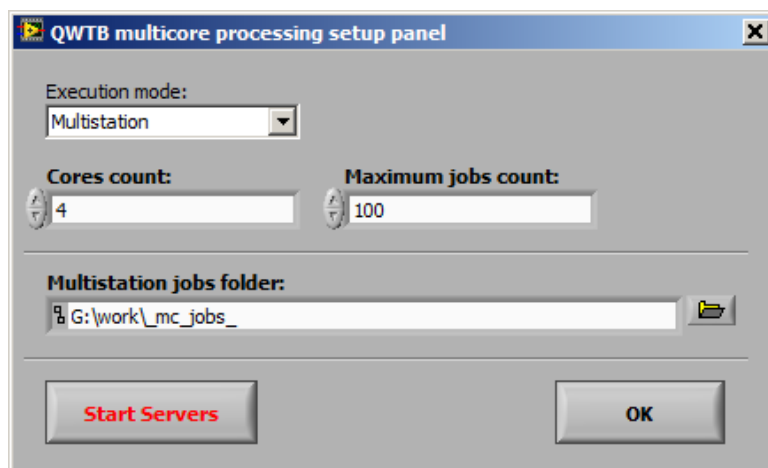
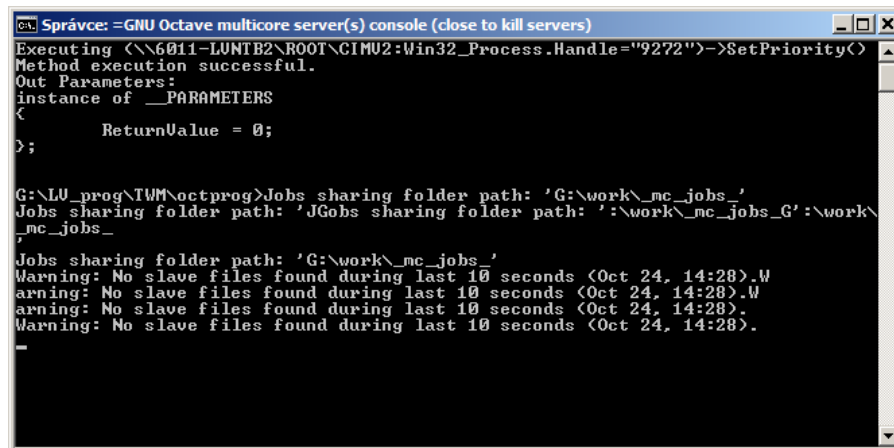


Figure 3.21: TWM multicore processing setup panel.



```

Správce: =GNU Octave multicore server(s) console (close to kill servers)
Executing <\\6011-LUNTB2\ROOT\CIMU2:Win32_Process.Handle="9272">->SetPriority<
Method execution successful.
Out Parameters:
instance of __PARAMETERS
<
    ReturnValue = 0;
>;

G:\LU_prog\TWM\octprog>Jobs sharing folder path: 'G:\work\_mc_jobs_'
Jobs sharing folder path: 'JGobs sharing folder path: ':\work\_mc_jobs_G'\work\_
\_mc_jobs_
Jobs sharing folder path: 'G:\work\_mc_jobs_'
Warning: No slave files found during last 10 seconds <Oct 24, 14:28>.W
arning: No slave files found during last 10 seconds <Oct 24, 14:28>.W
arning: No slave files found during last 10 seconds <Oct 24, 14:28>.
Warning: No slave files found during last 10 seconds <Oct 24, 14:28>.

```

Figure 3.22: TWM multicore processing GNU Octave servers.

#### 3.1.4.5 Initiating measurement

When everything is configured, the measurement can be initiated by pressing the **START** or **SETUP&START** buttons on the main panel. Note pressing the **START** will still ask for new setup if the HW configuration was changed. The ongoing measurement can be terminated by pressing the **STOP** button at any time.

#### 3.1.4.6 Viewing the results

User may inspect the digitized waveforms using the button **VIEW RECORD** at any time. The panel shown in Figure 3.23 will be displayed. This panel rereads the data from saved record on runtime, so it may be a little slow for the long records. That is why it is equipped by entry **Max samples to display** to limit the viewed data amount. The panel can be displayed permanently along with the TWM.

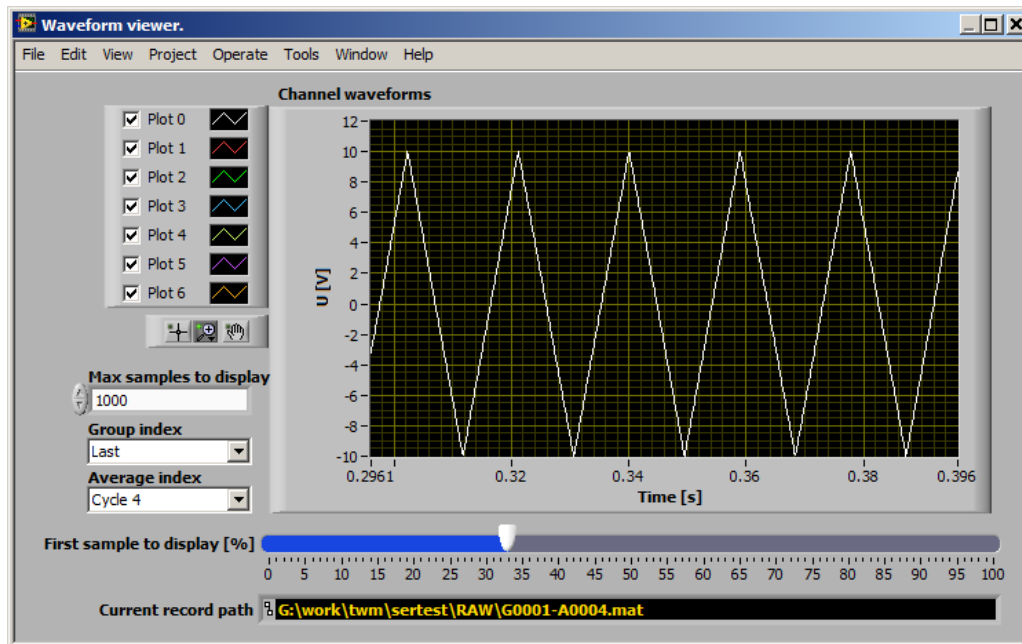


Figure 3.23: TWM record viewer panel.

If the algorithm contains the spectra of defined in the “qwtb\_list.info”, they can be displayed in dedicated panel shown in Figure 3.24. The panel can be shown by pressing button VIEW FFT on main panel Figure 3.3. The panel shows the spectra calculated by selected algorithm. So it will not display spectrum if processing is disabled or selected algorithms does not return it as one of the output quantities.

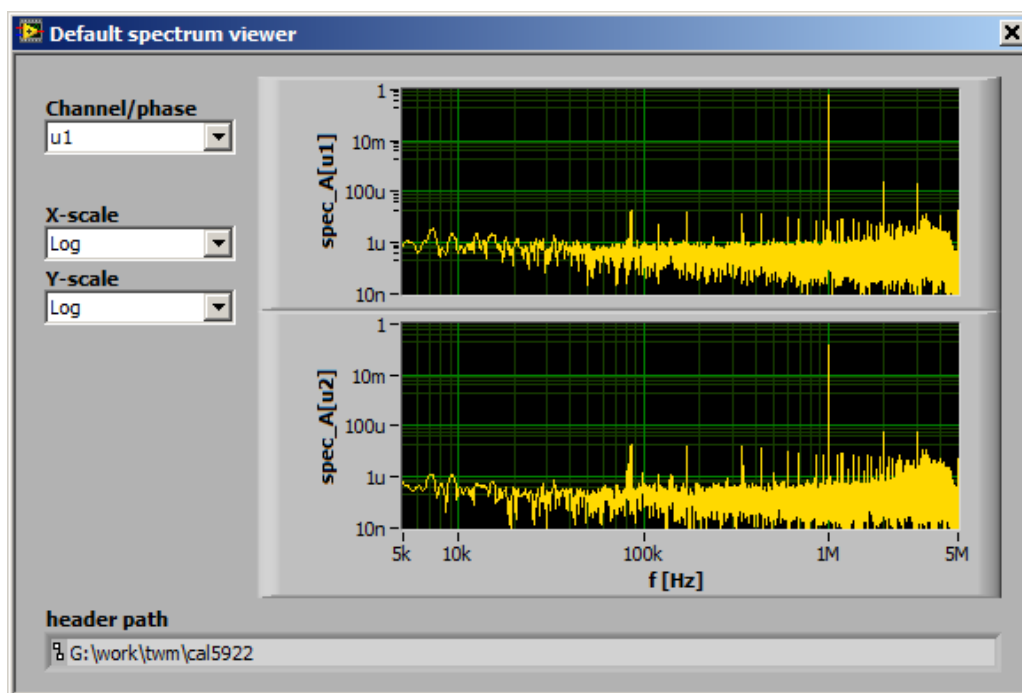


Figure 3.24: TWM spectrum viewer panel.



The results of the processing are displayed in the main panel of TWM. Depending on the processing mode, TWM will display either the **RAW** panel or **QWTB** results panel. The **RAW** panel is just a plain text. The **QWTB** is shown in Figure 3.3. First, it is important to mention the result viewer operates independently to the measurement. It can be used to view the results while TWM is digitizing and calculating new results. However, all the results formatting and querying is performed in GNU Octave/Matlab, so when the data are being processed, the display of results will be halted.

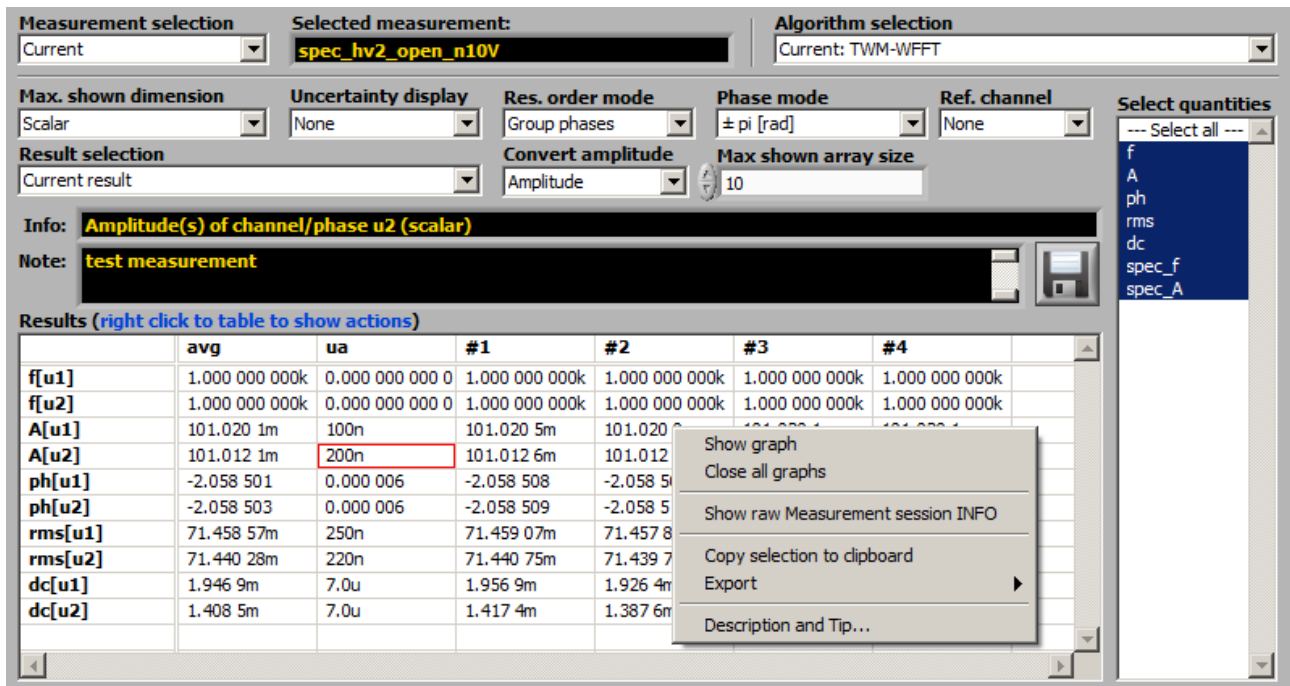


Figure 3.25: TWM processing results viewer.

First control to use is **Measurement selection**. To speed up the TWM operation, user may choose **None** to stop result viewer. Next option is **Current**, which will show currently measured results. Last option is **Load from file** to select previously processed results. Next control is **Algorithm selection**, which will contain names of all algorithms that were applied to the particular measurement. Next, user must select **Max. shown dimension** entry to define how the results should be displayed. Option **Scalar** means TWM will show only scalar quantities and it will show the results from all repetition cycles at once. Option **Vector** or **Matrix** will show scalars and vectors (and matrices), so it can show only one result at once. User may select desired result by entry **Result selection**. TWM can display **Current result**, selected one or **Average** of all available. Note the averaging for large results count may take considerable time. Next, user may **Select quantities** to display only needed. Next option is **Uncertainty display**, **Res. order mode** to regroup the quantities and **Phase mode** to select phase display format. **Max. shown array size** limits the size of vector and matrix quantities to be displayed, because TWM was not designed for showing large amounts of data as a table. If the size is exceeded, TWM will display “only graph” instead. **Ref. channel** is used to display phase differences between channels. This is useful e.g. for measuring inter-channel phase shift by PSFE or similar algorithm. Note the channels must have unique tags, e.g. either different phase indices or u/I transducer type, so



TWM can pick the reference channel. Next option is Convert amplitude, which will convert the quantities marked by “is amplitude” in “qwtb\_list.info” to the desired format, e.g. effective value.

The result quantities and their uncertainties are shown in the table Results. By selecting the row, TWM will display description from the QWTB toolbox. Also note there are several options available by right click to the table content (see Figure 3.25). First, the data can be exported to MS Excel (it must be installed first). Next, any row can be shown as a graph. This is useful for spectra or viewing the history of given quantity. Note the graphs are generated by GNU Octave/Matlab so they remain opened until closed manually or via **Close all graphs** option but it may take some time especially for GNU Octave for large datasets. Any selection can be copied to a clipboard and paste to Excel style editor. Note the exporting and copying to Excel will always try to convert data to numeric format.

#### 3.1.4.7 Batch processing

TWM can be used as a sampling tool only and the processing can be done later. Also user may need to calculate additional parameters from already digitized signals. TWM is equipped by the batch processing tool for this case. The tool shown in Figure 3.26 can be invoked by pressing **START QWTB CALC**. User must select the **Measurement session**. Next, the tool will show available **measurement groups** and **records**, which must be selected first. Next, the algorithm must be selected by pressing the **PROCESSING SETUP** button. After the selection, the processing can be started by pressing **START** and eventually terminated by pressing **STOP**. The new measurement results will be shown in the results viewer in the main panel. Note calculating repeatedly the same algorithm will always override past results for the same algorithm. However, the results from the other algorithms will be untouched and available for displaying.

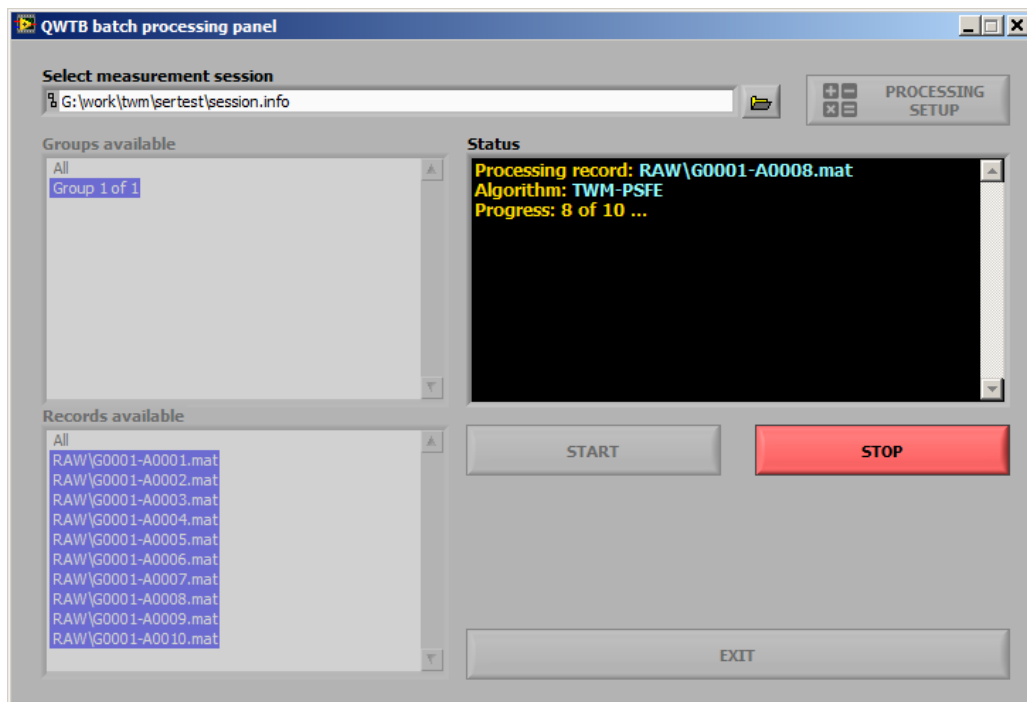


Figure 3.26: TWM QWTB batch processing panel.

## 3.2 TWM Corrections Reference Manual

Following section describes format of the correction data sets for digitizer and transducers for TWM or TPQA tools. This chapter does not describe calibration methods (not into details). It only describes different correction strategies and available corrections, their behaviour and format. For details on the possible calibration process of the components please refer to the chapter 2.

All correction files are based on the combination of INFO-STRINGS library [70] and ordinary CSV files. The combination was chosen to keep the format human readable and at the same time editable by commonly available SW tools.

The corrections are loaded automatically by the TWM tool and passed to the PQ algorithm wrapped in the QWTB toolbox [67]. The following text shows the formats of the correction data sets, behavior of the TWM corrections loader and naming of the correction values and tables that will be passed to the QWTB algorithm.

Note although ALL the corrections can be created and edited via graphical user interface of TWM tool, it is not possible to do that using TPQA tool and furthermore user must first know meaning and structure of the particular corrections.

### 3.2.1 CSV marices

Many of the correction matrices in the TWM tool are stored as CSV tables with values separated by semicolon “;”. Example are the frequency-amplitude transfers. This solution was chosen to ensure flexibility and easy editing for the user. All the matrices must have unified format which is shown in following text.

It may be a bit problematic to save CSV files in this format on computers with various language localizations, so when using e.g. Excel, it is important to carefully check if the saved CSV file contains semicolon as a value separator. This may be dependent on local setting in Windows. Some languages uses comma “,”, some semicolon “;”. It may be needed to switch this in (Windows Control Panel | Region and Language | Formats | Additional settings).

Note the table itself is read by TWM processing module which is written in Matlab/GNU Octave. These environments expect always decimal dot “.” as a decimal separator, so it is strongly recommended to switch the system decimal separator to dot (Windows Control Panel | Region and Language | Formats | Additional settings).

TWM tool distinguishes two variants of CSV matrices. First, one dimensional (1D) matrix typically used only for a frequency dependency and second, two dimensional (2D) matrices for frequency-amplitude dependencies. Each CSV matrix, 1D or 2D, can contain one or more quantities (and their uncertainties).

Example of 1D matrix with single quantity  $A$  dependent on axis  $Y$  is shown in Table 3.2. Example with multiple quantities  $A$ ,  $B$  and  $C$  is show in Table 3.3

Comment	
$Y$	$A$
$y_1$	$a_1$
$y_2$	$a_2$
$y_3$	$a_3$

Table 3.2: Example of 1D CSV table with one quantity

Comment			
$Y$	$A$	$B$	$C$
$y_1$	$a_1$	$b_1$	$c_1$
$y_2$	$a_2$	$b_2$	$c_2$
$y_3$	$a_3$	$b_3$	$c_3$

Table 3.3: Example of 1D CSV table with multiple quantities

The “comment” column can contain any string description of the content. The table header (quantity names) starts always in the second row even if comment cell is empty.

TWM CSV matrix loader was designed so it can load even matrix with missing elements such as shown in Table 3.4. The missing value  $a_2$  will be interpolated from  $a_1$  and  $a_3$  by the loader (linear interpolation). However, missing value  $b_1$  and  $c_3$  will be loaded as NaN because they are at the boundary of the matrix and extrapolation is disabled since the uncertainty of extrapolation cannot be properly evaluated.

Comment			
$Y$	$A$	$B$	$C$
$y_1$	$a_1$		$c_1$
$y_2$		$b_2$	$c_2$
$y_3$	$a_3$	$b_3$	

Table 3.4: Example of 1D CSV table with multiple quantities and missing elements

The 1D matrix can be also made independent on the axis  $Y$  if the matrix has only one row and the axis  $Y$  values are empty as shown in Table 3.5. All TWM functions will in this case ignore the axis  $Y$  and will assume the values  $a_1$ ,  $b_1$ ,  $c_3$  for any value of  $Y$ .

Comment			
$Y$	$A$	$B$	$C$
	$a_1$	$b_1$	$c_1$

Table 3.5: Example of 1D CSV table with multiple quantities independent to axis  $Y$ 

TWM also supports 2D matrices dependent on two axes  $X$  and  $Y$ . Example of such matrix with single quantity is shown in Table 3.6. The matrix can contain any number of quantities

( $A$ ,  $B$ ,  $C$ , etc.).  $Y$  axis is identical as in 1D matrices.  $X$  axis is horizontal and its values  $x_1$ ,  $x_2$ , etc. are repeated for each quantity. All quantities must have identical number of  $X$  values. Example is shown in Table 3.7.

Comment			
	$A$	$A$	$A$
$Y \setminus X$	$x_1$	$x_2$	$x_3$
$y_1$	$a_{11}$	$a_{12}$	$a_{13}$
$y_2$	$a_{21}$	$a_{22}$	$a_{23}$
$y_3$	$a_{31}$	$a_{32}$	$a_{33}$

Table 3.6: Example of 2D CSV matrix with single quantity

Comment						
	$A$	$A$	$B$	$B$	$C$	$C$
$Y \setminus X$	$x_1$	$x_2$	$x_1$	$x_2$	$x_1$	$x_2$
$y_1$	$a_{11}$	$a_{12}$	$b_{11}$	$b_{12}$	$c_{11}$	$c_{12}$
$y_2$	$a_{21}$	$a_{22}$	$b_{21}$	$b_{22}$	$c_{21}$	$c_{22}$
$y_3$	$a_{31}$	$a_{32}$	$b_{31}$	$b_{32}$	$c_{31}$	$c_{32}$

Table 3.7: Example of 2D CSV matrix with multiple quantities

The 2D matrix can be also independent on  $Y$  axis as shown in Table 3.8 or independent on  $X$  axis as shown in Table 3.9. The example of matrix independent on both axes  $X$  and  $Y$  is shown in Table 3.10.

The 2D matrix can of course also contain empty cells same as for 1D variant. The interpolation of missing cells is performed per columns.

Comment						
	$A$	$A$	$B$	$B$	$C$	$C$
$Y \setminus X$	$x_1$	$x_2$	$x_1$	$x_2$	$x_1$	$x_2$
	$a_{11}$	$a_{12}$	$b_{11}$	$b_{12}$	$c_{11}$	$c_{12}$

Table 3.8: Example of 2D CSV matrix with multiple quantities independent on axis  $Y$ 

Comment			
	$A$	$B$	$C$
$Y \setminus X$			
$y_1$	$a_{11}$	$b_{11}$	$c_{11}$
$y_2$	$a_{21}$	$b_{21}$	$c_{21}$
$y_3$	$a_{31}$	$b_{31}$	$c_{31}$

Table 3.9: Example of 2D CSV matrix with multiple quantities independent on axis  $X$

Comment			
	$A$	$B$	$C$
$Y \setminus X$			
	$a_{11}$	$b_{11}$	$c_{11}$

Table 3.10: Example of 2D CSV matrix with multiple quantities independent on both axes  $X$  and  $Y$

### 3.2.2 Correction model

The TWM tool and the implemented algorithms perform corrections to the errors introduced by the digitizer and transducer. However, when the transducer is connected to the digitizer via cable, the transducer's transfer will be affected by the loading effects due to finite input impedance of the digitizer and capacitance of the cable. This effect can be corrected if the lumped impedance model of the transducer terminals, cables and digitizer is known. Thus a special function dealing with this problem for single-ended and differential connection of the transducer to digitizer channels was developed and each algorithm should employ it. The function is able to calculate corrections in four different configurations shown in Figure 3.27, Figure 3.28, Figure 3.29 and Figure 3.30. TWM will choose single-ended or differential based on the configuration of the transducer corrections. The buffered mode is enabled by including the buffer output impedance “Z\_buf” to the transducer corrections (see details below).

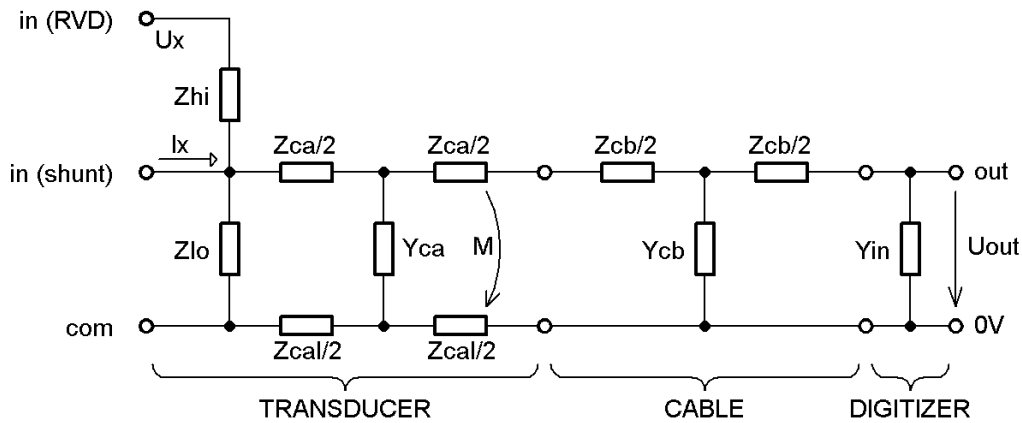


Figure 3.27: Transducer-digitizer loading correction model for single ended connections.

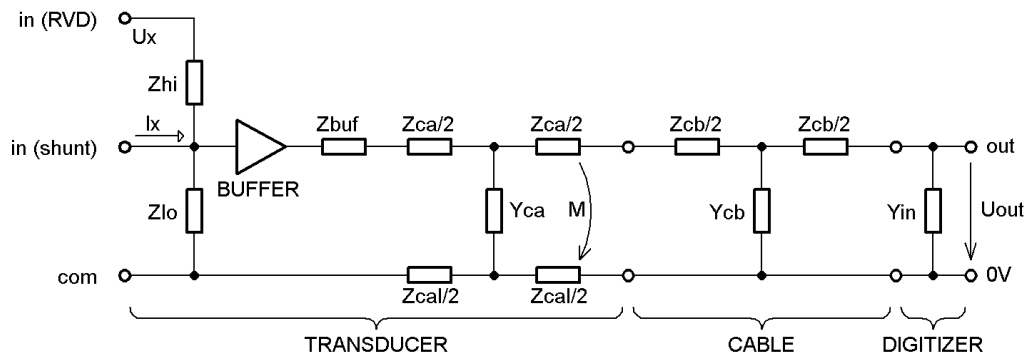


Figure 3.28: Transducer-digitizer loading correction model for single ended connections with buffer amplifier.

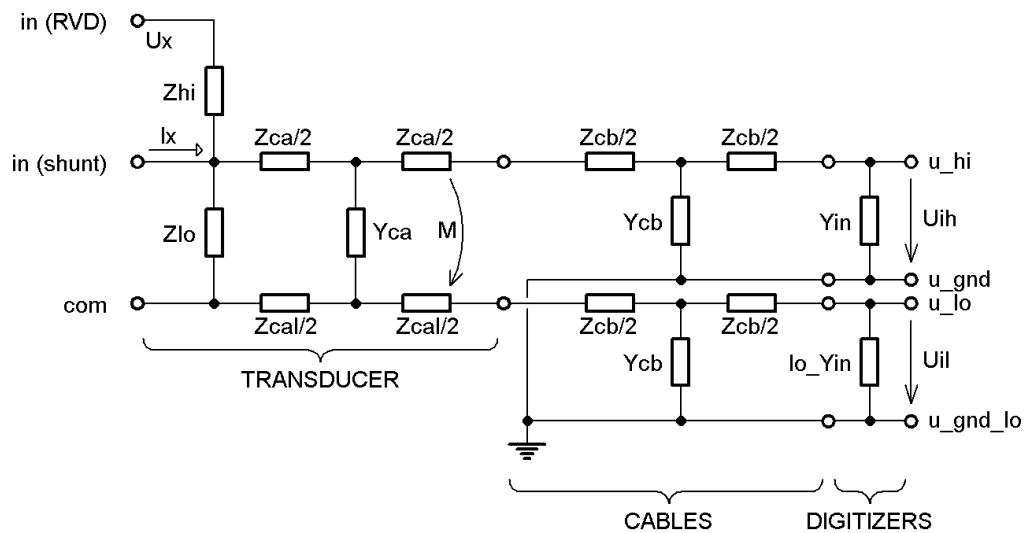


Figure 3.29: Transducer-digitizer loading correction model for differential connection.

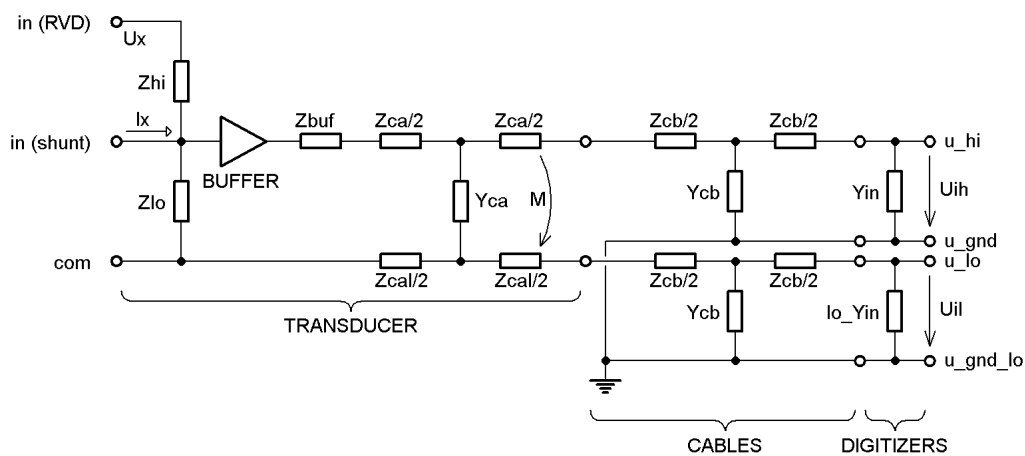


Figure 3.30: Transducer-digitizer loading correction model for differential connection with buffer amplifier.

The impedance components “ $Y_{in}$ ” (and “ $lo\_Yin$ ”) comes from the digitizer channel corrections, whereas the rest of the model components are loaded from the transducer correction file.

### 3.2.3 Calibration concept

TWM concept allows variety of calibration strategies. The basic concept shown in Figure 3.31 is to calibrate all components separately, i.e.: (i) Transducer(s); (ii) Digitizer(s); (iii) Cables (impedance model). In this concept the transducer is calibrated with reference planes at its terminals under no loading condition at the output. The absolute minimum is to calibrate nominal ratio, gain transfer, phase transfer and low-side impedance for the RVD divider. Digitizer is also calibrated at its terminals. Minimum required parameters to be calibrated are nominal gain, gain transfer, phase transfer and its input impedance. However in this concept TWM must perform loading correction according the section 3.2.2. To make this correction work, it is necessary to calibrate at least cable impedance parameters “ $Z_{cb}$ ” and “ $Y_{cb}$ ”. If there is also an adapter between the transducer and cable, typically coaxial to two BNCs, it is also reasonable to calibrate the impedance model of the adapter “ $Z_{ca}$ ”, “ $Z_{cal}$ ”, “ $Y_{ca}$ ” and “ $M$ ”. Eventually, if buffer is part of the transducer, the buffer output impedance “ $Z_{buf}$ ” can be calibrated.

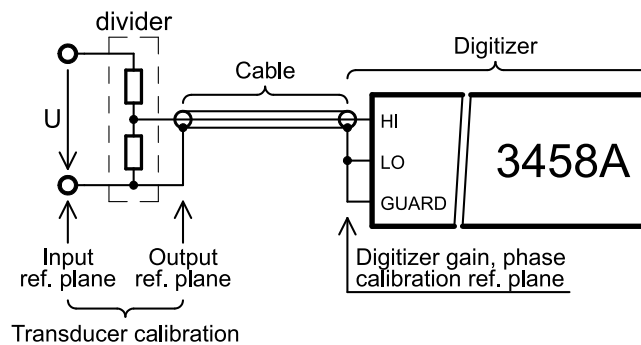


Figure 3.31: Separate transducer-cable-digitizer calibration.

The next concept is to merge the digitizer with cable as shown in Figure 3.32. This is in most cases the method of choice, because mostly the same cable is used for all transducers. Therefore it is not necessary to calibrate it separately. The digitizer is calibrated at the end of the cable, so the gain and phase effect of the cable becomes part of the digitizer gain and phase transfers. The shunting impedance of the cable “ $Y_{cb}$ ” becomes part of the digitizer input admittance “ $Y_{in}$ ” as they are measured together. Transducer will be calibrated same as in the first case. The components “ $Z_{cb}$ ” and “ $Y_{cb}$ ” are left unassigned. Analogically it is possible to merge transducer with the cable, however that is less common solution.



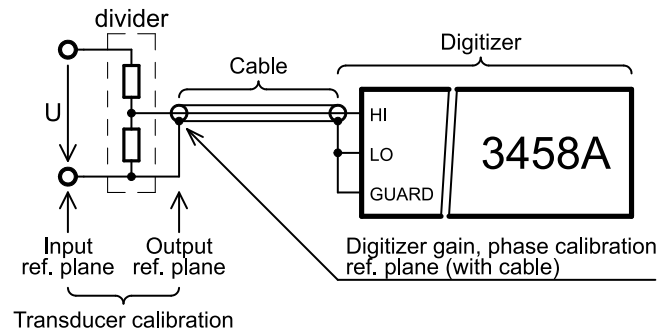


Figure 3.32: Separate transducer-(cable+digitizer) calibration.

Last possible option is so called system calibration as shown in Figure 3.33 (described also in section 2.5), where the whole input path is taken as one device. This concept requires a reference system that can measure simultaneously with TWM at the input of the TWM transducer. The deviation of TWM and the reference system is used to build gain and phase correction. Such correction can be stored to either transducer gain-phase matrices, or digitizer gain-phase matrices, because the effect is somewhat identical. All other components in the impedance model remain unassigned. Note this method is not suitable for differential connection as it would not be possible to evaluate the leakage current due to the common mode voltage at low-side input of the digitizer.

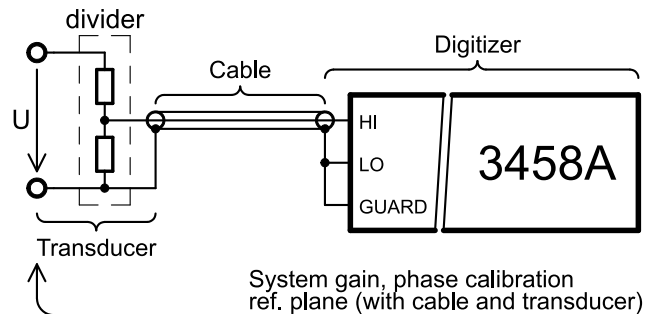


Figure 3.33: System calibration concept.

### 3.2.4 Transducer corrections

TWM recognizes two types of transducer corrections: “divider” and “shunt”. Format of the correction file is identical for both. File starts with the identifier **type** which defines the transducer type. **name** and **serial number** is description of the transducer. Optional item **linked to digitizer channel** can restrict the use of the transducer correction file to particular digitizer channel which may be needed when the transducer and digitizer channel were calibrated together. Next, the main correction data follows (description below). Example of the file for a shunt:

```
1 // type of the correction:
2 type:: shunt
3
4 // name of the transducer:
```

```

5 name:: Current shunt 1A
6
7 // serial number of the transducer:
8 serial number:: CMI/1A/1/13
9
10 // identifier of the channel of the digitizer if the transducer was calibrated together with the digitizer:
11 // note: leave empty or remove if not needed
12 linked to digitizer channel:: HP3458A, sn. MY45053095
13
14 // nominal/DC ratio: V/A for shunt, Vin/Vout for divider:
15 nominal ratio:: 0.600005
16 nominal ratio uncertainty:: 0.000009
17
18 // frequency transfer of the transducer — amplitude (input/output):
19 // 2D CSV table:
20 // y-axis: frequency
21 // x-axis: input rms value
22 // quantity 1: in/out transfer values
23 // quantity 2: absolute uncertainties
24 amplitude transfer path:: csv\tfer_amp.csv
25
26 // frequency transfer of the transducer — phase (input — output):
27 // 2D CSV table identical format to amp. transfer.
28 phase transfer path:: csv\tfer_phi.csv
29
30 // frequency dependence of impedance of the low—side resistor of RVD:
31 // 2D CSV table,
32 // y-axis: fundamental frequency
33 // x-axis: fundamental amplitude
34 // quantities order: sfdr [dB], u(sfdr)
35 sfdr path:: csv\sfdr.csv
36
37 // --- loading correction components ---
38 // frequency dependence of series impedance of transducer's high—side terminal:
39 // 1D CSV table, y-axis: frequency, quantities order: Rs, Ls, u(Rs), u(Ls)
40 output terminals series impedance path:: csv\Zca.csv
41
42 // frequency dependence of series impedance of transducer's low—side terminal:
43 // 1D CSV table, y-axis: frequency, quantities order: Rs, Ls, u(Rs), u(Ls)
44 output terminals series impedance path (low—side):: csv\Zcal.csv
45
46 // frequency dependence of mutual inductance between transducer's terminals:
47 // 1D CSV table, y-axis: frequency, quantities order: M, u(M)
48 output terminals mutual inductance path:: csv\Zcam.csv
49
50 // frequency dependence of loss admittance between the transducer's terminals:
51 // 1D CSV table, y-axis: frequency, quantities order: Cp, D, u(Cp), u(D)
52 output terminals shunting admittance path:: csv\Yca.csv
53
54 // frequency dependence of series impedance of the cable to digitizer input:
55 // 1D CSV table, y-axis: frequency, quantities order: Rs, Ls, u(Rs), u(Ls)
56 output cable series impedance path:: csv\Zcb.csv
57
58 // frequency dependence of shunting admittance of the cable to digitizer input:
59 // 1D CSV table, y-axis: frequency, quantities order: Cp, D, u(Cp), u(D)

```

```

60 output cable shunting admittance path:: csv\Ycb.csv
61
62 // frequency dependence of impedance of the low-side resistor of RVD:
63 // 1D CSV table, y-axis: frequency, quantities order: Rp, Cp, u(Rp), u(Cp)
64 rvd low side impedance path:: csv\Z_low.csv
65
66 // frequency dependence of impedance of the buffer output series impedance (leave out to disable buffer!):
67 // 1D CSV table, y-axis: frequency, quantities order: Rs, Ls, u(Rs), u(Ls)
68 buffer output series impedance path:: csv\Z_buf.csv

```

### 3.2.4.1 Transducer correction items

Following paragraphs describe particular correction components. It will always show format of the correction data and naming of the correction data quantities that will be passed to the QWTB algorithm.

#### 3.2.4.1.1 Nominal ratio

Nominal ratio item **nominal ratio** is scalar real value that defines nominal (typically DC) ratio of the transducer. For shunt it is value in Ohms. For divider it is input-to-output ratio voltage. The value has also associated absolute uncertainty **nominal ratio uncertainty**. Both values are mandatory. Note it is possible to use these items to store nominal gain for any frequency, e.g. 50 Hz. It is not restricted to DC. The relative amplitude transfers [3.2.4.1.3](#) will be always relative to this value. So the choice is up to the user.

#### 3.2.4.1.2 Amplitude transfer (optional)

**amplitude transfer path** is path to the CSV files with 2D frequency-amplitude transfer relative to the nominal ratio. If the correction is not defined, TWMM will assume neutral value of 1.0 for **amplitude**. It is important the user should always define the correction down to zero frequency in order to make algorithms requiring DC value work. It may be also needed to define frequency dependence up to the Nyquist frequency for the FFT based algorithms. The same applies for the rms level axis. If the correction is made dependent on the rms level, the rms-axis values must start at zero and range safely above the highest measured rms level. Otherwise algorithm may report error such as “Not sufficient frequency or amplitude range of correction”.

Note the x-axis is dependent on input voltage (or current), not on the output one. The correction loader will always combine **nominal ratio** and **amplitude transfer path** into a single absolute correction table:

$$\text{absolute gain} = \text{nominal ratio} \cdot \text{gain}, \quad (3.2)$$

$$u(\text{absolute gain}) = \sqrt{\text{nominal ratio uncertainty}^2 \cdot u(\text{gain})^2}. \quad (3.3)$$

Note the “absolute gain” and its uncertainty will be automatically inverted by TWM loader for a shunt so the “absolute gain” is always a ratio of measured input quantity (voltage or current) and transducer output voltage. Which means the “gain” from the correction matrix for divider is relative dependence of input-to-output division ratio, whereas “gain” for shunt is relative dependence of impedance of the shunt.

Following example explains the loading process more clearly. Example measurement of current shunt impedance is shown in Table 3.11. Nominal ratio is chosen as a DC value of the shunt:

**nominal ratio** = 0.600000,

**nominal ratio uncertainty** = 0.000001,

and CSV **amplitude transfer path** matrix is shown in Table 3.12.

$f$ [kHz]	$Z$ [ $\Omega$ ]	$u(Z)$ [ $\Omega$ ]
0	0.600 000	0.000 001
1	0.600 006	0.000 003
10	0.600 060	0.000 030
100	0.600 600	0.000 060

Table 3.11: Example of measured impedance of a current shunt.

My shunt description		
	gain	u(gain)
f \ rms		
0	1.000000	0.000000
1	1.000010	0.000005
10	1.000100	0.000050
100	1.001000	0.000100

Table 3.12: Example of gain transfer CSV matrix corresponding to the Table 3.11 measured impedance of a current shunt.

The CSV matrix header example is shown in the Table 3.13. Naming convention of the quantities passed to the QWTB algorithm is shown in Table 3.14.

comment				
	gain	...	u(gain)	...
f \ rms				

Table 3.13: CSV matrix header for amplitude transfer correction.  $f$ : frequency axis [Hz];  $rms$ : input rms value [V] or [A];  $gain$ : relative transfer [V/V] or [A/A];  $u(gain)$ : absolute std. uncertainty of gain.

QWTB name	Default value	Meaning
*tr_gain.f.v	<input type="text"/>	Frequency axis [Hz]
*tr_gain.a.v	<input type="text"/>	Input RMS value axis [V] or [A]
*tr_gain.v	1	Gain
*tr_gain.u	0	Abs. std. uncertainty of Gain

\* - transducer prefix [71] (i.e. “u\_” or “i\_” or nothing)

Table 3.14: Quantity names passed to the QWTB algorithm.

### 3.2.4.1.3 Phase transfer (optional)

**phase transfer path** is path to the CSV files with 2D frequency-amplitude phase transfer. If the correction is not defined, TWM will assume neutral value of 0 for **phase transfer path**. It is important the user should always define the correction down to zero frequency in order to make algorithms requiring DC value work. It may be also needed to define frequency dependence up to the Nyquist frequency for the FFT based algorithms. The same applies for the rms level axis. If the correction is made dependent on the rms level, the rms-axis values must start at zero and range safely above the highest measured rms level. Otherwise algorithm may report error such as “Not sufficient frequency or amplitude range of correction”.

The CSV matrix header example is shown in the Table 3.15. Naming convention of the quantities passed to the QWTB algorithm is shown in Table 3.16. Note the x-axis is dependent on input voltage (or current), not on the output one.

comment				
	phi	...	u(phi)	...
f \ rms				

Table 3.15: CSV matrix header for phase transfer correction. *f*: frequency axis [Hz]; *rms*: input rms value [V] or [A]; *phi*: phase shift [rad]; *u(phi)*: absolute std. uncertainty of phi [rad].

QWTB name	Default value	Meaning
*tr_phi.f.v	<input type="text"/>	Frequency axis [Hz]
*tr_phi.a.v	<input type="text"/>	Input RMS value axis [V] or [A]
*tr_phi.v	0	Phase shift [rad]
*tr_phi.u	0	Abs. std. uncertainty of Phase shift [rad]

\* - transducer prefix [71] (i.e. “u\_” or “i\_” or nothing)

Table 3.16: Quantity names passed to the QWTB algorithm.

### 3.2.4.1.4 Transducer SFDR value (optional)

Defines effects of distortion of the transducer. The **sfdr path** is path to the 2D CSV file with measured SFDR values dependent on amplitude and frequency of fundamental component of

the signal. The values are given in [dB]. Note the values are positive, i.e.: 120 dB means max spur amplitude is  $A_0 \cdot 10^{-(120/20)}$ , where  $A_0$  is fundamental amplitude. It is not a correction, it is used just to estimate uncertainty caused by THD of the transducer.

The CSV martix header example is shown in the Table 3.17. Naming convention of the quantities passed to the QWTB algorithm is shown in Table 3.18. Note the x-axis (amplitude) is dependent on the input voltage (or current), not on the output one.

comment		
	sfdr	...
f \ a		

Table 3.17: CSV matrix header for SFDR correction.  $f$ : frequency axis [Hz];  $a$ : input amplitude value [V] or [A];  $sfdr$ : SFDR value [dB].

QWTB name	Default value	Meaning
*tr_sfdr_f.v		Frequency axis [Hz]
*tr_sfdr_a.v		Input amplitude value axis [V] or [A]
*tr_sfdr.v	180	Positive SFDR value [dB]

\* - transducer prefix [71] (i.e. “u\_” or “i\_” or nothing)

Table 3.18: Quantity names passed to the QWTB algorithm.

### 3.2.4.1.5 Transducer low-side RVD impedance (optional)

1D CSV table **rvd low side impedance path** defines rough impedance of the low-side resistor for RVDs. This value is needed only for RVDs and it is used to calculate the loading effect of the cable and digitizer input to the transfer of the transducer. It is a “Zlo” component in the connection diagrams in section 3.2.2. Typically it is not necessary to calibrate the value to uncertainty below 0.1 % if the resistance of the RVD is up to few hundred ohms and total impedance is above 1 M $\Omega$ . For a shunt the value is ignored as the impedance of shunt can be calculated from the absolute complex transfer.

The CSV martix header example is shown in the Table 3.19. Naming convention of the quantities passed to the QWTB algorithm is shown in Table 3.20.

comment				
f	Rp	Cp	u(Rp)	u(Cp)

Table 3.19: CSV matrix header for RVD low-side impedance correction.  $f$ : frequency axis [Hz];  $Rp$ : Parallel resistance value [ $\Omega$ ];  $Cp$ : Parallel capacitance value [F];  $u(Rp)$ : Abs. std. uncertainty of  $Rp$  [ $\Omega$ ];  $u(Cp)$ : Abs. std. uncertainty of  $Cp$  [F].

QWTB name	Default value	Meaning
*tr_Zlo_f.v	$\square$	Frequency axis [Hz]
*tr_Zlo_Rp.v	1	Parallel resistance [ $\Omega$ ]
*tr_Zlo_Rp.u	0	Abs. standard uncertainty of Rp [ $\Omega$ ]
*tr_Zlo_Cp.v	0	Parallel capacitance [F]
*tr_Zlo_Cp.u	0	Abs. standard uncertainty of Cp [F]

\* - transducer prefix [71] (i.e. “u\_” or “i\_” or nothing)

Table 3.20: Quantity names passed to the QWTB algorithm.

### 3.2.4.1.6 Transducer high-side output terminal series impedance (optional)

1D CSV table **output terminals series impedance path** is estimate of the series impedance of the transducer’s high-side output terminal (component “Zca” in the correction diagram in section 3.2.2). It is part of the transducer loading corrections. The value is usually not measurable, but at least its uncertainty should be estimated in order to take the loading effect into the uncertainty budget.

The CSV matrix header example is shown in the Table 3.21. Naming convention of the quantities passed to the QWTB algorithm is shown in Table 3.22.

comment				
f	Rs	Ls	u(Rs)	u(Ls)

Table 3.21: CSV matrix header for transducer terminal high-side series impedance.  $f$ : frequency axis [Hz];  $R_s$ : Series resistance [ $\Omega$ ];  $L_s$ : Series inductance [H];  $u(R_s)$ : Abs. std. uncertainty of  $R_s$  [ $\Omega$ ];  $u(L_s)$ : Abs. std. uncertainty of  $L_s$  [H].

QWTB name	Default value	Meaning
*tr_Zca_f.v	$\square$	Frequency axis [Hz]
*tr_Zca_Rs.v	1e-9	Series resistance [ $\Omega$ ]
*tr_Zca_Rs.u	0	Abs. standard uncertainty of Rs [ $\Omega$ ]
*tr_Zca_Ls.v	1e-12	Series inductance [H]
*tr_Zca_Ls.u	0	Abs. standard uncertainty of Ls [H]

\* - transducer prefix [71] (i.e. “u\_” or “i\_” or nothing)

Table 3.22: Quantity names passed to the QWTB algorithm.

### 3.2.4.1.7 Transducer low-side output terminal series impedance (optional)

1D CSV table **output terminals series impedance path (low-side)** is estimate of the series impedance of the transducer’s low-side output terminal (component “Zcal” in the correction diagram in section 3.2.2). It is part of the transducer loading corrections. The value

is usually not measurable, but at least its uncertainty should be estimated in order take the loading effect into the uncertainty budget. Note for the single-ended connection this component can be part of the high-side impedance “Zca” and this correction can be left unassigned.

The CSV martix header example is shown in the Table 3.23. Naming convention of the quantities passed to the QWTB algorithm is shown in Table 3.24.

comment				
f	Rs	Ls	u(Rs)	u(Ls)

Table 3.23: CSV matrix header for transducer terminal low-side series impedance.  $f$ : frequency axis [Hz];  $Rs$ : Series resistance [ $\Omega$ ];  $Ls$ : Series inductance [H];  $u(Rs)$ : Abs. std. uncertainty of  $Rs$  [ $\Omega$ ];  $u(Ls)$ : Abs. std. uncertainty of  $Ls$  [H].

QWTB name	Default value	Meaning
*tr_Zcal.f.v		Frequency axis [Hz]
*tr_Zcal_Rs.v	1e-9	Series resistance [ $\Omega$ ]
*tr_Zcal_Rs.u	0	Abs. standard uncertainty of $Rs$ [ $\Omega$ ]
*tr_Zcal_Ls.v	1e-12	Series inductance [H]
*tr_Zcal_Ls.u	0	Abs. standard uncertainty of $Ls$ [H]

\* - transducer prefix [71] (i.e. “u\_” or “i\_” or nothing)

Table 3.24: Quantity names passed to the QWTB algorithm.

### 3.2.4.1.8 Transducer output terminals mutual inductance (optional)

1D CSV table **output terminals mutual inductance** is estimate of the mutual inductance between the transducer’s output terminals (component “M” in the correction diagram in section 3.2.2). It is part of the transducer loading corrections. The value is usually not measurable, but at least its uncertainty should be estimated in order take the loading effect into the uncertainty budget. Note for the single-ended connection the values of impedances “M”, “Zcal” and “Zca” can be combined to the correction “Zca”:

$$Z_{ca}(f) = Z_{ca}(f) + Z_{cal}(f) - j \cdot 4\pi \cdot f \cdot M, \quad (3.4)$$

where  $f$  is frequency. In that case this correction and low-terminal series impedance correction “Zca” can be left empty. However, for differential mode the values of “Zca”, “Zcal” and “M” should be at least estimated especially for high frequency measurements. Otherwise the correction mechanism cannot provide meaningful estimation of the loading error uncertainty.

The CSV martix header example is shown in the Table 3.25. Naming convention of the quantities passed to the QWTB algorithm is shown in Table 3.26.



comment		
f	M	u(M)

Table 3.25: CSV matrix header for transducer terminals mutual inductance.  $f$ : frequency axis [Hz];  $M$ : Mutual inductance [H];  $u(M)$ : Abs. std. uncertainty of  $M$  [H].

QWTB name	Default value	Meaning
*tr_Zcam.f.v	[]	Frequency axis [Hz]
*tr_Zcam.M.v	1e-12	Mutual inductance inductance [H]
*tr_Zcam.M.u	0	Abs. standard uncertainty of M [H]

\* - transducer prefix [71] (i.e. “u\_” or “i\_” or nothing)

Table 3.26: Quantity names passed to the QWTB algorithm.

### 3.2.4.1.9 Transducer output terminals shunting admittance (optional)

1D CSV table **output terminals shunting admittance path** is estimate of the shunting admittance between the transducer’s output terminals (component “Yca” in the correction diagram in section 3.2.2). It is part of the transducer loading corrections. The value is usually not measurable, but at least its uncertainty should be estimated in order take the loading effect into the uncertainty budget.

The CSV matrix header example is shown in the Table 3.27. Naming convention of the quantities passed to the QWTB algorithm is shown in Table 3.28.

comment				
f	Cp	D	u(Cp)	u(D)

Table 3.27: CSV matrix header for transducer terminals shunting admittance.  $f$ : frequency axis [Hz];  $C_p$ : Parallel capacitance [F];  $D$ : Loss tangent [-];  $u(C_p)$ : Abs. std. uncertainty of  $C_p$  [F];  $u(D)$ : Abs. std. uncertainty of  $D$  [-].

QWTB name	Default value	Meaning
*tr_Yca.f.v	[]	Frequency axis [Hz]
*tr_Yca.Cp.v	1e-15	Parallel capacitance [F]
*tr_Yca.Cp.u	0	Abs. standard uncertainty of $C_p$ [F]
*tr_Yca.D.v	0	Loss tangent [-]
*tr_Yca.D.u	0	Abs. standard uncertainty of $D$ [-]

\* - transducer prefix [71] (i.e. “u\_” or “i\_” or nothing)

Table 3.28: Quantity names passed to the QWTB algorithm.

### 3.2.4.1.10 Optional buffer output series impedance (optional)

1D CSV table **buffer output series impedance path** is effective series output impedance of the buffer placed between transducer and output terminals “Zca”/“Zcal”. The buffer presence is identified by this correction, so **do not assign it to tell TWM that no buffer is used**.

The CSV matrix header example is shown in the Table 3.29. Naming convention of the quantities passed to the QWTB algorithm is shown in Table 3.30.

comment				
f	Rs	Ls	u(Rs)	u(Ls)

Table 3.29: CSV matrix header for transducer buffer output impedance.  $f$ : frequency axis [Hz];  $Rs$ : Series resistance [ $\Omega$ ];  $Ls$ : Series inductance [H];  $u(Rs)$ : Abs. std. uncertainty of  $Rs$  [ $\Omega$ ];  $u(Ls)$ : Abs. std. uncertainty of  $Ls$  [H].

QWTB name	Default value	Meaning
*tr_Zbuf.f.v	[]	Frequency axis [Hz]
*tr_Zbuf.Rs.v	0	Series resistance [ $\Omega$ ]
*tr_Zbuf.Rs.u	0	Abs. standard uncertainty of $Rs$ [ $\Omega$ ]
*tr_Zbuf.Ls.v	0	Series inductance [H]
*tr_Zbuf.Ls.u	0	Abs. standard uncertainty of $Ls$ [H]

\* - transducer prefix [71] (i.e. “u\_” or “i\_” or nothing)

Table 3.30: Quantity names passed to the QWTB algorithm.

### 3.2.4.1.11 Cable(s) series impedance (optional)

1D CSV table **output cable series impedance path** is effective series impedance of the cable between transducer and digitizer (component “Zcb” in the correction diagram in section 3.2.2). It is part of the transducer loading corrections. In differential mode the both high- and low-side cables are expected to be identical! Note the cable correction can be omitted if the transducer was calibrated together with the cable.

The CSV matrix header example is shown in the Table 3.31. Naming convention of the quantities passed to the QWTB algorithm is shown in Table 3.32.

comment				
f	Rs	Ls	u(Rs)	u(Ls)

Table 3.31: CSV matrix header for cable series impedance.  $f$ : frequency axis [Hz];  $Rs$ : Series resistance [ $\Omega$ ];  $Ls$ : Series inductance [H];  $u(Rs)$ : Abs. std. uncertainty of  $Rs$  [ $\Omega$ ];  $u(Ls)$ : Abs. std. uncertainty of  $Ls$  [H].

QWTB name	Default value	Meaning
*tr_Zcb.f.v	$\square$	Frequency axis [Hz]
*tr_Zcb.Rs.v	1e-9	Series resistance [ $\Omega$ ]
*tr_Zcb.Rs.u	0	Abs. standard uncertainty of Rs [ $\Omega$ ]
*tr_Zcb.Ls.v	1e-12	Series inductance [H]
*tr_Zcb.Ls.u	0	Abs. standard uncertainty of Ls [H]

\* - transducer prefix [71] (i.e. “u\_” or “i\_” or nothing)

Table 3.32: Quantity names passed to the QWTB algorithm.

### 3.2.4.1.12 Cable(s) shunting admittance (optional)

1D CSV table **output cable shunting admittance path** is estimate of the shunting admittance between the transducer’s output terminals (component “Ycb” in the correction diagram in section 3.2.2). It is part of the transducer loading corrections. In differential mode both the high- and low-side cables are expected to be identical! Note the cable correction can be omitted if the transducer was calibrated together with the cable.

The CSV matrix header example is shown in the Table 3.33. Naming convention of the quantities passed to the QWTB algorithm is shown in Table 3.34.

comment				
f	Cp	D	u(Cp)	u(D)

Table 3.33: CSV matrix header for cables shunting admittance.  $f$ : frequency axis [Hz];  $C_p$ : Parallel capacitance [F];  $D$ : Loss tangent [-];  $u(C_p)$ : Abs. std. uncertainty of  $C_p$  [F];  $u(D)$ : Abs. std. uncertainty of  $D$  [-].

QWTB name	Default value	Meaning
*tr_Yca.f.v	$\square$	Frequency axis [Hz]
*tr_Yca.Cp.v	1e-15	Parallel capacitance [F]
*tr_Yca.Cp.u	0	Abs. standard uncertainty of Cp [F]
*tr_Yca.D.v	0	Loss tangent [-]
*tr_Yca.D.u	0	Abs. standard uncertainty of D [-]

\* - transducer prefix [71] (i.e. “u\_” or “i\_” or nothing)

Table 3.34: Quantity names passed to the QWTB algorithm.

## 3.2.5 Digitizer corrections

Digitizer correction datasets consist of the two parts:

- Definition of the whole digitizer (interchannel corrections),

- Definition of the particular channels (corrections that are independent to another channel or HW).

### 3.2.5.1 Digitizer correction files format

Before the particular corrections are described it is important to explain the format and structuring. The format of every correction matrix for the digitizer and its channels is identical. The format was designed so the so it allows following:

- Filtering the correction file by attributes of the digitizer.
- Automatic selection or interpolation of the correction data by the configuration (parameters) of the digitizer.
- Loading either embedded numeric matrices or CSV matrices.

The correction data are always enclosed in the INFO file section, where the **my correction name** is the name of the correction:

```
1 #startsection:: my correction name
2 // correction content
3 #endsection:: my correction name
```

The correction must contain at least the matrix with the correction data named **value**:

```
1 #startsection:: my correction name
2
3 // up to 2D matrix with the list of values of the correction:
4 #startmatrix:: value
5 0.0; 0.10000; 0.20000
6 0.0; 0.10000; 0.20000
7 0.0; 0.01000; 0.02000
8 #endmatrix:: value
9
10 #endsection:: my correction name
```

The value may be scalar, vector or 2D matrix of real numbers. If nothing else is present in the correction section, the correction loader will load the table of values as it is and will pass it to the QWTB algorithm under quantity name defined by the particular correction (see particular correction descriptions). The value may also contain relative path(s) to the CSV tables (single, vector of CSV files or 2D matrix of CSV files) that contains CSV table with 1D or 2D dependence (see introduction). Example for single CSV matrix:

```
1 #startsection:: my correction name
2
3 // correction defined by CSV matrix:
4 #startmatrix:: value
5 csv\my_csv_table.csv
6 #endmatrix:: value
7
8 #endsection:: my correction name
```

Example for multiple matrices:

```

1  #startsection:: my correction name
2
3      // correction defined by multiple CSV matrices:
4      #startmatrix:: value
5          csv\gain_tfer_fs_50kHz.csv
6          csv\gain_tfer_fs_500kHz.csv
7          csv\gain_tfer_fs_5MHz.csv
8      #endmatrix:: value
9
10 #endsection:: my correction name

```

For CSV matrix mode the uncertainty is directly part of the CSV matrix. If the **value** contains only real numbers, the TWM can also load associated absolute std. uncertainty from complementary matrix **uncertainty** which has to be of the same dimensions as the **value** matrix:

```

1  #startsection:: my correction name
2
3      // .....
4      #startmatrix:: uncertainty
5          0.00; 0.00010; 0.00020
6          0.00; 0.00010; 0.00020
7          0.00; 0.00011; 0.00022
8      #endmatrix:: uncertainty
9
10 #endsection:: my correction name

```

Any correction can be disabled without removing the correction section by inserting line:

```

1  #startsection:: my correction name
2
3      // .....
4      disabled:: 1
5
6  #endsection:: my correction name

```

The correction loader can automatically select or interpolate between the values in the matrices **value** (and **uncertainty**) based on the value of any attribute (parameter) of the digitizer that is present in the measurement header file. This is useful whenever the correction value depends on some setting of the digitizer. For example the measurement header always contains parameter **voltage ranges [V]** with range of the digitizer so it is possible to insert following section to the correction:

```

1  #startsection:: my correction name
2
3      // .....
4
5      // ---- List of parameters on which the correction values depends: ----
6      // primary parameter (remove if not used):
7      #startsection:: primary parameter
8

```

```

9          // name of the HW parameter:
10         // note: it must be exact name of the parameter that appears in measurement header
11         name:: voltage ranges [V]
12
13         // is this parameter interpolable?
14         // note: set to 0 or remove if not interpolable
15         interpolable:: 0
16
17         // list of supported values of a primary parameter on which the correction depends:
18         // eg.: range of the digitizer
19         #startmatrix:: value
20             1
21             10
22             100
23         #endmatrix:: value
24
25         #endsection:: primary parameter
26
27     #endsection:: my correction name

```

The section **primary parameter** defines vertical axis of interpolation (selection) of the **value** matrix. I.e. for range value “10”, it will select second row of table **value**. The **value** of the interpolation parameter may be string as well as numeric. If it is numeric and the **interpolable** is non-zero, the loader will interpolate the **value** vertically per columns.

If section **secondary parameter** is added to the correction section, it will do the same as **primary parameter** except in horizontal direction. Note each parameter reduces size of the **value** matrix by one dimension by the interpolation/selection, so when it is 2D matrix and one parameter is used, it will be interpolated to 1D vector (horizontal or vertical). If two parameters are defined, it will be interpolated to scalar value.

If the **value** matrix of the correction data is matrix of paths to CSV files, the loader will select/interpolate between the CSV matrices as well. It will first interpolate content of all involved CSV matrices to identical x- and y-axes, then it will interpolate between the matrices by the **primary parameter** and **secondary parameter**, so the result is one CSV matrix. This is useful for example for the frequency dependence of the digitizer channel gain which may be dependent on the aperture and range of the digitizer.

Last supported feature of the correction section is filtering the corrections by attribute of the digitizer. Let’s assume the measurement header contains parameter **sampling mode**. The filter may look like this:

```

1  #startsection:: my correction name
2
3      // .....
4
5      // --- Filtering of the correction by HW attributes: ---
6      // this is the list of channel specific attributes for which the correction is valid
7      // anything put here will be checked with the digitizer setup stored in the header file
8      // of the measurement and if it does not match, the loader will return an error
9      #startmatrix:: valid for attributes
10         sampling mode

```

```

11      #endmatrix:: valid for attributes
12
13      // list of allowed values of attribute 1 (eg.: sampling mode):
14      #startmatrix:: sampling mode
15          DSDC
16          DSAC
17      #endmatrix:: sampling mode
18
19  #endsection:: my correction name

```

The **valid for attributes** list defines list of measurement header attributes which are used for filtering. Each attribute has its own list of allowed string values. In this case matrix **sampling mode** contains values “DSDC” and “DSAC”. If any other value is found in the measurement header or the **sampling mode** attribute is not found at all, the loader will return an error, which signalizes the correction is not compatible with selected HW and/or its current configuration.

### 3.2.5.2 Digitizer corrections

The digitizer correction defines the digitizer as a whole system. It contains list of all channels (e.g. sampling multimeters used in the setup). It also contains correction data which somehow defines relation between multiple channels, such as inter-channel time shifts. Example of the digitizer correction header INFO file is show in the following text:

```

1  // correction type:
2  type:: digitizer
3
4  // description of the digitizer corrections:
5  name:: Demonstration corrections for setup with two 3458A digitizers
6
7  // names of the channels as they appear in the digitizer identification:
8  // these are exact unique names of the channels in the order that will be loaded to the SW
9  #startmatrix:: channel identifiers
10     HP3458A, sn. MY45053095
11     HP3458A, sn. MY45053104
12     HP3458A, sn. MY45053107
13  #endmatrix:: channel identifiers
14
15  // relative links to the files with channel corrections for each channel:
16  #startmatrix:: channel correction paths
17     ..\channel.MY45053095\HP3458_MY45053095.info
18     ..\channel.MY45053104\HP3458_MY45053104.info
19     ..\channel.MY45053107\HP3458_MY45053107.info
20  #endmatrix:: channel correction paths
21
22  // here follows definitions of ANY correction tables
23  // .....

```

The identifier of the correction **type** must be set to value “digitizer”. The **name** is any string describing the correction data file. Next, there is a list of a digitizer channel identifiers **channel**

**identifiers.** This is the list of digitizer channel identification strings exactly as they are returned during the instrument identification in the TWM tool digitizer configuration panel. These are used to restrict the correction file to use with particular instruments. Otherwise the TWM tool will return an error if the processing of data is initiated. The TWM processing mechanism is design so it can operate incomplete digitizer, i.e. if only first two of the instruments in the example above are present, it will still be valid file for such setup. Next item is **channel correction paths** which are relative paths to the files with the channel corrections, one for each channel of the digitizer. Next, the correction data tables follows.

### 3.2.5.2.1 Inter-channel time-shift correction (optional)

The matrix **interchannel timeshift** defines correction values for time shifts between the channels of the digitizer. It must be a row vector of values, one for each digitizer channel. It defines correction of time shift of each channel relative to the first channel in the **channel identifiers** list, e.g. for three channels:

```

1  #startsection:: interchannel timeshift
2
3      #startmatrix:: value
4          0.0; 0.010000; 0.020000
5      #endmatrix:: value
6      #startmatrix:: uncertainty
7          0.0; 0.000012; 0.000011
8      #endmatrix:: uncertainty
9
10 #endsection:: interchannel timeshift

```

Note the first value is always zero. Shown example means second channel correction is  $(0.010\,000 \pm 0.000\,012)$  s, and third correction is  $(0.020\,000 \pm 0.000\,011)$  s. Note it is a correction factor, not a time shift, so the sign of the values is opposite to the measured time shifts. The correction is optional. By default the time shifts and uncertainty is zero.

Typical way of determining the correction value is by TWM tool itself. All channels of the digitizer are connected together and algorithm capable of estimating the phase is used to measure inter-channel phase shift. The time shift correction is then calculated as:

$$\Delta t(n) = -\frac{\Delta \phi(n)}{2\pi \cdot f}, \quad (3.5)$$

where  $f$  is measured frequency and  $\Delta \phi$  measured phase shift of channel  $n$  to first channel in radians. It is of course necessary to disable all corrections before performing such measurement, otherwise such measurement would be just a difference to current set of the corrections. Note this method will correct timeshift and thus inter-channel phase error only at the frequency at which it is performed, e.g. 50 Hz. It may be enough for measurement of power at 50 Hz, however the residual phase difference between the channels for other frequencies should be corrected as well by phase correction shown in section 3.2.5.6.

Note the values of the time shift are combined with the time stamps coming from the digitizers and are passed to the QWTB algorithm according to the rules defined in [71]. The power



algorithms will always correct interchannel time shift, because they receive the correction in separate QWTB quantity “time\_shift”. But for single input algorithms such as PSFE harmonic estimator, there is no such possibility. The time shift correction can be performed only relative to a common time reference, each channel (phase) separately, so the algorithms receive the time shift correction combined with eventual time stamp from the digitizer in QWTB quantity “time\_stamp”. It may be not desirable to perform such correction every time, so these algorithms have always a **user parameter “comp\_timestamp”**. **This parameter must be set to “1” if the algorithm should apply the correction!**

### 3.2.5.2.2 Timebase correction (optional)

The correction **timebase correction** defines relative correction to the error of time base of the digitizer. It is optional parameter. E.g.: value of  $+10^{-7}$  means the actual time base of the digitizer  $f_{\text{ref}}$  is  $f_{\text{ref}} = f_{\text{nom}} \cdot (1 + 10^{-7})$ . That also means the estimated frequency of the signal will be decreased by  $-10^{-7}$  after the correction. Note the value is common for all channels thus it was placed in the digitizer correction instead of a channel correction. The quantity name under which it is passed to the QWTB algorithm is shown in Table 3.35.

This correction can be also measured by TWM tool itself when known frequency source is connected to the digitizer input(s). However, this correction must be disabled before the measurement.

QWTB name	Default value	Meaning
adc_freq.v	0	Value of correction [Hz/Hz]
adc_freq.u	0	Absolute standard uncertainty [Hz/Hz]

Table 3.35: Quantity names passed to the QWTB algorithm.

### 3.2.5.2.3 Inter-channel crosstalk

**To be defined!**. Currently no algorithm in TWM set supports this type of correction as no general and effective way of performing it was found for the case with multiple phase systems. The correction in principle requires to estimate parameters of ALL involved channels, so e.g. 6 for three phase power and applying correction between each pair. This is currently not even possible withing the used data exchange mechanism.

### 3.2.5.3 Channel corrections

Channel corrections define corrections that apply only to a single channel of the digitizer. Example of the channel correction file header:

```

1 // type of the correction
2 type:: channel
3
4 // correction name string
```

```

5 name:: Channel correction HP3458A, sn. MY45053095
6
7 // device/channel identification as it appears in the digitizer identification
8 // note: leave empty or remove if this correction should be independent of the instrument/channel
9 channel identifier:: HP3458A, sn. MY45053095
10
11 // here follows definitions of ANY correction tables
12 // .....

```

The **type** must be “channel” for the channel correction file. **name** is any string describing the correction file. **channel identifier** is optional item that will cause the TWM correction loader will throw an error if this channel correction is applied to a digitizer channel with different identification. It must be the exact string as returned by the TWM tool during digitizer identification. It may be removed if it is not required.

### 3.2.5.4 Nominal gain (optional)

Optional correction **nominal gain** defines DC gain of the digitizer and its std. uncertainty. The value is combined with relative channel frequency transfer to absolute transfer (see below). Example:

```

1 #startsection:: nominal gain
2
3     #startmatrix:: value
4         1.000005
5     #endmatrix:: value
6     #startmatrix:: uncertainty
7         0.000003
8     #endmatrix:: uncertainty
9
10 #endsection:: nominal gain

```

### 3.2.5.5 Gain frequency transfer (optional)

Optional correction **gain transfer** defines relative frequency dependence of the gain of the digitizer channel. It is combined with the nominal gain to absolute gain transfer:

$$\text{absolute gain} = \text{nominal gain} \cdot \text{gain}, \quad (3.6)$$

$$u(\text{absolute gain}) = \sqrt{u(\text{nominal gain})^2 \cdot u(\text{gain})^2}. \quad (3.7)$$

The calculated “absolute gain” value is multiplied by the measured amplitude to get actual amplitude of the input signal. The correction data is 2D CSV matrix dependent on the frequency and amplitude. Example of the correction section:

```

1 #startsection:: gain transfer
2
3     #startmatrix:: value

```

```

4          csv\tfer_gain.csv
5      #endmatrix:: value
6
7  #endsection:: gain transfer

```

The CSV matrix header example is shown in the Table 3.36. Naming convention of the quantities passed to the QWTB algorithm is shown in Table 3.37.

comment				
	gain	...	u(gain)	...
f \ a				

Table 3.36: CSV matrix header for digitizer gain correction.  $f$ : frequency axis [Hz];  $a$ : input amplitude axis [V];  $gain$ : gain correction [V/V];  $u(gain)$ : absolute std. uncertainty of gain [V/V].

QWTB name	Default value	Meaning
*adc_gain.f.v	□	Frequency axis [Hz]
*adc_gain.a.v	□	Amplitude axis [V]
*adc_gain.v	1	Gain correction [V/V]
*adc_gain.u	0	Abs. standard uncertainty of gain [V/V]

\* - transducer prefix [71] (e.g. “u\_”, “i\_”, “u\_lo”, etc.)

Table 3.37: Quantity names passed to the QWTB algorithm.

### 3.2.5.6 Phase frequency transfer (optional)

Optional correction **phase transfer** defines frequency dependence of the correction to the phase error of the digitizer channel. It is the value which must be added to the measured phase of the harmonic component to get actual phase angle of the input signal. The correction data is 2D CSV table dependent on the frequency and amplitude. Example of the correction section:

```

1  #startsection:: phase transfer
2
3      #startmatrix:: value
4          csv\tfer_phi.csv
5      #endmatrix:: value
6
7  #endsection:: phase transfer

```

The CSV matrix header example is shown in the Table 3.38. Naming convention of the quantities passed to the QWTB algorithm is shown in Table 3.39.

comment				
	phi	...	u(phi)	...
f \ a				

Table 3.38: CSV matrix header for digitizer phase correction.  $f$ : frequency axis [Hz];  $a$ : input amplitude axis [V];  $\phi$ : phase correction [rad];  $u(\phi)$ : absolute std. uncertainty of phase [rad].

QWTB name	Default value	Meaning
*adc_phi.f.v		Frequency axis [Hz]
*adc_phi.a.v		Amplitude axis [V]
*adc_phi.v	0	Phase correction [rad]
*adc_phi.u	0	Abs. standard uncertainty of phase [rad]

\* - transducer prefix [71] (e.g. “u\_”, “i\_”, “u\_lo”, etc.)

Table 3.39: Quantity names passed to the QWTB algorithm.

### 3.2.5.7 DC offset (optional)

Correction **dc offset** defines DC offset of the digitizer and its uncertainty. Note it is a measured DC offset, not a correction! The correction is passed to the QWTB algorithm under the quantity names defined in Table 3.40. Example of the correction section:

```

1  #startsection:: dc offset
2
3      #startmatrix:: value
4          1.234e-6
5      #endmatrix:: value
6      #startmatrix:: uncertainty
7          2.500e-6
8      #endmatrix:: uncertainty
9
10 #endsection:: dc offset

```

QWTB name	Default value	Meaning
*adc_offset.v	0	DC offset [V]
*adc_offset.u	0	Abs. standard uncertainty of offset [V]

\* - transducer prefix [71] (e.g. “u\_”, “i\_”, “u\_lo”, etc.)

Table 3.40: Quantity names passed to the QWTB algorithm.

### 3.2.5.8 Aperture correction (optional)

Correction **aperture correction** defines whether the TWM algorithms should perform gain and phase correction to the effect of the aperture time of the ADC. The correction has effect

only for digitizers that have aperture parameter such as 3458A. It will perform corrections:

$$\delta A = \frac{T_A \pi f}{\sin(T_A \pi f)}, \quad (3.8)$$

$$\Delta \phi = T_A \pi f, \quad (3.9)$$

where the  $T_A$  is aperture time from measurement header [s],  $f$  is frequency component [Hz],  $\delta A$  is the relative correction of component gain [V/V] and  $\Delta \phi$  absolute correction of component phase [rad]. Example of the correction section:

```

1  #startsection:: aperture correction
2
3      #startmatrix:: value
4          1
5      #endmatrix:: value
6
7  #endsection:: aperture correction

```

The correction is enable by default. Non-zero value enables the correction. This correction has no uncertainty value. It is recommended to let this correction enabled. It will have no effect on the digitizer without aperture parameter such as NI 5922, but it will significantly reduce the amplitude error on sampling multimeters such as 3458A. When calibration of the DMM gain error is performed using the TWM tool itself, the correction of the residual channel gain errors will be much smaller, when this correction is enabled. The correction is passed to the QWTB algorithm under the quantity names defined in Table 3.41.

QWTB name	Default value	Meaning
*adc_aper_corr.v	1	0 - disable, 1 to enable the correction

\* - transducer prefix [71] (e.g. “u\_”, “i\_”, “u\_lo”, etc.)

Table 3.41: Quantity names passed to the QWTB algorithm.

### 3.2.5.9 SFDR value (optional)

Correction **sfdr** defines effects of the distortion of the digitizer. It is defined as 2D CSV matrix of SFDR values dependent on fundamental component amplitude and frequency. It is a value in dB. Note the values are positive, i.e.: 120 dB means max spur amplitude is  $A_0 \cdot 10^{-(120/20)}$ . The SFDR value is not correction as SFDR cannot be used to correct anything. It is just used by the TWM algorithms to estimate uncertainty caused by the SFDR.

The CSV martix header example is shown in the Table 3.42. Naming convention of the quantities passed to the QWTB algorithm is shown in Table 3.43. Example of the correction section:

```

1  #startsection:: sfdr
2
3      #startmatrix:: value
4          csv\sfdr.csv
5      #endmatrix:: value
6
7  #endsection:: sfdr

```

comment		
	sfdr	...
f \ a		

Table 3.42: CSV matrix header for digitizer SFDR correction.  $f$ : frequency axis [Hz];  $a$ : amplitude axis value [V];  $sfdr$ : SFDR value [dB].

QWTB name	Default value	Meaning
*adc_sfdr.f.v		Frequency axis [Hz]
*adc_sfdr.a.v		Input amplitude axis [V]
*adc_sfdr.v	180	Positive SFDR value [dB]

\* - transducer prefix [71] (e.g. “u\_”, “i\_”, “u\_lo”, etc.)

Table 3.43: Quantity names passed to the QWTB algorithm.

### 3.2.5.10 RMS jitter (optional)

Correction **rms jitter** defines rms value of the channel sampling time jitter in [s]. This is used just for uncertainty estimation. The correction value is passed to the QWTB algorithm under names defined in Table 3.44. Example of the jitter correction section:

```

1 #startsection:: rms jitter
2
3 #startmatrix:: value
4     1e-8
5 #endmatrix:: value
6
7 #endsection:: rms jitter

```

QWTB name	Default value	Meaning
*adc_jitter.v	0	RMS sampling jitter value [s]

\* - transducer prefix [71] (e.g. “u\_”, “i\_”, “u\_lo”, etc.)

Table 3.44: Quantity names passed to the QWTB algorithm.

### 3.2.5.11 Input admittance (optional)

Correction **input admittance** defines input admittance of the digitizer channel. It is used as a part of the transducer loading corrections according section 3.2.2 where it is component “Yin” (and “lo\_Yin” for differential connection). The correction data are in form of 1D CSV matrix dependent on frequency only. The CSV matrix header example is shown in the Table 3.45. Naming convention of the quantities passed to the QWTB algorithm is shown in Table 3.46. Example of the correction section:

```

1  #startsection:: input admittance
2
3      #startmatrix:: value
4          csv\Y_inp.csv
5      #endmatrix:: value
6
7  #endsection:: input admittance

```

comment				
f	Cp	Gp	u(Cp)	u(Gp)

Table 3.45: CSV matrix header for input admittance of digitizer channel.  $f$ : frequency axis [Hz];  $C_p$ : Parallel capacitance [F];  $G_p$ : Parallel loss conductance [S];  $u(C_p)$ : Abs. std. uncertainty of  $C_p$  [F];  $u(G_p)$ : Abs. std. uncertainty of  $G_p$  [S].

QWTB name	Default value	Meaning
*adc_Yin_f.v		Frequency axis [Hz]
*adc_Yin_Cp.v	0	Parallel capacitance [F]
*adc_Yin_Cp.u	0	Abs. standard uncertainty of $C_p$ [F]
*adc_Yin_Gp.v	1e-12	Parallel loss conductance [S]
*adc_Yin_Gp.u	0	Abs. standard uncertainty of $G_p$ [S]

\* - transducer prefix [71] (e.g. “u\_”, “i\_”, “u\_lo”, etc.)

Table 3.46: Quantity names passed to the QWTB algorithm.

### 3.3 Software introduction - TPQA manual - LabWindows Environnement

Following chapters will describe installation and basic usage of the TPQA tool [72] based on information from the report on the software tool "A245 TPQA structure" [73].

#### 3.3.1 Installation of drivers and development environments

Before running and installing of TPQA the user must complete the following steps and install several components:

1. Download and unpacking of the TPQA tool itself from GitHub [72]
2. Installation of the prerequisites for the running of TPQA open tool project:
  - (a) LabWindows 2013 Runtime Engine. This is needed to run any LabWindows application;
  - (b) Drivers of all integrated instruments, which are currently:
    - i. NI VISA drivers for handling of DMMs via GPIB IEEE-488.2 bus;
    - ii. niScope drivers for handling of NI PXI 5922 digitizers.
3. Installation of the Matlab for data processing.
4. After downloading of TPQA.zip file, unpack it to desired folder and in the Matlab console run the file `reg_matlab_dlls.m` for registering Matlab DLLs (`\bin\win32`), or add manually the path to the DLLs to the Windows environment variable `PATH`. Example path of the DLLs is following: `C:\Program Files (x86)\MATLAB\R2013a\bin\win32`.

Steps (1), to (4) are mandatory. Current version of TPQA is built for DMM HP3458 and NI-PXI5922 digitizers. It is necessary to install VISA drivers even for use with NI 5922 cards and "niScope" drivers and even for use only with Agilent 3458A multimeters.

Step (3) is needed when processing of the recorder waveforms is performed off-line but the Matlab must be installed on the PC. For on-line processing TPQA offers an addition GUI interface. In that case, the algorithms employed for waveform analysis are based on specific functions distributed under Measurement LabWindows library. The 15RPT04 TracePQM protocol establishes that only the algorithm contained into QWTB should be validated. So, the output data coming from TPQA on-line processing module have not been validated. Their validation might be performed as additional task from end-users.

##### 3.3.1.1 Installing TPQA tool

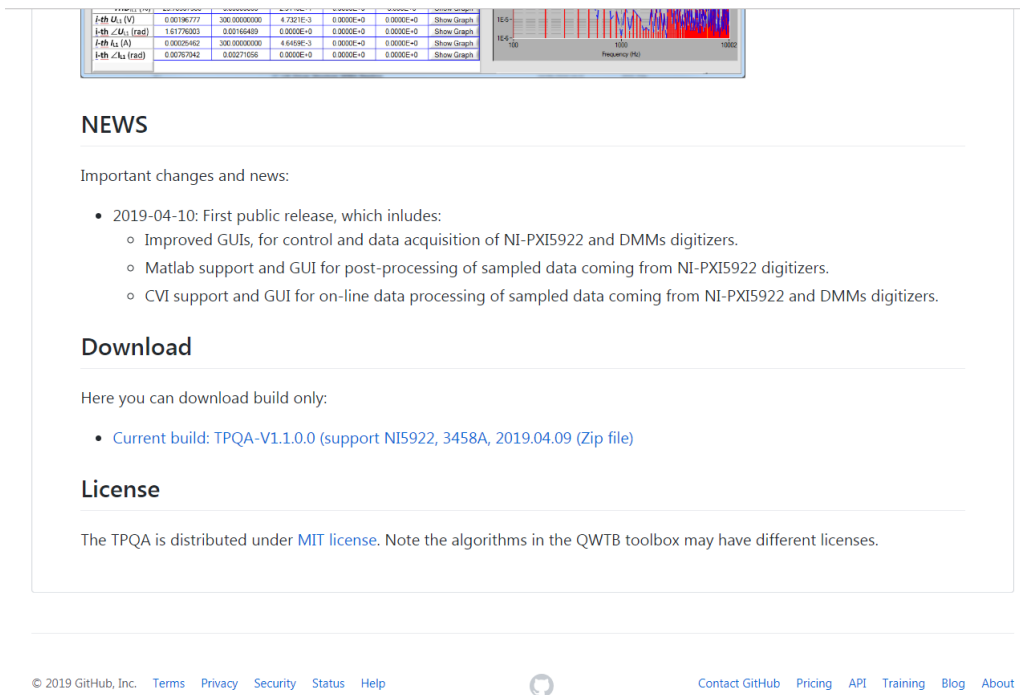
TPQA tool requires no installation. Its files just must be unpacked from the ZIP to any user folder, e.g.:



C:\TPQA\TPQA\_1.1.0

It can be downloaded from GitHub webpage (see Figure 3.34).

However, user may also download development version which will run only with development version of LabWindows/CVI minimum version 2013. The development version can be obtained downloading the GitHub as a ZIP file (see Figure 3.34).



**PARAMETERS**

Parameter	Value	Unit	Min	Max	Step	Default	Min	Max	Step	Default	Min	Max	Step	Default	Min	Max	Step	Default
$f_{th}$ $U_1$ (V)	0.00196777	V	0.00000000	0.00200000	0.00000000	0.00196777	0.00000000	0.00200000	0.00000000	0.00196777	0.00000000	0.00200000	0.00000000	0.00196777	0.00000000	0.00200000	0.00000000	0.00196777
$f_{th}$ $\angle U_1$ (rad)	1.57739033	rad	0.00000000	0.00000000	0.00000000	1.57739033	0.00000000	0.00000000	0.00000000	1.57739033	0.00000000	0.00000000	0.00000000	1.57739033	0.00000000	0.00000000	0.00000000	1.57739033
$f_{th}$ $I_{L1}$ (A)	0.00025462	A	0.00000000	0.00000000	0.00000000	0.00025462	0.00000000	0.00000000	0.00000000	0.00025462	0.00000000	0.00000000	0.00000000	0.00025462	0.00000000	0.00000000	0.00000000	0.00025462
$f_{th}$ $\angle I_{L1}$ (rad)	0.00757042	rad	0.00000000	0.00000000	0.00000000	0.00757042	0.00000000	0.00000000	0.00000000	0.00757042	0.00000000	0.00000000	0.00000000	0.00757042	0.00000000	0.00000000	0.00000000	0.00757042

**NEWS**

Important changes and news:

- 2019-04-10: First public release, which includes:
  - Improved GUIs, for control and data acquisition of NI-PXI5922 and DMMs digitizers.
  - Matlab support and GUI for post-processing of sampled data coming from NI-PXI5922 digitizers.
  - CVI support and GUI for on-line data processing of sampled data coming from NI-PXI5922 and DMMs digitizers.

**Download**

Here you can download build only:

- Current build: [TPQA-V1.1.0.0 \(support NI5922, 3458A, 2019.04.09 \(Zip file\)\)](#)

**License**

The TPQA is distributed under [MIT license](#). Note the algorithms in the QWTB toolbox may have different licenses.

© 2019 GitHub, Inc. [Terms](#) [Privacy](#) [Security](#) [Status](#) [Help](#) [Contact GitHub](#) [Pricing](#) [API](#) [Training](#) [Blog](#) [About](#)

Figure 3.34: Location of TPQA download on the TPQA GitHub webpage.

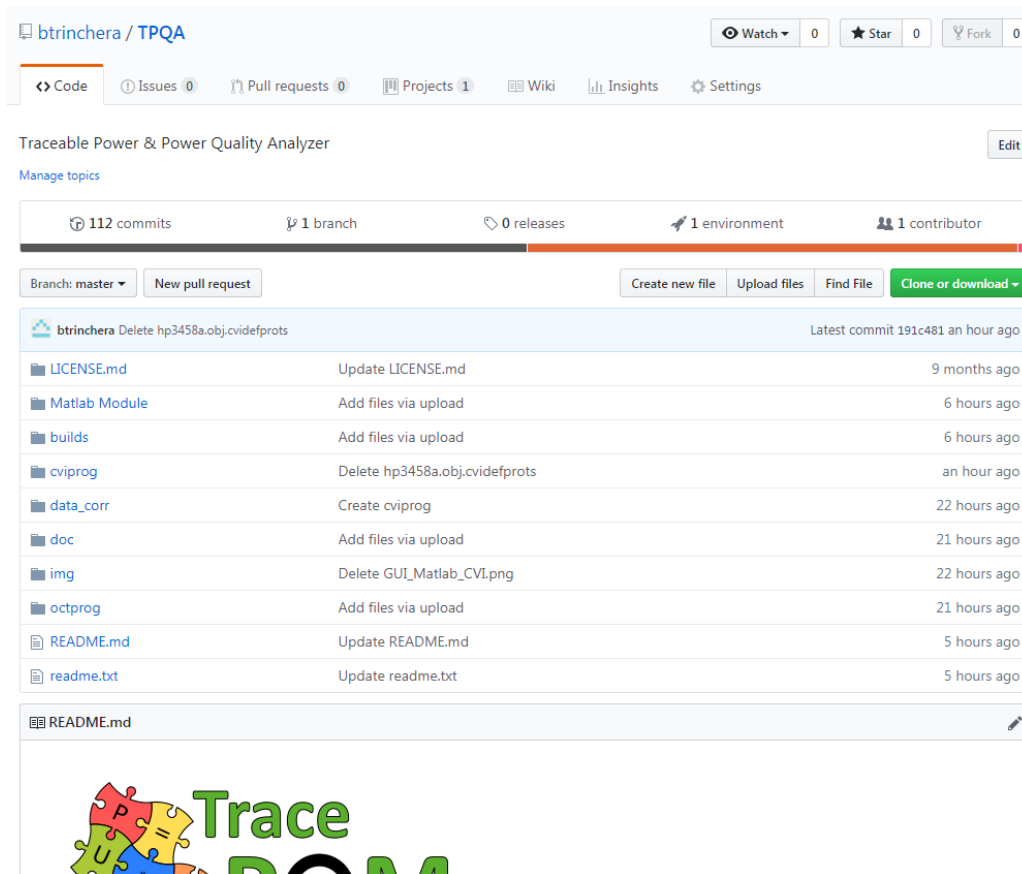


Figure 3.35: Downloading development version of TPQA from GitHub webpage.

### 3.3.1.2 Installing TPQA prerequisites

LabWindows applications in general requires large amount of external libraries and drivers to run. First required is LabWindows 2013 Runtime Engine 32bit [58]. The version must be 32bit as the TPQA is built as a 32bit application.

Next component are the VISA drivers, which are needed for communication via GPIB. At least version 5.4 should be installed. The newer versions are partially compatible, see [59] for selection.

Last needed component are niScope drivers, which are used to communicate with NI 5922 digitizers. These supported versions are 4.0.5 to 16.1 (see [60] for details).

### 3.3.1.3 Installing Matlab

Matlab [63] is the only processing environment for the TPQA, however it should be totally compatible. TPQA was tested with versions 2007b and later. Typical Matlab installation should contain all required packages and they are loaded automatically, so no additional actions after installation should be required.

### 3.3.2 Startup

When all required components are installed, the TPQA can be started by its executable `TPQA_32bit.exe`. When no component is missing, the front panel should appear with no error messages. If some driver is missing, LabWindows will show an error with explanation which component cannot be located. Typical missing components are "niScope.dll", "niTcl.dll" (part of "niScope" drivers) or VISA drivers. If TPQA requests the libraries, follow the installation guidance in section 3.3.1. TPQA requires no other configurations prior starting the application itself.

### 3.3.3 User guide

Main panel of TPQA is shown in Figure 3.36. All subpanels with particular configurations can be invoked from the main panel. Error indicator at the bottom will show eventual error message of the TPQA. User must configure the system before any measurement can be taken. This is done by the main panel and from additional control buttons situated into panel **Acquisition and Processing Control**. The additional control buttons are as follows:

- **LF-Setup DMMs** for configuration of low frequency setup based on HP 3458 digitizers;
- **HW Corrections** for selection of the transducer and digitizer connection and correction
- **QWTB processing** for off-line data processing based on Matlab algorithms;
- **CVI Data processing** for on-line data processing based on LabWindows algorithms.

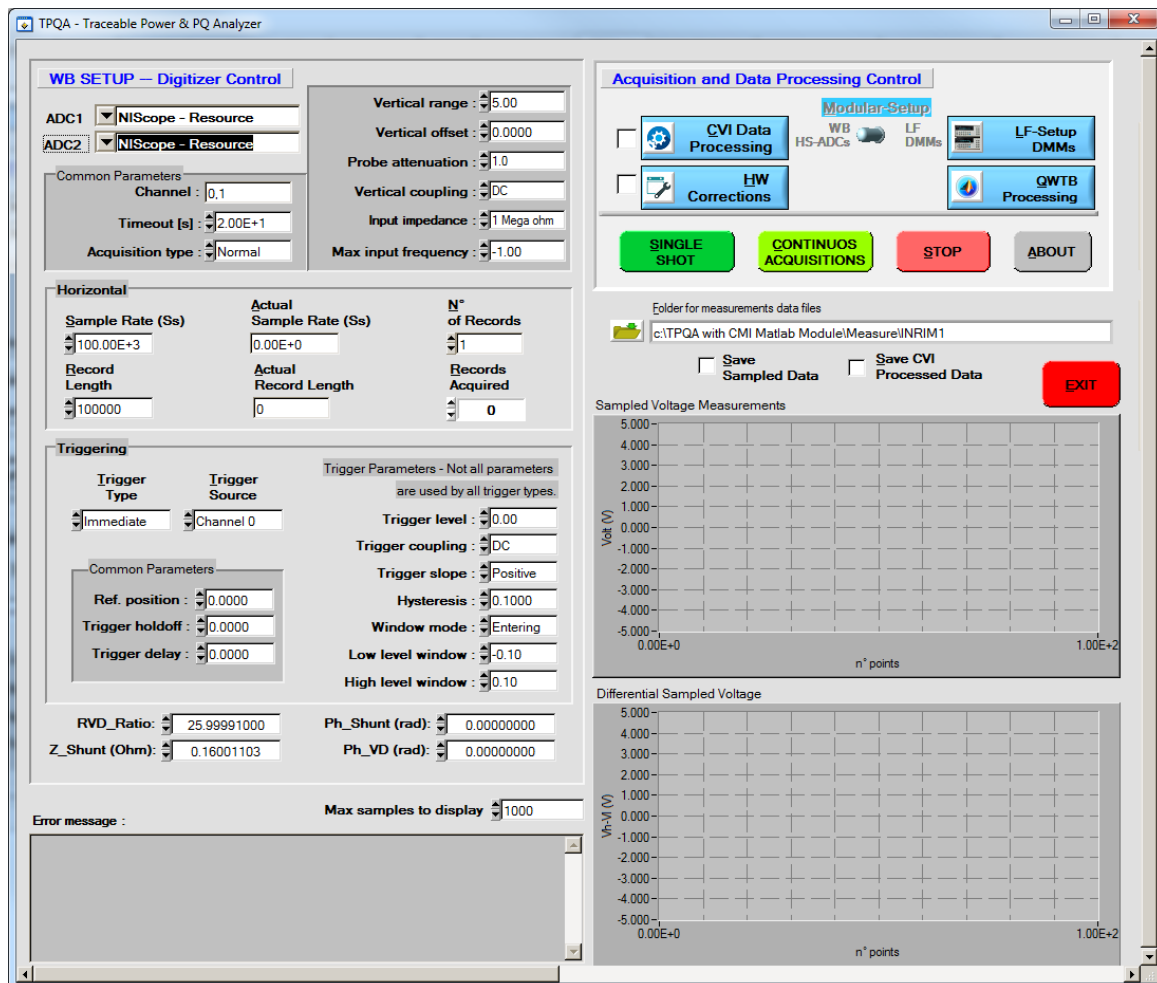


Figure 3.36: Front panel of TPQA.

### 3.3.3.1 Configuring digitizers for a new measurement setup

TPQA contains two distinct subpanels for the configuration of high precision digitizers and measurement setup.

The first subpanel concerns the configuration of high-speed digitizers employed for wideband power and power quality measurements, e.g. NI 5922, and is visible into TPQA main panel. The second one is focused on the configuration of high precision sampling DMMs mainly used for LF power and PQ measurements at power line frequency, e.g. HP-3458A.

#### 1. Configuration subpanel for high-speed PXI-5922 digitizer

All the useful parameters for configuring high speed digitizers are inside the subpanel **WB SETUP – Digitizer Control**, as shown in Figure 3.37 Below is reported a brief description of main control windings. Further explanations about the operation of the buttons and controls are reported in A2.4.5 report describing the TPQA part of the open software project, located within \doc directory of TPQA project.

- The overall configuration of high speed digitizers is divided in three steps:
  - Selecting digitizers and physical channels: using **ADC1** and **ADC2** it is possible to select all PXI-5922 resources recognized by niScope driver. Within **Common parameters** box it is possible to configure all physical channels of individual digitizing cards. Figure 3.37 gives an example on how to configure digitizing cards for single-ended or differential voltage measurements according to power and PQ experimental setup specifications.

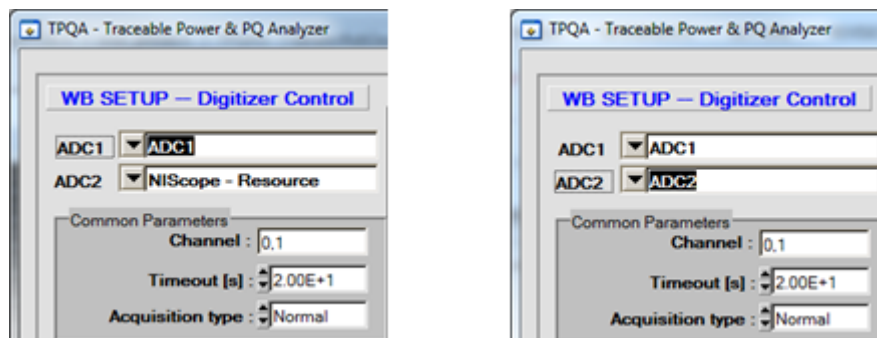


Figure 3.37: TPQA - (Left) single-ended measurements; (Right) differential measurements.

- Configuring vertical and horizontal digitizer parameters: Figure 3.38 shows the control parameters allowing the configuration of each physical channel of the digitizer. Vertical setting comprises common parameters as **Vertical range**, **offset** and **coupling**. **Input impedance** and additional parameters as **Probe attenuation** and **Max Input frequency**. Horizontal setting comprises common parameters as **Sample Rate** and **Record Length**, which must be set manually by users.

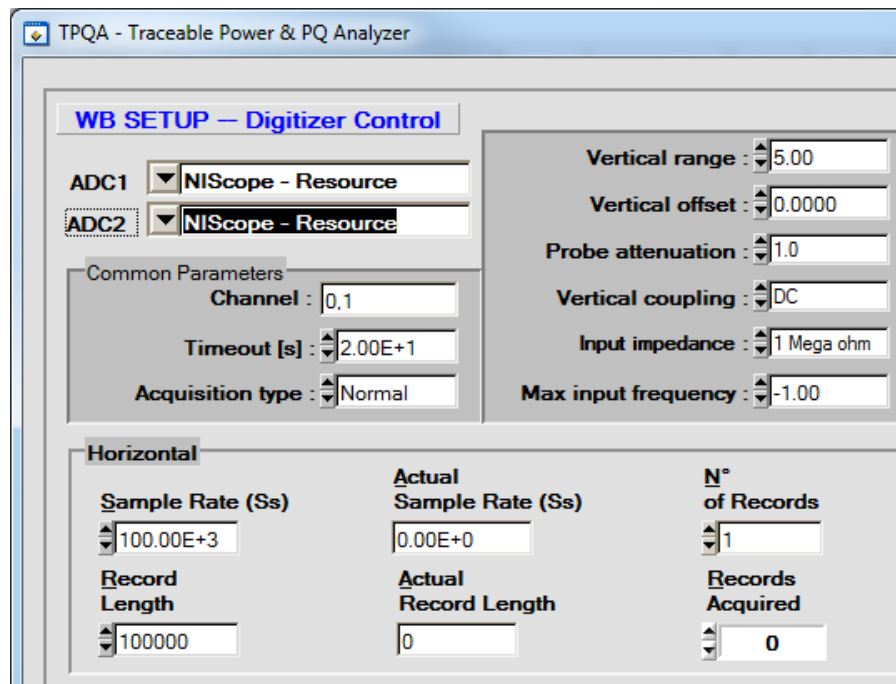


Figure 3.38: TPQA configuration panel for vertical and horizontal setting of digitizer physical channels.

- Trigger setting: Figure 3.39 shows the panel aimed at setting and arming digitizer trigger during the measurements. **Trigger Type** and **Trigger Source** are used to arm and set the input source of the trigger. For setting the parameters shown on the left, consult the PXI-5922 datasheet.

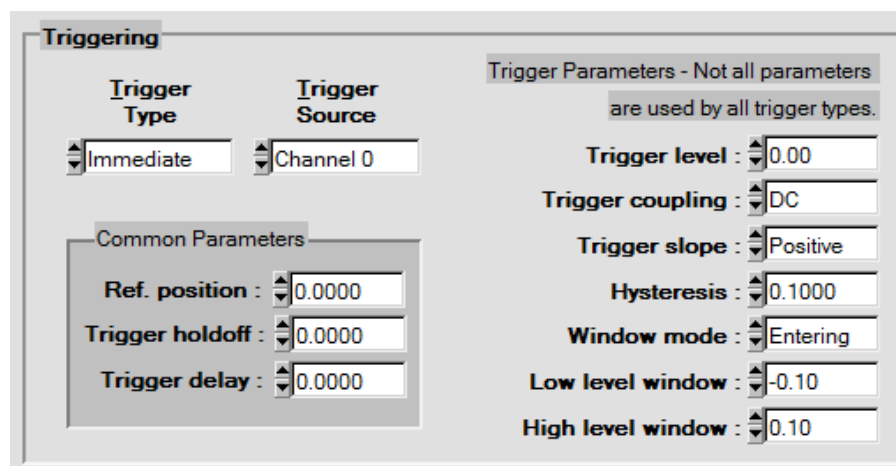


Figure 3.39: TPQA configuration panel for trigger resources and setting.

## 2. Configuration subpanel for HP-3458 sampling DMMs

The subpanel developed to assist the user during the configuration low frequency macro setup based on high precision HP-3458 sampling DMMs is activated by pressing the button

LF-Setup DMMs into Acquisition and Data processing Control box. Figure 3.40 shows the panel for HP-3458 DMMs digitizers configuration.

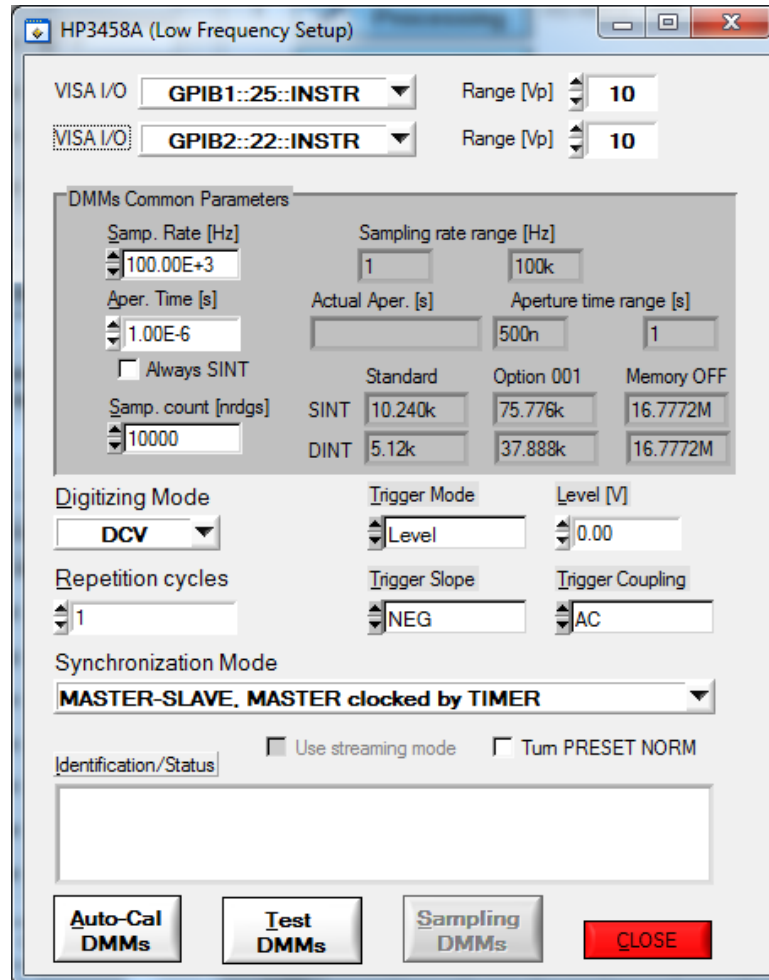


Figure 3.40: TPQA configuration panel for HP-3458a DMMs digitizer.

It is composed of three main steps:

(a) DMMs selecting:

- **VISA I/O:** Selects the GPIB address of the Master DMM;
- **VISA I/O:** Selects the GPIB address of the Slave DMM.

(b) DMMs common parameters settings:

- **Sampling Rate:** Reciprocal of the time interval state by the TIMER;
- **Aperture Time [s]:** the DMMs A/D converter's integration time;
- **Actual aperture:** reports the effective Aperture time value inserted;
- **Aperture time range:** max and min value allowed according to sampling rate (please read the 3458A Manual [14]);

- **Sampling rate range:** it is made up all frequencies between the highest and lowest sampling frequency of DMMs;
- **Sampling Count:** the total number of samples that the A/D must acquire;
- **SINT (Single Integer):** is one type of output formats for readings and it is composed by two bytes, is used during low-resolution measurement;
- **DINT (Double Integer):** is one type of output formats for readings and it is composed by two bytes, is used during high-resolution measurement.
- **Standard, Option 001 and Memory OFF:** indicate three measurement mode (please read Sampling with 3458A book [7] for more details).

**Note:** The parameters placed in the zone of subpanel highlighted in grey are automatically calculated by software.

(c) Sampling settings:

- **Digitizing mode:** Selects the digitizing method of DMMs;
- **Trigger property:**
  - **Trigger mode:** the trigger mode indicates the signal condition that allows the representation of the acquired waveform starts. The user can choose three types of triggers (external, immediate and level). External means that there is another trigger of s different device. Immediate means that when the DMM starts acquiring, the waveform is also displayed. Finally, the level indicates the value of the trigger starting voltage;
  - **Trigger slope:** indicates if the trigger must be on negative or positive slope of waveform;
  - **Trigger coupling:** indicates the coupling type between trigger circuit and ADC channels. It can be DC or AC, without or with capacitive coupling;
  - **Level:** in this slash the User can put in the voltage value of trigger level if him chosen the level as trigger mode option.
- **Synchronization Mode:** indicates how multiple DMMs are synchronized. There are different type through them are synchronized: MASTER-SLAVE, MASTER clocked by TIMER, MASTER-SLAVE, MASTER clocked by AWG, All clocked by AWG e All clocked by TIMER. For more details refer to [65].

At the bottom of the subpanel the user can choose to auto call or to test DMMs by pressing **Auto-Cal DMMs** or **Test DMMs**. When the user has finished to configure the HP3458 for sampling can to close the subpanel by pressing **CLOSE**.

### 3.3.3.2 Configuration of measurement corrections

User must upload transducers corrections files before doing any meaningful measurement. This is done by pressing **HW Corrections** on the main panel, which will invoke panel shown in



Figure 3.41.

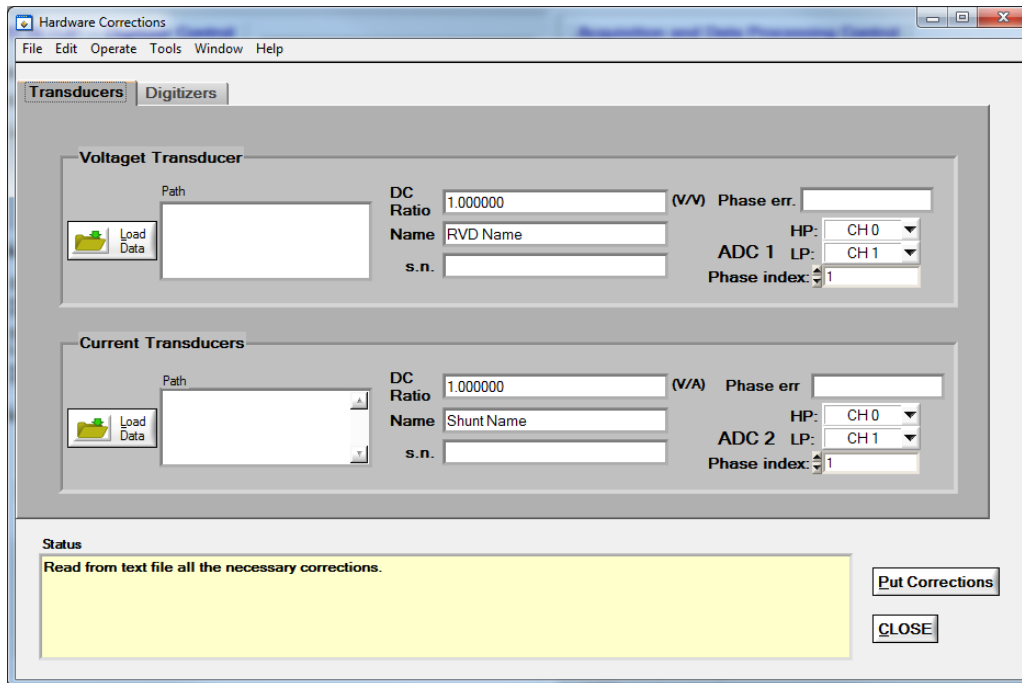


Figure 3.41: TPQA hardware corrections configuration panel.

In the HW Corrections menu, there are two pages where to apply corrections: the first one is related to voltage and current transducers and the second one for Digitizer. The formats of the correction files is described in "A231 Corrections Files Reference Manual" [64]. Also in the same panel is possible to set how the transducers are connected to the experimental setup. Below it is given an example for single-ended and differential transducer configuration using the selectors **High (HP)** and **Low (LP)** to map the transducer outputs to particular digitizer virtual channels.

### 1. Transducers corrections

In the transducers page there are two sections where it is possible to upload the corrections for Voltage and Current transducers for both single-phase power and power quality measurements. The corrections for each transducer are loaded by pressing the button **Load Data**. Note that TPQA installation contains examples including "dummy" divider and shunt correction with unity transfers in the TPQA folder:

```
./data/corrections/transducers.
```

Once uploaded the respective files, the following boxes will be automatically filled with the related data: **DC Ratio**, **Name**, **Serial number** and **Phase error**.

For the ADC samplers it is instead required the channel selection depending on the type of measurement.

If the measurement is single-ended, the transducers are connected to the same ADC module, so **ADC1** and **ADC2** must be set only for the high potential as shown in Figure 3.42. The

low potential **LP** box must be set as not used.

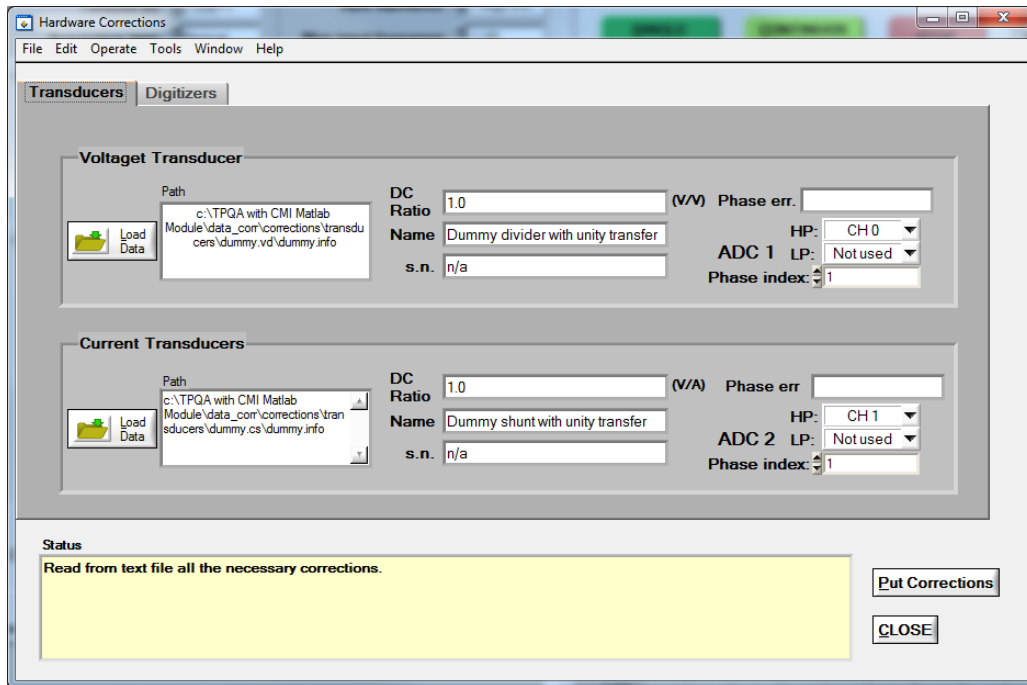


Figure 3.42: TPQA - Example of transducers configuration when ADC1 and ADC2 are set Single-ended mode.

If the measurement is differential, the transducers are connected to different ADC boards and the channels parameters must be set as shown in Figure 3.43. Both **ADC1** and **ADC2** use the **HP** and **LP** boxes, set either on channel zero and channel one.

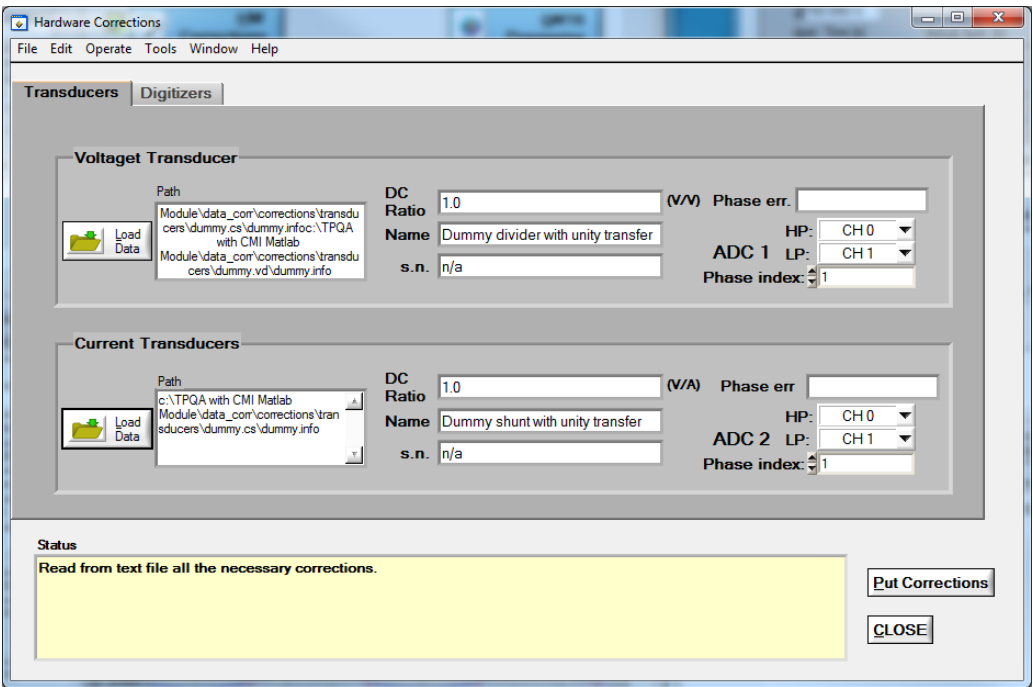


Figure 3.43: TPQA - Example of transducers configuration when ADC1 and ADC2 are set in Differential mode.

2. **Digitizer corrections** In the second page it is possible to upload the digitizer corrections as shown in Figure 3.44.

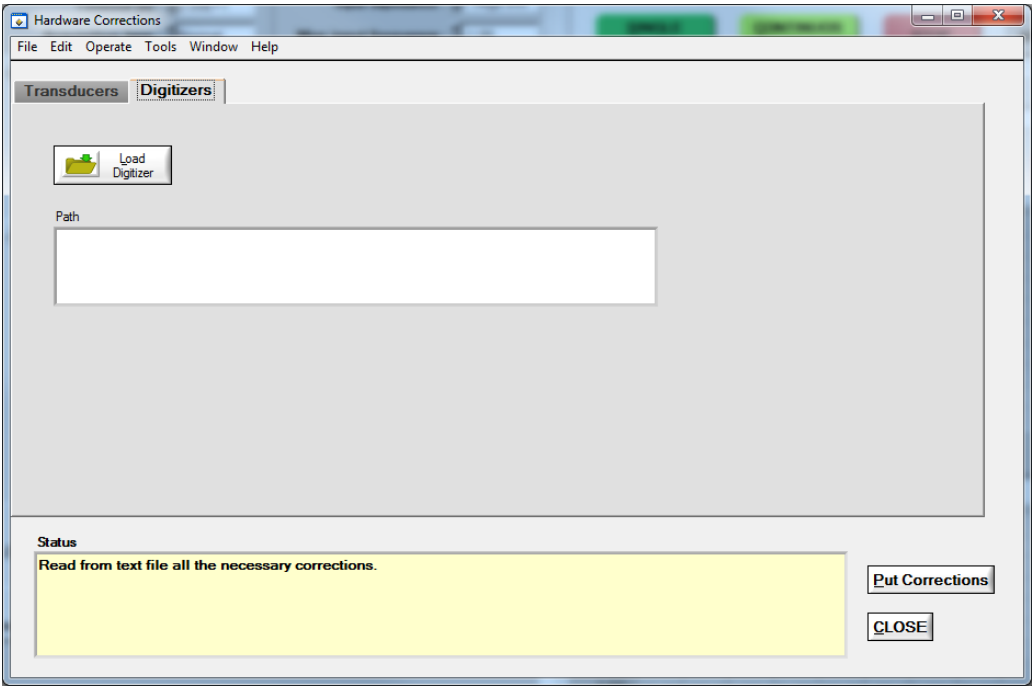


Figure 3.44: TPQA - Example of digitizer configuration panel.

For further information about the digitizer corrections refer to section [3.1.4.3.2](#).

### 3.3.3.3 TPQA data processing

TPQA data processing is performed using two approaches: i) QWTB Processing for post-processing of raw data coming from ADCs; ii) CVI data processing for quasi real-time processing. Both modalities can be performed using the same set of data. Below is reported a description of both approaches.

#### 1. TPQA – QWTB Processing (post-processing)

This method of data processing is described in the activity “A214 [\[74\]](#) The concept for the interface between the data processing module and the control and data acquisition module”, of TracePQM-15RPT04, and only describes the concept for interfacing LabWindows/CVI to MATLAB tool. The report describes the off-line method, which performs the calculation of power and power quality parameters, according to the algorithms, using a set of static sampled data.

Here we report a brief description on how to use the same interface for the post-processing of sampled data coming from a single measurement session. All the considerations about this post-processing approach with respect to the data exchange are identical to those described for TWM open software tool project. For more details refer to the following reports:

- Section [3.2](#) “Corrections Files Reference Manual”;
- “A231 – Data exchange format and file formats”, [\[65\]](#);
- “A232 – Algorithm Exchange Format”, [\[71\]](#);
- “A244 – TWM algorithms description”, [\[66\]](#) or brief version in section [3.6](#).

Once the measurement session has been configured, see section [3.4.2.2](#) “Measurement configuration for LabWindows environment (TPQA)” for an example of configuration, where is described as the user can use TWM algorithm on TPQA. This is done by pressing the button **QWTB Processing** on the main TPQA panel, which will invoke panel shown in Figure [3.45](#) and the user must wait until the message (Please wait, starting Matlab interface ... done) will not appear on the box Processing status (see Figure [3.45](#)).

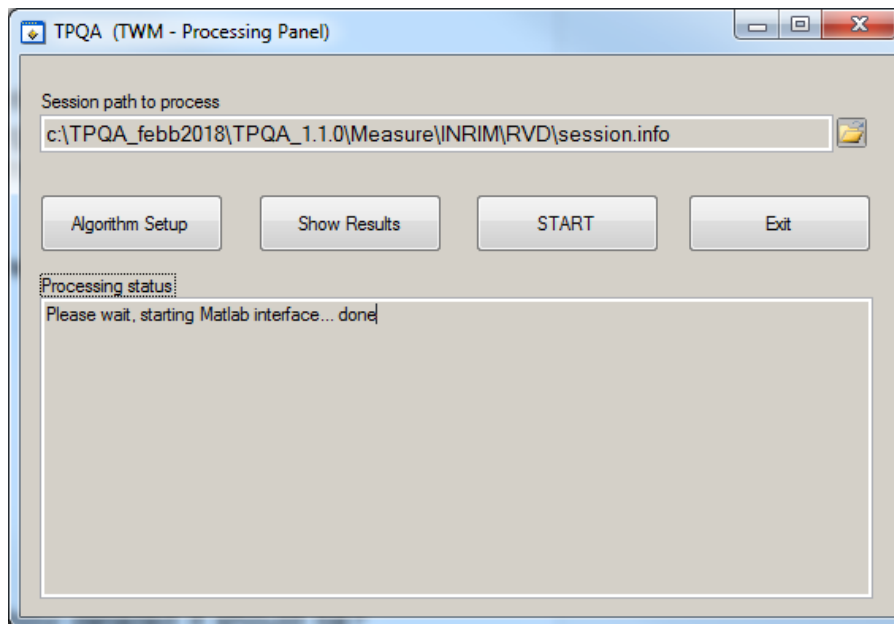


Figure 3.45: TPQA (TWM processing panel).

The user must check if the **Session path** to process is correctly linked to the directory containing the session.info file generated during the measurements.

The User must press the button **Algorithm Setup** and the new panel **QWTB processing algorithms**, shown in Figure 3.46, will be invoked.

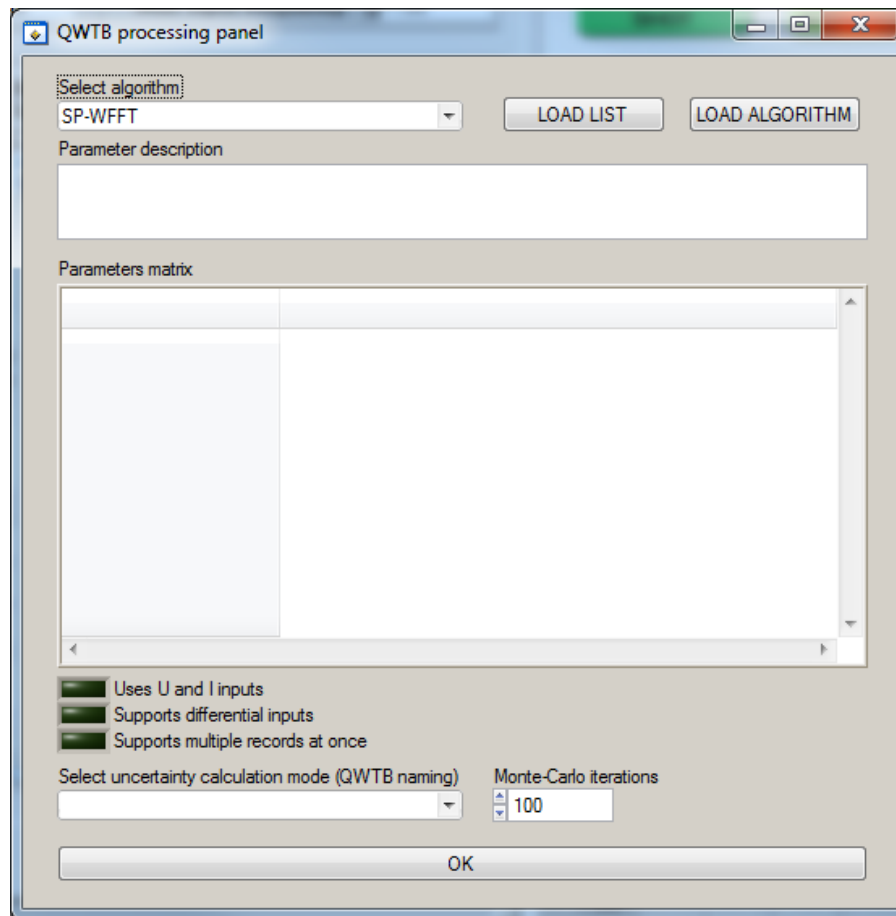


Figure 3.46: TPQA - Algorithm setup panel.

By pressing the button **LOAD LIST** all the available algorithms will be ready to be selected. The User can select the algorithm from a list of algorithms that appears pressing the button **Select Algorithm**. At the end by pressing **OK**, will invoke again the TPQA (TWM - Processing panel Figure 3.45).

To continue with the post-processing of data the user must press the button **START**, which enables the data processing using the selected algorithms. In the **Processing Status** box a progressive number will appear, which indicates the record number under processing as shown in Figure 3.47. User may need to calculate additional parameters from already digitized signals. TPQA is equipped by the batch processing tool for this case similar to TWM project. By selecting new algorithms and repeating the same procedure on the same set of digitized data new processing results will be available.

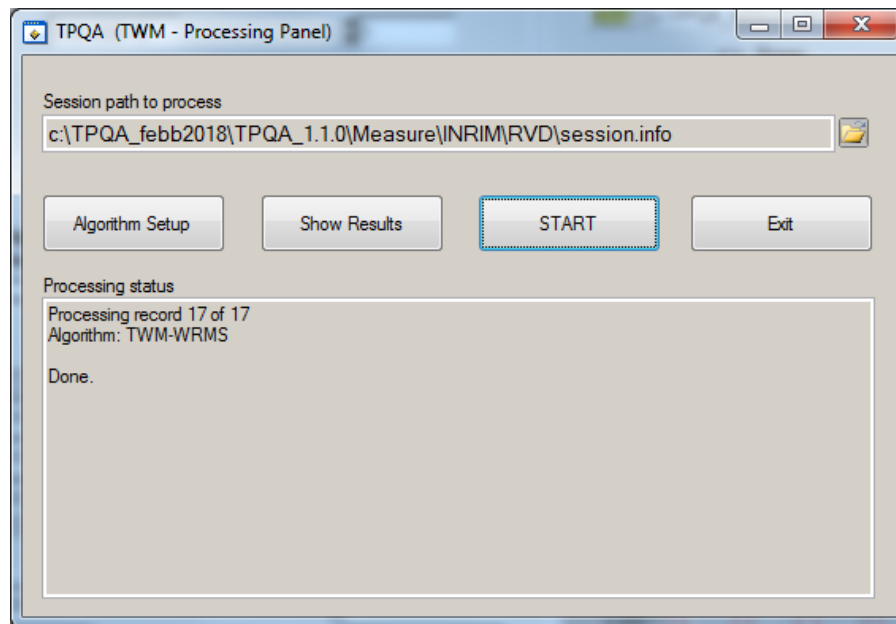


Figure 3.47: TPQA (TWM processing panel) when processing record is finished.

To view the results of processing press the button **Show results** and a new panel will be invoked as shown in Figure 3.48. Before to view results the user must check if the folder uploaded in the **Result file** box (see Figure 3.48) is the same where have been uploaded the processing data. To view the results the user must press on **REFRESH** button and after this must control that all performed elaboration in batch processing show in the **Result matrix** box.

User by selecting the processing that a specific algorithm is responsible for (**Select Algorithm** button), can have access to all the measurement results.

The user by pressing the button **Select result** can change the visualization mode of the results.

If the user need to do other later processing with the results can use the copy and paste mode from panel.

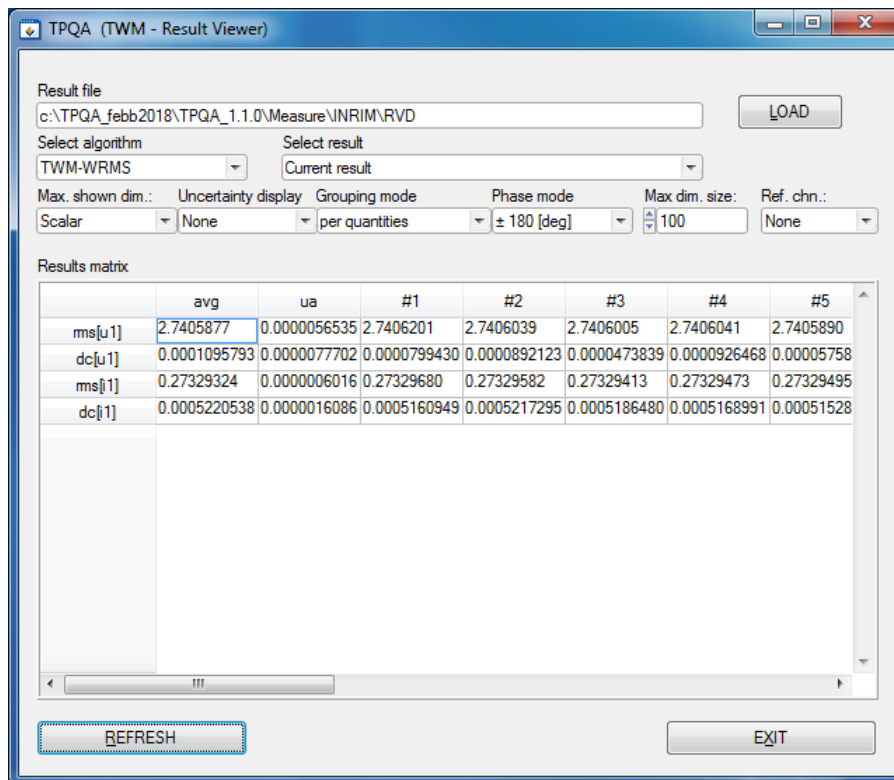


Figure 3.48: TPQA (TWM-Result Viewer).

## 2. TPQA - CVI Data Processing (quasi real-time processing)

The second GUI for data processing elaboration can be activated by pressing “**CVI Data Processing**” command button, Figure 3.49, which opens the panel shown in Figure 3.50.



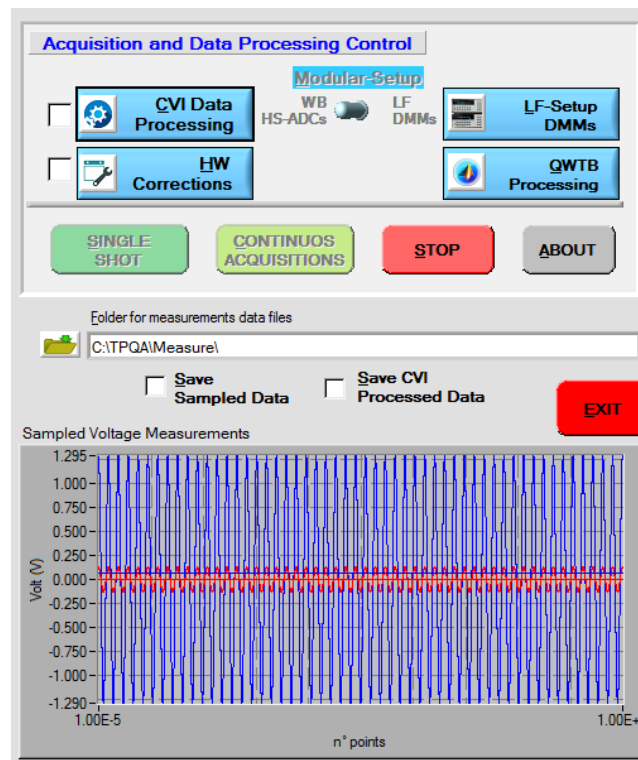


Figure 3.49: TPQA - Acquisition and Data Processing Control section and the measurement plot.

It can be activated in continuous acquisition mode and it is possible to activate additional control panels as follows:

- (a) **CVI Data Processing** command button opens the panel shown in Figure 3.50. Here there are situated the main waveform parameters computed using native algorithms furnished by NI (National Instruments).

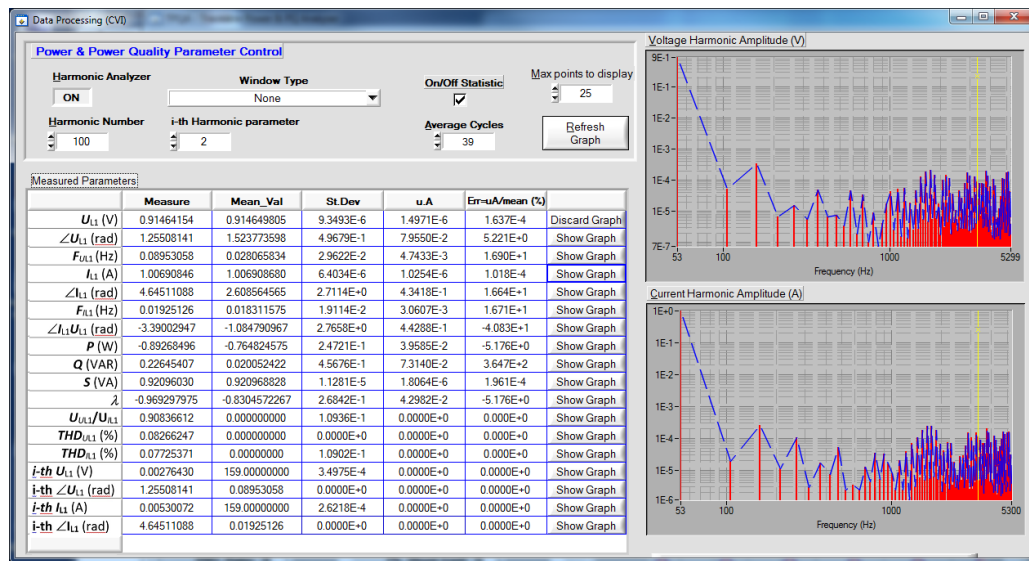


Figure 3.50: TPQA - Preliminary (on-line) data processing using NI-CVI FFT algorithms.

- **Harmonic analyzer ON/OFF:** this button allows according to the parameters set to “**Harmonic Number**” and “**Window Type**” to carry out an analysis on the frequency domain on the sampled waveforms. When enabled it shows on the right-side of the panel the harmonic graphs plotted against frequency. The first graph plotted refers to **Voltage harmonic amplitude (V)** and the second one to **Current harmonic amplitude (A)**; both start from the characteristic frequency of 53 Hz until the selected Harmonic parameter;
- **Window type:** it permits to the user to select a specific type of window which enables different filters on the measured parameters. The program will set by default **None** of these options;
- **On/Off Statistic:** this flag allows computing statistical parameters such as **mean value**, **standard deviation**, **uncertainty A** and the **percentage error** of measured values. Everything will be displayed in the grid next to the measured values;
- **Average cycles:** this counter shows the number of samples that the system takes into account to evaluate the statistical parameters;
- **Max points to display:** it sets the maximum number of points to plot the graphs;
- **Refresh Graph:** update the harmonic graphs of Voltage and Current;
- **Show Graph:** these series of buttons next to each parameter in the grid invoke a new window displaying the corresponding measured value over time as shown in Figure 3.51.
- **CLOSE:** this button allows to exit from the data processing panel.

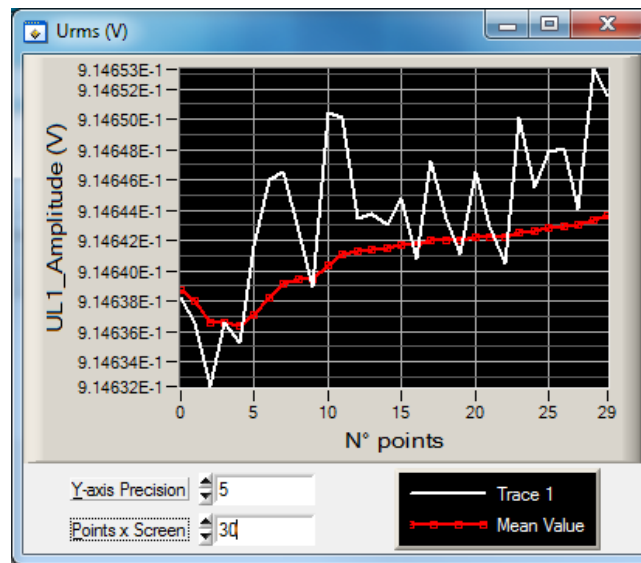


Figure 3.51: TPQA - Selected Measured value graph.

- (b) **Save Sampled Data:** this flag allows to save the measured parameter in the selected Folder for measurements data files path, as a .MATH or .INFO file;
- (c) **Save CVI Processed Data:** this flag allows to save all data extracted from the waveforms. It extract the whole grid containing the measured values plus all the statistical parameters as a .MATH or .INFO file.

## 3.4 Software configuration of the built-in digitizers

### 3.4.1 DMM 3458A

#### 3.4.1.1 Voltage range selection

As the most current and voltage transducers are designed to have output voltages equal or below 0.8 V, the digitizers are usually calibrated and used only at the 1 V range of the DCV function. If required, the different ranges of the digitizers can be selected in **Digitizer configuration panel**. For any ranges, the corresponding inter- and intra-channel corrections should be used in the correction files. The corrections can be set for the different ranges, sampling rates and the measurement frequencies by separate \*.csv corrections files.

#### 3.4.1.2 Input frequency bandwidth

The input frequency bandwidth (the frequency range where the gain is more than -3 dB) of the digitizer should be considered when selecting the voltage range and the digitizing mode, see **Digitizer configuration panel**. The input bandwidth for the different input ranges and the different digitizing modes can be found from the user's manual of the multimeter 3458A [14]. In general, the same voltage range (1 V or 10 V) at both channels in combination with the DCV digitizing mode allows better accuracy. The DCV mode introduces systematic errors due to lower cutoff frequencies. The model describing the frequency response in the DCV mode was studied in [75].

#### 3.4.1.3 Aperture time

Selection of the aperture time affects significantly the performance of the digitizer. The gain error and the frequency dependence on the aperture time were studied in [76] and in [45], respectively. The reported transition point at the aperture time of 100  $\mu$ s corresponds to a change in the internal configuration of the multimeter.

Temperature coefficients in order of 10  $\mu$ V/V $^{\circ}$ C were reported in [53] for the multimeter gains at the aperture times below 100  $\mu$ s. A temperature controlled environment is recommended at the aperture times below 100  $\mu$ s.

#### 3.4.1.4 Sampling rate

In the available digitizing modes DCV, DSDC and DSAC the sampling rates up to 100 kHz are allowed. The sampling time should be set to a higher value than the aperture time to allow the 3458A to process the reading. The minimum differences between the sampling time and the aperture time are described in details in [7]. For the DCV sampling mode, it is safe to reserve 23  $\mu$ s for the processing time for the aperture times above 100  $\mu$ s and 10  $\mu$ s for the aperture

times below 100  $\mu$ s. In the DS mode the aperture time is fixed to 2 ns and cannot be affected by user.

#### 3.4.1.5 Samples count

The number of samples  $N$  defines frequency resolution and the number of periods to be processed by an algorithm. The recommended values for the number of samples and the number of periods required for the stable operation of an algorithm can be found from the description of algorithms in the present guide. In general, for many algorithms the longer record reduces standard deviation roughly with factor  $\sqrt{N}$ . However, for very long records the drifts of the digitizer may prevail, so it may be beneficial to repeat measurement e.g. ten times with one tenth of the record size. Such setting enabled user to view the drift in a graph. Also note some algorithms may not work properly with too long records.

### 3.4.2 Digitizer NI PXI 5922

Here is reported an example of the configuration of the TPQA open software tool to be used for power and PQ measurements. The example covers the configuration of the build-in digitizers with particular emphasis of the use of wide band macro setup based on PXI-5922 digitizers. ADCs as well as voltage and current digitizers are configured for single ended measurements. The example also reports how to configure the data processing for quasi real-time processing using CVI native algorithms and QWTB processing tool box. The TPQA open software project setup has been tested as an executable file on INRIM new and existing measurement setup.

#### 3.4.2.1 Measurement setup for testing TPQA

TPQA handles measurement setups identified for low-frequency (LF) and wide band (WB) power and PQ measurements, according to WP1: Design and validation of the modular power and PQ measurement setup.

For WB measurements the system is based on single or dual NI-5922 digitizers. The digitizing boards can be configured for asynchronous or synchronous acquisitions using a common frequency reference. The macro setup based on NI-5922 digitizers has the advantage of being easily adaptable from a single phase to three phase measurements system.

With respect to the use of precision digitizers for the design of the WB system, the main features are:

- flexible vertical resolution depending on the sampling frequency;
- several synchronization and clocking strategies depending on the kind of PQ parameters under investigation;
- reconfigurable digital platforms for traditional, real time measurements and continuous acquisition for long time measurements beyond the capabilities of internal memory;

- simple synchronization of single digitizers for a polyphaser digitizer suitable for three-phase PQ measurements.

Figure 3.52 shows a prototype modular system which comprises both LF and WB macro-setups developed at INRIM. Both LF and WB digitizers are handled by the same PXI chassis which has a control unit for remote control of both LF and WB digitizers based on a NI mainstream unit.

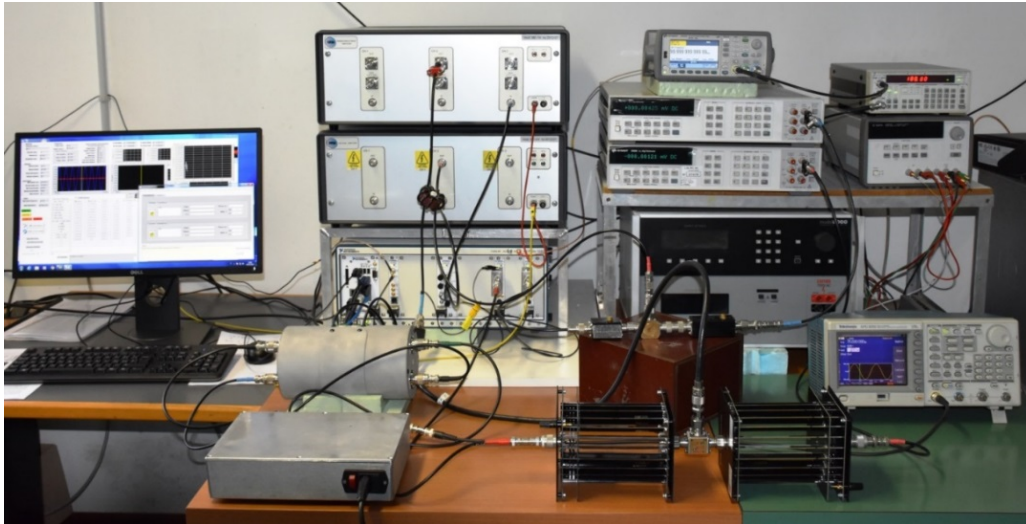


Figure 3.52: Macro setups modular system

#### 3.4.2.2 Measurement configuration for LabWindows environment (TPQA)

The following gives a typical configuration being used with TPQA software using a PXI-5922 digitizer configured for single ended power and PQ measurements.

The TPQA was developed and tested using the following hardware components:

- PXIe chassis mod.1085 equipped with NI-PXIe-8840 embedded controller for real time measurements.
- Two high-bandwidth digitizers NI PXI-5922, to carry out differential sampled voltage measurement;
- Arbitrary waveform generator or clock generator, e.g., Agilent 331/332xxA, Agilent 335/336xxA, SRs CG635;
- Two USB ports of the NI-PXIe-8840 embedded controller are dedicated of interfacing of HP3458A digitizers using independent GPIB-USB-HS controllers
- NI PXI-8840 or equivalent mainstream unit with MS Windows Windows 7 or higher equipped with two or more USB ports.

##### 1. Configuration of WB digitizers, e.g. PXI-5922

- Select the digitizer from **WB-SETUP-Digitizer Control** menu on main panel control (see Figure 3.36). For single-ended measurement select only the first digitizer, e.g. **ADC1** select the name on PXI-5922 board recognized by Ni-Scope driver.
- In the subpanel **Common Parameters** check and/or set:
  - **Channel**: set to 0,1;
  - **Time out [s]**: don't set lower than 20 s;
  - **Acquisition type**: set to Normal;
  - **Vertical range**: setup second the PXI 5922 vertical specifications;
  - **Vertical coupling**: select AC, DC or GND (default DC);
  - **Input impedance**: select 1 M $\Omega$  or 50  $\Omega$  (default 1 M $\Omega$ ).
- In the subpanel **Horizontal** set:
  - **Sample Rate (s)**: set the sampling rate frequency of WB digitizer (default 100 kSs, maximum 15 MSs);
  - **Record Length**: set the number of points to be acquired (maximum  $\approx$  8 MS).
- In the subpanel **Triggering** set:
  - **Trigger Type**: set to desired mode (default Immediate, for synchronized measurements set Edge mode);
  - **Trigger source**: set to **channel 0** for **Edge** mode triggering;
  - For all further parameters see the PXI-5922 datasheet [15].

## 2. Transducers Corrections

- For correction to be used follow all steps described in section 3.3.3.2. Remember to specify how the voltage and current transducers are connected by selecting single or differential mode of operation.

## 3. Data saving

- User must select, for proper data saving and further elaboration, a directory specified in **Folder for measurement data files** placed in the main panel by pressing the related button. After selecting and or creating a new folder, e.g. press C:\TPQA\TPQA\_1.1.0\Measure\INRIM\press Done in the shown window;
- **Save Sampled Data**: used to save all acquired data, otherwise the TPQA will not save any data and no data processing will be available. In this mode it will be possible to save sampled data to be used for off-line data processing using **QWTB** tool box or other algorithms. After pressing **SINGLE SHOT** or **CONTINUOUS ACQUISITION** button the TPQA will open window where to store sequential bunches of data streaming, e.g. ADC\_nnnn.txt;



- **Save CVI Processed Data:** pressing this button TPQA will ask for additional file for storing processed data using CVI algorithms, based on FFT approach.

#### 4. Data acquisition

The user can collect data in two ways, by pressing the following buttons:

- **SINGLE SHOT:** for a single acquisition;
- **CONTINUOUS ACQUISITION:** for a dynamic acquisition. In this mode TPQA always collect data and save them into specified folder by adding a progressive index in each file, e.g: ADC\_nnnn.txt. The index number  $n$  appears in the numeric control **N° of Records**.

#### 5. Data Processing

There are two modes to show the elaboration of results on the acquired data:

- (a) Using QWTB tool box and its algorithms for off-line data processing as specified in the TWM guide in section 3.1. This can be done pressing **QWTB Processing** button placed in the **Acquisition and Data Processing** control of the main panel window. This mode of operation is similar to those described in “QWTB batch processing panel” in section 3.1.4.7. After to have press **QWTB Processing** button, the **TPQA (TWM-processing panel)** will appear and the user must complete the following steps:
  - Press **Algorithm Setup** button and select the proper algorithm in **Select algorithm** control box and then press OK;
  - Press **START** button. In the processing status data log box will appear the name of algorithm and the processing records. Please wait until Done comes up.
  - Press **Show Results** button and the window **TWM result viewer** appears, otherwise user must select the **Measurement session**:
    - Check if the **Result file** reports the path containing measured data;
    - Press **Refresh** and in the **Select Algorithm** will appear the name of QWTB algorithm. The results shown in **Results matrix** can be copied and pasted in a spreadsheet, e.g. \*.csv;
    - On the same set of data the user can test all the available algorithms developed according to the TracePQM project.
- (b) Pressing **CVI Data Processing** an additional window for on-line data processing appears. This mode of introducing the results is useful to get a preliminary and partially traceable evaluation of the results in terms of common power and PQ parameters as described in section 3.3.3.3 and paragraph “CVI data processing”.

By using both the processing tool box, i.e. QWTB and CVI, it is also possible to perform a direct comparison between the common algorithms used for the estimation of main electrical power and PQ parameters on the same set of sampled data.



## 3.5 Integration of new types of digitizers

### 3.5.1 LabVIEW environment

TWM was designed as a modular setup capable of extension by new digitizers without affecting the rest of the SW tool or algorithms. The addition of support for new digitizer requires modification of the LabVIEW part of TWM tool. The programming details are beyond scope of this guide. Therefore, the details are available in a standalone document "A245 TWM Structure" [77] which describes internal structure of TWM and steps needed to include new digitizer.

### 3.5.2 LabWindows environment

TPQA open tool software employed in CVI environment has a modular structure which enable the possibility to fit new digitizers by developing prototype functions, which will be able to interact with the digitizer under test using vendor drivers through a translation layer. Before showing an example, it is important giving the concept of the flow chart developed for TPQA open tool software.

#### 3.5.2.1 Flow chart LabWindowsTM/CVI environment

The TPQA is organized according to the flow chart diagram shown Figure 3.53. The whole TPQA application consists of two parts:

1. LabWindows modules (Control and Processing) that controls the instruments, initiates processing and serves as a user interface
2. Calculation or Processing module based on a double mechanism suitable to process digitized data using:
  - quasi real-time approach for dynamic data processing based on FFT algorithms developed in Labwindows/CVI;
  - post processing and formatting the data for displaying and generation of the measurement report (summary of the results formatted in compact form). The acquired data may be processed at any time. It is possible to just record batch of measurements without processing which may be helpful for time consuming calculations. The processing of the whole batch of measurements can be initiated later either via TWM or on a supercomputer. For further details the interested user can refers to TWM open software tool [57].

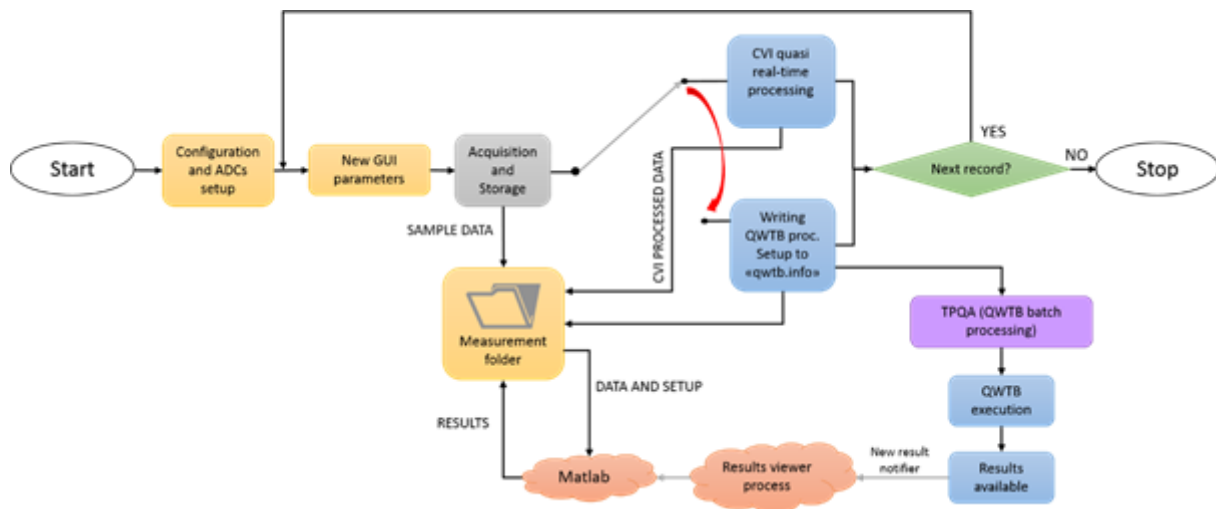


Figure 3.53: Flow chart for TPQA open software tool.

### 3.5.2.2 Integration of new digitizers in LabWindows/CVI environment

The concept of the modular driver has been developed in order to avoid the direct access directly the drivers of particular instruments. It was verified that accessing directly of instrument drivers requires a different approach for each particular ADC board. It was substituted such an approach with a different mechanism which uses a \*.c function translator able to interact as an interface layer between the data acquisition module and the physical instrument drivers which is called **Virtual driver**.

In TPQA open software project such an interface is composed for a specific board, e.g. PXI-NI-5922 digitizer, by two files a (\*.c file and a header \*.h) file:

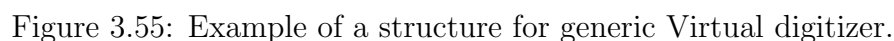
```
GenericMultiDeviceConfiguredAcquisitionTClk.c
GenericMultiDeviceConfiguredAcquisitionTClk.h
```

Only some remarks to take into account regard to the data storing of sampled data when the digitizer runs continually. The solution adopted aims to collect the sampled data and then stored them directly on hard drive while the ADCs runs continually.

In Figure 3.54 is shown the \*.h file (header file) employed as translator for the virtual driver used with ni.Scope driver.

An example of the flow chart developed to describe the virtual driver employed with “niScope” driver is shown in Figure 3.55. New virtual drivers could be inserted into the flow chart, substituting them with those highlighted in the flow chart in blue (see Figure 3.55). This means that the user will rewrite part of the code according to the vendor driver specifications.

Figure 3.54: Header structure of the translator used with ni.scope driver.



Page 230 of 245

## 3.6 Power and PQ tests - Algorithms

### 3.6.1 Existing algorithms

Total of 12 algorithms were developed in scope of TracePQM project. Each of the algorithms was developed, equipped by an uncertainty estimator or Monte Carlo calculator and validated using numeric simulation. The list of algorithms is shown in following table [3.47](#).

Name	Uncertainty	Verification	Description
TWM-PSFE	GUF	Yes	Single-harmonic estimation (amplitude, frequency and phase)
TWM-FPNLSF	GUF	Yes	Single-harmonic estimation (offset, amplitude, frequency and phase)
TWM-MFSF	GUF, MCM	Yes	Multi-harmonic estimation (offset, amplitudes, phases, frequency)
TWM-WRMS	GUF, MCM	Yes	RMS level calculation in time-domain
TWM-WFFT	GUF	Yes	Multi-harmonic estimation (offset, amplitudes, phases)
TWM-PWRTDI	GUF, MCM	Yes	Power parameters estimation in time domain
TWM-PWRFFT	GUF	Yes	Power parameters estimation in frequency domain
TWM-Flicker	GUF	Yes	Flicker measurement following IEC 61000-4-15
TWM-MODTDPS	GUF	Yes	Amplitude modulation estimator
TWM-HCRMS	GUF	Yes	Half-cycle RMS detector following IEC 62586
TWM-InDiSwell	GUF	Yes	Events detector IEC 61000-4-30
TWM-THDWFFT	GUF	Yes	Harmonics and THD estimator
TWM-InpZ	None	No	Estimation of digitizer input impedance

Table 3.47: List of algorithms in scope of TracePQM project.

The algorithms are briefly described in following sections. Up to date details of each algorithm can be found online [\[66\]](#).

#### 3.6.1.1 TWM-PSFE - Phase Sensitive Frequency Estimator

TWM-PSFE is a TWM wrapper for the Phase Sensitive Frequency Estimator algorithm (PSFE). PSFE is an algorithm for estimating the frequency, amplitude, and phase of the fundamental component in harmonically distorted waveforms. The algorithm minimizes the phase difference between the sine model and the sampled waveform by effectively minimizing the influence of the harmonic components. It uses a three-parameter sine-fitting algorithm for all phase calculations.

The resulting estimates show up to two orders of magnitude smaller sensitivity to harmonic distortions than the results of the four-parameter sine fitting algorithm. The algorithm generally works better for higher samples count per period (if possible at least 10).

The TWM wrapper TWM-PSFE is designed for single-ended transducers only. It will only estimate frequency in the differential input transducer mode. The algorithm is equipped by a fast uncertainty estimator for the frequency quantity only.

### **3.6.1.2 TWM-FPNLSF - Four Parameter Non Linear Sine Fit**

This algorithm fits a sine wave to the recorded data by means of non-linear least squares fitting method using 4 parameter (frequency, amplitude, phase and offset) model. Due to non-linear characteristic, convergence is not always achieved. When run in Matlab, function “lsqnonlin” in Optimization toolbox is used. When run in GNU Octave, function “leasqr” in GNU Octave Forge package optim is used. Therefore results can differ.

This algorithm, in general, is not suitable for distorted signals. It offers good results for signals with low harmonic content if at least 10 periods of signal are recorded with preferably at least 50 samples per period. The algorithm also requires initial estimate of the frequency accurate to 500 ppm. The algorithm generally works better for higher samples count per period (if possible at least 10, optimally over 50).

The algorithm supports differential transducer connection. The integrated uncertainty estimator was developed only for the GNU Octave version. This should be still kept in mind when using the algorithm with Matlab despite the Matlab version seems to give always more accurate results than GNU Octave.

### **3.6.1.3 TWM-MFSF - Multi-Frequency Sine Fit**

TWM-MFSF is an algorithm for estimating the frequency, amplitude, and phase of the fundamental and harmonic components in a waveform. Amplitudes and phases of harmonic components are adjusted to find minimal sum of squared differences between sampled signal and multi-harmonic model. When all sampled signal harmonics are included in the model, the algorithm is efficient and produces no bias. It can even handle aliased harmonics, if they are not aliased back exactly at frequencies where other harmonics are already present. Further, it can also handle non harmonic components, when their frequency ratio to the fundamental frequency is exactly known a-priori. The algorithm generally works better for higher samples count per period (if possible at least 10 per period).

The TWM wrapper TWM-MFSF is equipped with a Monte Carlo uncertainty calculator and also a fast uncertainty estimator limited for certain types of signal and algorithm setup.

#### 3.6.1.4 TWM-WRMS - RMS value by Windowed Time Domain Integration

TWM-WRMS is an algorithm for calculation RMS value and DC component of signal a time domain integration of windowed signal  $y(t)$ . The windowing function eliminates effects of non-coherent sampling. Therefore, it does work even for non-coherently sampled waveforms. The algorithm itself without contribution of corrections can easily reach errors below  $1 \mu\text{V/V}$  with proper selection of a sampling rate and window size. That is ideally at least 10 samples per period and at least 10 periods of fundamental component recorded.

The TWM-WRMS algorithm wrapper is able to use single-ended or differential input sensors. The algorithm is also equipped by a fast uncertainty estimator and the Monte Carlo uncertainty calculation method for more accurate but slower uncertainty evaluation.

#### 3.6.1.5 TWM-WFFT - Windowed FFT spectrum analysis

Algorithm for single or multi-tone harmonic analysis using windowed FFT. The algorithm performs windowed FFT of the signal, applies TWM corrections and extracts FFT bin(s) with selected frequencies. It also calculates RMS value estimate, however RMS will be usable only for coherent sampling. The main purpose of the algorithm is inter-channel phase shift and voltage ratio analysis. That will work even for non-coherent sampling, when non-rectangular window is used.

Note the harmonics spacing in the spectrum must be higher, then width of the selected window! E.g. the wide “flattop\_248D” needs at least some 25 FFT bins spacing. Also note the wider windows have higher equivalent noise bandwidth, so the noise in the analyzed harmonic is amplified.

The TWM-WFFT algorithm wrapper is able to use single-ended or differential input sensors. The algorithm is also equipped with a fast uncertainty estimator for the harmonic components.

#### 3.6.1.6 TWM-THDWFFT - THD from Windowed FFT

This algorithm is designed for calculation of the harmonics and Total Harmonic Distortion (THD) of the non-coherently sampled signal. It uses windowed FFT to detect the harmonic amplitudes, which limits the achievable accuracy of the harmonics detection due to the window scalloping effect. However, the algorithm was initially designed for THD calculation of the low-distortion signals, where the accuracy was not critical. The relative expanded uncertainty of the harmonics is at least 0.015 % (or 0.005 % after highly experimental correction method). On the other hand, the algorithm was designed to compensate the spectral leakage of the noise to the harmonics near noise level, so it offers decent accuracy for the very low distortions near self-THD of the digitizer itself.

The algorithm supports direct processing of a multiple records which are used to produce averaged spectrum before the main calculation. This possibility should be preferred instead of repeated call of the algorithm for each record as it reduces the noise. The algorithm supports only single-ended transducer connection.

The algorithm returns: (i) Full spectrum; (ii) Identified harmonics; (iii) THD coefficients according various definitions; (iv) RMS noise estimate; (v) THD+Noise estimate.

Note the uncertainty is evaluated only for some of the returned parameters.

### 3.6.1.7 TWM-PWRTDI - Power by Time Domain Integration

TWM-PWRTDI is an algorithm for calculation of power parameters using a time domain integration of  $u(t) \cdot i(t)$  product. It is based on the use of window function to eliminate effects of non-coherent sampling. Therefore, it does work even for non-coherently sampled waveforms. The algorithm itself without correction effect can easily reach errors below  $1 \mu\text{W}/\text{VA}$  with proper selection of a sampling rate and windows size. That is ideally at least 10 samples per period and at least some 30 periods of fundamental component recorded.

The algorithm can calculate all basic parameters: active power  $P$ , reactive power  $Q$ , apparent power  $S$ , RMS voltage  $U$ , RMS current  $I$  and power factor  $PF$ . It also returns DC components separately:  $U_{\text{DC}}$ ,  $I_{\text{DC}}$  and  $P_{\text{DC}}$ . User may choose optional AC coupling mode by setting parameter  $ac\_coupling = 1$  in which case the  $U$ ,  $I$ ,  $P$ ,  $Q$ ,  $S$  and  $PF$  will be calculated without the AC component.

The windowed RMS method itself can calculate power in any quadrant, however it is not able to distinguish all four quadrants. The quadrant identification (proper signs for  $P$  and  $Q$ ) is obtained from an auxiliary windowed FFT algorithm which is running along the main RMS calculation. Note the quadrant selection may fail around  $PF = 0$  (the absolute values will be correct). The sign of  $Q$  is calculated using harmonic components method according Budenau definition, whereas the value of  $Q$  is obtained as  $S = \sqrt{S^2 - P^2}$ .

The TWM-PWRTDI algorithm is able to use single-ended or differential input sensors for voltage channel, current channel or both. The algorithm is also equipped by a fast uncertainty estimator and the Monte Carlo uncertainty calculation method for more accurate but slower uncertainty evaluation.

### 3.6.1.8 TWM-PWRFFT - Power by FFT

Algorithm for calculation of power parameters from FFT spectra of voltage and current channels. It calculates the power in full bandwidth. It designed for coherent sampling.

The algorithm can calculate all basic parameters: active power  $P$ , reactive power  $Q$ , apparent power  $S$ , RMS voltage  $U$ , RMS current  $I$  and power factor  $PF$ . It also returns DC components separately:  $U_{\text{dc}}$ ,  $I_{\text{dc}}$  and  $P_{\text{dc}}$ . User may choose optional AC coupling mode by setting parameter  $ac\_coupling = 1$  in which case the  $U$ ,  $I$ ,  $P$ ,  $Q$ ,  $S$  and  $PF$  will be calculated without the AC component. The definition of components is identical to the TWM-PWRTDI.

The TWM-PWRFFT algorithm wrapper is able to use single-ended or differential input sensors for voltage channel, current channel or both. The algorithm is also equipped by a fast uncertainty estimator.



### 3.6.1.9 TWM-Flicker - Flicker algorithm

The TWM wrapper TWM-Flicker is an algorithm for evaluation of the short term flicker parameters. It calculates instantaneous flicker sensation  $P_{inst}$  and short-term flicker severity  $P_{st}$ . Sampling rate has to be higher than 7 kHz. If sampling rate is higher than 23 kHz, signal will be down sampled by algorithm. More than 600 s of signal is required as the algorithm needs at least a minute to settle the filters. Typical sampling time value is above 660 s.

The algorithm requires either Signal Processing Toolbox when run in Matlab or a signal package when run in GNU Octave. Frequency of line (carrier frequency)  $f_{line}$  can be only 50 or 60 Hz.

The algorithm was implemented according IEC 61000-4-15.

The algorithm wrapper is equipped by a simple uncertainty estimator based on the worst observed error of the algorithm on the tabulated  $P_{st}$  values for various sampling rates.

Note the algorithm output slightly differ for Matlab and GNU Octave implementation. The cause of this difference was not yet identified. Also the observed performance in the Matlab 2017b was about five times higher then in GNU Octave 4.2.2 on the same computer.

### 3.6.1.10 TWM-MODTDPS - Modulation analyzer in Time Domain, by quadrature Phase Shifting

TWM-MODTDPS is algorithm for calculation of the amplitude modulation parameters of non-coherently sampled signal in time domain. It was designed for basic estimation of the modulation parameters of a sinusoidal carrier modulated by sine wave or rectangular wave with duty cycle 50%. It is intended as an alternative to the Flicker algorithm if it is required to measure only modulating parameters.

The algorithm operates in time domain and it is based on the analytical signal. It is capable to estimate the parameters up to modulating-to-carrier frequency ratio of 33%. The record must contain at least 3 periods of the modulating signal and it also requires at least 10 samples per period of carrier.

It is capable to use the differential transducer connection, however the uncertainty is not calculated for the differential mode. The algorithm is equipped by an uncertainty estimator, which covers most of the operating range. The estimator parameter space contains a few gaps where the algorithm may fail, which will be always indicated as an error message. These gaps problems may be prevented by changing the sampling parameters, e.g. by changing the samples count or a sampling rate.

### 3.6.1.11 TWM-HCRMS - Half Cycle RMS algorithm

Algorithm for calculation of the so called half cycle RMS values or sliding window RMS values of a single phase waveform. It calculates RMS value of signal in length of one period with window step defined by the method of calculation. That is, according to the IEC 61000-3-40: (i)



Class A - half-cycle step; (ii) Class S - “sliding window” step (20 windows per period for this implementation).

The algorithm is designed so it can handle non-coherent sampling and also it is capable to compensate slow frequency drifts. It uses PSFE and resampling technique to ensure coherent sampling internally. The user can enter signal frequency manually if coherent sampling was ensured by the digitizer.

In general, the algorithm will work better with higher sampling rates. At least 100 samples should be recorded per period of the fundamental component (= sampling rate 5 kSa/s for 50 Hz networks). The higher is better, because the RMS algorithm will better suppress the harmonic and inter-harmonic content.

The algorithm is for single-ended input only and it is equipped with fast uncertainty estimator.

#### **3.6.1.12 TWM-InDiSwell - Interruption, Dip, Swell event detector**

This algorithm detects power quality events “dip”, “swell” and “interruption” for a single phase systems according to the IEC 61000-3-40, “class A” (half-cycle step) or “class S” (sliding window). It returns relative event time, duration and its residual RMS value in percents relative to the entered nominal level. Note the result provided for the classes A and S should be identical as long as the event is synchronized with the nominal frequency zero-cross. However that is rarely the case of real life situations, so the selection must be made depending on the prescription for the given PQ meter test or PQ event calibrator.

The algorithm internally uses RMS envelope detector TWM-HCRMS, so the accuracy of the detection depends on its properties. In general, the algorithm will work better with higher sampling rates. At least 100 samples should be recorded per period of the fundamental component (= sampling rate 5 kSa/s for 50 Hz networks). The higher is better, because the RMS algorithm will better suppress the harmonic and inter-harmonic content.

The algorithm is for single-ended input only and it is equipped with fast uncertainty estimator.

#### **3.6.1.13 TWM-InpZ – Estimator of Digitizer Input Impedance**

This simple algorithm was designed to measure input impedance of digitizer channel. It is experimental algorithm designed as an addition to the main algorithms developed for PQ measurement. It is not equipped by any uncertainty evaluation.

### **3.6.2 Integration of new algorithms**

TWM and TPQA tools are designed so they can both use TWM processing module that runs in Matlab or GNU Octave. Thus following section applies for both tools. The processing module

described in [77] is an extension for QWTB toolbox [67]. The toolbox was designed for a simple addition of new algorithms by simply creating new folder with specified files. However, to make TWM work properly, the rules described in [71] for the naming of the input and output quantities in the newly developed algorithm must be followed, so all the data received from TWM processing module are recognized and processed correctly.

Each QWTB algorithm compatible with TWM processing module must contain at least following files in following file structure:

→ <b>.\octprog\QWTB</b>	QWTB toolbox root folder in the TWM 'octprog' folder
→ <b>alg_TWM-my_algorithm_name</b>	Algorithm 'TWM-my_algorithm_name' root folder
→ <b>alg_info.m</b>	Algorithm info definition file (see QWTB doc [67])
→ <b>alg_wrapper.m</b>	Algorithm wrapper (call to low level functions)
→ <b>*.*</b>	Auxiliary function of the wrapper

The **red** parts are mandatory names. The **bold** prefix in the algorithm name '**TWM-**' was chosen to distinguish the original QWTB algorithms that usually do not apply any corrections from the TWM algorithm extensions that do calculate corrections and their uncertainties. So it is recommended to follow this rule.

TWM always expect at least "alg\_info.m" file, which contains name, short description, references and definitions of input and output quantities. TWM then only requires main algorithm wrapper "alg\_wrapper.m", which may either call some low level functions, call another QWTB algorithms or contain the algorithm code directly. It must process all the received quantities with the sample data and corrections and return quantities to be saved and displayed by TWM. It also contains estimator or Monte Carlo calculator of uncertainty.

In order to make the newly added algorithm visible in TWM, one must first add its name to the filter of supported algorithms which is located in the file:

`.\octprog\qwtb_list.info`

This file is described to details in [65]. It must at least contain name of the algorithm in the list of supported algorithms:

```

1 // filter of the algorithms}
2 type:: qwtb list
3
4 // === list of the supported algorithms ===}
5 // note: enter algorithm ID's, e.g.: PSFE, SFDR, ...}
6 #startmatrix:: list of supported algorithms
7 ...
8 TWM-my_algorithm_name
9 ...
10 #endmatrix:: list of supported algorithms
11
12 ...

```

The newly integrated algorithm should automatically appear in the list of available algorithms in the QWTB processing panel of TWM show in Figure 3.20.

When implementing the algorithms, user should keep in mind the algorithm should be compatible with both GNU Octave and Matlab environments, so it is recommended to not use the extended Octave syntax and when possible also not the commercial packages where no equivalent for the other environment is available. Where needed, user may use if/else statement to distinguish Matlab and Octave code to reflect the differences or eventually throw an error with information the algorithm cannot run in given environment. Example of environment dependent code:

```
1 %% Check if running in Matlab or GNU Octave:
2 IS_OCTAVE = (exist('OCTAVE_VERSION') ~= 0);
3
4 %% Check available packages
5 if IS_OCTAVE
6     if not(exist('butter'))
7         pkg load signal
8         if not(exist('butter'))
9             error('This algorithm requires package "signal" from Octave Forge');
10        end
11    end
12 else
13     if not(exist('butter'))
14         error('This algorithm requires "Signal Processing Toolbox"');
15     end
16 end
```

More details on implementation of the algorithm are given in up to date version of document A232 Algorithms Exchange Format.docx available online [\[71\]](#).

# Bibliography

- [1] S. Svensson, "A wattmeter standard for the audio frequency range," *IEEE Transactions on Instrumentation and Measurement*, vol. 48, no. 2, pp. 431–433, Apr. 1999, ISSN: 0018-9456. DOI: [10.1109/19.769618](https://doi.org/10.1109/19.769618).
- [2] T. Bergsten, V. Tarasso, and K.-E. Rydler, "A calibration system for electric power at frequencies up to 1 MHz," in *17<sup>th</sup> International Congress of Metrology*, EDP Sciences, 2015, p. 10 003, ISBN: 978-2-7598-1866-2. DOI: [10.1051/metrology/20150010003](https://doi.org/10.1051/metrology/20150010003).
- [3] V. Tarasso, T. Bergsten, and K. Rydler, "Towards an electric power standard for frequencies up to 1 MHz," in *2012 Conference on Precision Electromagnetic Measurements*, Jul. 2012, pp. 128–129. DOI: [10.1109/CPEM.2012.6250694](https://doi.org/10.1109/CPEM.2012.6250694).
- [4] E. Houtzager, G. Rietveld, and H. E. van den Brom, "Switching Sampling Power Meter for Frequencies Up to 1 MHz," *IEEE Transactions on Instrumentation and Measurement*, vol. 62, no. 6, pp. 1423–1427, Jun. 2013, ISSN: 0018-9456. DOI: [10.1109/TIM.2013.2250151](https://doi.org/10.1109/TIM.2013.2250151).
- [5] G. Rietveld, D. Zhao, C. Kramer, E. Houtzager, O. Kristensen, C. de Lefte, and T. Lippert, "Characterization of a Wideband Digitizer for Power Measurements up to 1 MHz," *IEEE Transactions on Instrumentation and Measurement*, vol. 60, no. 7, pp. 2195–2201, Jul. 2011, ISSN: 0018-9456, 1557-9662. DOI: [10.1109/TIM.2011.2117330](https://doi.org/10.1109/TIM.2011.2117330).
- [6] S. Awan, B. Kibble, and J. Schurr, *Coaxial Electrical Circuits for Interference-Free Measurements*. Institution of Engineering and Technology, 2011, 351 pp., ISBN: 978-1-84919-069-5. [Online]. Available: <https://epdf.tips/coaxial-electrical-circuits-for-interference-free-measurements-iet-electrical-me.html> (visited on 05/04/2019).
- [7] R. Lapuh, *Sampling with 3458A: Understanding, Programming, Sampling and Signal Processing*, 1st. Ljubljana: Left Right d.o.o., 2018, ISBN: 978-961-94476-0-4.
- [8] N. M. Institute, *Precision 1000 v inductive voltage divider*, 2016. [Online]. Available: <https://www.measurement.gov.au/ScienceTechnology/Documents/Precision-1000V-Inductive-Voltage-Divider.pdf> (visited on 05/30/2019).
- [9] K.-. Rydler, S. Svensson, and V. Tarasso, "Voltage dividers with low phase angle errors for a wideband power measuring system," in *Conference Digest Conference on Precision Electromagnetic Measurements*, Jun. 2002, pp. 382–383. DOI: [10.1109/CPEM.2002.1034882](https://doi.org/10.1109/CPEM.2002.1034882).
- [10] M. Ouameur, F. Ziade, and Y. L. Bihan, "Novel Broadband Calibration Method of Current Shunts Based on VNA," *IEEE Transactions on Instrumentation and Measurement*, vol. 68, no. 3, pp. 854–863, Mar. 2019, ISSN: 0018-9456. DOI: [10.1109/TIM.2018.2855499](https://doi.org/10.1109/TIM.2018.2855499).

- [11] M. Ouameur, F. Ziadé, and Y. Le Bihan, “Electromagnetic Modelling of a new Broad-band Current Shunt,” in *18<sup>th</sup> International Symposium on Applied Electromagnetics and Mechanics (ISEM 2017)*, Chamonix, France, Sep. 2017, 2p.
- [12] M. Ouameur, F. Ziade, and Y. L. Bihan, “Design and Modelling of a Shunt for Current Measurements at 10 a and up to 1 MHz: A Theoretical Approach,” in *2018 Conference on Precision Electromagnetic Measurements (CPEM 2018)*, Jul. 2018, pp. 1–2. DOI: [10.1109/CPEM.2018.8500844](https://doi.org/10.1109/CPEM.2018.8500844).
- [13] N. M. Institute, *Precision multi-range current transformer mct-1*, 2018. [Online]. Available: <https://www.measurement.gov.au/ScienceTechnology/Documents/Precision-Multi-Range-Current-Transformer.pdf> (visited on 05/30/2019).
- [14] Agilent Technologies, *3458A Multimeter User’s Guide, 4<sup>th</sup> edition*, 2001.
- [15] National Instruments, *NI PXI/PCI-5922 Specifications*, 2014.
- [16] N. M. Oldham and O. Petersons, “Calibration of Standard Wattmeters Using a Capacitance Bridge and a Digital Generator,” *IEEE Transactions on Instrumentation and Measurement*, vol. IM-34, no. 4, pp. 521–524, Dec. 1985, ISSN: 0018-9456. DOI: [10.1109/TIM.1985.4315395](https://doi.org/10.1109/TIM.1985.4315395).
- [17] N. Oldham, “Power Calibration Standard Based On Digitally Synthesized Sinewaves,” *IEEE Transactions on Power Apparatus and Systems*, vol. 104, no. 11, pp. 3117–3122, Nov. 1985, ISSN: 0018-9510. DOI: [10.1109/TPAS.1985.318820](https://doi.org/10.1109/TPAS.1985.318820).
- [18] P. N. Miljanic, “Calibrator for alternating voltage, current, and power,” *IEEE Transactions on Instrumentation and Measurement*, vol. 38, no. 2, pp. 384–389, Apr. 1989, ISSN: 0018-9456. DOI: [10.1109/19.192312](https://doi.org/10.1109/19.192312).
- [19] J. J. Hill and T. A. Deacon, “Voltage-Ratio Measurement with a Precision of Parts in 10<sup>9</sup> and Performance of Inductive Voltage Dividers,” *IEEE Transactions on Instrumentation and Measurement*, vol. 17, no. 4, pp. 269–278, Dec. 1968, ISSN: 0018-9456. DOI: [10.1109/TIM.1968.4313718](https://doi.org/10.1109/TIM.1968.4313718).
- [20] C. A. Hoer and W. L. Smith, “A 1-MHz Binary Inductive Voltage Divider with Ratios 2<sup>n</sup> to 1 or 6<sup>n</sup> dB,” *IEEE Transactions on Instrumentation and Measurement*, vol. 17, no. 4, pp. 278–284, Dec. 1968, ISSN: 0018-9456. DOI: [10.1109/TIM.1968.4313719](https://doi.org/10.1109/TIM.1968.4313719).
- [21] C. A. Hoer and W. L. Smith, “A 2:1 ratio inductive voltage divider with less than 0.1 ppm error to 1 MHz,” *Journal of Research of the National Bureau of Standards, Section C: Engineering and Instrumentation*, vol. 71, no. 2, pp. 101–109, 1967. [Online]. Available: [http://nvlpubs.nist.gov/nistpubs/jres/71C/jresv71Cn2p101\\_A1b.pdf](http://nvlpubs.nist.gov/nistpubs/jres/71C/jresv71Cn2p101_A1b.pdf) (visited on 04/25/2019).
- [22] T. M. Souders, “Wide-Band Two-Stage Current Transformers of High Accuracy,” *IEEE Transactions on Instrumentation and Measurement*, vol. 21, no. 4, pp. 340–345, Nov. 1972, ISSN: 0018-9456. DOI: [10.1109/TIM.1972.4314039](https://doi.org/10.1109/TIM.1972.4314039).
- [23] JCGM, *Evaluation of Measurement Data - Guide to the Expression of Uncertainty in Measurement*, JCGM, Ed. Bureau International des Poids et Mesures, 1995, ISBN: 92-67-10188-9.
- [24] —, *Evaluation of Measurement Data - Supplement 1 to the “Guide to the Expression of Uncertainty in Measurement” - Propagation of Distributions Using a Monte Carlo Method*, JCGM, Ed. Bureau International des Poids et Mesures, 2008.

- [25] —, *Evaluation of Measurement Data – Supplement 2 to the “Guide to the Expression of Uncertainty in Measurement” – Extension to Any Number of Output Quantities*, JCGM, Ed., October. Bureau International des Poids et Mesures, 2011.
- [26] K.-E. Rydler, “High precision automated measuring system for AC-DC current transfer standards,” *IEEE Transactions on Instrumentation and Measurement*, vol. 42, no. 2, pp. 608–611, Apr. 1993, ISSN: 0018-9456. DOI: [10.1109/19.278637](https://doi.org/10.1109/19.278637).
- [27] T. Funck and M. Klonz, “Improved AC-DC Current Transfer Step-Up With New Current Shunts and Potential Driven Guarding,” *IEEE Transactions on Instrumentation and Measurement*, vol. 56, no. 2, pp. 361–364, Apr. 2007, ISSN: 0018-9456. DOI: [10.1109/TIM.2007.890803](https://doi.org/10.1109/TIM.2007.890803).
- [28] S. Svensson, K.-. Rydler, and V. Tarasso, “Improved Model and Phase-Angle Verification of Current Shunts for AC And Power Measurements,” in *2004 Conference on Precision Electromagnetic Measurements*, Jun. 2004, pp. 82–83. DOI: [10.1109/CPEM.2004.305451](https://doi.org/10.1109/CPEM.2004.305451).
- [29] K. Rydler, T. Bergsten, and V. Tarasso, “Determination of phase angle errors of current shunts for wideband power measurement,” in *2012 Conference on Precision Electromagnetic Measurements*, Jul. 2012, pp. 284–285. DOI: [10.1109/CPEM.2012.6250913](https://doi.org/10.1109/CPEM.2012.6250913).
- [30] S. Mašláň, M. Šíra, T. Skalická, and T. Bergsten, “Four Terminal Pair Digital Sampling Impedance Bridge up to 1 MHz,” *IEEE Transactions on Instrumentation and Measurement*, pp. 1–1, 2019, ISSN: 0018-9456. DOI: [10.1109/TIM.2019.2908649](https://doi.org/10.1109/TIM.2019.2908649).
- [31] T. Bergsten and K. Rydler, “Realization of Absolute Phase and AC Resistance of Current Shunts by Ratio Measurements,” *IEEE Transactions on Instrumentation and Measurement*, vol. 68, no. 6, pp. 2041–2046, Jun. 2019, ISSN: 0018-9456. DOI: [10.1109/TIM.2018.2882927](https://doi.org/10.1109/TIM.2018.2882927).
- [32] U. Pogliano, B. Trinchera, and D. Serazio, “Wideband digital phase comparator for high current shunts,” *Metrologia*, vol. 49, no. 3, pp. 349–358, Apr. 2012, ISSN: 0026-1394. DOI: [10.1088/0026-1394/49/3/349](https://doi.org/10.1088/0026-1394/49/3/349).
- [33] S. Mašláň, M. Šíra, and T. Skalická, “Progress on Simple Resistance Standard with Calculable Time Constant,” in *2018 Conference on Precision Electromagnetic Measurements (CPEM 2018)*, Paris, France: IEEE, Jul. 2018, pp. 1–2, ISBN: 978-1-5386-0973-6. DOI: [10.1109/CPEM.2018.8501166](https://doi.org/10.1109/CPEM.2018.8501166).
- [34] I. Budovsky, “Measurement of Phase Angle Errors of Precision Current Shunts in the Frequency Range From 40 Hz to 200 kHz,” *IEEE Transactions on Instrumentation and Measurement*, vol. 56, no. 2, pp. 284–288, Apr. 2007, ISSN: 0018-9456. DOI: [10.1109/TIM.2007.891117](https://doi.org/10.1109/TIM.2007.891117).
- [35] G. Bosco, M. Garcocz, K. Lind, U. Pogliano, G. Rietveld, V. Tarasso, B. Voljc, and V. Zachovalová, “Phase Comparison of High-Current Shunts up to 100 kHz,” *IEEE Transactions on Instrumentation and Measurement*, vol. 60, no. 7, pp. 2359–2365, Jul. 2011, ISSN: 0018-9456. DOI: [10.1109/TIM.2011.2108553](https://doi.org/10.1109/TIM.2011.2108553).
- [36] X. Pan, J. Zhang, X. Ma, Y. Gu, W. Liu, B. Wang, Z. Lu, and D. Zhang, “A Coaxial Time Constant Standard for the Determination of Phase Angle Errors of Current Shunts,” *IEEE Transactions on Instrumentation and Measurement*, vol. 62, no. 1, pp. 199–204, Jan. 2013, ISSN: 0018-9456. DOI: [10.1109/TIM.2012.2212595](https://doi.org/10.1109/TIM.2012.2212595).
- [37] L. Lai, J. Feng, L. Shi, H. Shi, Y. Pan, and B. Zhou, “Measurement of the time constant of four-terminal resistor based on dissipation factor of capacitor,” in *2016 Conference*



- on *Precision Electromagnetic Measurements (CPEM 2016)*, Jul. 2016, pp. 1–2. DOI: [10.1109/CPEM.2016.7540607](https://doi.org/10.1109/CPEM.2016.7540607).
- [38] K. Rydler, T. Bergsten, and G. Eklund, “A Method for Realisation of Inductance and Quality Factor to 1 MHz,” in *2018 Conference on Precision Electromagnetic Measurements (CPEM 2018)*, Jul. 2018, pp. 1–2. DOI: [10.1109/CPEM.2018.8500813](https://doi.org/10.1109/CPEM.2018.8500813).
  - [39] R. Hadzhistoykova and T. Konstantinova, “Measurements for dc characterization of low resistance standards in bim,” in *Proceedings 28th International Scientific Symposium Metrology and Metrology Assurance 2018*, Sozopol, Bulgaria, Sep. 2018, pp. 106–110. [Online]. Available: <https://easychair.org/my/conference?conf=mmo2018>.
  - [40] U. Pogliano, B. Trinchera, M. Lanzillotti, and D. Serazio, “Characterization of resistive dividers for a wideband power analyzer,” in *29th Conference on Precision Electromagnetic Measurements (CPEM 2014)*, Aug. 2014, pp. 130–131. DOI: [10.1109/CPEM.2014.6898293](https://doi.org/10.1109/CPEM.2014.6898293).
  - [41] L. Lingzhang, Q. Zhongtai, and T. Guangqiu, “A new precision AC resistance divider,” *IEEE Transactions on Instrumentation and Measurement*, vol. 37, no. 3, pp. 462–464, Sep. 1988, ISSN: 0018-9456. DOI: [10.1109/19.7476](https://doi.org/10.1109/19.7476).
  - [42] T. Bergsten, V. Tarasso, and K. Rydler, “Precision measurement system for characterisation of phase displacement of voltage dividers up to 1 MHz,” in *CPEM 2010*, Jun. 2010, pp. 259–260. DOI: [10.1109/CPEM.2010.5545107](https://doi.org/10.1109/CPEM.2010.5545107).
  - [43] B. Trinchera, D. Serazio, and U. Pogliano, “Asynchronous Phase Comparator for Characterization of Devices for PMUs Calibrator,” *IEEE Transactions on Instrumentation and Measurement*, vol. 66, no. 6, pp. 1139–1145, Jun. 2017, ISSN: 0018-9456. DOI: [10.1109/TIM.2017.2648598](https://doi.org/10.1109/TIM.2017.2648598).
  - [44] T. Bergsten, V. Tarasso, and K. Rydler, “Determining voltage dependence of the phase response in voltage dividers,” in *2012 Conference on Precision Electromagnetic Measurements*, Jul. 2012, pp. 282–283. DOI: [10.1109/CPEM.2012.6250912](https://doi.org/10.1109/CPEM.2012.6250912).
  - [45] J. D. de Aguilar, J. R. Salinas, O. Kieler, R. Caballero, R. Behr, Y. A. Sanmamed, and Á. Méndez, “Characterization of an analog-to-digital converter frequency response by a Josephson arbitrary waveform synthesizer,” *Measurement Science and Technology*, vol. 30, no. 3, p. 035 006, Feb. 2019, ISSN: 0957-0233. DOI: [10.1088/1361-6501/aafb27](https://doi.org/10.1088/1361-6501/aafb27).
  - [46] IEEE Instrumentation and Measurement Society, Waveform Measurements and Analysis Committee, Institute of Electrical and Electronics Engineers, and American National Standards Institute, *IEEE Standard for Digitizing Waveform Recorders, IEEE Std 1057-2017 (Revision of IEEE Std 1057-2007)*. Jan. 2018, ISBN: 978-1-5044-4301-2. DOI: [10.1109/IEEESTD.2018.8291741](https://doi.org/10.1109/IEEESTD.2018.8291741).
  - [47] R. Lapuh, “Estimating the Fundamental Component of Harmonically Distorted Signals From Noncoherently Sampled Data,” *IEEE Transactions on Instrumentation and Measurement*, vol. 64, no. 6, pp. 1419–1424, Jun. 2015, ISSN: 0018-9456. DOI: [10.1109/TIM.2015.2401211](https://doi.org/10.1109/TIM.2015.2401211).
  - [48] B. Stott, “Interpolating between calibration points for an AC/DC transfer standard,” presented at the National Conference of Standards Laboratories, Monterey, CA, USA: Boulder, CO : National Conference of Standards Laboratories, ©1996., Aug. 25–29, 1996, p. 16. [Online]. Available: <http://citeseerx.ist.psu.edu/viewdoc/download?doi=10.1.1.527.5179&rep=rep1&type=pdf> (visited on 05/24/2019).
  - [49] A. Pokatilov, T. Kübarsepp, and V. Vabson, “Effect of Keysight 3458A Jitter on Precision of Phase Difference Measurement,” *IEEE Transactions on Instrumentation and Measurement*,

- vol. 65, no. 11, pp. 2595–2600, Nov. 2016, ISSN: 0018-9456. DOI: [10.1109/TIM.2016.2593965](https://doi.org/10.1109/TIM.2016.2593965).
- [50] R. Lapuh, B. Voljč, M. Lindič, and O. F. O. Kieler, “Keysight 3458A Noise Performance in DCV Sampling Mode,” *IEEE Transactions on Instrumentation and Measurement*, vol. 66, no. 6, pp. 1089–1094, Jun. 2017, ISSN: 0018-9456. DOI: [10.1109/TIM.2017.2681238](https://doi.org/10.1109/TIM.2017.2681238).
  - [51] R. Behr, O. F. O. Kieler, D. Schleußner, L. Palafox, and F. J. Ahlers, “Combining Josephson Systems for Spectrally Pure AC Waveforms With Large Amplitudes,” *IEEE Transactions on Instrumentation and Measurement*, vol. 62, no. 6, pp. 1634–1639, Jun. 2013, ISSN: 0018-9456. DOI: [10.1109/TIM.2013.2238433](https://doi.org/10.1109/TIM.2013.2238433).
  - [52] S. Benz, C. J. Burroughs, and P. D. Dresselhaus, “AC coupling technique for Josephson waveform synthesis,” *IEEE Transactions on Applied Superconductivity*, vol. 11, no. 1, pp. 612–616, Mar. 2001, ISSN: 10518223. DOI: [10.1109/77.919419](https://doi.org/10.1109/77.919419).
  - [53] F. Sandoval, G. Joya, Y. A. Sanmamed, R. Caballero, M. Neira, F. Garcia-Lagos, J. R. Salinas, and J. D. de Aguilar, “Study of Keysight 3458A Temperature Coefficient for Different Aperture Times in DCV Sampling Mode,” in *2018 Conference on Precision Electromagnetic Measurements (CPEM 2018)*, Jul. 2018, pp. 1–2. DOI: [10.1109/CPEM.2018.8500883](https://doi.org/10.1109/CPEM.2018.8500883).
  - [54] M. Šíra, O. Kieler, and R. Behr, “A Novel Method for Calibration of ADC Using JAWS,” *IEEE Transactions on Instrumentation and Measurement*, vol. 68, no. 6, pp. 2091–2099, Jun. 2019, ISSN: 0018-9456. DOI: [10.1109/TIM.2018.2888918](https://doi.org/10.1109/TIM.2018.2888918).
  - [55] W. Kester, “Understand SINAD, ENOB, SNR, THD, THD + N, and SFDR so You Don’t Get Lost in the Noise Floor,” Analog Devices, Inc., MT-003, Rev. A, 2009, p. 8. [Online]. Available: <https://www.analog.com/media/en/training-seminars/tutorials/MT-003.pdf> (visited on 05/24/2019).
  - [56] S. Svensson, K. Rydler, and V. Tarasso, “Upgrade of accuracy and traceability the SP Sampling Wattmeter,” in *2016 Conference on Precision Electromagnetic Measurements (CPEM 2016)*, Jul. 2016, pp. 1–2. DOI: [10.1109/CPEM.2016.7540707](https://doi.org/10.1109/CPEM.2016.7540707).
  - [57] S. Mašláň, *TWM - TracePQM Wattmeter*, Czech Metrology Institute. [Online]. Available: <https://github.com/smaslan/TWM> (visited on 05/24/2019).
  - [58] National Instruments, *LabVIEW Run-Time Engine 2013 (32-bit)*, 2013. [Online]. Available: <http://www.ni.com/download/labview-run-time-engine-2013/4059/en/>.
  - [59] —, (). NI-VISA and LabVIEW Version Compatibility, [Online]. Available: <http://www.ni.com/product-documentation/53413/en/> (visited on 05/24/2019).
  - [60] —, (). NI-SCOPE and LabVIEW Compatibility, [Online]. Available: <http://www.ni.com/product-documentation/53540/en/> (visited on 05/24/2019).
  - [61] J. W. Eaton, *GNU Octave*, 2018. [Online]. Available: <https://www.gnu.org/software/octave/>.
  - [62] M. Šíra and S. Mašláň, *Gnu Octave to Labview Pipes Interface*, Czech Metrology Institute. [Online]. Available: <https://github.com/KaeroDot/GOLPI> (visited on 05/24/2019).
  - [63] MathWorks, *Matlab*, 2012. [Online]. Available: <http://www.mathworks.com>.
  - [64] S. Mašláň, “Report A2.3.1: TWM correction datasets reference manual,” Czech Metrology Institute, A2.3.1, p. 19. [Online]. Available: <https://github.com/smaslan/TWM/blob/master/doc/A231%20Correction%20Files%20Reference%20Manual.docx> (visited on 05/24/2019).



- [65] —, “Report A2.3.1: Standardized model of data exchange,” Czech Metrology Institute, A2.3.1, p. 16. [Online]. Available: <https://github.com/smaslan/TWM/blob/master/doc/A231%20Data%20exchange%20format%20and%20file%20formats.docx> (visited on 05/24/2019).
- [66] —, “Report A2.4.4: TWM algorithms description,” Czech Metrology Institute, A2.4.4, p. 38. [Online]. Available: <https://github.com/smaslan/TWM/blob/master/doc/A244%20Algorithms%20description.pdf> (visited on 05/24/2019).
- [67] M. Šíra, *QWTB - Software Toolbox for Sampling Measurements*, Czech Metrology Insitute. [Online]. Available: <https://qwtb.github.io/qwtb/> (visited on 05/24/2019).
- [68] H. Fujiwara, J. Hájek, and O. Till, *Octave Forge - The 'parallel' package*. [Online]. Available: <https://octave.sourceforge.io/parallel/index.html> (visited on 05/24/2019).
- [69] S. Mašláň, M. Šíra, and M. Buehren, *Octave-multicore package*. [Online]. Available: <https://gitlab.com/KaeroDot/octave-multicore> (visited on 05/24/2019).
- [70] M. Šíra, *Info strings*, Czech Metrology Insitute. [Online]. Available: <https://github.com/KaeroDot/info-strings> (visited on 05/24/2019).
- [71] S. Mašláň, “Report A2.3.2: Algorithms exchange format,” Czech Metrology Institute, A2.3.2, p. 9. [Online]. Available: <https://github.com/smaslan/TWM/blob/master/doc/A232%20Algorithm%20Exchange%20Format.docx> (visited on 05/24/2019).
- [72] B. Trinchera, *TPQA tool*, Istituto Nazionale di Ricerca Metrologica Strada delle Cacce, 91 10135 Torino, ITALY, May 23, 2019. [Online]. Available: <https://github.com/btrinchera/TPQA>.
- [73] —, “Report A2.4.5: Report describing the open software tool TPQA developed in LabWindows/CVI environment,” Istituto Nazionale di Ricerca Metrologica Strada delle Cacce, 91 10135 Torino, ITALY, A2.4.5, p. 36. [Online]. Available: [https://github.com/btrinchera/TPQA/blob/master/doc/A245\\_TPQA%20Structure\\_extended.docx](https://github.com/btrinchera/TPQA/blob/master/doc/A245_TPQA%20Structure_extended.docx) (visited on 05/24/2019).
- [74] —, “Report A2.1.4: Concept of Interfacing LabWindows/CVI to Matlab,” Istituto Nazionale di Ricerca Metrologica Strada delle Cacce, 91 10135 Torino, ITALY, A2.1.4, p. 36. [Online]. Available: [https://github.com/btrinchera/TPQA/blob/master/doc/A214-%20LabWidowsCVI\\_to\\_Matlab\\_Interface.docx](https://github.com/btrinchera/TPQA/blob/master/doc/A214-%20LabWidowsCVI_to_Matlab_Interface.docx) (visited on 05/24/2019).
- [75] G. Crotti, D. Giordano, M. Luiso, and P. Pescetto, “Improvement of Agilent 3458A Performances in Wideband Complex Transfer Function Measurement,” *IEEE Transactions on Instrumentation and Measurement*, vol. 66, no. 6, pp. 1108–1116, Jun. 2017, ISSN: 0018-9456. DOI: [10.1109/TIM.2017.2661658](https://doi.org/10.1109/TIM.2017.2661658).
- [76] P. Espel, A. Poletaeff, and A. Bounouh, “Characterization of analogue-to-digital converters of a commercial digital voltmeter in the 20\hspace0.167emHz to 400\hspace0.167emHz frequency range,” *Metrologia*, vol. 46, no. 5, pp. 578–584, Sep. 2009, ISSN: 0026-1394. DOI: [10.1088/0026-1394/46/5/023](https://doi.org/10.1088/0026-1394/46/5/023).
- [77] S. Mašláň, “Report A2.4.5: TWM structure,” Czech Metrology Institute, A2.4.5, p. 38. [Online]. Available: <https://github.com/smaslan/TWM/blob/master/doc/A245%20TWM%20structure.docx> (visited on 05/24/2019).



<http://tracepqm.cmi.cz/>

Radoslava Hadzhistoykova, Antoaneta Yovcheva, Yolanda Álvarez Sanmamed, Javier Díaz de Aguilar, Stanislav Mašláň, Martin Šíra, Věra Nováková Zachovalová, Bruno Trinchera, Kristian Ellingsberg, Helge Malmbeek, Soureche Soccalingame, Aristo Philominraj, Andrei Pokatilov, Oliver Power, Marko Berginc, Tobias Bergsten, Stefan Svensson, Hüseyin Çaycı, Özlem Yilmaz, Tansu Kefeli

Guide for sampling power and power quality measurements

Published by Czech Metrology Institute  
Okružní 31, Brno, 636 00, Czech Republic  
Typeset using pdfL<sup>A</sup>T<sub>E</sub>X

First edition, May 31, 2019  
ISBN 978-80-905619-3-9  
2019